

---

# Techniques for Measuring Existing Long-Term Stresses in Prestressed Concrete Bridges, Vol. 1: Analytical, Laboratory, and Field Studies

---

PUBLICATION NO. FHWA-RD-99-178

SEPTEMBER 1999



U.S. Department of Transportation  
**Federal Highway Administration**

Research, Development, and Technology  
Turner-Fairbank Highway Research Center  
6300 Georgetown Pike  
McLean, VA 22101-2296

REPRODUCED BY:  
U.S. Department of Commerce  
National Technical Information Service  
Springfield, Virginia 22161



## FOREWORD

This report, *Techniques for Measuring Existing Long-Term Stresses in Prestressed Concrete Bridges: Volume I. Analytical, Laboratory, and Field Studies*, presents the techniques studied by Construction Technology Laboratories under a contract with the Federal Highway Administration, Department of Transportation, Washington, DC.

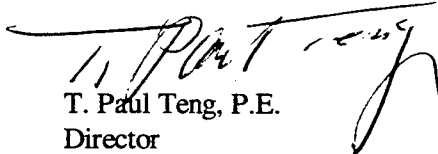
Volume I is the first of a 3-part series. It summarizes the analytical, laboratory, and field studies conducted to evaluate and improve flat-jack direct stress measurement techniques. Volume II presents a manual of instruction for using the equipment, while Volume III (previously published) summarizes the findings of the entire project.

This research was conducted to develop a technique for measuring the existing state of stress in prestressed concrete bridge members. This is needed to be able to evaluate the actual prestressing force and load capacity of prestressed concrete bridge members that may have been damaged. This report summarizes the results of analytical studies and laboratory tests on a concept that involves making small semi-circular saw cuts into the concrete member and subsequent progressive use of a set of small flat hydraulic jacks to measure existing stresses in prestressed concrete bridge girders. This report discusses the degree of accuracy that may be achieved and limitation on use of the technique.

Several strain relief methods, including boring and slitting techniques, were evaluated by performing analytical studies. The flat-jack slitting technique was determined to be the most promising. Laboratory tests were performed on unreinforced, reinforced, and prestressed concrete specimens. Additional variables included member thickness, magnitude of stress, and stress distribution. Various linear regression analyses were performed to determine the best relationship between flat-jack canceling pressure and internal concrete stress. Direct stress measurements taken on a 25-year-old prestressed concrete highway girder were similar to those determined from laboratory testing on companion girders.

Copies of this report are available from the National Technical Information Service (NTIS), 5285 Port Royal Road, Springfield, VA 22161.

PROTECTED UNDER INTERNATIONAL COPYRIGHT  
ALL RIGHTS RESERVED.  
NATIONAL TECHNICAL INFORMATION SERVICE  
U.S. DEPARTMENT OF COMMERCE

  
T. Paul Teng, P.E.  
Director  
Office of Infrastructure  
Research and Development

Reproduced from  
best available copy.



## NOTICE

This document is disseminated under the sponsorship of the Department of Transportation in the interest of information exchange. The United States Government assumes no liability for its contents or use thereof. This report does not constitute a standard, specification, or regulation.

The United States Government does not endorse products or manufacturers. Trademarks or manufacturers' names appear herein only because they are considered essential to the object of this document.

1. Report No. FHWA-RD- 99-17 8		2. Government Accession No.		3. Recipient's Catalog No.													
4. Title and Subtitle TECHNIQUES FOR MEASURING EXISTING LONG-TERM STRESSES IN PRESTRESSED CONCRETE BRIDGES Vol. 1. Analytical, Laboratory, and Field Studies				5. Report Date September 1999													
				6. Performing Organization Code													
7. Author(s) T. R. Overman, N. W. Hanson, B. G. Rabbat, B. J. Morgan, R. I. Zwiers, K. N. Shiu				8. Performing Organization Report No. CR-4995-4321-1													
9. Performing Organization Name and Address Construction Technology Laboratories 5420 Old Orchard Road Skokie, Illinois 60077-4321				10. Work Unit No. (TRAIS)													
				11. Contract or Grant No. DOT-FH-61-82-C-00020													
12. Sponsoring Agency Name and Address Offices of Research and Development Federal Highway Administration U. S. Department of Transportation Washington, D.C. 20590				13. Type of Report and Period Covered Final July 1982 - December 1985													
				14. Sponsoring Agency Code													
15. Supplementary Notes  FHWA Contract Manager: C. A. Ballinger (HNR-10)																	
16. Abstract This volume summarizes the state-of-the-art, analytical, laboratory, and field studies performed to evaluate the feasibility of the flat-jack direct stress measurement technique to be used on prestressed concrete bridges. Several strain relief methods, including boring and slitting techniques, were evaluated by performing analytical studies. The flat-jack slitting technique was determined to be the most promising.  Laboratory studies indicated that concrete internal stress could be measured to within $\pm 125$ psi with a 90 percent confidence level. Laboratory tests were performed on unreinforced, reinforced, and prestressed concrete specimens. Additional variables included member thickness, magnitude of stress, and stress distribution. Various linear regression analyses were performed to determine the best relationship between flat-jack canceling pressure and internal concrete stress. Direct stress measurements taken on a 25-year-old prestressed concrete highway girder were similar to those determined from laboratory testing on companion girders. There are three reports in the series:  <table border="0" style="width: 100%;"> <thead> <tr> <th style="text-align: left;"><u>Vol. No.</u></th> <th style="text-align: left;"><u>FHWA No.</u></th> <th style="text-align: left;"><u>Short Title</u></th> </tr> </thead> <tbody> <tr> <td>-</td> <td>FHWA-RD-85-</td> <td>Executive Summary Report</td> </tr> <tr> <td>1</td> <td>FHWA-RD- 99-17 8</td> <td>Analytical, Laboratory, and Field Studies</td> </tr> <tr> <td>2</td> <td>FHWA-RD- 99-179</td> <td>Manual of Instruction</td> </tr> </tbody> </table>						<u>Vol. No.</u>	<u>FHWA No.</u>	<u>Short Title</u>	-	FHWA-RD-85-	Executive Summary Report	1	FHWA-RD- 99-17 8	Analytical, Laboratory, and Field Studies	2	FHWA-RD- 99-179	Manual of Instruction
<u>Vol. No.</u>	<u>FHWA No.</u>	<u>Short Title</u>															
-	FHWA-RD-85-	Executive Summary Report															
1	FHWA-RD- 99-17 8	Analytical, Laboratory, and Field Studies															
2	FHWA-RD- 99-179	Manual of Instruction															
17. Key Words Nondestructive tests, normal stress, strain, residual stress, reinforced concrete, prestressed concrete, field tests, determination of stress			18. Distribution Statement No restrictions. This document is available to the public through the National Technical Information Service, Springfield, Virginia 22161														
19. Security Classif. (of this report) Unclassified		20. Security Classif. (of this page) Unclassified		21. No. of Pages 288	22. Price												

# SI\* (MODERN METRIC) CONVERSION FACTORS

## APPROXIMATE CONVERSIONS TO SI UNITS

Symbol	When You Know	Multiply By	To Find	Symbol
<b>LENGTH</b>				
in	inches	25.4	millimeters	mm
ft	feet	0.305	meters	m
yd	yards	0.914	meters	m
mi	miles	1.61	kilometers	km
<b>AREA</b>				
in <sup>2</sup>	square inches	645.2	square millimeters	mm <sup>2</sup>
ft <sup>2</sup>	square feet	0.093	square meters	m <sup>2</sup>
yd <sup>2</sup>	square yards	0.836	square meters	m <sup>2</sup>
ac	acres	0.405	hectares	ha
mi <sup>2</sup>	square miles	2.59	square kilometers	km <sup>2</sup>
<b>VOLUME</b>				
fl oz	fluid ounces	29.57	milliliters	mL
gal	gallons	3.785	liters	L
ft <sup>3</sup>	cubic feet	0.028	cubic meters	m <sup>3</sup>
yd <sup>3</sup>	cubic yards	0.765	cubic meters	m <sup>3</sup>

NOTE: Volumes greater than 1000 l shall be shown in m<sup>3</sup>.

Symbol	When You Know	Multiply By	To Find	Symbol
<b>LENGTH</b>				
in	inches	0.039	inches	in
ft	feet	3.28	feet	ft
yd	yards	1.09	yards	yd
mi	miles	0.621	miles	mi
<b>AREA</b>				
in <sup>2</sup>	square inches	0.0016	square inches	in <sup>2</sup>
ft <sup>2</sup>	square feet	10.764	square feet	ft <sup>2</sup>
yd <sup>2</sup>	square yards	1.195	square yards	yd <sup>2</sup>
ac	acres	2.47	acres	ac
mi <sup>2</sup>	square miles	0.386	square miles	mi <sup>2</sup>
<b>VOLUME</b>				
fl oz	fluid ounces	0.034	fluid ounces	fl oz
gal	gallons	0.264	gallons	gal
ft <sup>3</sup>	cubic feet	35.71	cubic feet	ft <sup>3</sup>
yd <sup>3</sup>	cubic yards	1.307	cubic yards	yd <sup>3</sup>
<b>MASS</b>				
oz	ounces	0.035	ounces	oz
lb	pounds	2.202	pounds	lb
T	short tons (2000 lb)	1.103	short tons (2000 lb)	T
<b>TEMPERATURE (exact)</b>				
°F	Fahrenheit temperature	1.8C + 32	Celcius temperature	°C
°F	Fahrenheit temperature	1.8C + 32	Fahrenheit temperature	°F
<b>ILLUMINATION</b>				
fc	foot-candles	0.0929	foot-candles	fc
fl	foot-Lamberts	0.2919	foot-Lamberts	fl
<b>FORCE and PRESSURE or STRESS</b>				
lbf	poundforce	0.225	poundforce	lbf
lbf/in <sup>2</sup>	poundforce per square inch	0.145	poundforce per square inch	lbf/in <sup>2</sup>
N	newtons		newtons	N
kPa	kilopascals		kilopascals	kPa

\* SI is the symbol for the International System of Units. Appropriate rounding should be made to comply with Section 4 of ASTM E380. (Revised September 1993)

## TABLE OF CONTENTS

1.0	INTRODUCTION	1
1.1	Widespread Use of Prestressed Concrete Bridges	1
1.2	Need for Stress Measurement in Prestressed Concrete Bridges	2
2.0	OBJECTIVE AND SCOPE	4
3.0	TASK A - STATE-OF-THE-ART SURVEY	5
3.1	Stress Measurement Techniques	5
3.1.1	Instrumentation During Construction	5
3.1.2	Instrumentation After Construction	9
3.2	Evaluation of Techniques	19
3.2.1	Techniques of Strain Relief	20
3.2.2	Location of Strain Relief	21
3.2.3	Stress-Strain Relationship	23
3.2.4	Measurement of Relieved Strain	24
3.3	Potential Stress Measurement Techniques	29
3.3.1	Flat-Jack Method	29
3.3.2	Borehole Deformation Method	30
3.3.3	Dilatometer Method	30
3.3.4	General Considerations	30
4.0	TASK B - ANALYTICAL STUDIES	32
4.1	Analytical Investigations of Measurement Techniques	32
4.1.1	Evaluation of Boring and Slitting Techniques	32
4.1.2	Model to Analyze the Flat-Jack Method of Strain Relief	38
4.1.3	Accuracy of Flat-Jack Method	50
4.2	Variables Affecting Stress Measurements	68
4.2.1	Shrinkage	70
4.2.2	Coefficient of Linear Thermal Expansion	72
4.2.3	Creep	72
4.3	Considerations for Field Tests	74
5.0	TASK C - LABORATORY STUDIES	75
5.1	Flat-Jack Measurement Technique	75

## TABLE OF CONTENTS

5.0	TASK C - LABORATORY STUDIES (Continued)	
5.2	Stress Measuring Equipment	78
5.2.1	Slitting Jig	78
5.2.2	Flat Jack	80
5.2.3	Pfender (Mechanical) Gage	82
5.2.4	Clip Gage	82
5.3	Laboratory Specimens	86
5.3.1	Specimen S1	91
5.3.2	Specimen S2	91
5.3.3	Specimen S3	91
5.3.4	Specimen S4	92
5.3.5	Specimen S5	92
5.3.6	Loading Scheme	92
5.4	Discussion of Test Results	92
5.4.1	Slot Displacement	94
5.4.2	Effects of Mineral Oil Coolant	96
5.4.3	Data Reduction	100
5.4.4	Data Analysis	102
5.4.5	Multiple Variant Linear Regression Analysis	106
5.4.6	Variables Affecting Canceling Pressures	113
6.0	TASK D - FIELD STUDIES	124
6.1	Girder Slots	125
6.2	Data Analysis	128
7.0	CONCLUSIONS AND RECOMMENDATIONS	131
7.1	Conclusions	131
7.2	Recommendations	133
8.0	REFERENCES	135
9.0	APPENDIX A - DISPLACEMENT DUE TO CUTTING INTO STRESSED PLATES	140
9.1	Circular Hole in a Stressed Plate	140
9.2	Slot in a Stressed Plate	143
10.0	APPENDIX B - LABORATORY TEST RESULTS	146
11.0	APPENDIX C - FIELD TEST RESULTS	260

## LIST OF FIGURES

Figure 1. Strain relief measured adjacent to relieved area.	11
Figure 2. Strain relief measured within relieved area.	14
Figure 3. Doorstopper strain relief method.	15
Figure 4. Strain relief method of measuring diameter change of overcored borehole.	16
Figure 5. Measurement points on plate.	34
Figure 6. Slotted bridge girder.	39
Figure 7. Two-dimensional model.	41
Figure 8. Symmetric opposite edge cracks.	43
Figure 9. Stress flow near slot.	45
Figure 10. Finite element mesh for a 12-in-thick section.	49
Figure 11. Reconstruction of a stress gradient.	57
Figure 12. Stress distributions.	61
Figure 13. Half-depth shrinkage stress model.	64
Figure 14. Full-depth shrinkage stress model.	69
Figure 15. Shrinkage stress distribution. <sup>[53]</sup>	71
Figure 16. Variation of creep with time. <sup>[54]</sup>	73
Figure 17. Creep and creep recovery. <sup>[48]</sup>	73
Figure 18. Saw assembly with raised blade.	79
Figure 19. Saw assembly with lowered blade.	81
Figure 20. Photograph of flat jacks.	83
Figure 21. Schematic of flat jacks.	84
Figure 22. Pfender gage.	85
Figure 23. Clip gage.	85
Figure 24. Elevations of Specimens S1, S3, and S4.	87
Figure 25. Sections of Specimens S1, S3, and S4.	88
Figure 26. Specimen S2.	89
Figure 27. Specimen S5.	90
Figure 28. Schematic of test setup.	93
Figure 29. Linear pressure versus clip gage displacement relationship.	95
Figure 30. Knife edge orientation.	97
Figure 31. Pfender point layout.	98

## LIST OF FIGURES (Continued)

Figure 32. Lubricated cut stress profile.	99
Figure 33. Effect of moisture on slot displacement.	101
Figure 34. Uncorrected results of specimen cuts.	103
Figure 35. Distribution of uncorrected canceling pressures.	104
Figure 36. Canceling pressures at various applied stresses.	105
Figure 37. Corrected results of 30- to 80-mm cuts on Specimens S4 and S5.	111
Figure 38. Distribution of corrected concrete stress.	112
Figure 39. Effect of flat jacks on stress distribution for Specimen S2.	114
Figure 40. Effect of time on stress distribution for Specimen S5 Slot N1.	115
Figure 41. Measured canceling pressures before and after application and removal of load.	117
Figure 42. Effect of gradient on measured transverse canceling pressures.	118
Figure 43. Effect of cutting into reinforcement.	119
Figure 44. Measured to applied stress at various pressures and plate spacings.	122
Figure 45. Girder cut locations.	126
Figure 46. Cross section cut locations.	127
Figure 47. Measured stresses.	129
Figure 48. Infinite plate models.	141
Figure 49. Uncorrected stress profile for 1S1V50/55T20MM.	149
Figure 50. Uncorrected stress profile for 1S1V50/55B.	151
Figure 51. Uncorrected stress profile for 1S2V00/00T.	153
Figure 52. Uncorrected stress profile for 1S2V00/00B60MM.	155
Figure 53. Uncorrected stress profile for 1S4V38/49TK.	157
Figure 54. Uncorrected stress profile for 1S4V38/49B.	159
Figure 55. Uncorrected stress profile for 1S5H50/50W.	161
Figure 56. Uncorrected stress profile for 2S3V50/50T.	163
Figure 57. Uncorrected stress profile for 2S3V50/50M.	165
Figure 58. Uncorrected stress profile for 2S3V50/50B.	167



## LIST OF FIGURES (Continued)

Figure 59.	Uncorrected stress profile for 2S4V75/75T.	169
Figure 60.	Uncorrected stress profile for 2S4V75/75M.	171
Figure 61.	Uncorrected stress profile for 2S4V75/75B.	173
Figure 62.	Uncorrected stress profile for 2S5H50/50M.	175
Figure 63.	Uncorrected stress profile for 2S6H00/00M0FJ.	177
Figure 64.	Uncorrected stress profile for 2S6H00/00M1FJ.	179
Figure 65.	Uncorrected stress profile for 2S6H00/00M2FJ.	181
Figure 66.	Uncorrected stress profile for 3N2V70/75T.	183
Figure 67.	Uncorrected stress profile for 3N2V70/75B.	185
Figure 68.	Uncorrected stress profile for 3N3V51/42T.	187
Figure 69.	Uncorrected stress profile for 3N4V55/46T.	189
Figure 70.	Uncorrected stress profile for 3N4V55/46B.	191
Figure 71.	Uncorrected stress profile for 3S5H50/50E.	193
Figure 72.	Uncorrected stress profile for 3S5H50/50WK.	195
Figure 73.	Uncorrected stress profile for 3S6H00/00E.	197
Figure 74.	Uncorrected stress profile for 3S6H00/00WK.	199
Figure 75.	Uncorrected stress profile for 4N1V00/00T.	201
Figure 76.	Uncorrected stress profile for 4N1V00/00B.	203
Figure 77.	Uncorrected stress profile for 4N2V95/118T.	205
Figure 78.	Uncorrected stress profile for 4N3V93/22T.	207
Figure 79.	Uncorrected stress profile for 4N3V93/22B.	209
Figure 80.	Uncorrected stress profile for 4N4V84/37T.	211
Figure 81.	Uncorrected stress profile for 4N4V84/37B.	213
Figure 82.	Uncorrected stress profile for 4N5H88/22E.	215
Figure 83.	Uncorrected stress profile for 4N5H88/22W.	217
Figure 84.	Uncorrected stress profile for 4S6V23/117T.	219
Figure 85.	Uncorrected stress profile for 4S6V23/117B.	221
Figure 86.	Uncorrected stress profile for 5S0V43/87T.	223
Figure 87.	Uncorrected stress profile for 5S0V43/87B.	225
Figure 88.	Uncorrected stress profile for 5N1V82/54T00.	227
Figure 89.	Uncorrected stress profile for 5N1V82/54B00.	229
Figure 90.	Uncorrected stress profile for 5N1V82/54T10.	231
Figure 91.	Uncorrected stress profile for 5N1V82/54B10.	233

## LIST OF FIGURES (Continued)

Figure 92.	Uncorrected stress profile for 5N1V82/54T40.	235
Figure 93.	Uncorrected stress profile for 5N1V82/54B40.	237
Figure 94.	Uncorrected stress profile for 5S1V43/87T.	239
Figure 95.	Uncorrected stress profile for 5N4V72/48T.	241
Figure 96.	Uncorrected stress profile for 5N4V72/48B.	243
Figure 97.	Uncorrected stress profile for 5S4V39/82T.	245
Figure 98.	Uncorrected stress profile for 5S4V39/82B.	247
Figure 99.	Uncorrected stress profile for 5N5H79/46E.	249
Figure 101.	Uncorrected stress profile for 5N5H79/46W.	251
Figure 102.	Uncorrected stress profile for 5S5H38/80T.	253
Figure 103.	Uncorrected stress profile for 5S5H38/80B.	255
Figure 104.	Uncorrected stress profile for 5S6H38/80T.	257
Figure 105.	Uncorrected stress profile for 5S6H38/80B.	259
Figure 106.	Uncorrected stress profile for TWS1VT.	262
Figure 107.	Uncorrected stress profile for TWS1VB.	264
Figure 108.	Uncorrected stress profile for TWS2VT.	266
Figure 109.	Uncorrected stress profile for TWS2VB.	268
Figure 110.	Uncorrected stress profile for TWS3HE.	270
Figure 111.	Uncorrected stress profile for TWS3HW.	272
Figure 112.	Uncorrected stress profile for TWB4VN.	274
Figure 113.	Uncorrected stress profile for TWB4VS.	276
Figure 114.	Uncorrected stress profile for TWS5VT.	278
Figure 115.	Uncorrected stress profile for TWS5VB.	280
Figure 116.	Uncorrected stress profile for TWS6VT.	282
Figure 117.	Uncorrected stress profile for TWS6VB.	284
Figure 118.	Uncorrected stress profile for TWS7HE.	286
Figure 119.	Uncorrected stress profile for TWS7HW.	288

## LIST OF TABLES

Table 1.	Coefficients C and S for equations 4 and 5.	36
Table 2.	Displacements due to cutting into a stressed plate.	36
Table 3.	Radial stress near circular hole.	47
Table 4.	Displacement of slotted sections.	51
Table 5.	Displacements due to slitting a section under uniform stress.	53
Table 6.	Flat-jack pressure causing unit displacement.	55
Table 7.	Centroid of flat jacks.	58
Table 8.	Displacements due to slitting a section with bending stress gradient.	60
Table 9.	Restoring flat-jack pressure for bending stress gradient.	63
Table 10.	Error in reconstruction of a bending stress gradient.	63
Table 11.	Displacement due to slitting section with shrinkage stress distribution.	66
Table 12.	Restoring flat-jack pressures for shrinkage stress distribution.	66
Table 13.	Discrepancy in reconstruction of shrinkage stress distribution.	67
Table 14.	Schematic of flat jacks.	84
Table 15.	Results of multiple linear regression analyses.	107
Table 16.	Cumulative frequency data for combined equation.	108
Table 17.	Cumulative frequency data for recommended equation.	110
Table 18.	Stress measurement data for specimen 1S1V50/55T20MM.	148
Table 19.	Stress measurement data for specimen 1S1V50/55B.	150
Table 20.	Stress measurement data for specimen 1S2V00/00T.	152
Table 21.	Stress measurement data for specimen 1S2V00/00B60MM.	154
Table 22.	Stress measurement data for specimen 1S4V38/49TK.	156
Table 23.	Stress measurement data for specimen 1S4V38/49B.	158
Table 24.	Stress measurement data for specimen 1S5H50/50W.	160
Table 25.	Stress measurement data for specimen 2S3V50/50T.	162
Table 26.	Stress measurement data for specimen 2S3V50/50M.	164
Table 27.	Stress measurement data for specimen 2S3V50/50B.	166
Table 28.	Stress measurement data for specimen 2S4V75/75T.	168

LIST OF TABLES (Continued)

Table 29.	Stress measurement data for specimen 2S4V75/75M.	170
Table 30.	Stress measurement data for specimen 2S4V75/75B.	172
Table 31.	Stress measurement data for specimen 2S5H50/50M.	174
Table 32.	Stress measurement data for specimen 2S6H00/00M0FJ.	176
Table 33.	Stress measurement data for specimen 2S6H00/00M1FJ.	178
Table 34.	Stress measurement data for specimen 2S6H00/00M2FJ.	180
Table 35.	Stress measurement data for specimen 3N2V70/75T.	182
Table 36.	Stress measurement data for specimen 3N2V70/75B.	184
Table 37.	Stress measurement data for specimen 3N3V51/42T.	186
Table 38.	Stress measurement data for specimen 3N4V55/46T.	188
Table 39.	Stress measurement data for specimen 3N4V55/46B.	190
Table 40.	Stress measurement data for specimen 3S5H50/50E.	192
Table 41.	Stress measurement data for specimen 3S5H50/50WK.	194
Table 42.	Stress measurement data for specimen 3S6H00/00E.	196
Table 43.	Stress measurement data for specimen 3S6H00/00WK.	198
Table 44.	Stress measurement data for specimen 4N1V00/00T.	200
Table 45.	Stress measurement data for specimen 4N1V00/00B.	202
Table 46.	Stress measurement data for specimen 4N2V95/118T.	204
Table 47.	Stress measurement data for specimen 4N3V93/22T.	206
Table 48.	Stress measurement data for specimen 4N3V93/22B.	208
Table 49.	Stress measurement data for specimen 4N4V84/37T.	210
Table 50.	Stress measurement data for specimen 4N4V84/37B.	212
Table 51.	Stress measurement data for specimen 4N5H88/22E.	214
Table 52.	Stress measurement data for specimen 4N5H88/22W.	216
Table 53.	Stress measurement data for specimen 4S6V23/117T.	218
Table 54.	Stress measurement data for specimen 4S6V23/117B.	220
Table 55.	Stress measurement data for specimen 5S0V43/87T.	222
Table 56.	Stress measurement data for specimen 5S0V43/87B.	224
Table 57.	Stress measurement data for specimen 5N1V82/54T00.	226
Table 58.	Stress measurement data for specimen 5N1V82/54B00.	228
Table 59.	Stress measurement data for specimen 5N1V82/54T10.	230
Table 60.	Stress measurement data for specimen 5N1V82/54B10.	232
Table 61.	Stress measurement data for specimen 5N1V82/54T40.	234

## LIST OF TABLES (Continued)

Table 62.	Stress measurement data for specimen 5N1V82/54B40.	236
Table 63.	Stress measurement data for specimen 5S1V43/87T.	238
Table 64.	Stress measurement data for specimen 5N4V72/48T.	240
Table 65.	Stress measurement data for specimen 5N4V72/48B.	242
Table 66.	Stress measurement data for specimen 5S4V39/82T.	244
Table 67.	Stress measurement data for specimen 5S4V39/82B.	246
Table 68.	Stress measurement data for specimen 5N5H79/46E.	248
Table 69.	Stress measurement data for specimen 5N5H79/46W.	250
Table 70.	Stress measurement data for specimen 5S5H38/80T.	252
Table 71.	Stress measurement data for specimen 5S5H38/80B.	254
Table 72.	Stress measurement data for specimen 5S6H38/80T.	256
Table 73.	Stress measurement data for specimen 5S6H38/80B.	258
Table 74.	Stress measurement data for specimen TWS1VT.	261
Table 75.	Stress measurement data for specimen TWS1VB.	263
Table 76.	Stress measurement data for specimen TWS2VT.	265
Table 77.	Stress measurement data for specimen TWS2VB.	267
Table 78.	Stress measurement data for specimen TWS3HE.	269
Table 79.	Stress measurement data for specimen TWS3HW.	271
Table 80.	Stress measurement data for specimen TWB4VN.	273
Table 81.	Stress measurement data for specimen TWB4VS.	275
Table 82.	Stress measurement data for specimen TWS5VT.	277
Table 83.	Stress measurement data for specimen TWS5VB.	279
Table 84.	Stress measurement data for specimen TWS6VT.	281
Table 85.	Stress measurement data for specimen TWS6VB.	283
Table 86.	Stress measurement data for specimen TWS7HE.	285
Table 87.	Stress measurement data for specimen TWS7HW.	287



## 1.0 INTRODUCTION

In this introduction, application of prestressing to highway bridges is briefly reviewed. The need for measurement of internal concrete stresses in prestressed concrete bridges is emphasized.

### 1.1 Widespread Use of Prestressed Concrete Bridges

Since the Walnut Lane Bridge in Pennsylvania was built in 1949, application of prestressing in the transportation industry has grown rapidly. Annual reports of the Bureau of Public Roads for each fiscal year from 1954 through 1957 reported that "Use of prestressed concrete in bridge construction continued to grow in favor because in many situations it permits large savings in materials and cost."<sup>[2]</sup>

Most prestressed concrete highway bridges built in the United States in the 1960's and 1970's were constructed of precast prestressed girders with cast-in-place decks. This procedure has been used for spans up to 140 ft (43 m). In California, 85% of all bridges are cast-in-place post-tensioned box girders.<sup>[3]</sup>

In the last decade, post-tensioned segmental bridge construction has gained acceptance in North America. Originally developed in Western Europe in the 1950's,<sup>[4]</sup> this bridge type has proven to be the most economical for spans from roughly one hundred to several hundred feet long.<sup>[5]</sup> Although the major application of prestressed concrete in the highway field has been for bridge girders, it has also been used for deck elements, piers and pier caps, piling, and culverts.

A recent survey of highway agencies reports that "Generally, prestressed concrete bridges have displayed excellent performance" and "durability and performance of pretensioned bridge girders were very good."<sup>[3]</sup>

## 1.2 Need for Stress Measurement in Prestressed Concrete Bridges

In a prestressed concrete member, the prestressing force decreases continuously with time at a decreasing rate. Decrease of prestressing force is primarily due to creep and shrinkage of the concrete, and relaxation of the prestressing steel. Guidelines and procedures for estimating prestress losses are given in the AASHTO Specifications<sup>[6]</sup> and in ACI Committee 343 Report, "Concrete Bridge Design."<sup>[7]</sup> Efforts to simplify and improve the accuracy of estimating prestress losses are ongoing.<sup>[8]</sup> Recently, tests<sup>[9]</sup> were conducted at the Construction Technology Laboratories on prestressed concrete bridge girders after 25 years of service. Measured prestress losses were about 50% of values estimated using existing codes and standards.

Although there have been very few structural problems due to inaccuracies in estimating prestress losses, serviceability and alignment problems have occurred. Inaccurate estimate of losses can result in excessive camber or sag of prestressed girders, thus causing ride discomfort.

In segmental bridge construction, alignment problems have occurred where precast elements are used. These problems may be due to inaccurate estimates of prestress losses resulting from variable manufacturing conditions. The actual age and strength of the concrete at the time of prestressing may be controlled by the construction schedule rather than by the designer or specifications.

In segmental bridge construction, different prestressing systems may be utilized on one structure. Decks may be prestressed laterally. Webs may be prestressed in a vertical plane or diagonally across construction joints. Longitudinal prestressing is usually performed in stages as segments are erected. As a result, a complex state of stress exists in the bridge superstructure. Therefore, an accurate estimate of prestress losses and accordingly of concrete stresses is very difficult in segmental bridge construction.



Several other factors influence the effective prestressing force in tendons. In statically determinate bridge superstructures, temperature gradient across a cross-section may cause minor changes in concrete and reinforcing steel stresses. If the bridge superstructure is statically indeterminate, temperature variation and differential settlement of supports will induce large stresses in the structure. In all cases, redistribution of stresses in the concrete will occur due to creep. As a result, the magnitude of concrete stresses will vary with time. Therefore, the exact state of stress can only be determined through measurements on the actual structure.

In recent years, some of the first post-tensioned bridges have shown signs of distress.<sup>[10]</sup> In addition, every year, several incidences of damage to prestressed concrete bridge girders are reported due to fire or collision by overheight vehicles.<sup>[11]</sup> In these instances, it may be essential to determine the state of stress in the bridge to evaluate the extent of damage.

From the above, it follows that techniques are needed to measure the existing long-term stresses in prestressed concrete bridges.

## 2.0 OBJECTIVE AND SCOPE

The objective of this investigation was to develop techniques for measuring existing long-term stresses in prestressed concrete bridges.

The above objective was accomplished within the scope of five tasks.

1. In Task A, a state-of-the-art survey was conducted to determine previous and current techniques used to measure stresses in materials. Techniques inventoried were evaluated to determine the most suitable approach to measure existing stresses in prestressed concrete bridges.
2. Analytical studies were conducted in Task B to determine suitability and accuracy of measurement techniques and/or equipment to measure existing stresses in prestressed concrete bridges.
3. Task C included laboratory investigations to evaluate the developed techniques.
4. In Task D, field studies were conducted on a selected bridge member to evaluate the techniques under site conditions.
5. A Manual of Instruction was prepared in Task E for the users of developed techniques.

Presented in this Final Report is a summary of Tasks A through D. The Manual of Instruction (Task E) is published under separate cover.<sup>[1]</sup>

### 3.0 TASK A - STATE-OF-THE-ART SURVEY

Existing methods for measurement of stresses in materials are reviewed in this section. Inventoried techniques are then evaluated. Potential techniques for measurement of existing long-term stresses in prestressed concrete bridges are identified.

#### 3.1 Stress Measurement Techniques

Two approaches are possible to determine existing long-term stresses in a prestressed concrete bridge. The first is to instrument the bridge at construction time. The second is to instrument the bridge at some time after construction.

##### 3.1.1 Instrumentation During Construction

During construction, it is possible to embed instruments<sup>[12,13]</sup> and to install measuring stations to determine physical changes during the life of the structure. These changes may include support reaction, tendon force, deflection, displacement, curvature, temperature, humidity, strain, and stress.

Measurement of support reactions in a continuous structure provides a measurement of effectiveness of certain long-term predictions in design. Support reactions are not sufficient to determine the absolute stresses in the bridge. Hydraulic and electronic devices have been used to measure support reactions. A hydraulic load measuring capsule<sup>[14]</sup> developed in France can measure reactions with extreme accuracy (0.2 percent) over the life of a bridge. Measurement of a reaction requires several people and a combination of hydraulic and electronic hardware at the location. Such a device has shown the influence of temperature gradients on the abutment reaction of a continuous bridge. A day with good sunshine produced a diurnal variation of 26 percent in support reaction.<sup>[14]</sup>

Change in support reaction in a single day can be measured with less complexity by a hydraulic capsule or a strain gaged load cell connected to an automatic data acquisition system. However, confidence in the long-term reference to original zero may require the additional complexity such as in the French system. The additional complexity allows the load sensing device to remain in an unloaded condition except when readings are being made. Reference to zero load is then available at any time.

Measurement of tendon force, like measurement of support reaction, requires that instruments be installed at the time of construction. Force in an unbonded tendon may be monitored with a hydraulic or strain-gaged cell installed at the anchorage prior to stressing. Load measuring cells could also be adapted to replace a short length of tendon at a desired location.<sup>[15,16]</sup> Determination of loss of tension requires confidence in long-term reference to zero load that may not be provided by strain-gaged systems.

Tendon force has also been determined by measuring the natural frequency of vibration of a known length of tendon.<sup>[17]</sup> Although this technique has only been used in precasting plants prior to casting of concrete, it may potentially be applicable to members in which the strands are accessible. Remote recording requires a means of initiating, sensing, and measuring vibration frequency. Reference to initial zero is not required since each measurement directly results in a calculated tendon force. Strain gages mounted on individual wires of a tendon can also be used to monitor tendon strain. Tendon strain must then be interpreted to produce tendon force. Bonded strain gages do not provide the long-term reference to zero needed to give confidence in long-term accuracy. However, short-term changes in strain can be accurately recorded over the life of the bridge.

Long-term monitoring of deflection requires early installation of bench marks. These marks are used in precision level surveys to establish initial vertical position and as zero reference for recording data from instruments installed later.

Long-term monitoring of displacement and curvature requires early installation of reference points. Accurate measurement of distance between points can be used as zero reference to establish initial horizontal position. Reference points on initial parallel lines on the structure can be used to detect curvature changes.

Temperature gradients through sections are needed to define source of temperature effects. Embedded thermocouples and humidity sensors are placed at time of construction.

Sensors embedded in the concrete are used to determine strain. Strain is measured to give an indication of stress. The relationship between strain and stress is affected by time in the form of creep and shrinkage strains and temperature in the form of thermal strains. Strains are measured by embedding devices, such as Carlson\* strain meters,<sup>[12]</sup> at time of construction. Remote recording of data uses electrical equipment connected by cable to the meter. An alternative is to secure points to the concrete surface of the member. Distance change between points is measured externally through a mechanical gage, for example, Whittemore Gage.<sup>[18]</sup> The time-dependent deformations are then monitored individually.

Prestressed concrete box-girder bridges instrumented at time of construction in the United States include Turkey Run Bridge in Indiana, Kishwaukee River Bridge in Illinois, Denny Creek Bridge in the State of Washington, Linn Cove Viaduct in North Carolina, an experimental bridge in Pennsylvania, and Red River Bridge in Louisiana, and six one- or two-span bridges in California. The recently completed East Huntington Bridge over the Ohio River between Huntington, West Virginia and Proctorville, Ohio was also instrumented during construction. Two cable-stayed bridges currently under construction (1985) are also being instrumented. They are the Mississippi River Bridge at Quincy, Illinois and the Sunshine Skyway Bridge in Tampa, Florida.

\*The United States Government and the performing organization do not endorse products or manufacturers. Trade or manufacturer's names appear herein solely because they are considered essential to the object of this report.

In addition to measurement of strains and temperature at the bridge, data from control specimens are needed to properly interpret measurements made on the bridge. Creep and shrinkage properties of the Kishwaukee River Bridge concrete have been measured at the Construction Technology Laboratories<sup>[19]</sup> under environmental conditions similar to those at the bridge site. Periodic measurements at the bridge and on control cylinders have been used to evaluate and verify the time-dependent deformations and stresses in this segmental box-girder bridge.<sup>[20]</sup>

"Easy-to-measure" items such as temperature and humidity as well as more difficult items such as displacement, curvature, and strain are not easily converted into stress. For example, during a single day the temperature variation throughout a simple span bridge may cause major changes in deflection, displacement, curvature, and strain, without a corresponding change in stress. However, in a continuous structure, a similar temperature variation may produce major changes in stress.<sup>[14]</sup>

In addition to short term disturbances, there are long-term effects that are originally estimated in the design stage and included as loss of prestress. Shrinkage and creep of concrete and relaxation of steel combine as losses. Shrinkage has been measured<sup>[19]</sup> but the effect on the structure is a complex redistribution of stress between concrete and reinforcement. Creep of the concrete<sup>[19]</sup> and relaxation of the steel have also been measured using auxiliary tests. The final determination of stress may include an uncertainty in the eyes of the design engineer who is asking for accurate data to aid in minor adjustment of design prestress losses.

Direct measurement of stress has therefore been a major goal of experimental work on bridges within the last decade. It has been suggested that direct measurement of stress in concrete can be made with Carlson Stress Meters.<sup>[12]</sup> These large pressure meters are embedded in the concrete at time of construction. Measurements are recorded by electrical equipment connected by cable to the meter. It should be noted with caution that Carlson Stress Meters detect time-dependent movements and translate these movements

into stress. However, measured data must be corrected for sustained modulus of elasticity and temperature variations.

Stress meters of a different form have been used in Great Britain<sup>[21]</sup> for direct measurement of stress. Several bridges used the German-made Glotzl pressure cells with satisfactory results. At each measurement, it is necessary to connect hydraulic equipment for pressurizing the cell to balance the local stress. Automatic data acquisition is therefore not possible. Large size, high cost, and measurement complexity have inhibited extensive application of the Glotzl pressure cells.

Calculations of stress from strain in prestressed concrete members is therefore neither practical nor possible unless time-dependent deformations are taken into account. This necessitates measurement of creep and shrinkage strains in the concrete and relaxation in the tendons. For this reason, direct stress measurements, taken on prestressed concrete bridges, with instrumentation installed after construction, provide a more reliable indication of stresses over a long period of time.

### 3.1.2 Instrumentation After Construction

The second approach that may be used to determine long-term existing stresses is to instrument a structure at some time after construction. Two methods are available for determining existing stress fields in structures after construction.

1. Measure a property that is, of itself, a direct indicator of absolute stress.
2. Relieve the existing state of strain in a local area in the structure. The existing state of stress is calculated from measurements made before and after the strain relief process.

Methods currently used to determine absolute state of stress include, X-Ray Diffraction,<sup>[22]</sup> Surface Hardness Testing,<sup>[23]</sup> Ultrasonic

Techniques,<sup>[24]</sup> and Magnetic Measurements.<sup>[25]</sup> Of these methods, the only technique presently suited to concrete is Ultrasonic. This method utilizes the principle that the velocity of ultrasonic waves in a material changes as a function of the elastic modulus, which in turn, experiences a second order change as a function of stress. The second order modulus change and the corresponding velocity change are very small and highly dependent on physical and elastic properties of the material as well. The modulus of elasticity of concrete varies with concrete mix, curing conditions, age, and environmental conditions. Therefore, ultrasonic techniques do not appear practical for stress measurement in concrete structures.

State of stress in prestressing tendons can be determined by exposing a length of tendon and measuring its natural frequency of vibration.<sup>[17]</sup> This direct method has never been applied due to effort and danger involved in exposing a tendon.

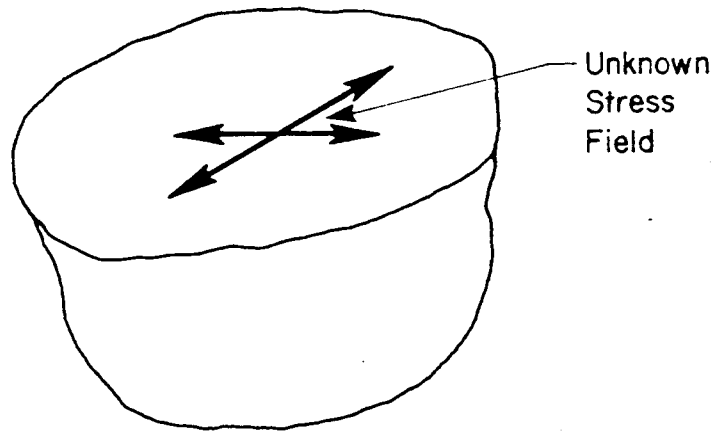
Strain relief methods have been used extensively to determine residual stress in metals and plastics, and to determine the existing state of stress in rock. The existing state of stress in rock masses is required to safely conduct mining operations. Strain relief applied to rock stress determination is a highly developed technology. Since the mining engineer works with a material similar to concrete, the geotechnical literature contains a wealth of information, experience, and techniques directly applicable to mass concrete. Applicability of these techniques to thin prestressed concrete members will be assessed after briefly reviewing existing strain relief methods.

Reference 24 is a bibliography published in 1971 listing 371 publications devoted to determining existing stresses in rock. The following is a brief summary of strain relief methods used in the geotechnical area.

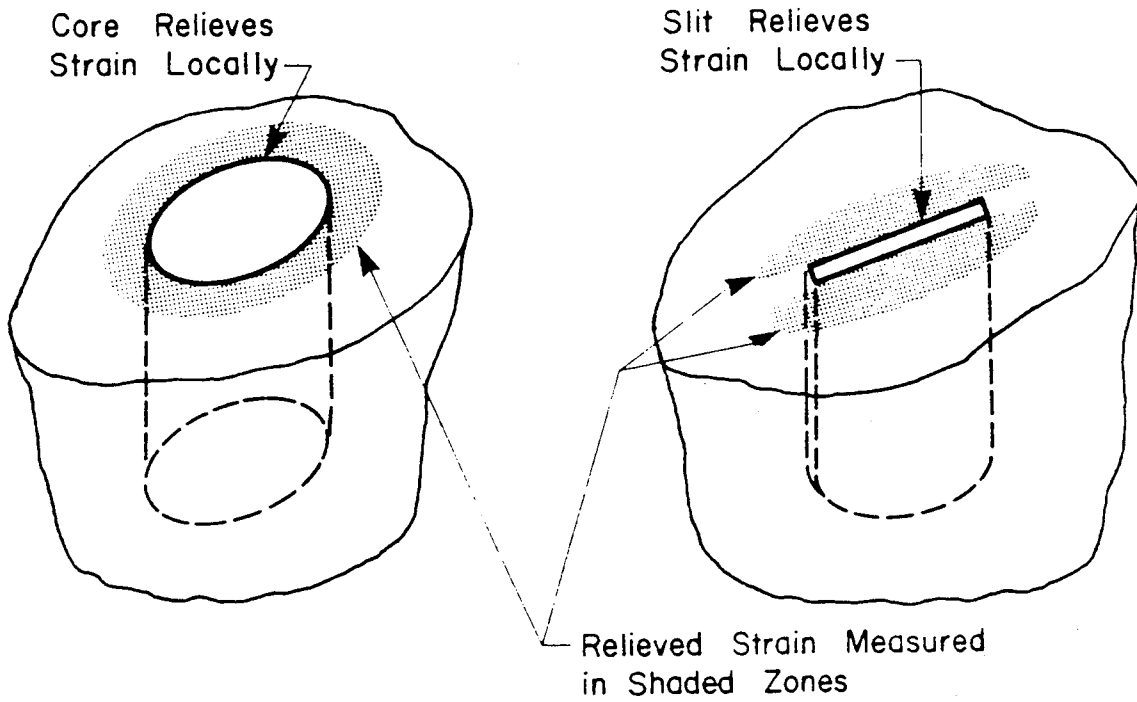
### 3.1.2.1 Strain Relief Measured Adjacent to Relieved Area

Figure 1 shows one basic approach to measurement of relieved strain. The strain field is relieved by drilling, coring, or slitting the material. The





(a) Stress field



(b) Core

(c) Slit

Figure 1. Strain relief measured adjacent to relieved area.

relaxation adjacent to the relieved area is measured either with bonded electrical resistance strain gages, mechanical displacement measuring devices, photoelastic coatings, or optical displacement grids. Using elasticity equations, the stress field existing in the material prior to the relief process is calculated from measured relieved strain, geometry of hole or slit, and elastic properties of the material.

It was noted that measurement of relieved strain with strain gages adjacent to a drilled hole is presently the most common method used to measure the existing state of stress in metals.<sup>[27]</sup> The technique is well developed and is extensively discussed in the literature.

One of the drawbacks to use of the above method in rock and concrete is the necessity of knowing the elastic properties of the material under investigation. In metals, this is not a major consideration since metals used in structural applications have elastic properties that do not vary appreciably from sample to sample or with respect of time. In rock and concrete, the elastic properties of the sample under study must be determined since environment, age, and moisture affect these properties. Elastic properties may be determined by testing the material taken from the relieved area. Another drawback of the strain relief method shown in figure 1 is that in reinforcing concrete, the reinforcing steel adjacent to the relieved area interferes with relief of concrete strain.

An interesting technique<sup>[28]</sup> used in conjunction with the slitting method of stress relief eliminates the need to know the elastic properties of the material. After the slit is cut and magnitude of relieved strain recorded, a flat pressure cell made to fit the slit is inserted. The cell, generally referred to as a "flat jack," is pressurized until the relieved (measured) strain is completely restored. The stress that existed in the material perpendicular to the slit prior to cutting the slit may be derived from the measured pressure in the flat jack. This method requires three slits to obtain magnitudes and directions of principal stresses.

Rocha and his colleagues at the Portugese National Laboratory of Civil Engineering in Lisbon are the leading proponents of the flat-jack technique and are the most expert in its application in the geotechnical field. Recently, based on the work of Rocha, Abdunur has utilized the flat-jack technique to determine absolute stresses in concrete structures.<sup>[29]</sup>

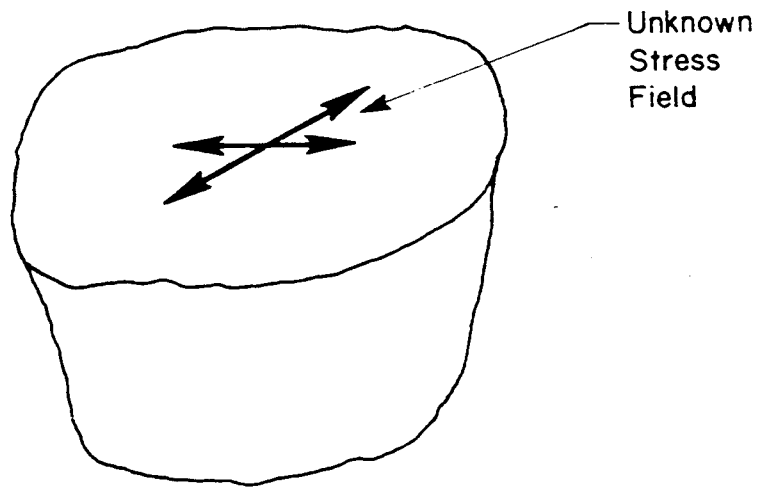
### 3.1.2.2 Strain Relief Measured Within Relieved Area

The second basic approach to measurement of relieved strain is shown in figure 2. In this method, the change in strain is measured within the relieved area instead of adjacent to the relieved area.

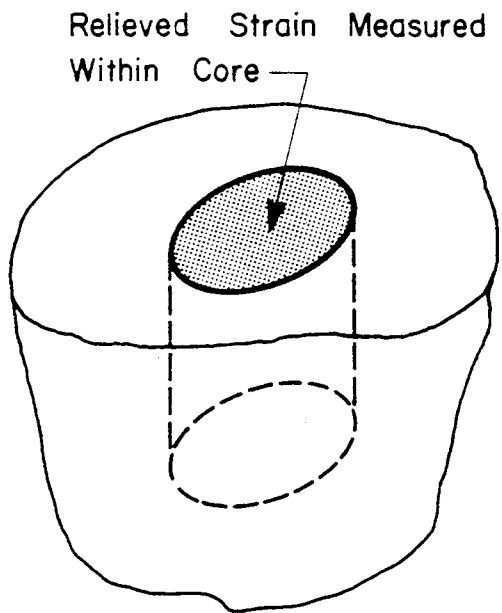
The area where the relieved strain is to be measured is first instrumented. The instrumentation may consist of electrical resistance strain gages, mechanical displacement measuring devices, or optical displacement grids. The instrumented area is relieved of strain by slitting or over-coring. Figures 3 and 4 illustrate commonly used overcoring techniques.

Figure 3 shows the "doorstopper" strain cell method pioneered by Leeman.<sup>[30,31]</sup> The doorstopper consists of a strain gage rosette prewired to a connector and molded into a waterproof cell. Cells are bonded in place and overcored either once to obtain surface conditions or successively to obtain relieved strain variation with depth. A complication in using this method to determine the variation of stress with depth is the stress concentration which is present at the bottom of the advancing cored hole as shown in figure 3d. The effect of the stress concentration must be compensated for in interpreting the relieved strain measured by the doorstopper.

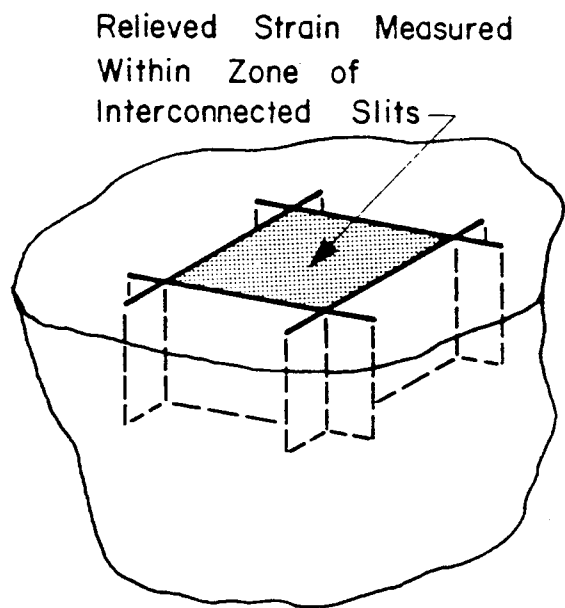
Research findings based on similar techniques have been published in Great Britain,<sup>[32]</sup> the United States,<sup>[33]</sup> and the Soviet Union.<sup>[34]</sup> However, the leading practitioners of this approach in the geotechnical community are Leeman and his associates at the National Mechanical Engineering Research Institute of the Council for Scientific and Industrial Research in Pretoria, South Africa. The method is highly developed and cells are



(a) Stress field



(b) Core



(c) Slit

Figure 2. Strain relief measured within relieved area.

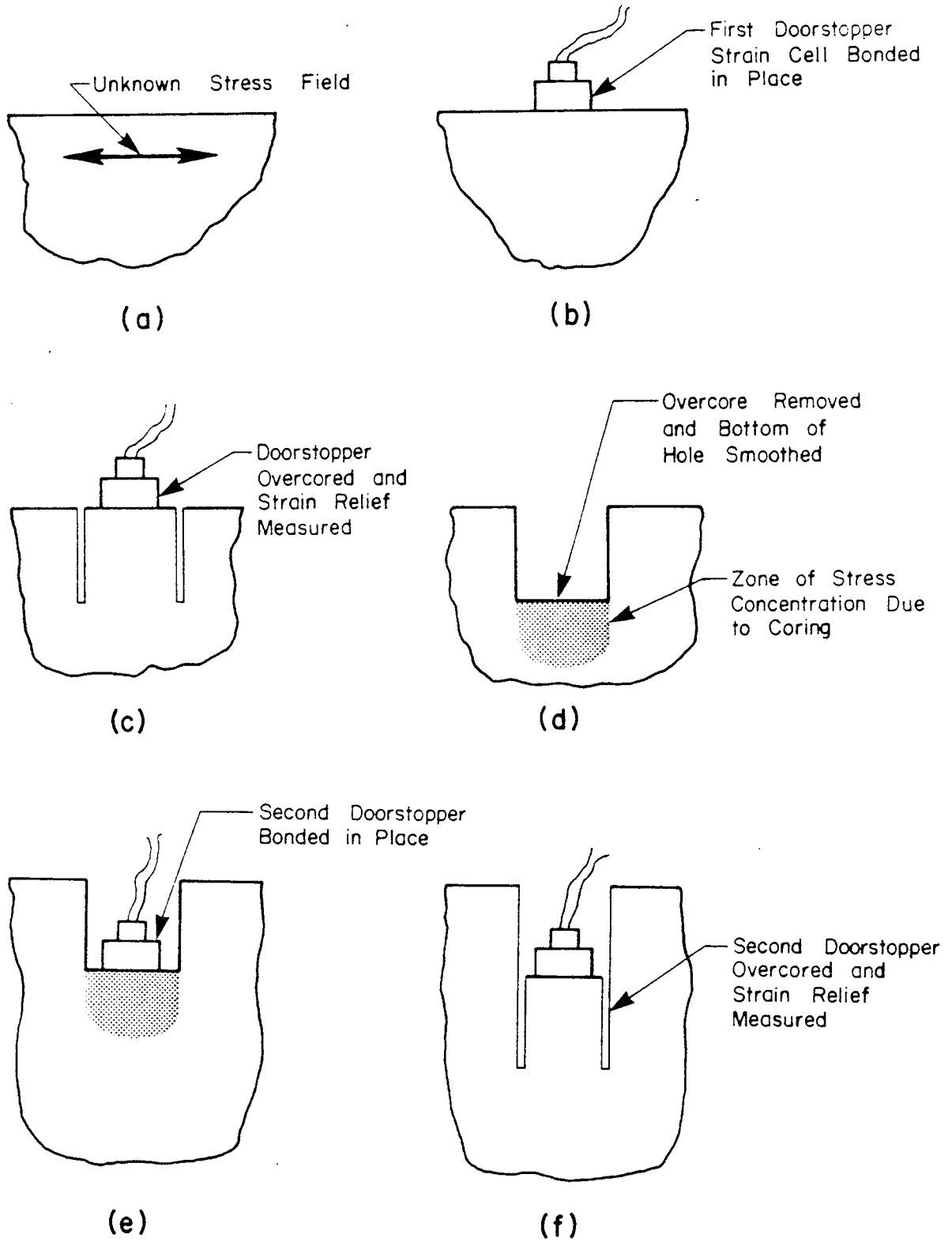


Figure 3. Doorstopper strain relief method.

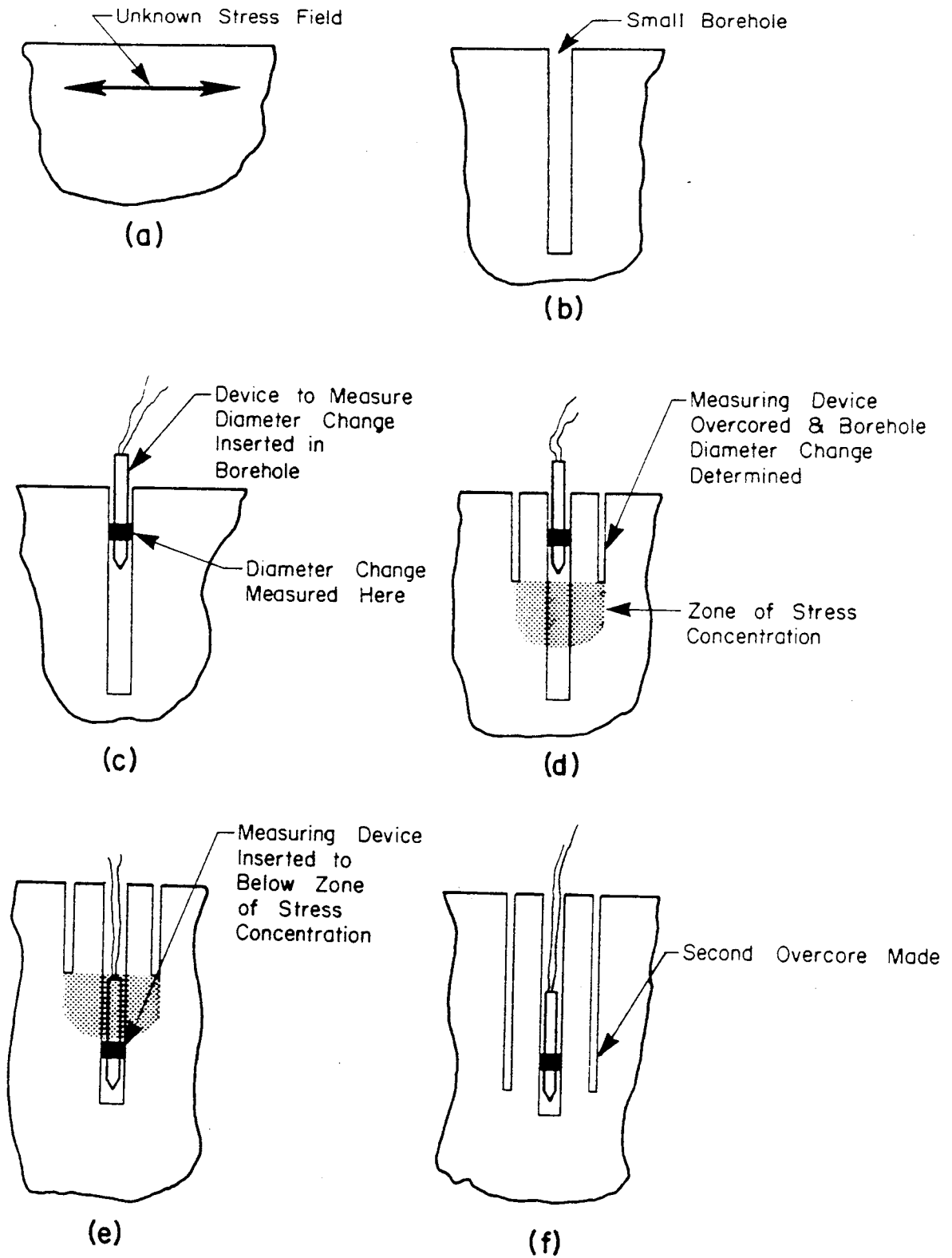


Figure 4. Strain relief method of measuring diameter change of overcored borehole.

commercially available. Leeman's standard cell is 1-3/8 in (34.9 mm) in diameter and is designed to be used in conjunction with a standard size diamond drilled borehole which is approximately 2-3/8 in (60 mm) in diameter.

The method generally used in the United States for stress measurement in rock is shown in figure 4. In this method, a small borehole is drilled well ahead of the overcoring advance. A device known as a borehole deformation gage, capable of measuring change in three diameters of the borehole, is inserted and overcored. The diameter changes have been measured with Linear Variable Differential Transformers (LVDT)<sup>[35]</sup> or with strain-gaged cantilever arms.<sup>[36,37]</sup> As shown in figure 4, the device is inserted well into the borehole so that it is out of the zone of stress concentration prior to overcoring. This method has been standardized by the United States Bureau of Mines.<sup>[36,37]</sup> The Bureau of Mines standard instrument is designed to be used in a 1-1/2-in-diameter (38.1-mm) borehole. The overcore is 6 in (152 mm) in diameter. The method was also adapted for use in determining existing stress in concrete dams by the United States Bureau of Reclamation.<sup>[38,39]</sup> The method has the advantage of using a sealed sensor which mechanically measures deformation rather than a bonded-in-place doorstopper cell which is less reliable under field conditions.

The two methods shown in figures 3 and 4 are used to measure two dimensional strain only. To obtain the complete three dimensional strain field utilizing these methods, three core holes with nonparallel axes must be used. The complete three dimensional strain field can be determined from a single overcoring operation, but additional measurements are required. Leeman<sup>[31]</sup> has utilized three strain gage rosettes, each having three strain gages, bonded to the wall of a small borehole similar to the borehole shown in figure 4. Relieved strains measured by these nine gages during overcoring are used to derive the three dimensional state of strain that originally existed in the rock mass.

A more elaborate borehole deformation gage has been developed by Bonnechere and Cornet.<sup>[40]</sup> The gage utilizes sensors to measure radial

and longitudinal displacements. The cell requires a 3-in-diameter (76.2-mm) borehole with a minimum length of 6 in (152 mm).

Numerous types of inclusions<sup>[41,42]</sup> have been designed to be bonded in boreholes prior to overcoring. The inclusions generally are instrumented with electrical resistance strain gages although an inclusion made of a solid photoelastic material<sup>[43]</sup> has also been used. The photoelastic inclusion has been used in concrete bridges. When the strain field is relieved by overcoring, the change in the shape of the drilled hole deforms the inclusion. The original strain field is determined from the measured deformation of the inclusion.

Inclusions have also been developed which incorporate flat pressure cells along their length.<sup>[44]</sup> When the strain field is relieved by overcoring, the change in pressure in the cells is used to derive the state of stress in the rock prior to the overcoring operation.

The methods of strain relief shown in figures 2, 3, and 4 require a knowledge of elastic properties of the material in order to derive stress from the measured strain. Although separate cores may be taken and tested to determine elastic properties, the common method used is to test the overcore obtained during the relief process. The overcore is placed in a pressure chamber with the instrumentation used to initially measure the relieved strain installed. Elastic properties are derived from the relationship between the applied pressure and the corresponding borehole measurements. Overcores may be tested immediately after removal from the structure in a portable chamber so that creep and shrinkage effects are minimized. This is the practice of the Bureau of Mines.<sup>[36]</sup>

A method analogous to the flat-jack method has been developed to determine stress directly by utilizing a variation of the pressure chamber technique.<sup>[31]</sup> A chamber capable of applying two pressures is used. Each pressure is applied to the overcore in ninety degree quadrants opposite each



other. The two pressures are varied until the relieved strain originally measured is completely restored. Principal stresses that existed in the material prior to coring are derived from the two pressures.

Elastic properties of rock have also been determined by expanding cylindrical pressure cells in boreholes using a dilatometer. The radial displacement is either measured directly<sup>[45]</sup> or indirectly by monitoring the volume change as the cell is pressurized.<sup>[46]</sup>

### 3.2 Evaluation of Techniques

Stress measurement based on instrumentation installed during construction can provide information on distribution of reactions, displacement response of the bridge to load and environmental conditions, and long-term behavior. Definition of stress at a selected location may also require continuing auxiliary tests to define material characteristics and long-term deformations. Uncertainty of stress results could be reduced if a specially designed pressure cell had been embedded during construction at the selected location. Size of available pressure cells relative to cross-sectional dimensions and cost may prohibit such embedment. Therefore, even the best application of early installation of instrumentation may need the help of an on-site determination if stress at a specific location is to be defined.

Strain relief or stress relief methods may provide the solution to on-site determination of existing long-term stresses. However, developmental work is required to adapt existing methods for use on bridges.

There are four basic elements of any strain relief method which must be considered in determining which method to use:

1. Techniques of strain relief
2. Location of strain relief

### 3. Stress-strain relationship

### 4. Measurement of relieved strain

These four considerations are discussed in the following sections.

#### 3.2.1 Techniques of Strain Relief

There are methods of cutting concrete without mechanical contact. These methods include burning or use of laser. However, as a practical matter, mechanical cutting continues to be the preferred technique. To be generally applicable to concrete bridges, the strain relief, and therefore the cutting, must take place from one side. To achieve sufficient surface speed to efficiently cut concrete, the mechanical cutting action must take place on the periphery of a rotating tool. There are four mechanical methods of strain relief.

The first strain relief method is by sawing. With the rotating axis parallel to the surface, a thin circular blade is used and the cut is a slit as shown in figures 1 and 2. The edge of the blade is generally surfaced with a hard abrasive, such as diamond.

The second strain relief method is by drilling. The rotating axis of the cutting tool is perpendicular to the surface. The cutting action produces round holes. For comparatively small diameters, the entire cross-section of the hole is abraded by the end of the tool.

The third strain relief method is by using percussion drills. The hole is partially or completely advanced by impacting the concrete with the end of the tool, thus locally fracturing the concrete immediately ahead of the tool. Percussion drilling is not suitable for strain relief work as it not only fractures the concrete immediately ahead of the tool, but to the sides as well. This interferes with the measuring process that is the key element in any strain relief method.

The fourth strain relief method is by coring. For larger holes, a tubular cutting tool (core barrel) is used. The leading edge of the rotating tube cuts a circular slit which is advanced into the concrete. The material in the center goes into the tube as cutting takes place and is periodically broken off and removed. The cutting edges of core barrels are generally surfaced with hard abrasive material.

Since concrete sawing, drilling, and coring are abrasion cutting methods, heat is generated during the process. Typically, some form of cooling is employed. Water is commonly used. Oil has been used. Cooling has also been accomplished with jets of compressed air. Abdunur's experience<sup>[47]</sup> indicates that water cooling is undesirable. The water causes dimensional changes in the concrete which disturb the strain measurement process. Abdunur has successfully used air cooling, but has had to supercool the air with a bath of liquid nitrogen prior to directing it on the cutting tool.

In summary, for all strain relief methods considered, the strain is relieved by concrete sawing, drilling or coring, without using water cooling.

### 3.2.2 Location of Strain Relief

Strain may be measured adjacent to the relieved area, figure 1, or within the relieved area, figure 2. Also, strain may be measured either on or below the surface, although measuring below the surface and adjacent to the relieved area would be difficult to accomplish. Measurement within the relieved area requires an area large enough to permit accurate measurement. This means that inherently a larger area is affected by the relief process when measurement is made within the relieved area than when measurement is made adjacent to the relieved area.

Sawing affects a long but thin area compared to drilling or coring which requires a large volume of concrete to be removed. A saw cut 3 in (76.2 mm) deep at the center, made with a 12-in-diameter (305-mm) blade, leaves a slot 10-3/8 in (264 mm) long on the surface, whereas it is feasible to relieve

strain with a drilled hole about 2 in (50 mm) in diameter. Three separate sawing operations are required to obtain principal strains. Only one coring operation is required to determine principal strains.

A disadvantage of measurement adjacent to the relieved area is that reinforcing steel positioned around the area will interfere to some extent with relief of the concrete strain. As discussed in the next section on stress-strain relationships, material testing done in conjunction with this method should be done in place, so that the material relationships obtained will include the effect of reinforcement.

Another disadvantage of measurement adjacent to the relieved area is that surface strains are measured. Relieved surface strains contain the effects of shrinkage as well as strains due to load. The need to separate shrinkage and load strains is a drawback to any method that uses surface strain measurements. Using a method that utilizes strain measured below the surface has the advantage of minimal interference from shrinkage strain. However, it has the disadvantage of interference from stress concentrations that are induced by the penetration made in the concrete to permit the below surface strain to be measured. This difficulty is discussed in greater detail in section 3.2.4.4.

A desirable attribute of a relief method is the capacity to determine strain or stress gradients due to bending and axial loads. If the method is sufficiently accurate, this can be accomplished in conjunction with measuring strain adjacent to the relieved area by relieving the strain in discrete steps, incrementally cutting deeper at each step while measuring the relieved strain. Strain variation with depth can theoretically be determined in conjunction with measuring strain within the relieved area in the same way.

Measuring displacements in a borehole within the relieved area has the advantage that relieved strain can be measured at several discrete points below the surface at the same time, as the strain relief progresses. Obtaining measurements at a number of points below the surface simultaneously

during the strain relief process results in a much superior strain profile than can be obtained by taking measurements only on the surface or at one depth.

### 3.2.3 Stress-Strain Relationship

In homogeneous materials, stress distributions are derived from measured strain by use of stress-strain relationships. Depending on the degree of homogeneity, these relationships are either based on published data, tests of separately cast specimens, or determined from tests of material samples taken from the actual structure being studied. For example, in metals, stress-strain relationships are commonly taken from published data of tests of like composition material. Metals are highly homogeneous and even at small scale have only minor variations in constitutive relationships for a wide range of samples of material with similar composition and hardening treatment.

On the other hand, rock and concrete are less homogeneous and generally are tested for stress-strain relationship on a case-by-case basis. Testing is needed particularly in old concrete, like the concrete in existing bridges, since age effects add even more variability to constitutive relationships.

The flat-jack technique has the advantage of determining original stress in the concrete directly. This is the method used by Abdunur.<sup>[29]</sup> The flat-jack method overcomes the basic problem of reinforcement interference with the relief process. However, since relieved strain is measured on the surface, stresses due to shrinkage as well as load release are measured. As discussed previously, the ability to separate shrinkage and load stresses is a drawback to this method.

If the strain is relieved by drilling or coring, then a cylindrical pressure cell dilatometer<sup>[45,46]</sup> inserted in the hole should be used to determine the response of the measurement system to known internal pressures. Again, this method suffers from the fact that surface strain is measured.

Figure 2 shows strain measured within a cored area or an area of interconnected slits. Since the stress-strain curve of the material would be required, the interconnected slit approach is less attractive than the coring approach. The process of coring and testing cores is more straightforward than slitting and testing a straight-sided specimen.

If the strain is to be measured within a cored area, then the core itself can be removed and tested in a portable cell with a single pressure<sup>[36]</sup> or in an assimilator<sup>[31]</sup> with two pressures. The assimilator has the advantage of the flat-jack method in that original strain pattern restoration takes place and original material stresses are derived directly from pressure measurements. This method has the additional advantages over the flat-jack method of being compatible with measurement techniques that measure strain below the surface away from high shrinkage strains, and of being able to determine principal stresses with one relief operation.

#### 3.2.4 Measurement of Relieved Strain

Historically, relieved strain has been measured by a great number of methods based on a variety of principles. The most common methods are:

1. Optical - relieved strain is indicated by a change in the optical characteristics of a material bonded to the material under study.
2. Electrical - average relieved strain is indicated by a change in the electrical characteristics of a material bonded to the material under study.
3. Mechanical - average relieved strain is computed from the measurement of a length change divided by the original length.

These three methods are described below followed by a subsection which discusses strain measurement below the surface.

#### 3.2.4.1 Optical Methods

There are two optical methods of strain measurement. The Moirè technique detects changes in geometry of a pattern. The photoelastic technique detects changes in optical properties. Roberts points out in reference 43 that one of the principal advantages of the photoelastic technique of strain measurement is that it measures strain on a point-by-point basis. While this is an advantage for many materials, it is a disadvantage for strain relief measurement in concrete for the following reason.

Prior to strain relief, the photoelastic coating would be bonded to the surface of the structure. It would therefore be uniformly bonded to aggregates as well as cement paste. After strain relief, the coating would respond to the different strain changes occurring in the different constituents of the concrete. Even aggregates below the surface could affect readings. The resultant fringe pattern would be highly distorted locally and therefore would be uninterpretable. This same difficulty would be present in application of the Moirè technique.

Application of optical methods to concrete under field conditions would present many practical problems. While optical methods have been used in the field, as discussed by Roberts,<sup>[43]</sup> they require various pieces of auxiliary apparatus, such as light sources, viewers, cameras, etc. that require special training to use and that are more suited for use in a laboratory environment.

For the above reasons, optical methods were not considered for the experimental phase of this project.

#### 3.2.4.2 Electrical Methods

The bonded electrical resistance strain gage is currently the most widely used instrument for strain measurement. One of the principal advantages of strain measurement with strain gages is that it lends itself to automatic recording of data. This is a major advantage when many stages of measurement are to be made. A strain gage measures average strain over the length of its

sensing element, referred to as its gage length. Strain gages are available in gage lengths of less than 1/8 in (3.2 mm). Small gage length is one of the features that make strain gages attractive for general use since the measurement of strain at a point can be approached. However, in concrete, strain measurement at a point is not desired. In fact, it is generally recommended that gage lengths of three to four times the maximum aggregate size be used to compensate for the non-homogeneous nature of concrete.<sup>[48]</sup>

Gages of three to four times maximum aggregate size, or effectively a minimum length of 3 to 4 in (76 to 102 mm), would be too long to satisfactorily respond to the local strain gradients that exist adjacent to an area of strain relief. Gages of this length would be acceptable, however, for measurement of strain within a relieved area, but would generally require a larger relieved area than mechanical techniques.

It would be possible to install a strain gage with a small gage length on the polished surface of an aggregate particle. During the relief process, the gage would respond to the change in strain of a near homogeneous material. Since the particle modulus of elasticity and loading would be unknown, it would be necessary to rely on post-relief tests to determine the response of the particle to known forces. While it is feasible to use post-relief testing to determine the overall response of a relieved area, it is not feasible to expect a post-relief test to strain an individual aggregate particle in the same manner it was strained prior to strain relief. Therefore, small gage length strain gages would not have application for strain relief measurement of concrete.

The strain gage rosette used in Leeman's<sup>[31]</sup> standard doorstopper cell is 1 in (25.4 mm) in diameter. This diameter is too small for direct application to concrete strain measurement.

While many advances have been made in the techniques of strain gage installation, it is still an exacting procedure not easily accomplished in the field. The gage length required to measure concrete strain with a strain gage would be approximately the same as that required by mechanical strain



measurement, as discussed in the next section. Since this is the case, there would be no advantage from a measurement standpoint to the use of strain gages over mechanical gages which are considerably easier to use in the field.

#### 3.2.4.3 Mechanical Methods

Strain was first measured mechanically. Before optical and electrical methods, it was the only method available and many variations of instruments were developed. A major disadvantage of mechanical methods for general strain measurement work has been the comparatively long gage length required. A gage length on the order of inches is required so that the change in length is large enough to be within the resolution of the instruments available. In concrete, gage lengths of several inches are required to average out nonhomogeneity. Therefore, large gage length needed by each gage is not a disadvantage.

Mechanical gages are well suited to field measurement as they can be more easily designed to be resistant to adverse field environments, such as, moisture and dust, than electric or optical gages. This is true even if the mechanical gage includes optical or electrical components. These can be made environment-proof during construction of the gage.

#### 3.2.4.4 Measurement of Strain Below the Surface

In an existing bridge, the only possible way to measure relieved strain below the surface is to first penetrate the surface to a given depth, place a measurement device below the surface, and then relieve the strain around the penetration. Two methods of measurement below the surface are shown in figures 3 and 4. The most common way to get below the surface is to first drill a small diameter hole as shown in figure 4. However, it is noted that even a small hole partially relieves the strain field in the area adjacent to it. The equations of elasticity are used to account for the fact that the strain field has been partially relieved. However, if reinforcement exists

in the area, it may interfere with the relief resulting from even a small diameter hole, thus giving an erroneous indication of total strain relief during overcoring.

As discussed previously, the area surrounding the bottom of a hole in a stress field is subject to stress concentration as shown in figures 3 and 4. If an instrument is placed in this zone prior to overcoring, it will respond to the relief of the stress concentration and not the original stress distribution in the material. Theoretically, the effect of the stress concentration can be compensated for analytically. Practically, the added complication due to stress concentration is a definite drawback to the use of Doorstopper strain cells (figure 3). The measurement of relieved strain in boreholes (figure 4) does not suffer from this difficulty.

Once the hole has been drilled, there are many methods of measuring the relieved strain. The method shown in figure 4 measures the change in diameter of the drilled hole when the strain around the hole is relieved by overcoring. As pointed out previously, this method has been extensively developed by the Bureau of Mines<sup>[36,37]</sup> and is the current standard method in the United States for strain relief measurement in rock. Also as discussed previously, the method has been used for strain relief measurement in concrete dams.<sup>[38,39]</sup> The instrument measures the change in three diameters at a given level during overcoring. It is possible therefore to derive principal strains from the measurements.

Another method for measuring relieved strain within the drilled hole is to bond strain gages directly to the wall of the hole prior to overcoring.<sup>[31]</sup> Strain gages in general would not be well suited for strain relief measurement in concrete particularly when compared to other methods available.

Although there are numerous examples in the geotechnical literature of the use of inclusions bonded in place in boreholes which are subsequently overcored, there appears to be no clear advantage to them over direct

measurement of the change in diameter of the borehole. They could not easily be reused and any procedure requiring bonding to concrete in the field would be undesirable.

Based on the above discussion, mechanical strain measurement should be used if relieved strain is to be measured on the surface. Since the measurement must take place across the area where the relief cut is actually taking place, there would be no advantage to having a system that automatically records strain since it would have to be moved each time the relief cut is made deeper. A hand-type mechanical method would therefore be satisfactory.

### 3.3 Potential Stress Measurement Techniques

Existing techniques for stress measurement in rock and in steel have been summarized in previous sections. The following are candidate stress measurement techniques that could be adapted to concrete.

#### 3.3.1 Flat-Jack Method

Abdunur's work in France<sup>[29]</sup> with the flat-jack technique as applied to reinforced concrete focused attention on the flat-jack method. Abdunur not only constructed and tested flat jacks, but also developed the peripheral slitting and measurement procedures required to make the method suitable for use in reinforced and prestressed concrete structures. Although reference to strain relief work in concrete is made in the geotechnical literature, it appears that no other strain relief method is developed for use in concrete to the extent and with the apparent success of Abdunur's flat-jack method.

Abdunur's flat-jack method utilized stress-relief procedures and techniques that were entirely consistent with those summarized in the previous sections. Abdunur claimed that he could measure compressive as well as tensile stresses to an accuracy of 0.3 MPa (43.5 psi).<sup>[29]</sup>

### 3.3.2 Borehole Deformation Method

The borehole deformation method could have application in concrete. It has already been used for this purpose<sup>[38,39]</sup> in massive non-reinforced concrete structures. The main disadvantage of this approach is that the existing devices used in rock are too large for direct use in concrete bridges. Smaller boreholes and overcores, on the order of 1 and 4 in (25.4 and 102 mm) maximum diameters, respectively, would be required. While mechanical design could be patterned after what was being used in rock, miniaturized prototype hardware would require design and extensive development.

### 3.3.3 Dilatometer Method

The use of a dilatometer in conjunction with drilling to obtain strain relief and the measurement of strain adjacent to the relieved area has good potential. This method has the potential of requiring the smallest area of damage and most complete stress picture of any method. However, this technique also would require design and extensive development for miniaturization.

### 3.3.4 General Considerations

In evaluating various direct stress measurement systems, three factors are important: costs, time to take measurements, and accuracy. Additional factors include ease of measurement, level of preliminary work, level of expertise required, acceptance of the concept by bridge engineers, and extent of damage incurred when using the technique.

More peripheral considerations include (1) costs for review of drawings and initial calculations, (2) direct equipment use, (3) time-on-site, (4) further development, refinement, and calibration of equipment, (5) repair of damage, (6) transporting equipment, (7) auxiliary testing of materials, (8) development of custom analysis of each structure, and (9) analysis of data.

Existing stress-relief methods require cutting a slot or coring a hole in a bridge member, therefore, unrepairable damage to the structure is an inherent part of measuring systems. The extent of damage must be limited because the usefulness of a measuring scheme is dependent on the significance of damage. A useful method must not destroy a structure's function.

As a result of temperature and humidity variations, stresses in a continuous structure vary with time, therefore, it is important to limit the time required to take stress measurements. Considering this factor, faster methods would be more accurate because the stress variations with time are minimized.

The most important factor in considering various stress measurement techniques is their accuracy. To justify costs and damage to a structure, and to gain the acceptance of bridge engineers, a stress measurement method must be accurate and reliable.

Acceptance of a concept is dependent on confidence in results and understanding of the method. A well conceived approach based on clear engineering principles should be readily accepted by bridge engineers if results are within the accuracy needed.

In order to determine the accuracy of the above three potential stress measurement techniques, mathematical analyses were performed. Results of these analyses are reported in the next section.

## 4.0 TASK B - ANALYTICAL STUDIES

Results of analyses are reported in this section. The analyses were intended to establish accuracy of slitting and boring techniques in determining stresses. The time-dependent effects of creep and shrinkage on measurement technique are reviewed. The importance of considering these effects is emphasized.

### 4.1 Analytical Investigations of Measurement Techniques

In the following investigation, the boring and slitting techniques of stress measurement are compared. From the analysis, it is determined that the slitting technique, that is, the flat-jack method, can yield more accurate stress measurements than the boring technique. The accuracy with which compensating flat-jack pressures can be measured is then determined for various slot depths and gage lengths across the slot. The accuracy of the flat-jack model in reconstructing uniform, bending, and shrinkage stress distributions is also evaluated. As a result of the findings of analytical studies, recommendations for further analytical investigations are presented.

#### 4.1.1 Evaluation of Boring and Slitting Techniques

Following a review of potential stress measurement methods, three techniques were selected for further investigation. Two techniques (borehole and dilatometer) involved boring a hole into the structure, while the third (flat jack) involved slitting the structure. As was discussed in previous sections, there are many factors to consider in determining which method of stress measurement should be used. Sensitivity and accuracy of the method are of prime importance. The purpose of this section is to discuss one such factor, that is, magnitude of displacement relative to size and shape of cut.

In general, the larger the displacement that can be obtained by cutting into a stressed medium, the more accurate the stress measurement. However, a stress measurement technique that requires a smaller hole will have a wider range of applications and will minimize damage to the structure. In this

section, investigation of displacements caused by boring and slitting in a stressed medium, is based on analyses of an infinitely long plate under uniform axial load.

As shown in figure 5a, to analyze displacements due to cutting a circular hole of diameter  $2a$  in a stressed plate, two points a distance  $2(a + e)$  apart are selected on the plate. The displacement,  $d_c$ , between the two points is

$$d_c = \frac{Ta^2}{E(a + e)^3} [4a^2 + (5 + \nu)(2ae + e^2)] \quad (1)$$

where  $T$  = uniform axial stress that existed in the plate before the hole was cut

$a$  = radius of hole

$e$  = distance from edge of hole to the point where displacement is measured

$E$  = modulus of elasticity

$\nu$  = Poisson's ratio

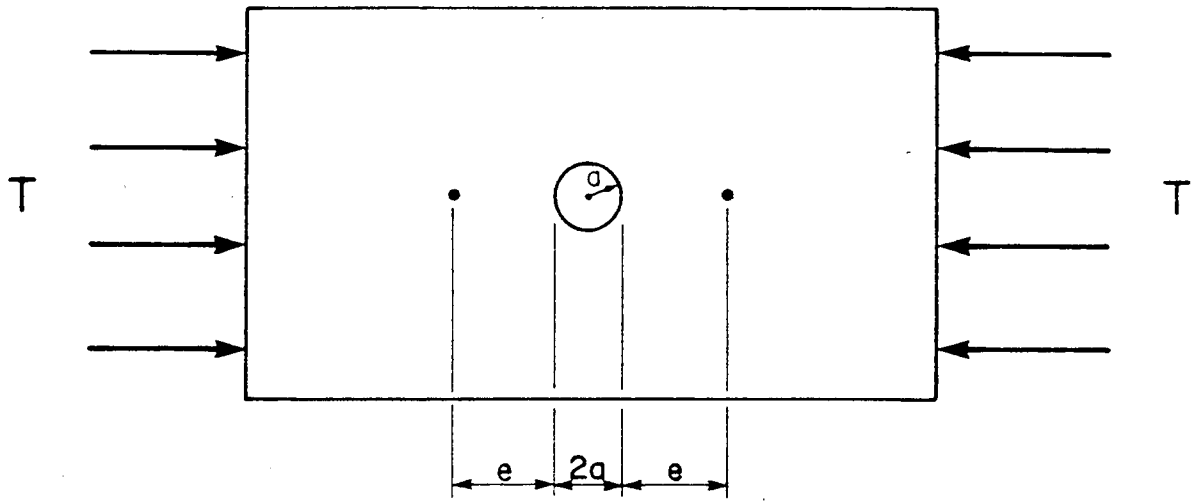
Derivation of equation 1 is presented in section 10.0

A similar equation is derived for displacement caused by slitting a stressed plate. This time, two points a distance  $2e$  apart are selected on the plate. When a slot of length  $2a$  is cut into the stressed plate as shown in figure 5b, the displacement,  $d_s$ , between the two points is

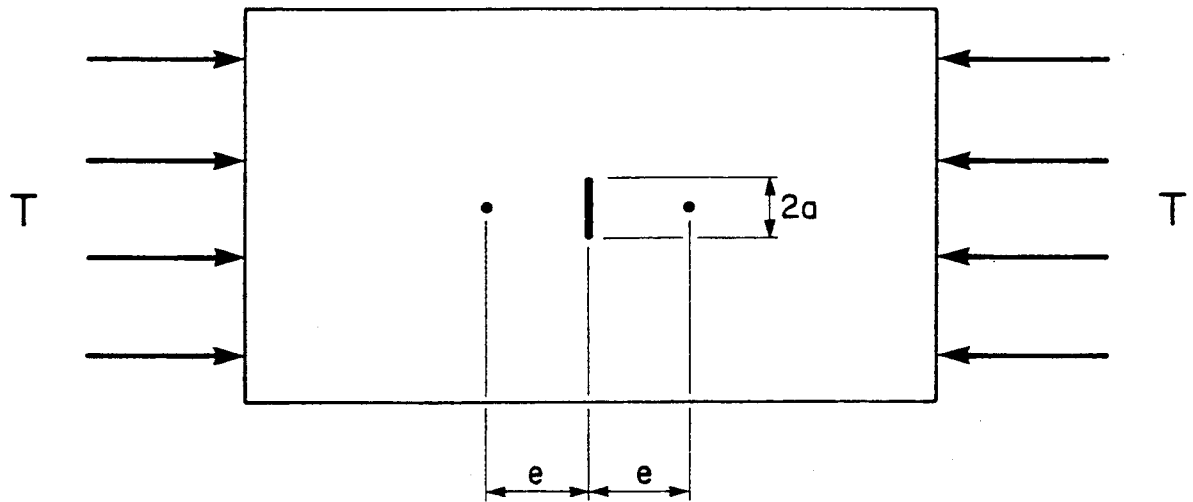
$$d_s = \frac{2T}{E} \left[ \frac{2a^2 + e^2 (1 - \nu)}{\sqrt{a^2 + e^2}} - e(1 - \nu) \right] \quad (2)$$

Derivation of equation 2 is also given in section 10.0. For analysis purposes, width of the slot is assumed negligible. The distance from the edge of the slot to the point where the displacement is measured is termed "e."

To determine how displacements are related to the shape of the cut, equations 1 and 2 were analyzed for various distances,  $e$ . If the displacement is measured at the edge of the cut ( $e = 0$ ), equations 1 and 2 reduce to



(a) Measurement points for plate with circular hole



(b) Measurement points for plate with slot

Figure 5. Measurement points on plate.



$$d_c = d_s = \frac{4Ta}{E} \quad (3)$$

In the above equation, displacements due to cutting a circular hole of Diameter  $2a$  and a slot of Length  $2a$  are identical. In other words, when displacements are measured at the edge of the cut, the magnitude of the displacement is determined by the size of the cut in a direction perpendicular to the displacement, that is, length of cut. The displacements  $d_c$  and  $d_s$  do not depend on the size of the cut in a direction parallel to the displacement, that is, width of cut.

To investigate displacements at points away from the cut equations 1 and 2 are simplified as follows:

$$d_c = \frac{CTa}{E} \quad (4)$$

and

$$d_s = \frac{STa}{E} \quad (5)$$

where 
$$C = \frac{n[4n^2 + (5 + \nu)(2n + 1)]}{(n + 1)^3}$$

$$S = 2 \left[ \frac{2n^2 + (1 - \nu)}{\sqrt{n^4 + n^2}} - \frac{(1 - \nu)}{n} \right]$$

$$n = \frac{a}{e}$$

In the above equations,  $C$  and  $S$  are constants determined by Poisson's ratio and the ratio of  $e/a$ . For concrete, Poisson's ratio,  $\nu$ , varies between 0.11 and 0.21.<sup>[49]</sup> For this analysis, Poisson's ratio was taken as 0.17. Values of  $C$  and  $S$  for  $\nu = 0.17$  and various ratios of  $e/a$  are listed in table 1. Table 1, along with equations 4 and 5, indicate that when  $0 < e/a < 1/2$  displacements are about 1% larger for the slot, while for  $e/a > 1/2$  displacements are larger for the hole. The further the measurements are taken from the edge of the cut the more significant the difference between the two cuts becomes. At  $e/a = 10$ , for example, displacement caused by cutting the slot is only 67% of the displacement caused by boring a hole.

Table 1. Coefficients C and S for equations 4 and 5.\*

e/a	C	S	Percent Difference in Displacements $d_c$ and $d_s$
0	4.00	4.00	0
1/8	3.77	3.79	1
1/4	3.54	3.57	1
1/2	3.11	3.12	1
3/4	2.74	2.71	1
1	2.44	2.34	4
2	1.68	1.44	14
4	1.02	0.77	25
10	0.47	0.32	33

\*Above values were calculated using  $\nu = 0.17$

Table 2. Displacements due to cutting into a stressed plate.\*

Distance from Edge of Cut (in)	Displacements (millionths in)		Difference in Displacement due to Hole and Slot (millionths in)
	Due to Circular Hole	Due to Slot	
0.00	200.0	200.0	0.0
0.25	188.7	189.4	-0.6
0.50	176.8	178.3	-1.5
1.00	155.5	155.9	-0.4
2.00	121.9	117.1	4.8
4.00	84.0	71.9	12.1
8.00	51.2	38.6	12.6
20.00	23.5	15.8	7.7

\*Displacements are computed from equations 4 and 5 with  
 $T = 100$  psi,  $\nu = 0.17$ ,  $E = 4 \times 10^6$  psi,  $a = 2$  in

Metric Equivalents:

1 in = 25.4 mm

1 psi = 6.895 kPa

Displacements taken far from the cut, however, are significantly smaller than displacements near the cut. For example, displacements that would occur with  $E = 4 \times 10^6$  psi (27,580 MPa),  $\nu = 0.17$ ,  $T = 100$  psi (0.69 MPa), and  $a = 2$  in (51 mm) are listed in table 2. At the edge of the hole or slot, the displacement is 200 millionths of an inch (0.005 mm). However, at  $e = 20$  in (508 mm), the displacement due to cutting the circular hole is 23.5 millionths (0.0006 mm). At the same point, the displacement due to slitting is 15.8 millionths of an inch (0.0004 mm). Since larger displacements lead to more accurate stress measurements, it is advantageous to take measurements as close as possible to the edge of the cut.

For the displacements listed in table 2, the difference in displacement due to boring and slitting is not significant if gage accuracy is considered. The smallest unit displacement that can be measured with the Pfender (mechanical) gage is 39.4 millionths of an inch (0.001 mm). In table 2, the maximum difference in displacements between boring and slitting is 12.6 millionths of an inch (0.00032 mm). This is less than half the minimum unit displacement that can be measured with a Pfender gage.

If a stress of  $T = 1000$  psi (6.9 MPa) is considered, then all displacements in table 2 must be multiplied by 10. Since the maximum Pfender gage length is about 4 in (100 mm), that is 2 in (51 mm) on each side of the slot, only displacements for  $e \leq 2.0$  in (51 mm) will be considered. For these cases, the maximum difference between  $d_c$  and  $d_s$  is 4.8 millionths of an inch (0.000122 mm). This would be a difference of only about one-tenth of a unit on a Pfender gage.

The above examples indicate that for a large plate under a uniform axial load the measurable difference in deflection caused by boring a hole of Diameter  $2a$  or cutting a slot of length  $2a$  is negligible. Clearly, however, the amount of material that would be cut from the plate in boring a hole of Diameter  $2a$  is greater than the amount of material that would be removed in cutting a slot of length  $2a$ .

Moreover, if coring is used, the practical range for the diameter of the core is 2 to 3 in (51 to 76 mm). With slitting, the length of the slot can

be as large as 12 in (305 mm) with a depth of only 3 in (76 mm). Since displacements increase with increasing cut length, larger displacements can be obtained with the slitting technique than with the boring technique. If  $T = 100$  psi (0.69 MPa), equation 4 indicates that at  $e = 0.25$  in (6.35 mm), the displacement due to boring a hole with a radius of 3 in (76 mm) would only be 289 millionths of an inch (0.0073 mm). For a 12-in (305-mm) slot, however, the displacement at the same point would be 590 millionths of an inch (0.015 mm) as indicated in equation 5.

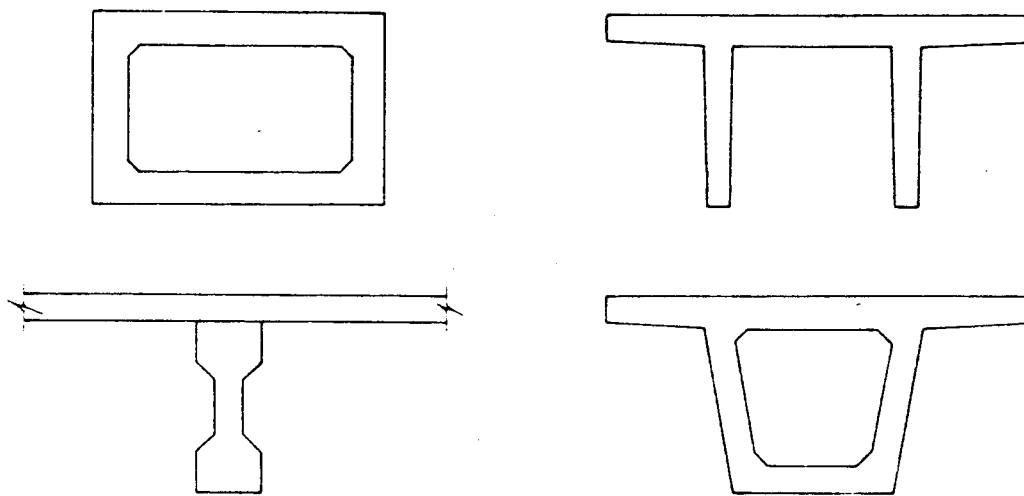
The slitting technique leads to larger displacements with less damage to the structure than the boring technique. Since larger displacements yield more accurate stress measurements, the slitting technique is preferable to the boring technique. Therefore, in the remainder of this section only the slitting technique, that is, the flat-jack method of stress measurement will be investigated.

#### 4.1.2 Model to Analyze the Flat-Jack Method of Strain Relief

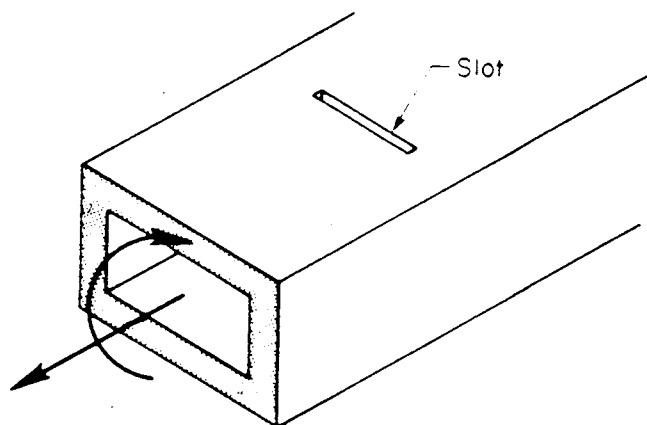
The above analysis dealt with a slot in an infinite section under uniform axial stress. However, to evaluate the flat-jack technique more precisely, a slot at the edge of a finite section was considered. Also, in addition to the uniform stress distribution, both bending and shrinkage stress distributions were investigated. Since simple closed form solutions do not exist for these additional cases, finite element analyses were used for further evaluations of the flat-jack technique.

##### 4.1.2.1 Two-Dimensional Model

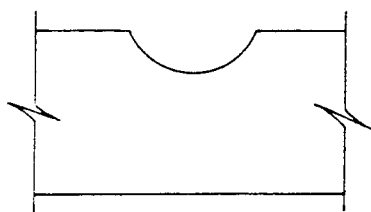
Cross sections of different bridge girders are shown in figure 6a. When the flat-jack method of stress measurement is used to determine existing stresses in portions of these girders, a slot is cut in the member perpendicular to the direction of the unknown stresses. A slotted box girder is shown in figure 6b. As a result of the slitting, a displacement occurs across the slot. A flat jack is then inserted in the slot and a uniform



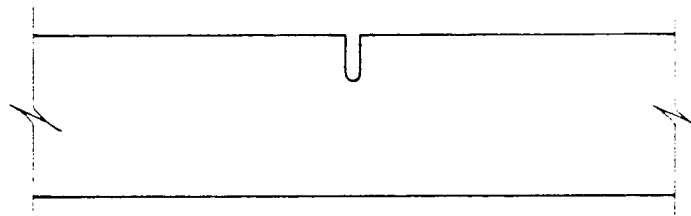
(a) Sample bridge girder cross sections



(b) Box girder with slot



(c) Cross section of wall with slot



(d) Longitudinal section of wall with slot

Figure 6. Slotted bridge girder.

restoring pressure is applied to the walls of the slot. The purpose of this analysis is to determine how accurately the restoring pressure represents the existing stress in the structure.

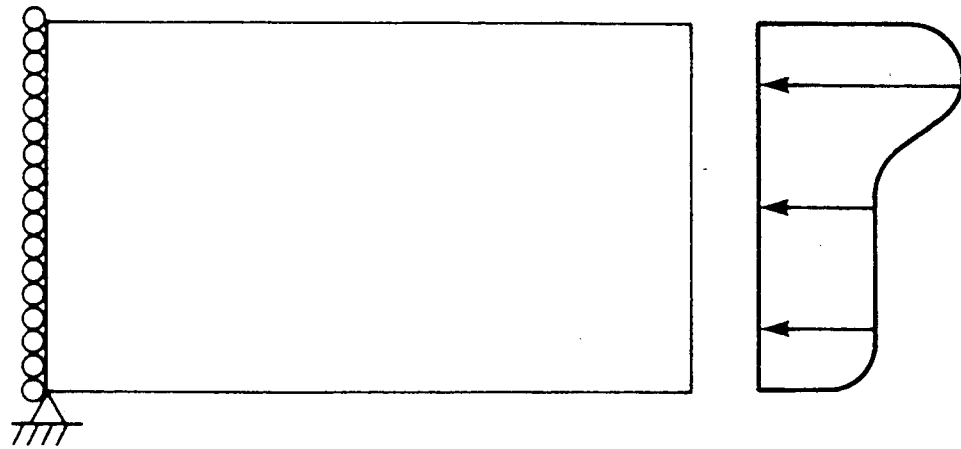
A cross section of the slot is shown in figure 6c. In order to model the slotted girder accurately, a three-dimensional model has to be used. However, analysis of such a complex model is beyond the scope of this investigation. Approximate displacements associated with the method of strain relief by slitting can be obtained by analyzing a two-dimensional plane strain model of the section.

#### 4.1.2.2 Boundary Conditions

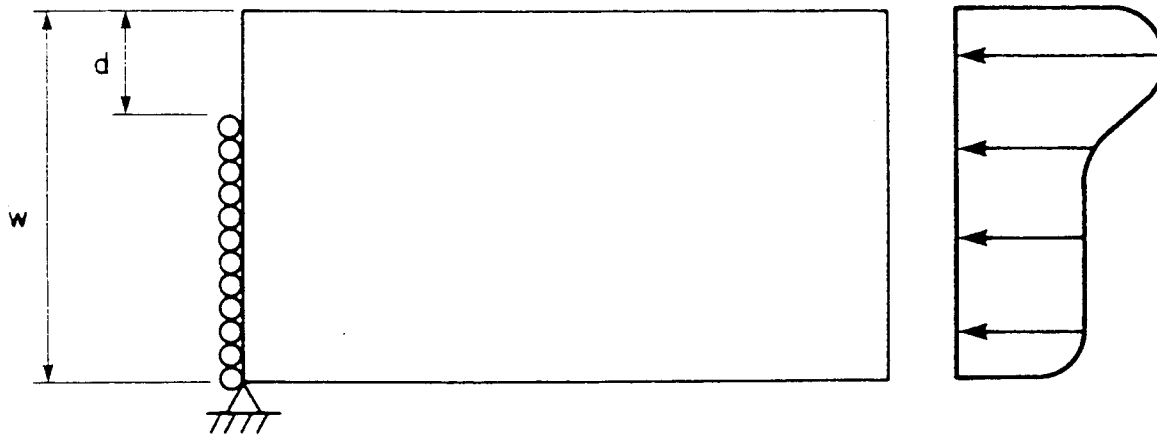
A two-dimensional model obtained by cutting a longitudinal strip from the wall of a bridge girder is shown in figure 6d. Results of analyses discussed in the previous section indicate that displacements due to cutting a small hole in a stressed plate are not significantly affected by the size of the hole in the direction of displacement measurement. The width of the slot can therefore be neglected and the simplified model shown in figure 7 used. In this model, the slot is modelled as a straight, free edge. Slot depth is determined by the number of rollers removed from the left edge. A section with no slot is modelled by restraining all horizontal displacements along the left edge. To model the slot, horizontal restraints are limited to the area below the slot. A model without a slot is shown in figure 7a, and a model with a slot is shown in figure 7b. The rollers along the edge allow the material to expand and contract vertically when a horizontal load is applied. This prevents the development of additional stresses due to Poisson's effect. A vertical support is provided at the bottom left corner of the model to prevent rigid body motion.

#### 4.1.2.3 Dimensions of the Model

Displacements that would occur when the section in figure 7 is subjected to various stress distributions were determined by a finite element analysis.



(a) Model without slot



(b) Model with slot

Figure 7. Two-dimensional model.

Since costs of computer runs depend directly on the number of elements in the finite element model, it was advantageous to minimize the model's dimensions.

The walls of prestressed concrete bridge girders are usually 6 to 12 in (152 to 305 mm) thick. For sections without slots, displacements due to axial, bending, or shrinkage stresses can be found by analyzing a half-depth model of the section. To determine whether such an approach would be valid for sections with slots, consideration of stresses near the slot is necessary.

When a section is slotted, large stresses known as stress concentrations may develop near the slot. Stress concentration factors are used to describe the magnitude of the maximum stress in the slotted section. For a section under uniform axial stress, the stress concentration factor is the ratio of the maximum stress in the slotted section to the constant stress in the unslotted section.

While the stress concentration factor depends, in part, on the shape of the slot, it is mainly determined by the ratio of the slot depth,  $d$ , to the section depth,  $w$  (ratio  $d/w$ ). For a section of infinite depth, the stress concentration factor does not change with changing slot depths. For finite-depth sections, it has been found that for low values of ratio  $d/w$ , the stress concentration factors remain constant. However, when ratio  $d/w$  exceeds a certain value, the stress concentration factor increases significantly with increasing values of  $d/w$ .

Presently, stress concentration factors are not available for the model shown in figure 7b. However, they are available for the case of the tension strip with symmetric opposite edge cracks shown in figure 8. The stress concentration factor for opposite edge cracks<sup>[50]</sup> remains approximately constant if

$$\frac{2d}{w} \leq 0.25 \quad (6)$$

where  $d$  = depth of each crack  
 $w$  = width of section



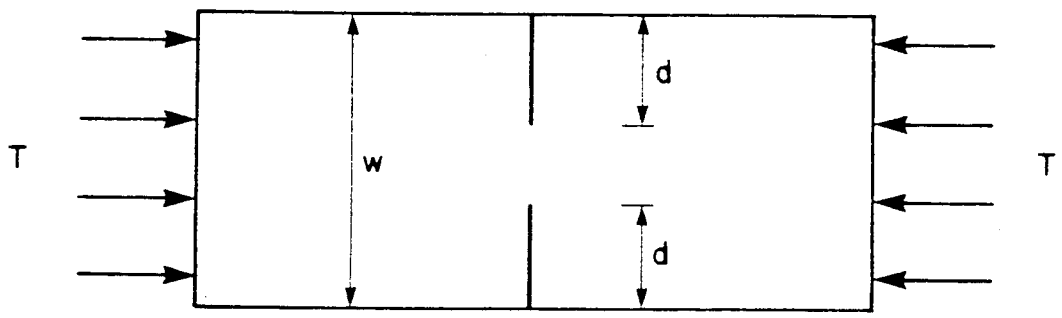


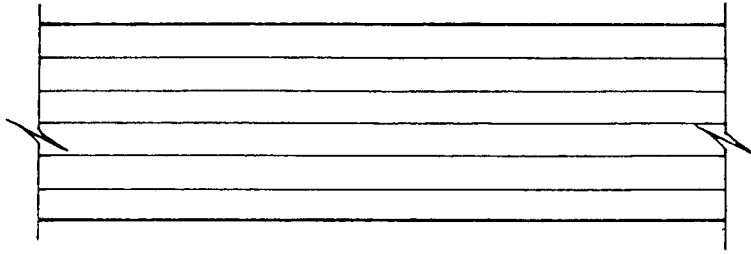
Figure 8. Symmetric opposite edge cracks.

The above relation gives conservative values for the case of a single slot in a tension strip. For a slot depth of 3 in (76 mm), the stress concentration factors will be constant for sections deeper than 24 in (610 mm). For a slot depth of 0.8 in (20.3 mm), the stress concentration factor will be constant for sections deeper than 6.4 in (163 mm).

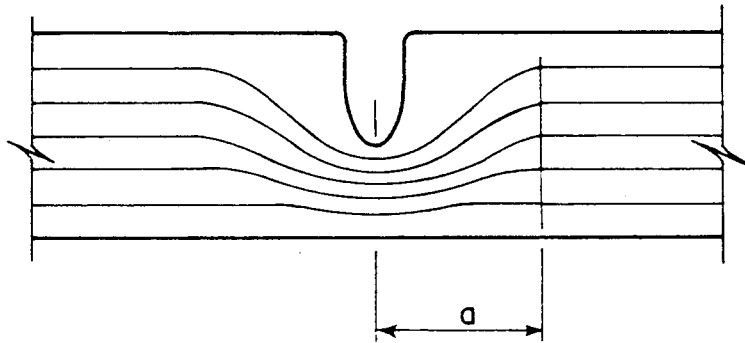
Equation 6 indicates that for small sections and large slot depths, half-depth models of the section should not be used. If, for example, a 12-in (305-mm) section were modelled as a 6-in (152-mm) section (with appropriate boundary conditions), then for slot depths greater than about 0.8 in (20.3 mm), stresses calculated using the half-depth, 6-in (152-mm) model would be significantly larger than those found by analyzing the full-depth, 12-in (305-mm) model. For slots with depths less than 0.8 in (20.3 mm), however, approximately the same stresses would be found with each model.

Since slots under consideration are at least 0.8-in (20.3-mm) deep, and since stress concentration effects become more significant with larger slots, full-depth models were used when possible. Half-depth models were used only for analysis of shrinkage stresses. This was done to take advantage of the already developed finite element model. While results with these half-depth models are useful in analyzing the flat-jack method of stress measurement, they do not represent the behavior of slotted wall sections in bridge girders. To determine the effects of slitting a bridge girder under shrinkage stresses, a full-depth model of the particular wall should be used.

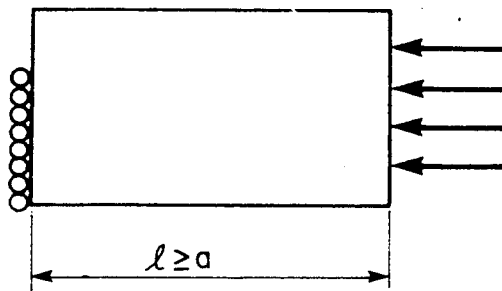
The length of the model was also determined by considering stress distributions around the slot. St. Venant's principle indicates that if a hole is cut in a stressed medium, the stress distribution in the neighborhood of the hole changes.<sup>[51]</sup> However, at distances that are large compared to the size of the hole, the change in the stress distribution is negligible. A strip under uniform tensile stress is presented in figure 9. Figure 9a shows the stress flow in a strip with no slot, while figure 9b shows the stress flow in a strip with a slot. Near the slot the stress distribution



(a) Stress flow before slitting



(b) Stress flow after slitting



(c) Length of section

Figure 9. Stress flow near slot.

is affected by the slot. At distances far from the slot, the slot has no effect on the stress distribution in the section.

It is possible to calculate stresses near the slot by modelling only a section of the strip as shown in figure 9c. This type of model, however, is valid only if the section is taken sufficiently far from the slot. If "a" is the minimum distance from the slot at which the stress distribution is no longer affected by the slot, then the stress distribution in the model and in the actual strip correspond only if the length of the model is greater than or equal to "a". If the length is less than "a", then the model will not reflect the stress distribution in the slotted strip.

Since no exact solutions were available to determine a minimum length for the model, an approximate initial dimension was chosen. The approximate dimension was based on an exact solution for stresses due to a uniform axial load on an infinite plate with a circular hole. The radial stress in the direction of the axial load is:<sup>[51]</sup>

$$\sigma_r = T - \frac{T}{2} \left( \frac{5a^2}{r^2} - \frac{3a^4}{r^4} \right) \quad (7)$$

where T = the uniform axial stress

a = radius of the hole

r = radial distance from the center of the hole to the point where the stress is measured

Values of  $\sigma_r$  for various r/a ratios are listed in table 3. As long as  $r/a \geq 8$ , the change in the stress distribution away from the hole is less than 5%. Since the maximum slot depth would be about 3 in (76 mm), a length of 23 in (584 mm) was used for the initial model. If a finite element analysis of this 23-in (584-mm) model had indicated that the length was inadequate, a longer model would have been developed.

#### 4.1.2.4 The Finite Element Model

SAPIV, "A Structural Analysis Program for Static and Dynamic Response of Linear Systems"<sup>[52]</sup> was used to analyze the model in the linear elastic

Table 3. Radial stress near circular hole.

$r/a^*$	$\sigma_r/T^{**}$
1	0
2	0.47
5	0.90
8	0.96
10	0.98
50	1.00

\*a is the radius of the hole, r is the distance from the center of the hole to the point where stress is measured.

\*\*T is the uniform axial stress.

range. A 6x23-in (152x584-mm) model and a 12x23-in (305x584-mm) model were developed. Both of these models were divided into 1052 rectangular plane strain elements. The 12x23-in (305x584-mm) model is shown in figure 10. Thirty-three elements were used in each row of the mesh and thirty-two elements were used in each column of the mesh. Small elements were used where steep stress gradients were expected. For example, to model shrinkage stresses along the surface, four rows of elements 0.1-in (2.5-mm) deep were used. Near the slot, where large stress concentrations due to the slot were expected, elements were either 0.1 in (2.5 mm) square or 0.1x0.2 in (2.5x 5.1 mm). The largest element in the mesh was 1.0x1.5 in (25.4x38.1 mm). Slot depths of 0.8, 1.6, 2.4, and 3.2 in (20.3, 40.6, 61.0, and 81.3 mm) were modeled. These depths approximately correspond to the flat-jack depths.

Stresses were applied in the form of element pressures. As discussed in detail later, shrinkage stresses were modeled throughout the element by varying nodal temperatures. The same linear elastic material was used in all elements. Values for modulus of elasticity and Poisson's ratio were, respectively,  $E = 4 \times 10^6$  psi (27,580 MPa) and  $\nu = 0.17$ . This modulus corresponds to a concrete compressive strength of 5000 psi (34.5 MPa).

#### 4.1.2.5 Verification of the Model's Dimensions

Computer analyses using the finite element models confirmed that an adequate length had been selected for the model. When subjected to a uniform stress, the stress distribution away from the slot remained relatively unchanged. In the 12-in (305-mm) model with the 3.2-in (81.3-mm) slot, the stress distribution 10 in (254 mm) away from the slot varied by less than 5% from the stress distribution at the loading edge. In the 6-in (152-mm) model with a 3.2-in (81.3-mm) slot, the stress distribution 6 in (152 mm) away from the slot varied by less than 5% from the stress distribution at the loading edge.

Comparison of displacements near the slot in a 6-in (152-mm) section and in a 12-in (305-mm) section confirmed the importance of using a full depth

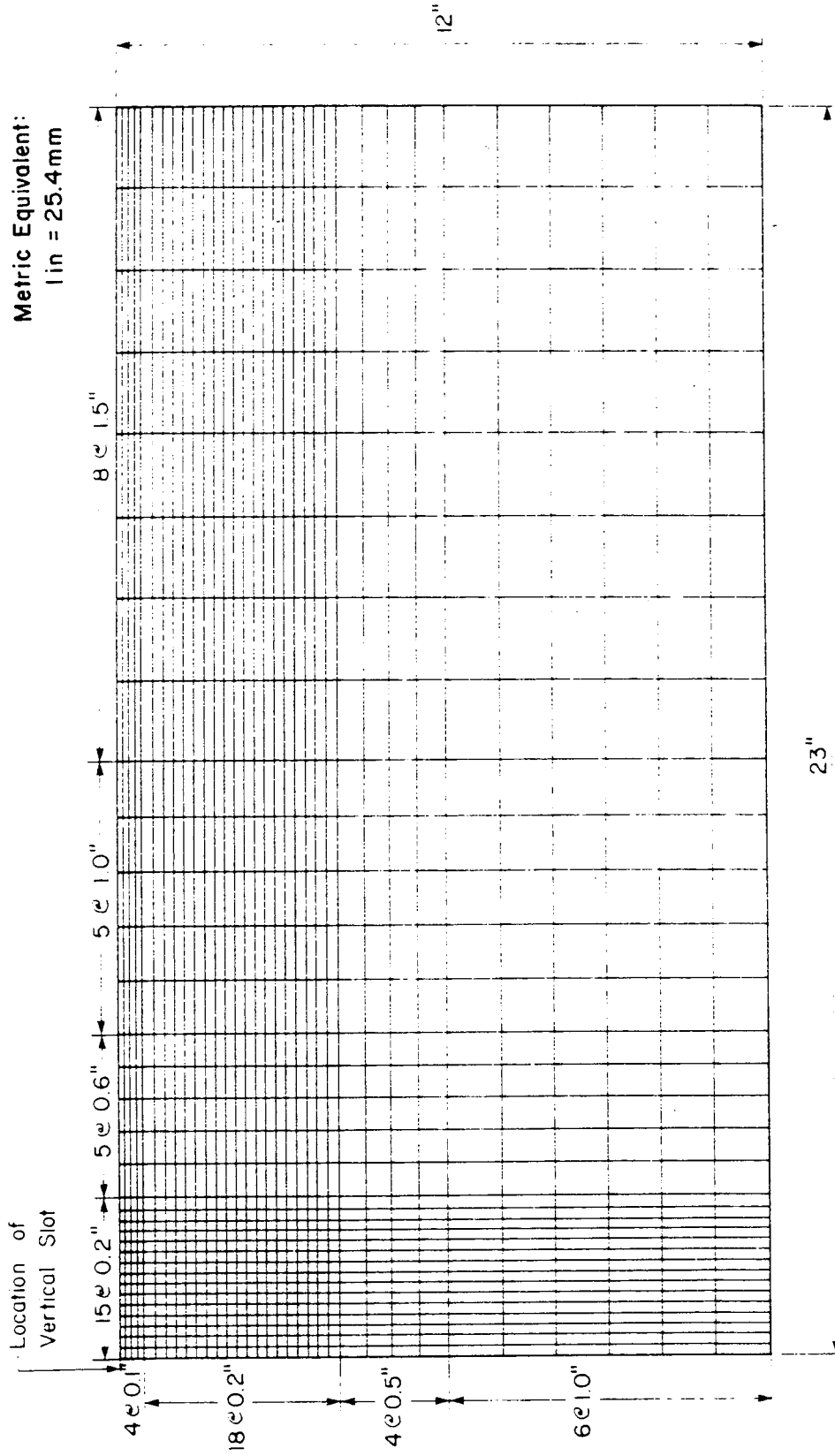


Figure 10. Finite element mesh for a 12-in-thick section.

section to model the girder's behavior. Displacements due to applying a uniform axial stress of 1000 psi (6.9 MPa) on a slotted section are listed in table 4 for models with various slot depths. The displacements are calculated along the top surface for points 0.4 in (10.2 mm) on either side of the slot. Displacements for both 6- and 12-in-deep (152- and 305-mm) sections are presented. For unslotted sections, displacements in the 6-in and 12-in (152- and 305-mm) models are equal. For a 0.8-in-deep (20.3-mm) slot, the displacement in the 6-in (152-mm) section is about 7% larger than the displacement in the 12-in (305-mm) section. The difference in displacement between the two sections increases with increasing slot size. For a 3.2-in (81.3-mm) slot, the displacement in the 6-in (152-mm) section is almost 160% larger than the displacement in the 12-in (305-mm) section.

#### 4.1.3 Accuracy of Flat-Jack Method

##### 4.1.3.1 Accuracy of Stress Measurements

Measurement of displacements is critical in determining stresses. Both displacements due to cutting a slot and those due to restoring the stress in a section by means of a flat jack must be measured accurately. Several types of gages are available for measuring displacements. The most sensitive of these is the Pfender gage. Each unit on the Pfender gage represents a displacement of 39.4 millionths (0.001 mm). Other gages, such as the Whittemore, Demec, and Huggenberger are less sensitive. For example, a unit on the Whittemore and Huggenberger gages represents a displacement of 100 millionths of an inch (0.00254 mm), while each unit on a Demec represents a displacement of 200 millionths of an inch (0.005 mm).

The amount of displacement that each unit on a gage represents gives some indication of the accuracy with which displacements can actually be measured. However, laboratory and field measurements using a particular gage must be made to verify repeatability of measurement accuracy. For example, experimental data may show that it is possible to repeat measurements consistently to an accuracy of half a unit. On a Pfender gage that would mean an accuracy



Table 4. Displacement of slotted sections.

Slot Depth (in)	Displacements* (thousandths in)	
	6-in Section	12-in Section
0	0.194	0.194
0.8	1.153	1.074
1.6	3.149	2.420
2.4	7.224	4.110
3.2	17.032	6.462

\*Displacements are calculated along the top surface 0.4 in from the edge of the slot. Displacements are due to a uniform axial stress of 1000 psi (6.9 MPa).

Metric Equivalent:  
1 in = 25.4 mm

of 19.7 millionths of an inch (0.0005 mm). On the other hand, tests may show that consistent readings can only be made to an accuracy of two units. With a Pfender gage that would mean an error of 78.8 millionths of an inch (0.002 mm). Once the accuracy with which a displacement can be measured is known, the analysis in this section can be used to determine accuracy of stress measurements.

Six- and 12-in (152- and 305-mm) sections under a uniform axial load of 1000 psi (6.9 MPa) were analyzed to determine displacements due to slitting. First, the displacements in an unslotted section with a 1000 psi (6.9 MPa) stress were obtained. Then the finite element model was used to obtain displacement in a slotted section under a stress of 1000 psi (6.9 MPa). The difference in the two solutions is the displacement due to slitting a section under a 1000-psi (6.9-MPa) stress.

Displacements due to slitting 6- and 12-in (152- and 305-mm) sections under a uniform stress of 1000 psi (6.9 MPa) are listed in table 5. These are displacements that would be measured across the slot. They are listed for various slot depths. The slot depths are approximately equal to the depth of flat jacks described later in section 5.0. The displacements have been computed along the top surface for points 0.4 in, 0.8 in, 1.2 in and 2.0 in (10.2, 20.2, 30.5, and 50.8 mm) from the slot. These are the points at which displacements could be measured using a Pfender gage.

#### 4.1.3.2 Accuracy of Uniform Stress Reconstruction

Analytically, it is clear that if slitting a section under uniform stress,  $T$ , causes a displacement,  $d$ , then to restore the section to its original position a uniform stress of magnitude  $T$  would have to be applied to the slot. It is unlikely, however, that actual measurements using a flat jack and Pfender gage will reproduce the uniform stress,  $T$ , exactly. The flat-jack restoring force may vary somewhat from the actual uniform stress in the section due to the limited accuracy of the gage. However, if the

Table 5. Displacements due to slitting a section under uniform stress.\*

Slot Depth (in)	Displacement (thousandths in)							
	6-in Section				12-in Section			
	Distance from Slot (in)				Distance from Slot (in)			
	0.4	0.8	1.2	2.0	0.4	0.8	1.2	2.0
0.8	0.959	0.749	0.605	0.460	0.880	0.670	0.521	0.359
1.6	2.954	2.727	2.502	2.164	2.225	2.001	1.777	1.414
2.4	7.030	6.810	6.577	6.156	3.915	3.742	3.492	3.050
3.2	16.838	16.625	16.397	15.956	6.268	6.060	5.836	5.374

\*Prior to slitting, section was under a uniform axial stress of 1000 psi

Metric Equivalent:

1 in = 25.4 mm

accuracy of the gage has been determined, then the error in stress measurement for various slot depths and measurement locations can be calculated.

The stress,  $\sigma_p$ , that corresponds to a unit displacement of a Pfender gage is:

$$\sigma_p = \frac{1000 \times 39.4 \times 10^{-6}}{d} \quad (8)$$

where  $d$  is the displacement taken from table 5. The displacement,  $d$ , varies with section depth, slot depth, and measurement location. In the above equation, 1000 corresponds to the uniform stress in the model while  $39.4 \times 10^{-6}$  represents a unit displacement on the Pfender gage. The stress,  $\sigma_p$ , is listed in table 6 for various size slots and measurement locations.

If it is determined that displacement can be measured to an accuracy of one Pfender gage unit, then  $\sigma_p$  is the error in stress measurement. The error in stress measurement decreases for smaller sections, deeper slots, or when measurements are taken closer to the slot. In other words, the error in stress measurement decreases when displacement increases.

If laboratory and field measurements indicate that the displacement can be measured to an accuracy of one-half a Pfender gage unit, then to determine the error in stress measurement, the values in table 6 should be divided by two. On the other hand, if tests indicate that the displacements can only be measured to an accuracy of two units, then all values in table 6 should be multiplied by two.

Accuracy of the flat-jack method of stress measurement depends mainly on two factors. First, as was discussed in the previous section, it depends on the accuracy of the displacement measurements. Secondly, as will be discussed in this section, it depends on the accuracy of the flat-jack model itself.

To analyze the accuracy of the flat-jack model, it is assumed that no errors exist in displacement measurements and that the measured flat-jack

Table 6. Flat-jack pressure causing unit displacement.\*

Slot Depth (in)	Flat-Jack Pressure (psi)							
	6-in Section				12-in Section			
	Distance from Slot (in)				Distance from Slot (in)			
	0.4	0.8	1.2	2.0	0.4	0.8	1.2	2.0
0.8	41	53	65	86	45	59	76	110
1.6	13	14	16	18	18	20	22	28
2.4	6	6	6	6	10	11	11	13
3.2	2	2	2	2	6	7	7	7

\*Unit displacement refers to a Pfender Gage unit which is equal to  $39.4 \times 10^{-6}$  in

Metric Equivalents:

1 in = 25.4 mm

1 psi = 6.895 kPa.

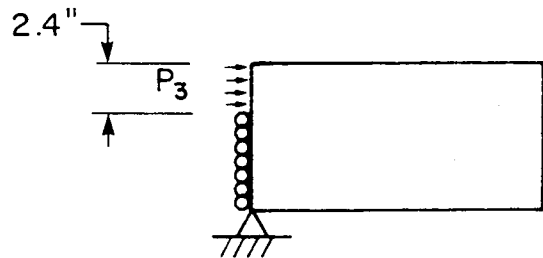
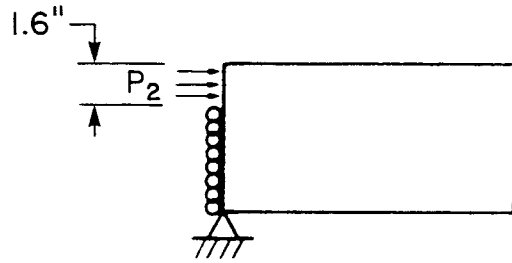
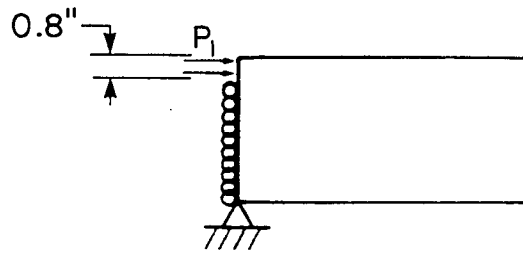
restoring pressures are exact. In other words, it is assumed that if a section under uniform stress,  $T$ , is slit, the restoring force in the flat jack is exactly  $T$ . Once the accuracy of the model has been determined, then the analysis of this section can be combined with that of the previous section to determine the accuracy of the method of strain relief by slitting.

#### 4.1.3.3 Accuracy of Stress Gradient Reconstruction

While the flat-jack model is exact for sections under uniform stress, it is not exact for sections with a non-uniform stress distribution. The error due to compensating for a non-uniform stress in the section by a uniform stress in the flat jack is investigated in this section. Two types of stress distributions are considered. The first type simulates a bending stress distribution, while the second type simulates a shrinkage stress distribution.

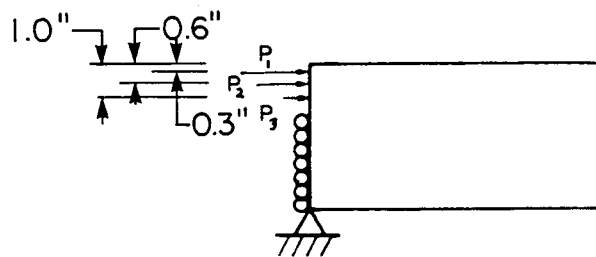
The method for determining a stress distribution in a section using the flat-jack model is illustrated in figure 11. First, restoring pressures for several slot depths are found as shown in figure 11a. A stress distribution for the slotted cross section is then constructed by distributing flat-jack pressures at the centroid of the flat jack as shown in figure 11b. If flat-jack stresses for all slot depths are the same, then a uniform stress distribution exists in the structure. This case was discussed in the previous section. If the flat-jack stresses are not the same for all slot depths, then a stress gradient exists in the structure.

The calculated centroids of the nominal flat-jack depths are listed in table 7. While the depth of flat jacks ranges from 0.8 in (20.3 mm) to about 3.2 in (81.3 mm), the location of their centroids ranges only from 0.3 in to 1.3 in (7.6 to 33.0 mm) below the surface. Therefore, currently available flat jacks, can determine stresses for points which are at most 1 in (25.4 mm) apart. If a stress gradient exists, the slope of this gradient must be determined from data in this 1-in (25.4-mm) area. If the slope of the stress distribution changes outside this 1-in (25.4-mm) area, the flat-jack technique does not help determine this change.



Metric Equivalent:  
1 in = 25.4 mm

(a) Flat-jack pressures



(b) Stresses at centroid of flat jacks

Figure 11. Reconstruction of a stress gradient.

Table 7. Centroid of flat jacks.

Nominal Flat Jack Depth (in)	Distance from Top of Flat Jack to Centroid (in)
0.8	0.322
1.6	0.648
2.4	0.979
3.2	1.316

Metric Equivalent:  
1 in = 25.4 mm



To determine the accuracy with which a bending stress gradient can be detected, the model shown in figure 7 was used. Both 6- and 12-in (152- and 305-mm) sections were analyzed under linear stress gradients with a maximum stress of 1000 psi as shown in figure 12b. Displacements due to cutting a slot are listed in table 8. These displacements were calculated using the procedure outlined for the case of a uniform stress. The displacements are computed across the slot.

To determine the uniform restoring pressure, displacements in table 8 were compared with the displacements in table 5. The ratio  $d_b/d_u$  was then calculated for all slot depths and measurement locations in a given section. In this ratio,  $d_b$  represents the displacements given in table 8 due to slitting a section with a bending stress gradient. Displacement,  $d_u$ , is given in table 5 and is due to slitting a section with a uniform stress distribution. The uniform 1000 psi (6.9 MPa) stress which caused the displacements in table 5 was multiplied by the above ratio. The resulting stress represents flat-jack restoring stress for a slotted section with a bending stress gradient.

For example, cutting a 1.6-in (40.6-mm) slot in a 12-in (305-mm) section with a bending stress gradient as shown in figure 12b, and measuring 0.4 in (10.2 mm) from the edge of the slot results in a displacement of 2.022 thousandths (0.051 mm). By pushing back on the slot with a pressure of 1000 psi (6.9 MPa) the magnitude of the displacement 0.4-in (10.2-mm) from the slot would be 2.225 thousandths (0.057 mm). To restore a displacement of 2.022 thousandths (0.051 mm), a stress of  $(2.002 \div 2.225) \times 1000$  psi or 909 psi (6.3 MPa) would have to be applied. According to the flat-jack model, the restoring stress of 909 psi is the stress in the section located at the centroid of the flat jack.

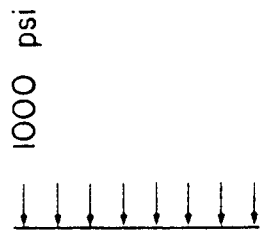
The centroid of a 1.6-in-deep (40.6-mm) flat jack is about 0.6 in (15.2 mm) below the surface. The actual stress at that point is about 890 psi (6.1 MPa). The flat-jack model, then, overestimates the stress at this point by about 2%. The stresses calculated using the flat-jack model

Table 8. Displacements due to slitting a section with bending stress gradient.\*

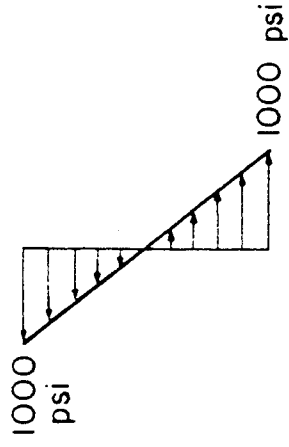
Slot Depth (in)	Displacements (thousandths in)							
	6-in Section				12-in Section			
	Distance from Slot (in)				Distance from Slot (in)			
	0.4	0.8	1.6	2.0	0.4	0.8	1.6	2.0
0.8	0.871	0.676	0.544	0.413	0.836	0.635	0.494	0.340
1.6	2.413	2.203	2.008	1.725	2.022	1.807	1.598	1.266
2.4	5.055	4.851	4.650	4.312	3.401	3.194	2.981	2.585
3.2	10.445	10.244	10.046	9.697	5.122	4.920	4.711	4.299

\*Prior to slitting, section was under linear stress gradient shown in figure 12b.

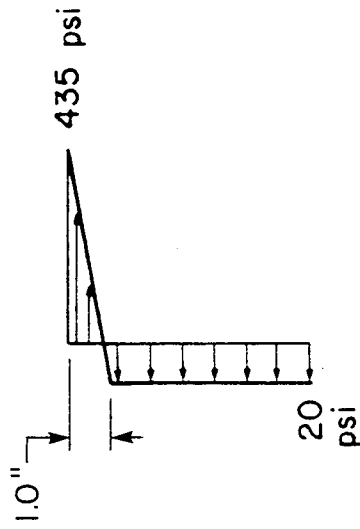
Metric Equivalent:  
1 in = 25.4 mm.



(a) Uniform compressive stress

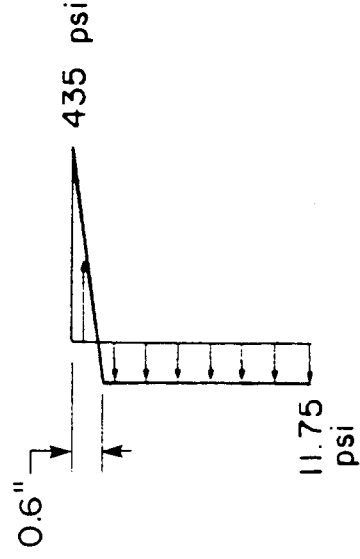


(b) Bending stress gradient



(c) Shrinkage stress gradient No. 1

Metric Equivalents:  
 1 in = 25.4 mm  
 1 psi = 6.895 kPa



(d) Shrinkage stress gradient No. 2

Figure 12. Stress distributions.

are listed in table 9. The errors in calculating stresses using the flat-jack model are listed in table 10. The flat-jack model overestimates the actual stresses by the percentages listed in this table.

With both the 6- and 12-in (152- and 305-mm) sections, the smallest errors occur when a 0.8-in (20.3 mm) slot is used and when measurements are taken 2.0 in (51 mm) from the slot. The largest errors occur in both sections when a 3.2-in (81.3-mm) slot is used and displacement measurements are made 0.4 in (10.2 mm) from the slot. Errors are larger for the 6-in (152-mm) section than for the 12-in (305-mm) section. The maximum error in the 6-in (152-mm) section is about 10%, while the maximum error in the 12-in (305-mm) section is about 5%.

A comparison of the results indicates that the accuracy of the flat-jack model in predicting bending stresses increases as the accuracy of measuring compensating flat-jack pressures decreases. As indicated by table 6 for uniform stress, accuracy of measuring compensating flat-jack pressures increases when measurements are taken near the slot, when larger slots are used, and when the depth of the section decreases. On the other hand, table 10 for bending stress shows that accuracy of the flat-jack model in predicting bending stresses increases when measurements are taken far from the slot, when shallow slots are used, and when the depth of the section increases.

#### 4.1.3.4 Accuracy of Shrinkage Stresses Reconstruction

To determine the accuracy with which a shrinkage stress distribution can be reconstructed using the flat-jack technique, the model shown in figure 13 was used. This model represents a half-depth section. Since shrinkage stress distributions in a section are symmetrical, a full-depth model would require a refined mesh along both the top and bottom surfaces. Rather than developing this new and larger finite element mesh, the mesh shown in figure 10 was used for this investigation. As shown in figure 13, vertical displacements were restrained along the bottom surface of the half-depth model. This reflects the fact that a full-depth symmetrical shrinkage stress

Table 9. Restoring flat-jack pressures for bending stress gradient.\*

Slot Depth (in)	Flat-Jack Pressure (psi)							
	6-in Section				12-in Section			
	Distance from Slot (in)				Distance from Slot (in)			
	0.4	0.8	1.6	2.0	0.4	0.8	1.6	2.0
0.8	908	903	900	900	951	948	947	945
1.6	817	809	802	797	909	903	900	896
2.4	719	712	707	700	869	854	854	848
3.2	620	616	613	608	817	812	807	800

\*Prior to slitting, section was under the linear stress gradient shown in figure 12b.

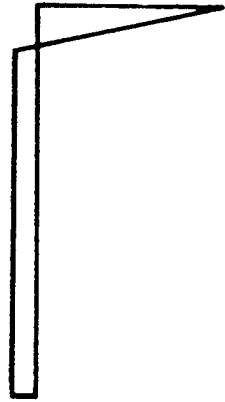
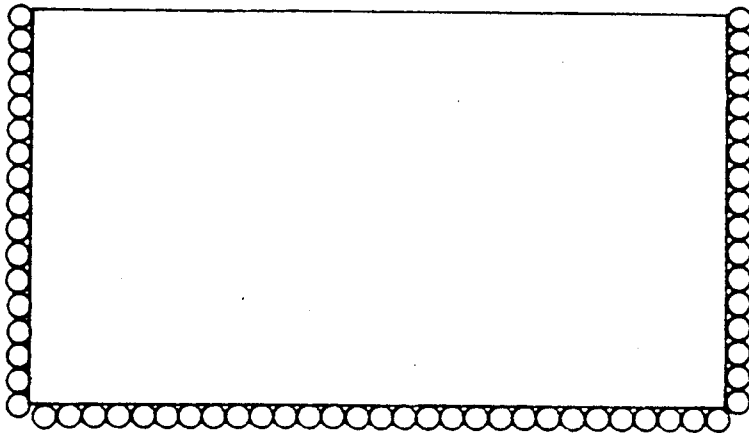
Metric Equivalent:  
1 in = 25.4 mm.

Table 10. Error in reconstruction of a bending stress gradient.\*

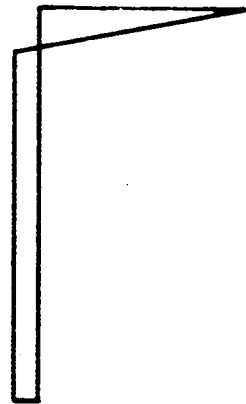
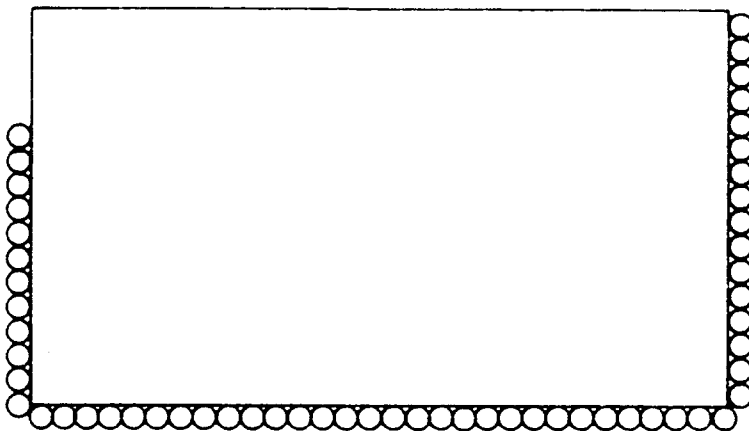
Slot Depth (in)	Error (percent)							
	6-in Section				12-in Section			
	Distance from Slot (in)				Distance from Slot (in)			
	0.4	0.8	1.6	2.0	0.4	0.8	1.6	2.0
0.8	1.7	1.2	1.0	0.9	0.9	0.5	0.5	0.2
1.6	4.0	2.9	2.2	1.5	2.0	1.4	1.1	0.6
2.4	5.9	4.9	4.1	3.1	3.8	2.0	2.0	1.3
3.2	9.6	8.9	8.3	7.4	4.8	4.1	3.5	2.6

\*Prior to slitting, section was under the linear stress gradient shown in figure 12b.

Metric Equivalent:  
1 in = 25.4 mm.



(a) Model without slot



(b) Model with slot

Figure 13. Half-depth shrinkage stress model.

distribution would not cause any vertical displacement along the middle plane of a full-depth section. Also, the right edge of the model was restrained against horizontal displacements. This insured a uniform stress distribution throughout the entire section.

Shrinkage stresses were simulated using a bilinear stress distribution. The magnitude of the maximum tensile stress was based on a shrinkage stress distribution given in reference 28. The magnitude of the compressive stress was chosen to equilibrate the internal tensile stresses. Shrinkage stresses were modeled in the finite element analysis by varying nodal temperatures. Once the required stress,  $\sigma$ , at each node was determined, the corresponding nodal temperature,  $t$ , was found from the following equation:

$$t = - \frac{\sigma (1 - \nu)}{\alpha E} \quad (9)$$

where  $\alpha$  is the coefficient of thermal expansion. A value of  $\alpha = 5.5$  millionths per °F (9.9 millionths per °C) was used. Two shrinkage stress distributions were modeled as shown in figures 12c and 12d. In both cases the maximum tensile stress was 435 psi (3 MPa). The depth of the tensile stress area in one distribution was 0.6 in (15.2 mm) while the depth of the tensile stress area in the other distribution was 1.0 in (25.4 mm). The half-depth model was then analyzed for slot depths of 0.8, 1.6, 2.4 and 3.2 in (20.3, 40.6, 61.0, and 81.3 mm).

Displacements due to cutting a slot in the stressed section were obtained by releasing the appropriate nodal restraints in the model. The displacements are listed in table 11. The magnitude of the flat-jack stresses required to restore the section to its original position are listed in table 12. These stresses were calculated using the procedure discussed for bending stress distributions.

According to the flat-jack model, the stresses in table 12 represent stresses at the centroid of the flat jack. The magnitudes by which the flat-jack technique overestimates or underestimates the actual shrinkage stresses are listed in table 13. The accuracy of the calculated stress is influenced by both the depth of the tensile shrinkage stress distribution and the depth of the slot.

Table 11. Displacements due to slitting sections with shrinkage stress distributions.

Slot Depth (in)	Displacements (thousandths in)							
	1.0-in-Deep Tensile Stress Distribution (figure 16c)				0.6-in-Deep Tensile Stress Distribution (figure 16d)			
	Distance from Slot (in)				Distance from Slot (in)			
	0.4	0.8	1.6	2.0	0.4	0.8	1.6	2.0
0.8	0.268	0.197	0.149	0.096	0.204	0.145	0.109	0.070
1.6	0.430	0.356	0.296	0.212	0.292	0.232	0.189	0.133
2.4	0.502	0.428	0.368	0.278	0.332	0.273	0.229	0.171
3.2	0.540	0.466	0.406	0.316	0.354	0.295	0.252	0.193

\*Values are calculated for the 12-in, half-depth model shown in figure 13b.

Table 12. Restoring flat-jack pressures\* for shrinkage stress distributions.

Slot Depth (in)	Flat-Jack Pressure (psi)							
	1.0-in-Deep-Tensile Stress Distribution (figure 12c)				0.6-in-Deep Tensile Stress Distribution (figure 12d)			
	Distance from Slot (in)				Distance from Slot (in)			
	0.4	0.8	1.6	2.0	0.4	0.8	1.6	2.0
0.8	305	294	285	268	232	216	209	193
1.6	193	178	167	150	131	116	106	94
2.4	128	114	105	91	85	73	66	56
3.2	86	77	70	59	56	49	43	36

\*Values are calculated for the 12-in, half-depth model shown in figure 13b.

Metric Equivalents:

1 in = 25.4 mm

1 psi = 6.895 kPa



Table 13. Discrepancy in reconstruction of shrinkage stress distributions.\*

Slot Depth (in)	Error (psi)							
	1.0-in-Deep Tensile Stress Distribution (figure 12c)				0.6-in-Deep Tensile Stress Distribution (figure 12d)			
	Distance from Slot (in)				Distance from Slot (in)			
	0.4	0.8	1.6	2.0	0.4	0.8	1.6	2.0
0.8	16	5	-3	-21	37	22	14	-2
1.6	53	38	26	10	143	128	118	106
2.4	138	124	115	101	97	85	77	68
3.2	106	97	90	79	68	60	55	48

\*Calculated for the 12-in, half-depth model shown in figure 13b.

Note: Negative values indicate magnitude of stress is underestimated.

Metric Equivalent:  
 1 in = 25.4 mm  
 1 psi = 6.895 kPa

The above results indicate that two difficulties arise in the reconstruction of shrinkage stress gradients using the flat-jack method. First of all, the flat-jack model does not accurately determine the shrinkage stresses in the structure at the centroid of the flat jack. Second, presently available flat jacks can only determine stresses at depths between 0.32 and 1.32 in (8.13 and 33.5 mm). Changes in the slope of the stress gradient outside this depth range cannot be accurately determined. Use of larger flat jacks would increase this area slightly.

Several possibilities exist for overcoming these difficulties. One possibility is to develop a method for monitoring displacements below the surface where shrinkage stresses are smaller. Measurement of displacements below the surface has disadvantages discussed earlier. A second possibility is to use parametric computer models to interpret the stress measurements. Both of these approaches should be investigated further. However, they are beyond the scope of this investigation.

If parametric investigations are made, full-depth models of a section should be used in all analyses. This includes analyses of shrinkage stresses. Such models will insure that stress concentration effects, which are dependent on slot depth to section depth ratios, are analyzed. A full-depth model for analysis of shrinkage stresses is shown in figure 14.

In light of the fact that analysis procedures and assumptions may change results somewhat, it does not appear that the flat-jack technique is suitable for measuring shrinkage stresses. This is contrary to Abdunur's<sup>[29]</sup> claims that he has measured shrinkage stresses using the flat-jack technique.

Laboratory results presented in section 5.0 confirm analytical studies. With the existing flat-jack equipment and refined techniques, shrinkage stresses cannot be determined using this technique.

#### 4.2 Variables Affecting Stress Measurements

It is well known that concrete shrinks during exposure to a drying environment. Upon application of stresses due to prestressing and dead load,

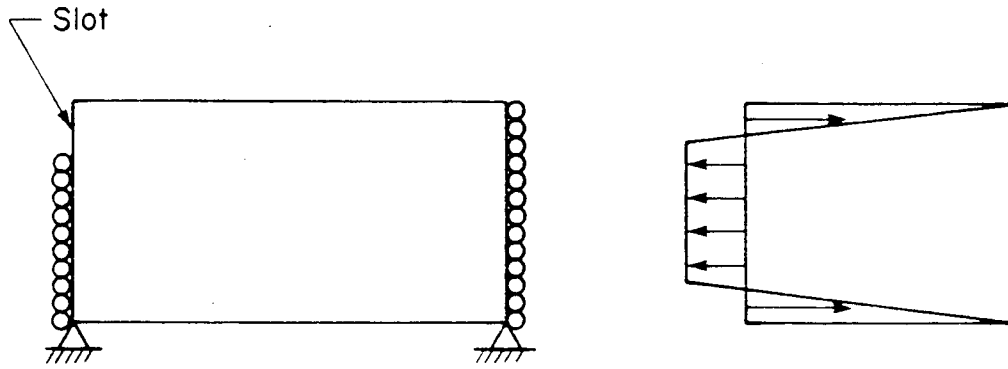


Figure 14. Full-depth shrinkage stress model.

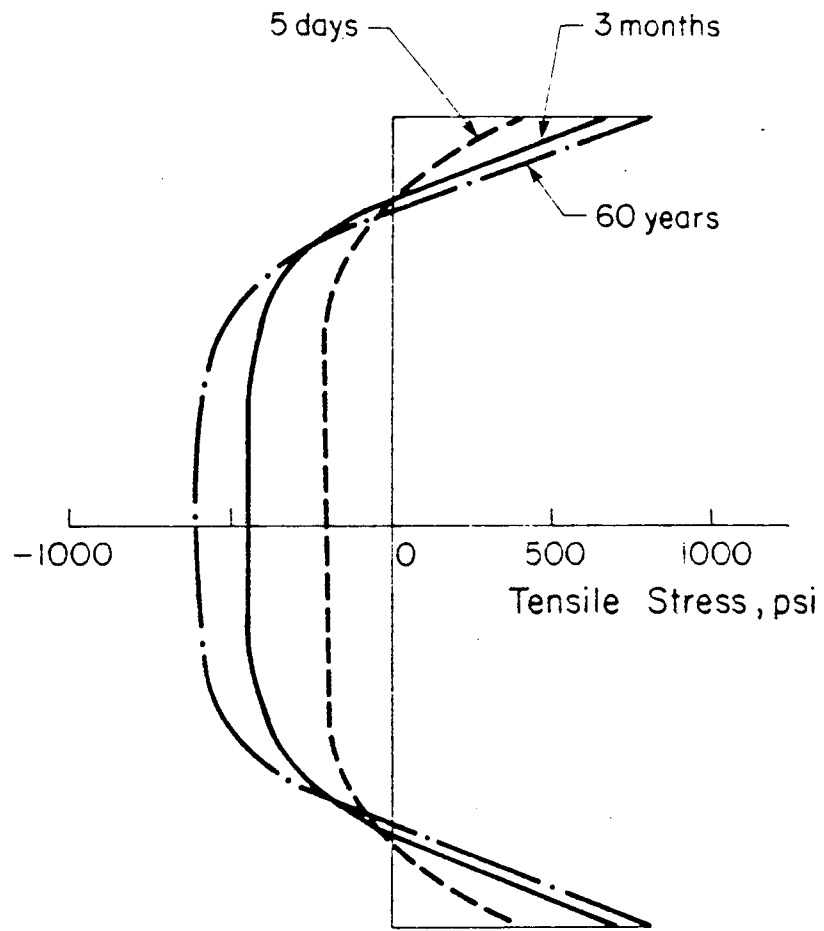
elastic deformations occur. Under sustained stress, concrete creeps with time. If exposed to a rise or fall of temperature, concrete expands or contracts, respectively. In the previous section, analyses indicated that the flat-jack method of stress measurement is the most promising technique for prestressed concrete applications. Therefore, this section will focus on how shrinkage, creep, and temperature variation can affect stresses measured by the flat-jack technique.

#### 4.2.1 Shrinkage

At time of casting, concrete has a pore humidity of 100%. Soon after stripping the forms and exposing the concrete surface to air, drying of the exposed concrete surface starts. Because of the diffusivity of concrete, drying starts at the exposed surfaces and spreads inside the concrete very slowly.

The moisture difference between the surface and the inside of the concrete causes a differential shrinkage.<sup>[53]</sup> The exposed skin of the concrete shrinks more than the rest of the concrete. Consequently, the exposed skin is restrained from shrinking by the center portion of the concrete. The result is that internal tensile and compressive stresses are induced in the concrete as shown schematically in figure 15. For equilibrium, the sum of tensile stresses equals the sum of compressive stresses. Procedures for computing shrinkage stresses have been suggested by Pickett<sup>[53]</sup> and Acker.<sup>[54]</sup> Although Abdunur<sup>[29]</sup> claims he can measure magnitude and distribution of the shrinkage stresses using flat jacks, analytical results discussed in section 4.1.3.4 indicate that shrinkage stresses may not be easy to measure with the flat-jack technique.

Several factors affect shrinkage stresses. One of the most important factors is the ambient relative humidity. Concrete shrinks with a loss in moisture and expands with a gain in moisture. Alternate wetting and drying of concrete causes cycles of shrinking and swelling.<sup>[55]</sup> Therefore, if stress measurement involves cutting the concrete, use of water to cool the saw blade should be avoided to prevent any changes in concrete shrinkage



Metric Equivalent:  
 1000 psi = 6.895 MPa

Figure 15. Shrinkage stress distribution. [53]

around the cut. Variation of the shrinkage strains can upset the measured stresses by several magnitudes.

#### 4.2.2 Coefficient of Linear Thermal Expansion

Concrete expands as temperature rises and contracts as temperature falls. An average value for the linear coefficient of thermal expansion of concrete is about 5.5 millionths per °F (9.9 millionths per °C), although values ranging from 3.2 to 7.0 millionths per °F (5.8 to 12.6 millionths per °C) have been observed.<sup>[55]</sup> Therefore, for restrained concrete with a modulus of elasticity of  $4 \times 10^6$  psi (27.6 GPa), rise of the temperature by 1°F (0.56°C) results in an increase of the compressive stress by 22 psi (152 kPa). Therefore, it will be important to maintain the temperature of the specimen and the ambient air as constant as possible.

#### 4.2.3 Creep

Creep is the time dependent deformation under sustained stress. Creep depends on (1) the magnitude of sustained stress, (2) age and strength of the concrete when stress is applied, and (3) the length of time the stress is sustained.

Creep curves for two concrete mixes<sup>[55]</sup> are shown in figure 16. Creep tests were made on 6x12-in (152x305-mm) concrete cylinders. Concrete compressive strength at 28 days was 3,000 psi (21 MPa) and 4,500 psi (31 MPa) for Specimens A and B, respectively. The specimens were loaded to 600 psi (4.14 MPa) at age 7 days. The figure indicates that an increase in the concrete compressive strength results in a reduction in creep. If a specimen is unloaded after a period of time, some instantaneous recovery occurs. This is followed by a creep recovery as shown in figure 17. However, even if the specimen remains unloaded, there is a residual deformation. The initial length is never recovered.

For the laboratory tests of Task C, constant loads were to be applied to the specimens. As it takes time to relieve the stresses and measure them,

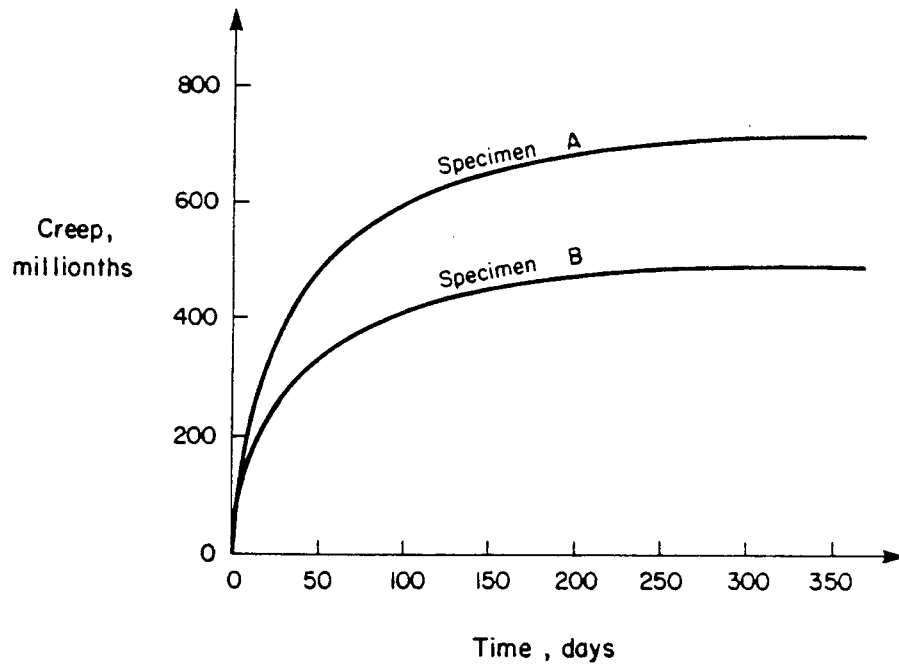


Figure 16. Variation of creep with time. [54]

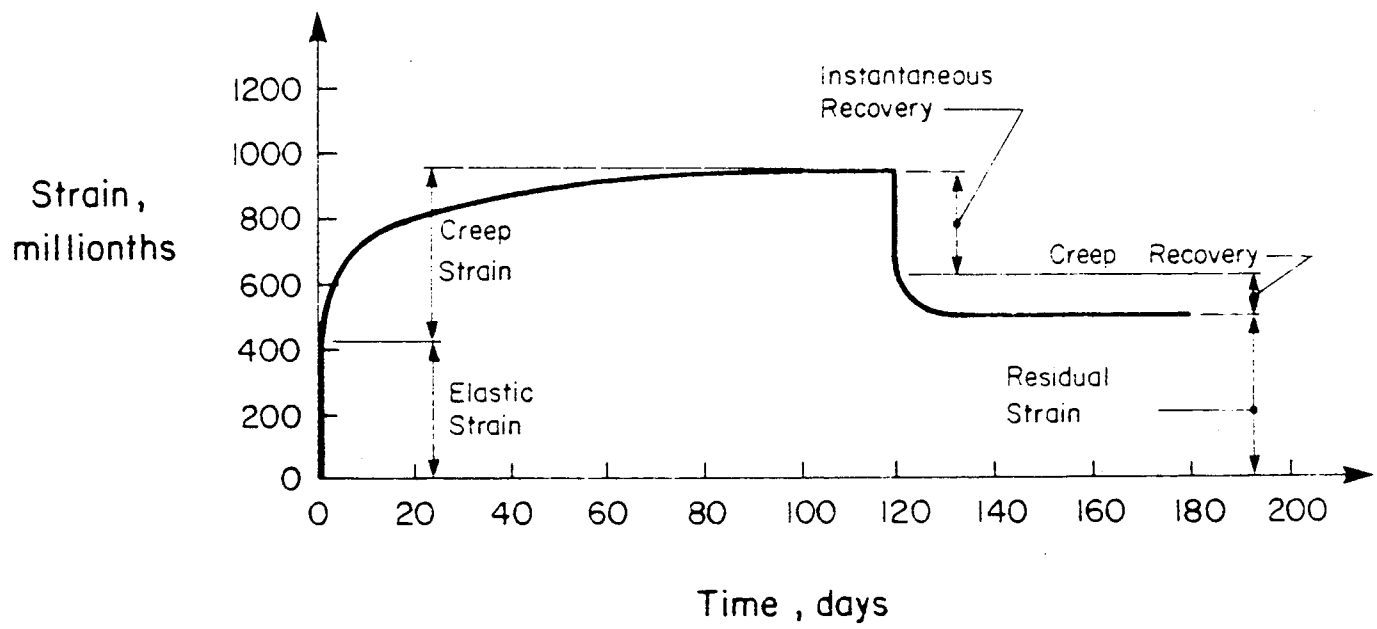


Figure 17. Creep and creep recovery. [48]

creep will occur. The rate of creep is higher immediately after loading as shown in figure 17. The rate of creep is also higher the younger the concrete. Therefore, to diminish the effect of creep on stress measurement, it was important to load the specimens as early as possible prior to testing. Also, specimens were aged as much as possible. For specimens previously loaded, but then unloaded to measure shrinkage stresses, it was necessary to wait after unloading to decrease the effect of creep recovery shown in figure 17.

The above discussion emphasizes the importance of shrinkage, temperature, and creep and how they can affect the stress measurement. Therefore, for the laboratory tests, it was important to monitor the strains at the slitting locations as well as away from the slitting locations.

#### 4.3 Considerations for Field Tests

In the field, bridges are exposed to continuously changing ambient humidity and temperature. Rain causes wetting of some of the bridge concrete. After the rain, wet concrete dries. Therefore, some of the bridge concrete experiences cycles of wetting and drying. Consequently, differential shrinkage occurs in different parts of the bridge concrete.

Concrete temperature varies seasonally and diurnally. Daily temperature variation induces transient thermal stresses. Stresses as high as 500 psi have been attributed to the effect of temperature.<sup>[56]</sup> In recent years, several procedures have been suggested to compute stresses due to temperature effects.<sup>[57]</sup> These stresses are superimposed with the stresses due to dead load, prestressing, and live loads.

Stress measurement using the flat-jack technique is accomplished in several steps discussed in detail in section 5.0, Laboratory Studies. Several hours may elapse between starting of the slitting and the stress measurement by the compensating flat-jack pressure. During this time, the stresses induced by temperature variation may vary. Therefore, it may be difficult to account for transient thermal stresses accurately.



## 5.0 TASK C - LABORATORY STUDIES

The flat-jack technique for measuring stresses in existing bridges is discussed in this section. The equipment required and test procedure are also described. Test variables and laboratory specimens are subsequently detailed. Finally, test results are presented and analyzed.

### 5.1 Flat-Jack Measurement Technique

Based on evaluation of existing techniques to measure stresses in materials outlined in the state-of-the-art survey in section 3.0 and the analyses performed in section 4.0, it was concluded that the most promising technique for measuring stresses in existing prestressed concrete bridges was the flat-jack technique. Abdunur summarized the technique as follows. "It consists of cutting a slot in the concrete, restoring the initial strain field with an ultra fine flat jack and measuring the pressure."

Details of the technique are better understood through a review of the test procedure. The following are the steps used in the stress measurement technique:

1. Location and orientation of the unknown stresses on the structure are determined.
2. The slitting jig is secured to the concrete surface such that the saw blade cuts a slot perpendicular to the selected orientation of the unknown stress.
3. Mechanical gage points are cemented to the concrete surface adjacent to the location of the proposed cut to monitor the strains. At this point a series of initial readings (zero readings) are taken using the gage points and a mechanical gage across the location of the proposed cut.

4. A slot is cut in the concrete to a predetermined depth (equal to the depth of the flat jack) using the saw. The saw blade is then removed from the slot.
5. The appropriate size flat jack is inserted in the slot. A series of mechanical gage readings are then taken and averaged to determine the zero pressure displacement.
6. The flat jack is pressurized incrementally. A series of mechanical gage readings is taken and averaged at each pressure increment.
7. All gage readings of displacements are adjusted as indicated by changes in the standard bar readings. A least-squares linear relationship is then determined from the multiple pressure and corresponding displacement readings. The pressure at which the least-squares line intersects zero displacement is the canceling pressure and corresponds to the initial zero reading.
8. Steps 4 through 7 are repeated for increasing slot depths selected to fit the available flat jacks.
9. The individual canceling pressures are then averaged to obtain the estimated concrete stress.

In Step 1, location and orientation of the slot are determined. The location is normally selected at the point of the required stress, but some modifications may be required to avoid cutting reinforcement. The stress measured with the flat jack is a function of the stress in the direction perpendicular to the slot. Where combined stresses exist, it may be necessary to make preliminary calculations to determine orientation of the principal stresses. If principal stresses are required, it is possible to make two cuts in orthogonal directions. In this case, the slots should not be too close to each other. Care should also be taken to avoid disturbing the strain field in the neighborhood of a slot prior to cutting the slot. When available,

construction drawings can be helpful to determine location and orientation of the slots to avoid cutting any reinforcing steel. However, Abdunur claims that existing stresses can be measured using the flat-jack technique even when reinforcing steel is cut.

In Step 2, the slitting jig is secured to the concrete surface. Details of the slitting jig are given in section 5.2.1. Expansion anchors are used to secure the slitting jig to the concrete. Location and orientation of the slitting jig will correspond with those of the slot.

In Step 3, mechanical gage points are cemented to the concrete surface. Gage points are used with the mechanical gage to measure the deformation across the slot. Optimum location of the mechanical gage points will be discussed later in section 5.4.1. Multiple readings are taken to accurately determine displacements.

The depth of the slot cut during Step 4 corresponds to the size of the flat jack. After a slot is cut, the blade is removed from the slot. In Steps 5 and 6, the flat jack is inserted, along with shims, into the slot. Shims are placed on both sides of the flat jack to reduce the jack expansion during pressurization and to allow easy removal after pressurization. Hydraulic pressure is applied to the jack. This causes change in displacement across the slot. Hydraulic pressure is applied in increments. After each increment, measurements are taken across the slot. The purpose is to determine the pressure in the flat jack that restores the initial reading taken with the mechanical gage. Care is taken not to overpressurize since overpressurization may crack adjacent concrete and disturb displacement readings. The compensating pressure is related to the stress in the concrete at the level of the center of gravity of the flat jack and is determined from a least squares linear regression analysis. To obtain more reliable results, it is necessary to measure the stress at different depths. For this reason, Steps 4 through 7 are repeated. This involves inserting the saw blade back in the slot and cutting a deeper slot. Then the blade is removed and a larger flat jack is inserted. This process can be repeated as many times as

the number of flat-jack sizes. The canceling pressures at various cut depths are then averaged to obtain the estimated concrete stress.

## 5.2 Stress Measuring Equipment

Equipment needed to measure stresses using the flat-jack technique includes:

1. Slitting jig
2. Flat jacks
3. Pfender (mechanical) gage and/or
4. Clip gage

### 5.2.1 Slitting Jig

The slitting jig consists of three main parts that facilitate sawing a slot in increments of depth into a concrete member. The three main parts are the base, the support frame, and the saw blade and motor assembly. The jig also provides for pivoting the cutting blade away from the slot location for stress measurement and then restoring the assembly for further cutting.

The base consists of a U-frame of steel that bolts to the concrete surface at three locations. The pivot is located on one edge of the frame as shown in figure 18.

The support frame consists of a frame, guide rods, and a positioner. The frame holds the guide rods at 90 degrees to the concrete surface. A matching half pivot on one side of the frame connects to the base pivot. A bolt connects the other side of the frame to the base.

The saw blade and motor assembly can be raised or lowered along the guide rods with location established by the positioner screw on the upper part of the support frame. The vernier shown in figure 18 is used to monitor cut

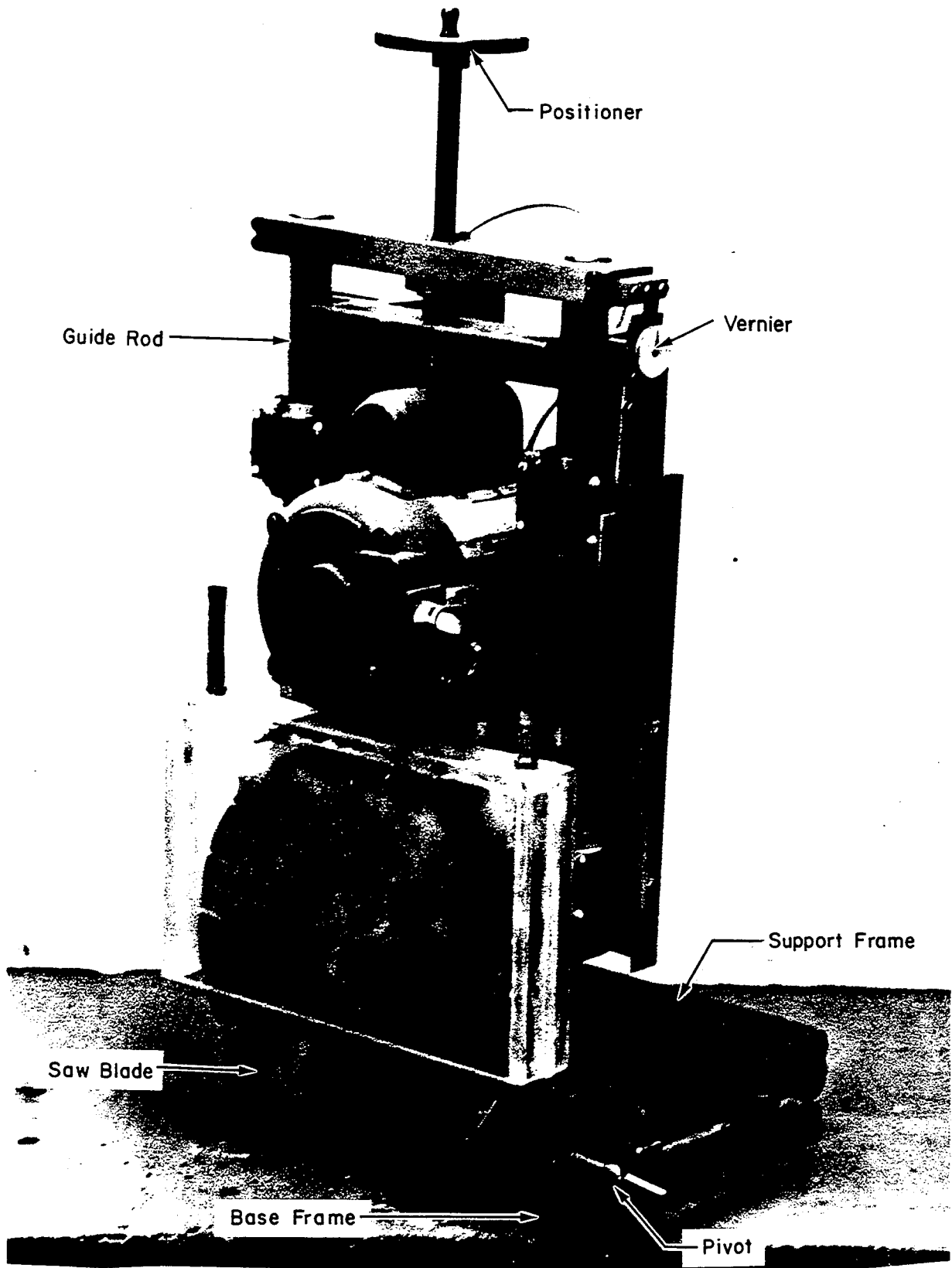


Figure 18. Saw assembly with raised blade.

depth. The raised and lowered positions are as shown in figures 18 and 19, respectively. The saw assembly and support frame can be tilted to one side using the pivot between the frame and the base.

To mount the slitting jig to the concrete surface, a template is used to define locations for three holes to be drilled to secure the slitting jig to the concrete surface. Holes are drilled and the base is bolted to the concrete through expansion anchors. The remainder of the jig is positioned on the base. A pivot pin is inserted on the one side, and a lock bolt is tightened on the other side to complete the mounting.

To lower the blade, the positioner hand wheel is turned to cause the rotating blade to cut a slot to a specified depth. The depth is indicated on a scale attached to the saw assembly. The saw is then raised to bring the rotating blade out of the sawed slot by again turning the positioner hand wheel. The lock bolt is removed and the saw is tilted to one side to provide access for measurement of stress. Further details are given in the User's Manual. [1]

The motor used in the slitting jig is 1.5 hp (1.12 kN.m/s) and uses an electric power supply of 110 volts. A diamond coated blade is used to obtain slots of uniform thickness and precise size to house the flat jack.

### 5.2.2 Flat Jack

The flat jack plays an important role in the direct stress measurement technique. The pressure applied by the flat jack to the walls of the slot is intended to simulate the stress in the concrete. Therefore, the flat jack should be sufficiently flexible to apply a uniform stress to the walls of the slot equal to the pressure in the flat jack. Moreover, the size of the flat jack should be reasonably small to facilitate use on prestressed concrete members.

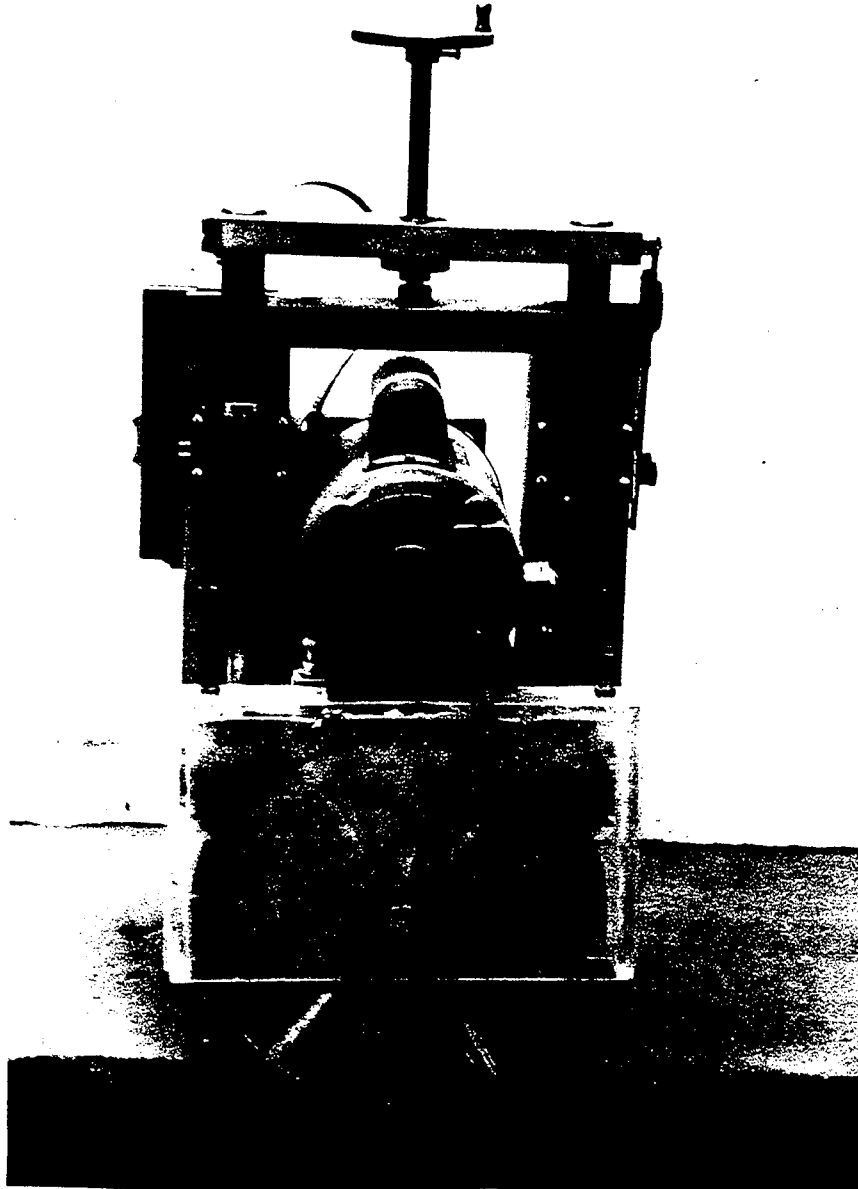


Figure 19. Saw assembly with lowered blade.

Flat jacks, developed for this research project, were manufactured in France. They have been developed over the last few years at the French government laboratory for bridges and highways (Laboratoire Central des Ponts et Chaussees). Details of the flat jacks have been patented in France and Europe, and a patent is pending in the United States.

A photograph of sample flat jacks is shown in figure 20. Dimensions of the flat jacks are given in figure 21. The thickness of the jacks is approximately 4 mm (0.157 in). Each jack consists of two sheet metal plates that are joined with a special weld detail. The two fittings secured to the end of the flat jacks permit air bleeding (bleed valve) and hydraulic pressure application (quick disconnect valve).

Peripheral equipment needed in conjunction with the flat jacks includes a hand pump, a calibrated pressure transducer, and a strain indicator. Hydraulic flat-jack pressure is measured with the calibrated pressure transducer connected to the strain indicator. This equipment is portable and does not require an external power source.

### 5.2.3 Pfender (Mechanical) Gage

The Pfender gage, shown in figure 22, is a mechanical hand-held device to measure displacement. It is manufactured in West Germany and has several features. The gage is sensitive, accurate, compact, and easy to transport. It has the capability of measuring deformations over gage lengths of 20, 40, 60, and 100 mm (0.79, 1.57, 2.36, and 3.94 in). The smallest unit on the dial gage is 0.001 mm (39.4 millionths in). Measurements can be repeated to better than  $\pm 0.0005$  mm (20 millionths in). The maximum range of displacement is  $\pm 0.5$  mm ( $\pm 0.02$  in). A standard bar is included with the Pfender gage to monitor changes in the gage itself.

### 5.2.4 Clip Gage

An electronic, detachable clip gage, as shown in figure 23, is also used to measure slot displacement. The clip gage, when connected to an amplifier



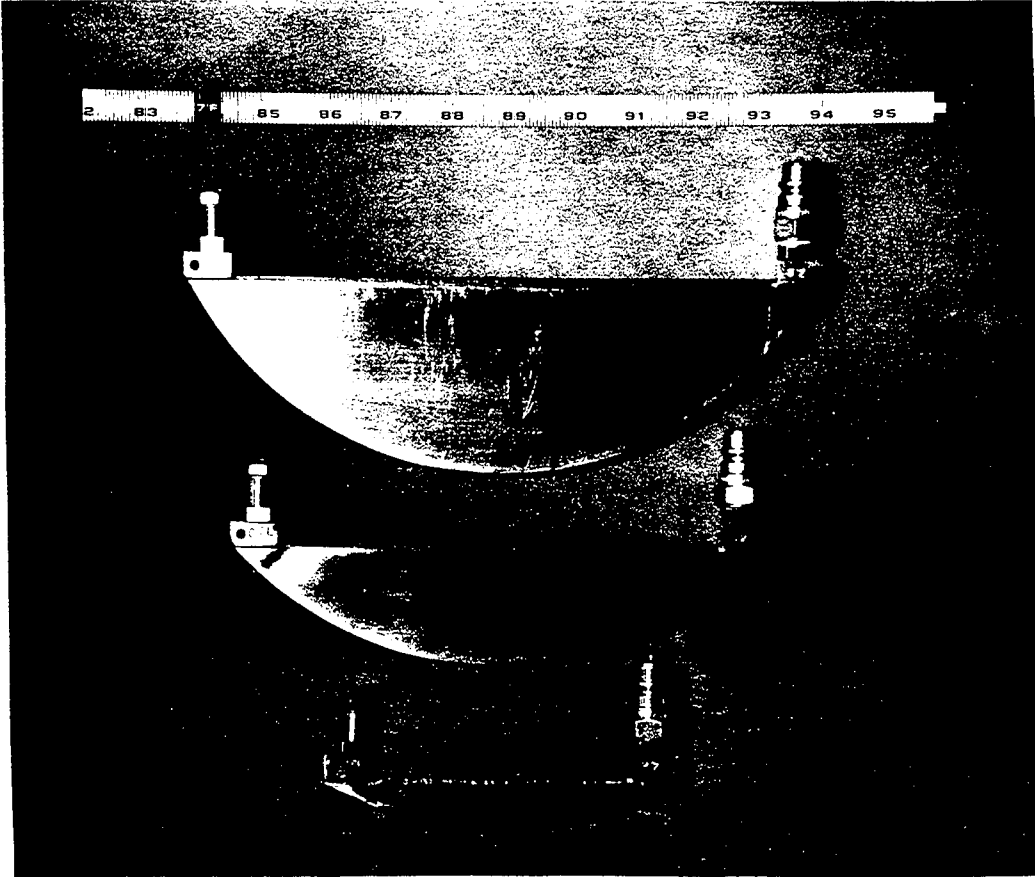


Figure 20. Photograph of flat jacks.

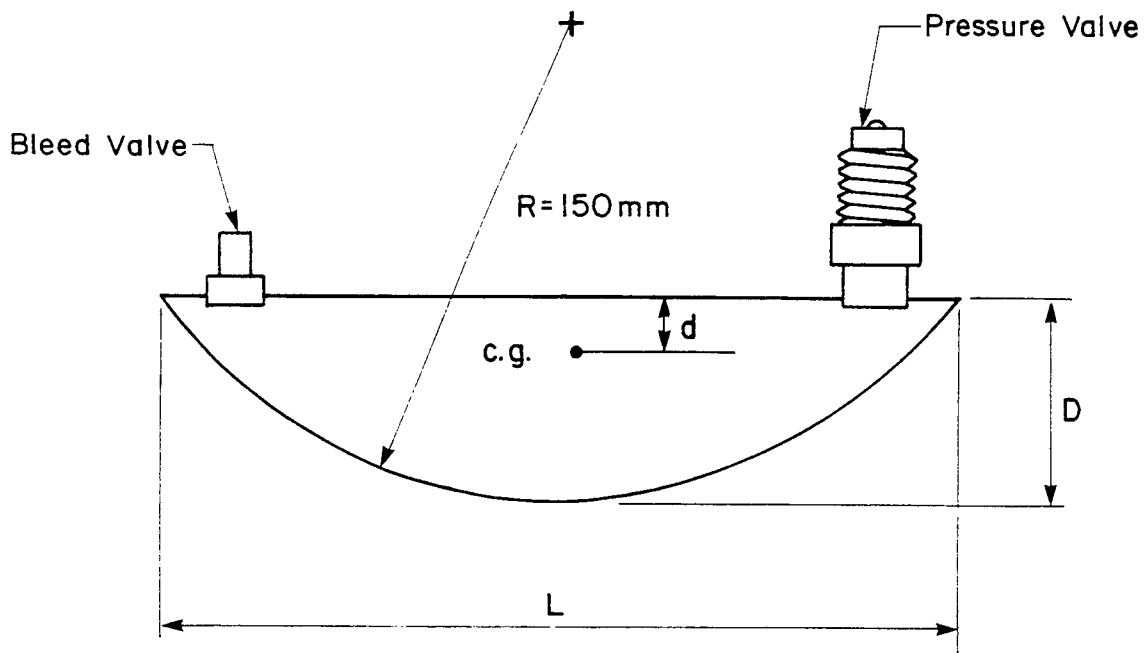


Figure 21. Schematic of flat jacks.

Table 14. Schematic of flat jacks.

D	mm	20	30	40	50	60	70	80
	in	0.79	1.18	1.57	1.97	2.36	2.76	3.15
d	mm	8.3	12.0	16.0	20.4	24.6	28.6	32.9
	in	0.33	0.47	0.63	0.80	0.97	1.12	1.30
L	mm	150	180	204	224	240	254	265
	in	5.9	7.1	8.0	8.8	9.5	10.0	10.5

Metric Equivalent:  
 1 mm = 0.0394 in

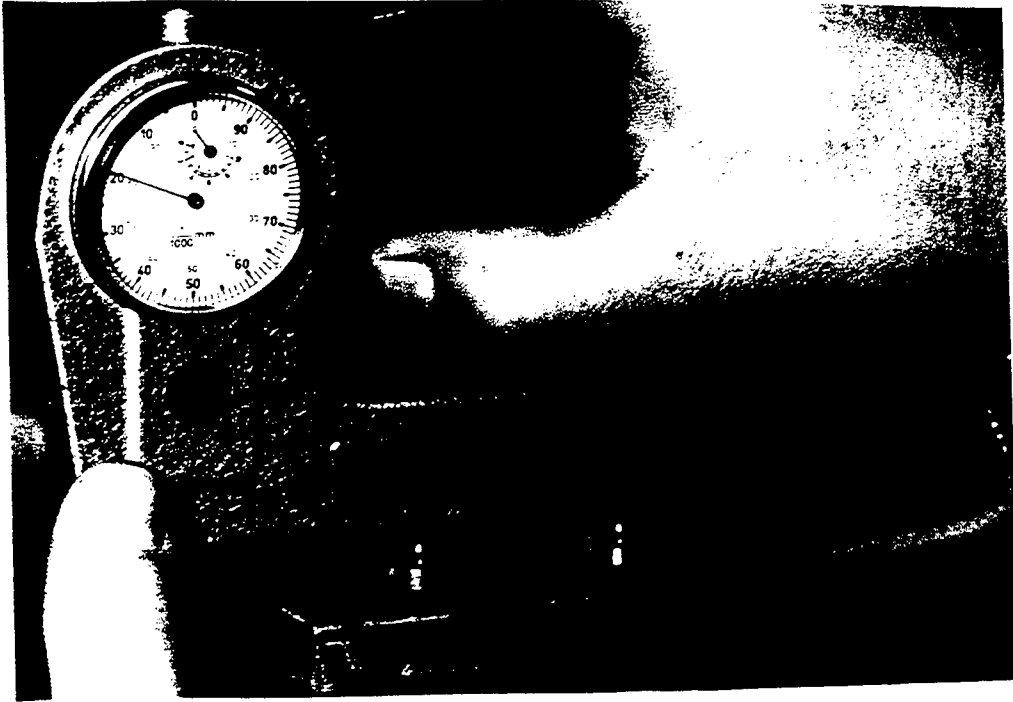


Figure 22. Pfender gage.

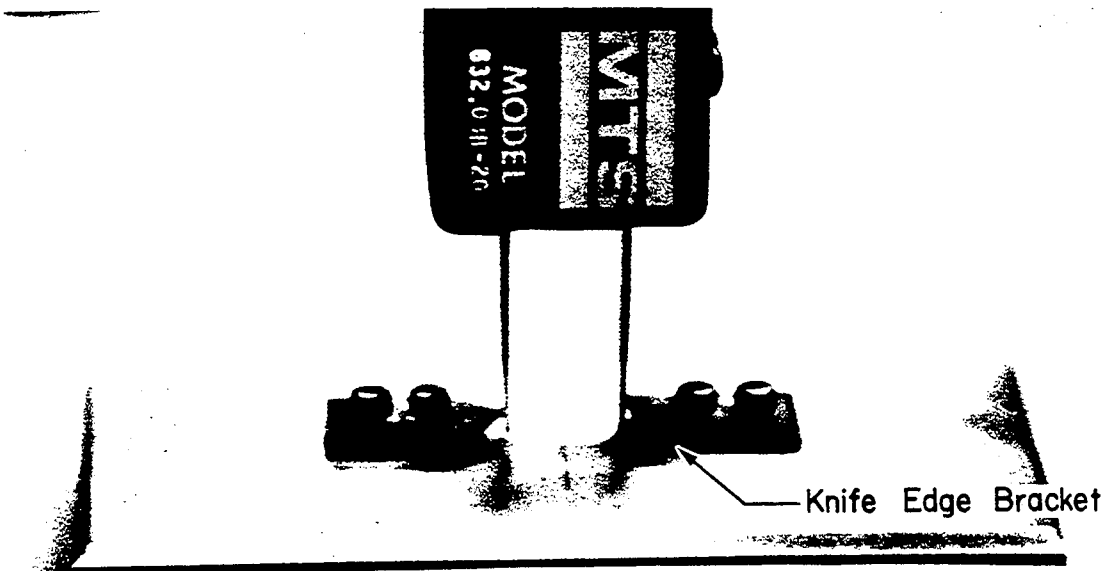


Figure 23. Clip gage.

and plotter, is capable of measuring displacements of 0.001 mm (39.4 millionths in) accurately. The working range of the clip gage used is 0.475 in (12.1 mm) to 0.625 in (15.9 mm). The gage length between the centers of the accompanying knife edges is 1.345 in (34.16 mm).

### 5.3 Laboratory Specimens

The main objectives of the laboratory tests were to experiment with the flat-jack technique of stress measurement and to determine the accuracy of the technique. To achieve these objectives, the following parameters were considered in planning the laboratory test specimens:

1. Plain, conventionally reinforced, and prestressed concrete elements
2. Member thickness
3. Magnitude of stresses
4. Stress distribution

Once laboratory experimentation began, it became apparent that other parameters were variable. These parameters, which will be discussed in detail, include:

1. Individual flat jack characteristics
2. Time effects including creep and creep recovery
3. Stress history of a member

To verify the accuracy of the technique, it was necessary to conduct tests under the simplest controlled conditions. Plain concrete specimens helped achieve a condition of uniform stress. In a conventionally reinforced specimen, stresses are resisted by the concrete and reinforcing steel. In a prestressed member, creep of the concrete plays an important role. Magnitude and distribution of shrinkage stresses in concrete are a function of the member thickness. In practice, a stress gradient exists in prestressed concrete members. Keeping the above parameters in mind, the five specimens shown in figures 24 through 27 were used in the laboratory tests. Details of

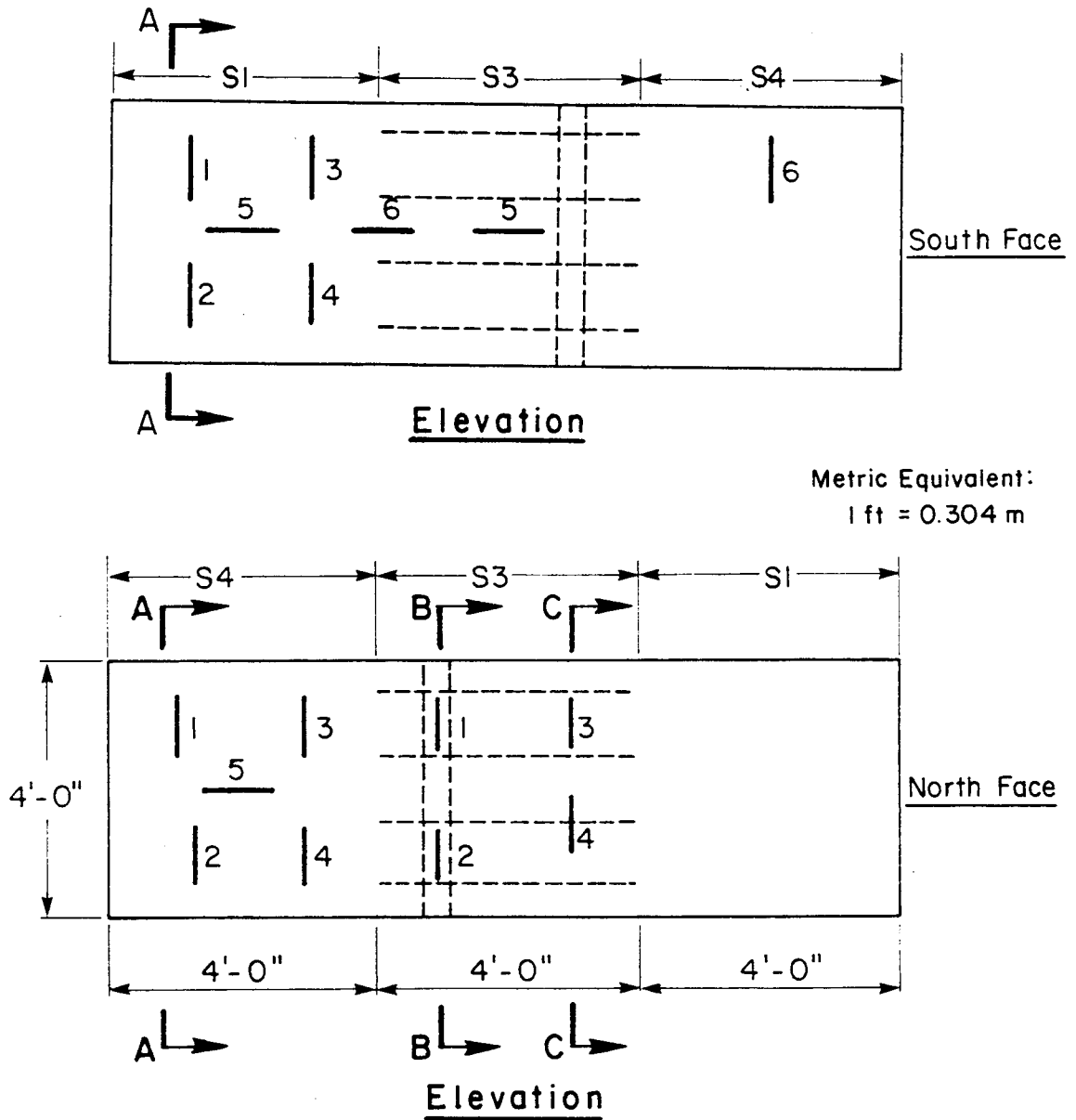


Figure 24. Elevations of Specimens S1, S3, and S4.

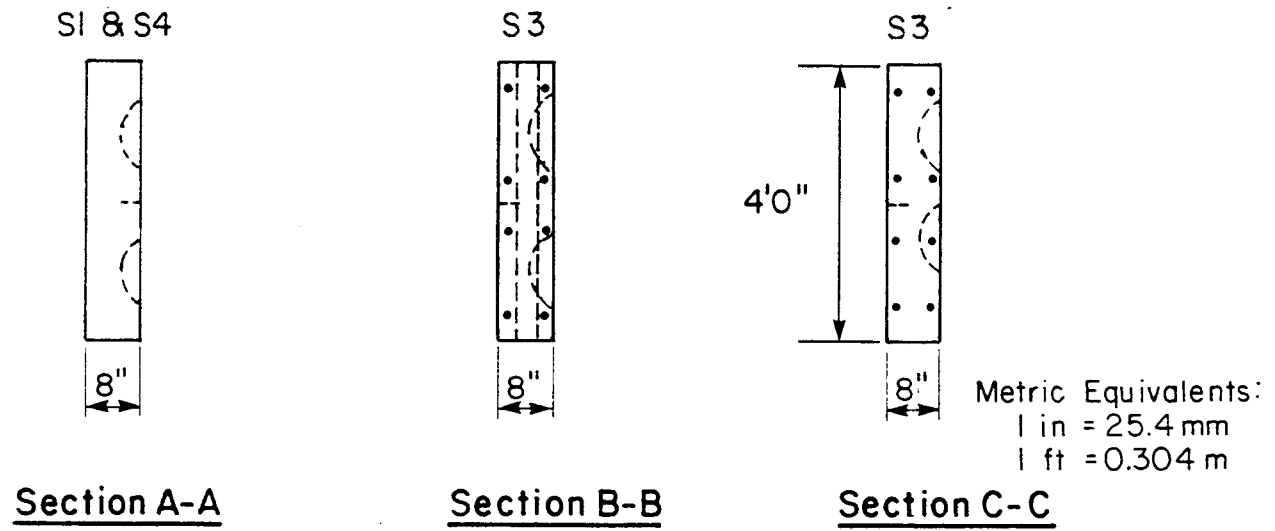
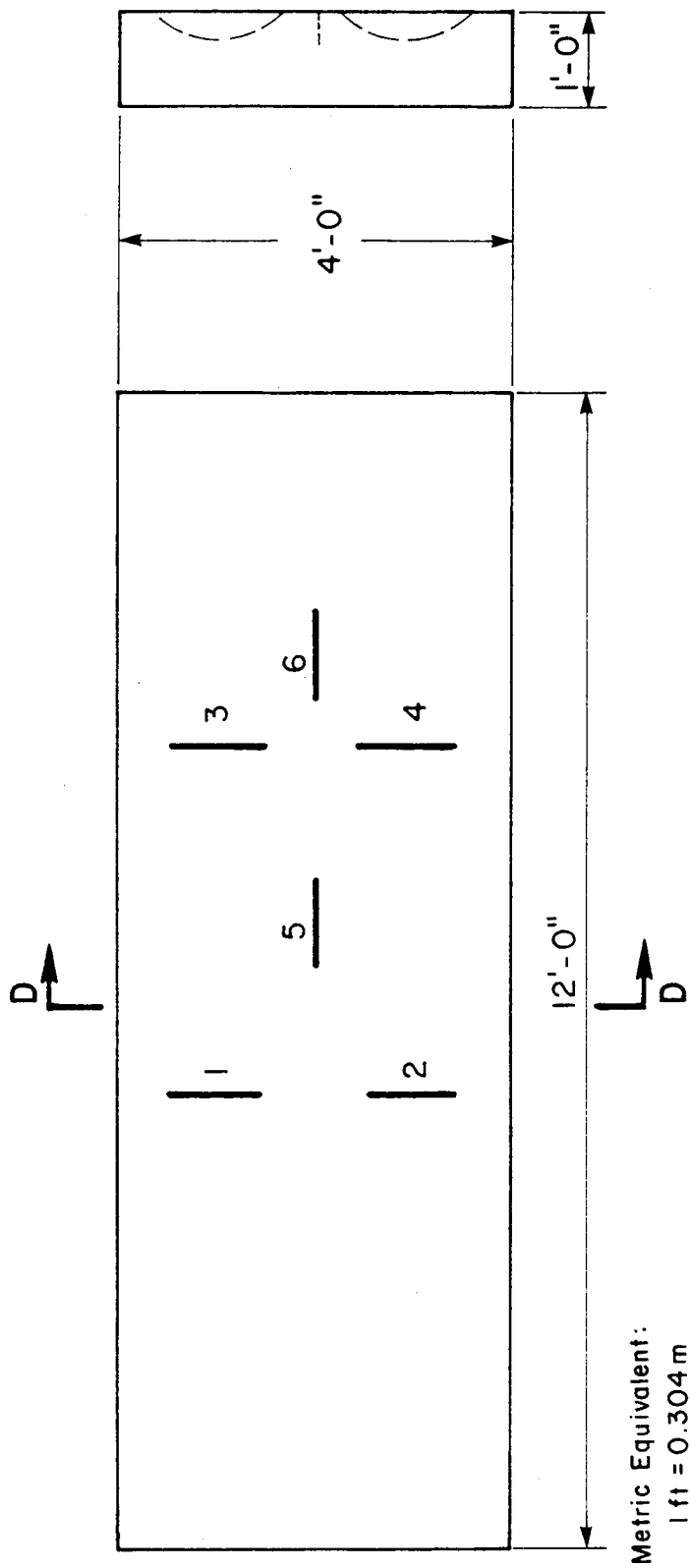


Figure 25. Sections of Specimens S1, S3, and S4.



Metric Equivalent:  
1 ft = 0.304 m

Elevation

Section D-D

Figure 26. Specimen S2.

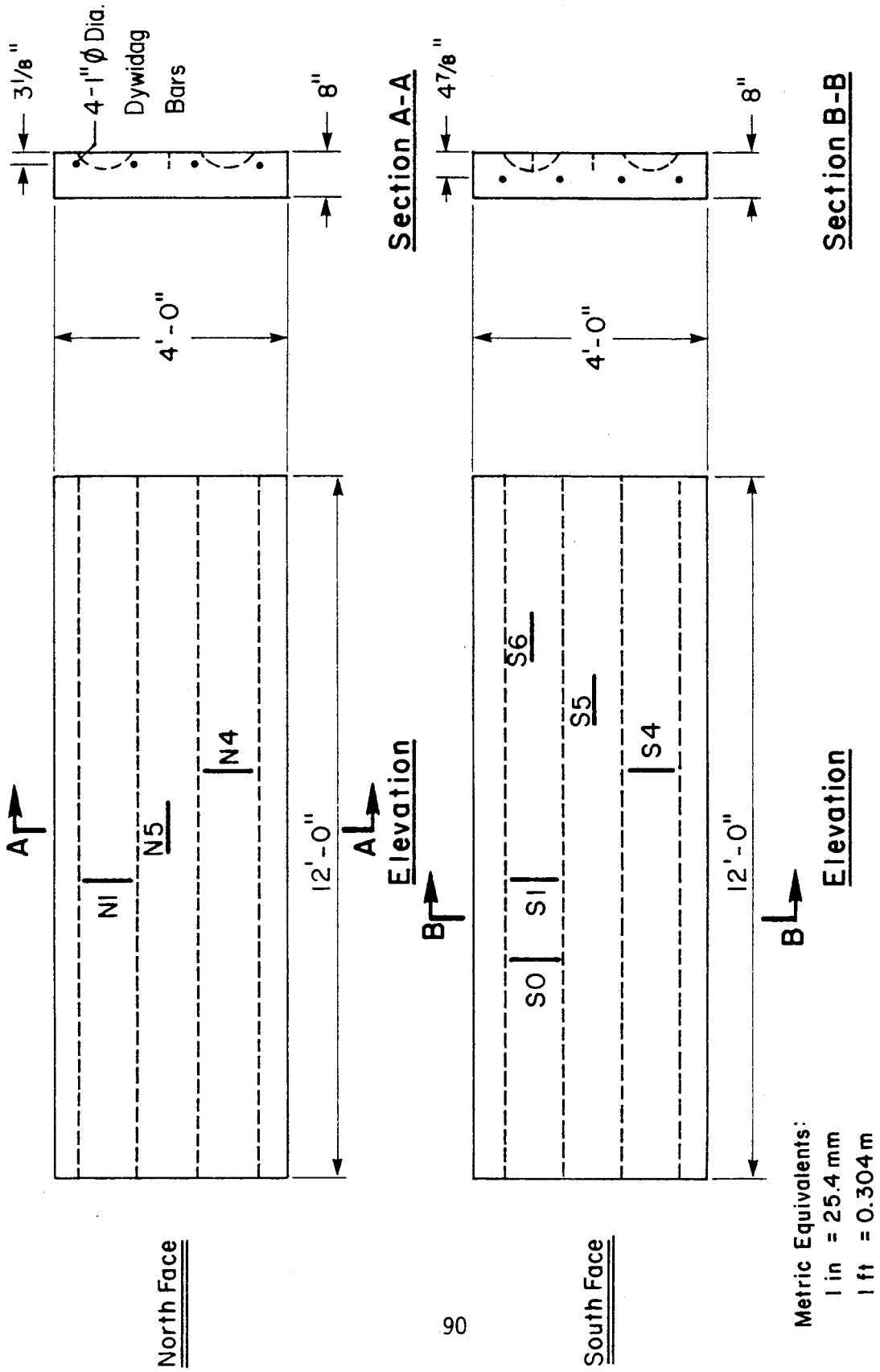


Figure 27. Specimen S5.



each specimen are given in sections 5.3.1 through 5.3.5. Specimens S1, S3, and S4 were incorporated into one concrete block. The target concrete strength for all specimens was 6000 psi (41.3 MPa).

#### 5.3.1 Specimen S1

Specimen S1 was made with 8-in-thick plain concrete. The intent was to determine how well the stress measurement technique predicted uniform internal stresses with no reinforcement present. A target uniform stress of approximately 500 psi (3.45 MPa) perpendicular to the plane of the slot was applied to the specimen while cutting Slots 1 and 4. No stress was applied while Slot 2 was cut. Canceling pressures were determined at 0, 200, 400, and 600 psi (4.14 MPa) at Slot 3. Slot 5, a transverse slot, was cut with a longitudinal applied stress of 500 psi (3.45 MPa).

#### 5.3.2 Specimen S2

Specimen S2 was similar to Specimen S1 except that it was 12 inches thick instead of 8 inches. The purpose of this specimen was to determine if member thickness affects stress measurements. A uniform stress of approximately 500 psi (3.45 MPa) was applied for Slots 1, 2, 3, and 5. A uniform stress of 750 psi (5.17 MPa) was applied for Slot 4. No external load was applied for Slot 6.

#### 5.3.3 Specimen S3

This specimen was similar to Specimen S1 but had No. 6 reinforcement in the vicinity of all slots. The intent was to determine how the presence of reinforcement affected the determination of stress. A uniform stress was applied perpendicular to the plane of Slots 2, 3, and 4. Slots 3 and 4 had only reinforcement orthogonal to the plane of the slot, while Slots 1 and 2 had additional reinforcement parallel to the slots. The reinforcement at Slot 4 was cut to determine the effects of cutting through reinforcement. Slots 5 and 6 had reinforcement parallel to the slots.

#### 5.3.4 Specimen S4

Specimen S4 was similar to Specimen S1 except that the applied force had a transverse eccentricity of approximately 0.85 in (21.6 mm). The purpose of this specimen was to determine how stress gradients affect stress measurements and to determine if the technique was sufficiently sensitive to detect gradients through a member. The result was a transverse stress gradient across the thickness of the specimen.

#### 5.3.5 Specimen S5

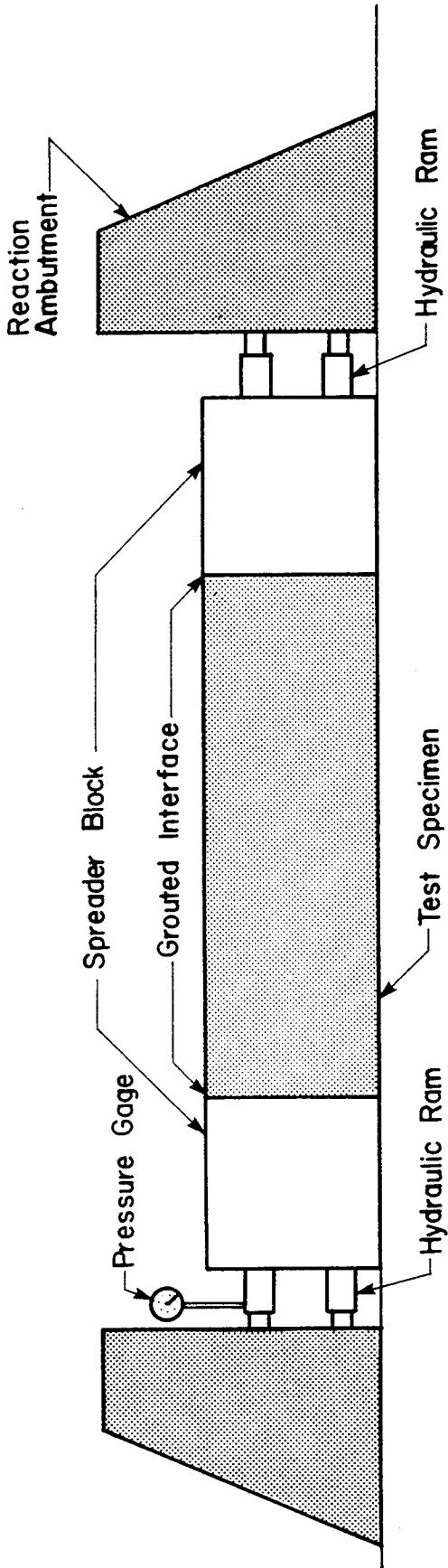
Specimen S5 was used to determine the accuracy of the method in a prestressed member. The prestressing force was eccentric to provide a transverse stress gradient. The gradient produced extreme fiber stress of approximately 450 and 800 psi (3.10 and 5.52 MPa). Load cells were used to monitor prestress force. Slots were cut on both sides of this specimen to determine the accuracy of the technique with positive and negative gradients.

#### 5.3.6 Loading Scheme

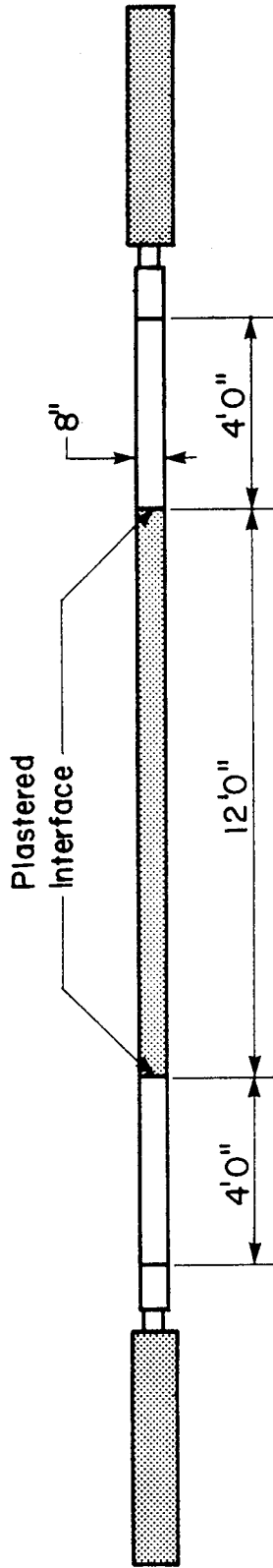
A schematic of how Specimens S1 through S4 were loaded in the laboratory is shown in figure 28. The reaction abutments were stressed to the laboratory floor. Load was calculated from pressure transducer readings. Specimen S5 was post-tensioned with four 1-in-diameter (25.4-mm) Dywidag bars. In all cases, loads were applied at least four hours before cutting slots.

### 5.4 Discussion of Test Results

The flat-jack direct stress measurement equipment and procedures were not well defined at the outset of this research project. As a result, experimentation was required to determine the best equipment and procedures. This section outlines (1) preliminary experimentation with displacement and



Elevation



Plan View

Metric Equivalents:  
 1 in = 25.4 mm.  
 1 ft = 0.304 m.

Figure 28. Schematic of test setup.

cutting equipment, (2) data reduction and analysis procedures, and (3) the results obtained using the recommended equipment and procedures on laboratory specimens.

Stress measurement data for all five specimens are given in section 10.0: Appendix B - Laboratory Test Results. The appendix also includes Pfender readings, linear regression line parameters, and graphs of measured canceling pressures plotted with the applied internal stress.

#### 5.4.1 Slot Displacement

To determine the best displacement measuring device, two types of equipment were tested: a detachable clip gage and a mechanical Pfender gage. The clip gage, when connected to an amplifier and a plotter, along with the pressure transducer, produced a continuous pressure versus displacement plot similar to those shown in figure 29. With the Pfender mechanical gage, displacements were taken at discrete intervals. Note that tensile canceling pressure was determined through extrapolation.

The clip gage measurement technique had several advantages and disadvantages. Continuous pressure versus displacement graphs could be produced quickly, by one person. In addition, canceling pressure could be determined directly from the plots, so data reduction was not required. Electrical drift, the need for extra equipment (that is clip gage, knife edges, amplifier and plotter) and problems with remounting the clip gage consistently on the knife edges were shortcomings of this technique.

An important concept was revealed by use of the clip gage. Plots of canceling pressure versus displacement were always linear when the clip gage was used as the displacement device. A sequence of lines connecting points of canceling pressure versus displacement measured by the Pfender gage often revealed a character other than a linear relationship. Pfender gage data could only be interpreted by a statistical method designed to remove the effect of random errors.

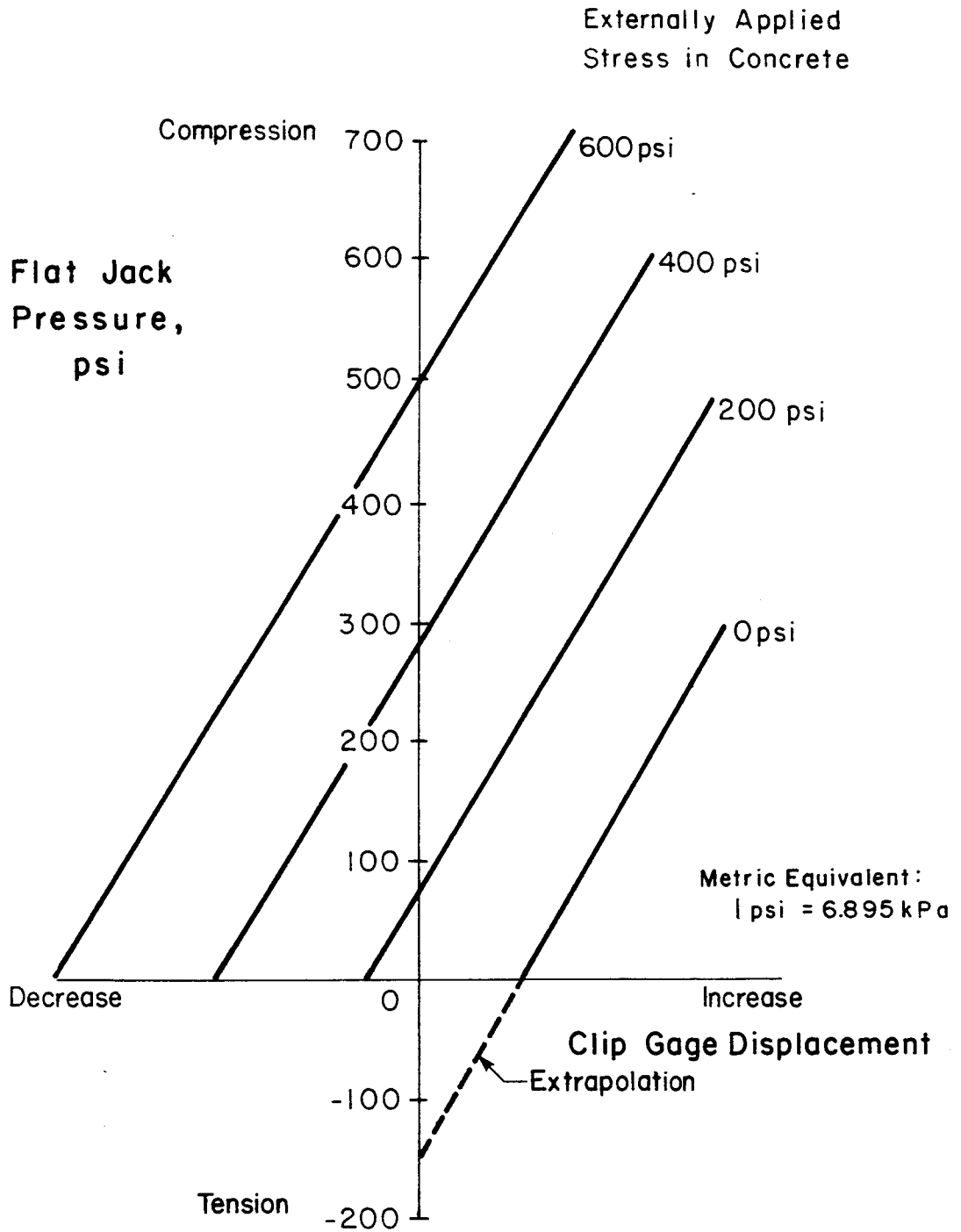


Figure 29. Linear pressure versus clip gage displacement relationship.

Remounting the clip gage inconsistently resulted in erroneous canceling pressures. This problem was overcome by using Pfender points mounted on the knife edges, as shown in figure 30, to determine the zero pressure displacement. Problems with electrical drift between readings were also eliminated with this technique. Speed and the ability to use only one person, which are associated with use of only the clip gage, were sacrificed as a result of use of the Pfender gage in conjunction with the clip gage.

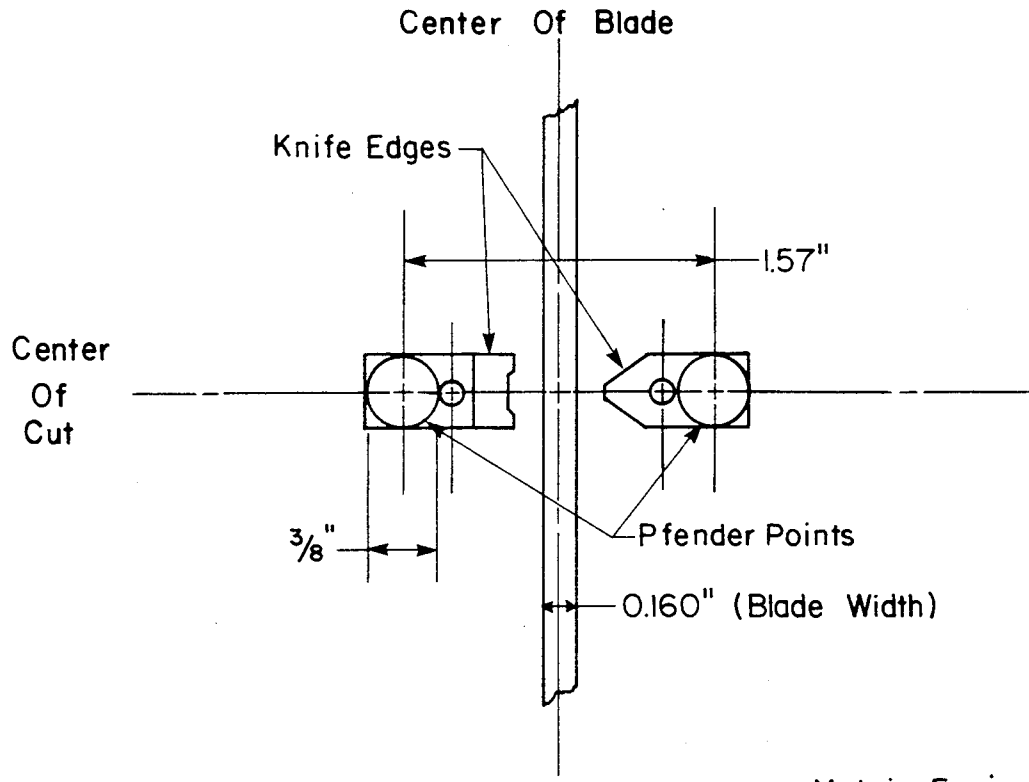
Laboratory experience and anticipated field problems indicated that the Pfender mechanical gage is the best displacement-measuring device. The clip gage requires too much peripheral equipment, including the Pfender gage, to be practical for field and laboratory use. The cycle time for Pfender readings, taken at four pressures, approximated the cycle time for continuous readings with the clip gage.

To determine the optimum Pfender reference point spacing, gage lengths of 20, 40, and 60 mm (0.79, 1.57, and 2.36 in) were used. A gage length of 40 mm (1.57 in) was determined to be optimum. Mounting the Pfender gage on points spaced at 20 mm (0.79 in) was difficult. The gage was unstable in tight quarters at this gage length. Points located 60 mm (2.36 in) apart were not sufficiently sensitive at most cut depths. The Pfender gage could be used comfortably, and the points were sufficiently sensitive at a spacing of 40 mm (1.57 in).

To increase the data base and to reduce sampling error, the Pfender point layout included two sets of reference points (4 points) as shown in figure 31. When two sets of measurements were taken on a slot (two sets of Pfender points or one set of Pfender points and one set of knife edges) the results were seldom identical, reflecting experimental scatter and effects of point spacing and location.

#### 5.4.2 Effects of Mineral Oil Coolant

Initial trial cuts were made using mineral oil as coolant. Figure 32 shows the flat jack canceling pressures plotted at the centroid of the



Metric Equivalent:  
1 in = 25.4 mm

Figure 30. Knife edge orientation.

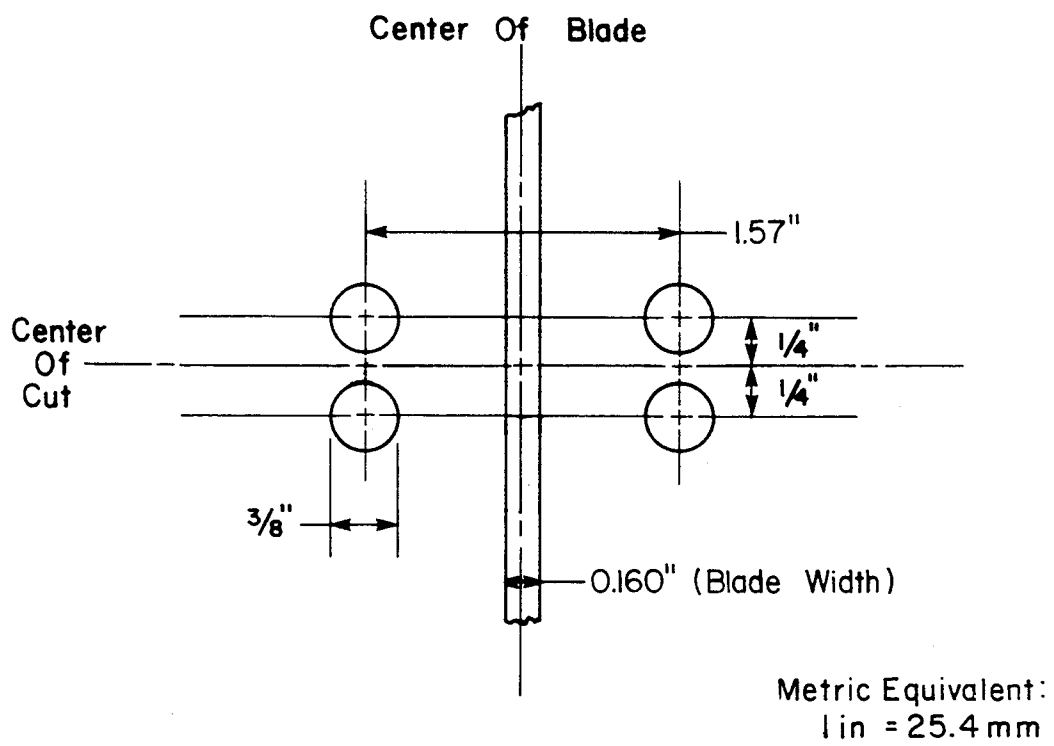
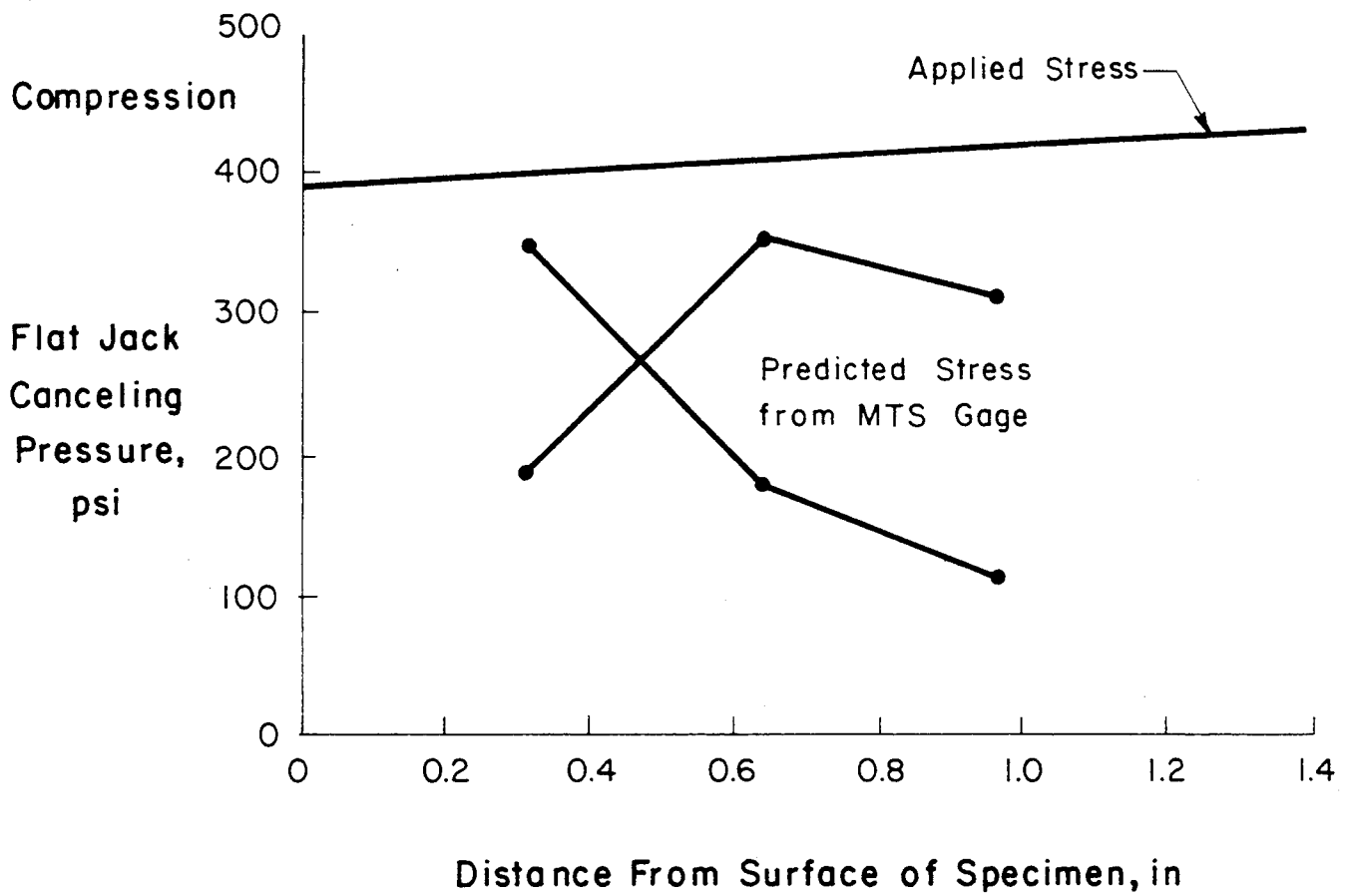


Figure 31. Pfender point layout.





Metric Equivalents:  
 1 in = 25.4 mm  
 1 psi = 6.895 kPa

Figure 32. Lubricated cut stress profile.

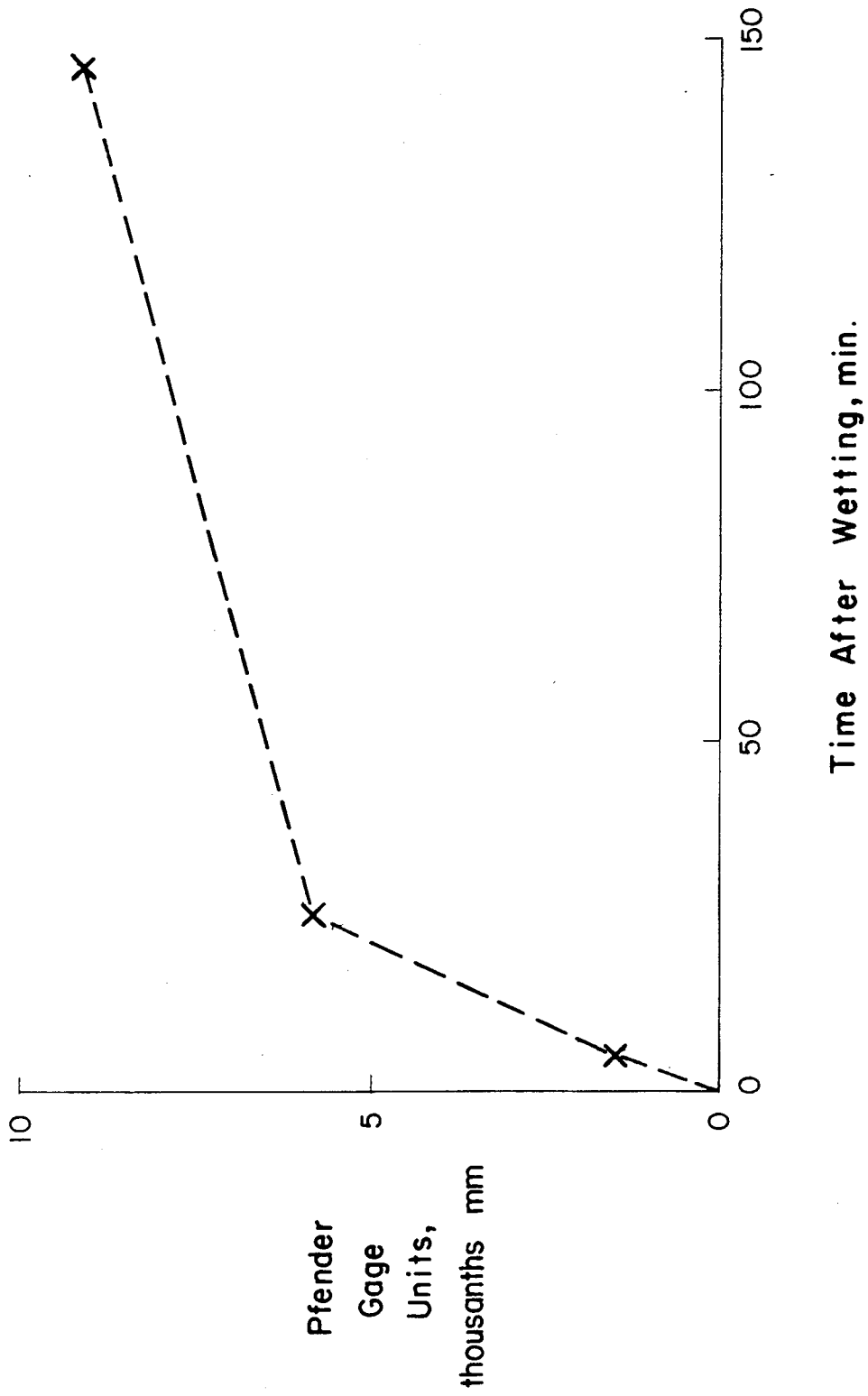
corresponding jacks and indicates the scatter between results of two slots sawn with the coolant. The slots were cut into concrete with the same applied stress level. The scatter is probably the result of swelling due to wetting of the concrete adjacent to the cuts. Eighty millimeter readings could not be taken on either cut because of loosened instrumentation. To determine how moisture affects slot displacement, an 80-mm (3.15-in) slot was soaked with water. Pfender gage readings were taken before and at 5, 25, and 145 minutes after wetting. Figure 33 shows the results of this experiment and indicates that moisture significantly affects displacement.

As a result of the problems associated with coolant cutting, all slots reported in the Task C test specimens were sawn without lubricant. Some increase in concrete temperature adjacent to the cuts was noted using the "dry" cutting technique, but initial trial cuts indicated that this temperature increase was generally less than 10°F (6°C).

#### 5.4.3 Data Reduction

The clip gage plots indicated a linear pressure versus displacement relationship, therefore a linear regression analysis was used to interpret Pfender gage results. The tables of linear regression parameters in section 10.0 indicate results of the linear regression analysis. The slope is related to the concrete modulus of elasticity. A unique slope exists at each cut depth for a given modulus. The Y-intercept indicates the canceling pressure. The correlation coefficient is a measure of "fit." This value varies from -1.0 to 1.0, with 1.0 being an exact positive fit or correlation and -1.0 being an exact negative fit, that is one variable moves opposite to the other variable. The large number of correlation coefficients that are approximately equal to 1.0 indicates that a linear relationship is appropriate. Values less than 0.95, which include many 20-mm cut results, are unreliable.

Calculation of concrete stress from canceling pressure assumes homogeneous behavior of the material near the slot. Surface stresses which produce



Metric Equivalent:  
1 mm = 0.039 in

Figure 33. Effect of moisture on slot displacement.

micro-cracking will destroy this homogeneity near the surface. As a result, shallow cuts often give invalid results.

The last parameter listed in the tables of section 10.0 is the standard error of estimate. This value is another indicator of correlation. The larger the number, the poorer the fit or correlation.

#### 5.4.4 Data Analysis

The measured flat-jack canceling pressures include the effects of shrinkage, creep, and peculiarities associated with each flat jack. Figures 34 and 35, which summarize all the vertical cut data from section 10.0, indicate that the measured canceling pressures are consistently lower than the applied concrete stress. The sloping line in figure 34 represents exact correlation between the two values. The cumulative frequency shown in figure 35 also shows the skewed distribution. To determine if the difference between measured and applied stress is a function of the applied stress, clip gage readings were taken on a slot at four different stress levels.

Figure 36, which summarizes data from section 10.0, indicates that the flat-jack technique accurately measures changes in applied stress. The graph shows canceling pressure at the centroids of the 20-, 40-, 60-, and 80-mm (0.79-, 1.57-, 2.36-, and 3.15-in) flat jacks for four applied stress levels. These results were obtained by making a cut to the desired depth, inserting the appropriate flat jack, and determining the canceling pressure. The applied stress was then increased 200 psi (1.38 MPa) and the canceling pressure was again determined. Two hundred psi increments were added until 800 psi (5.52 MPa) was reached. After canceling pressure was determined at all applied stresses for a given flat jack, the jack was removed and a deeper cut was made. The process continued at a unique slot until all four flat jacks had been used. This procedure was similar to the procedure used by Abdunur in that he cut slots prior to application of load "to eliminate internal stresses and offer a straightforward test of the release method." This procedure was helpful in the laboratory to verify Abdunur's technique

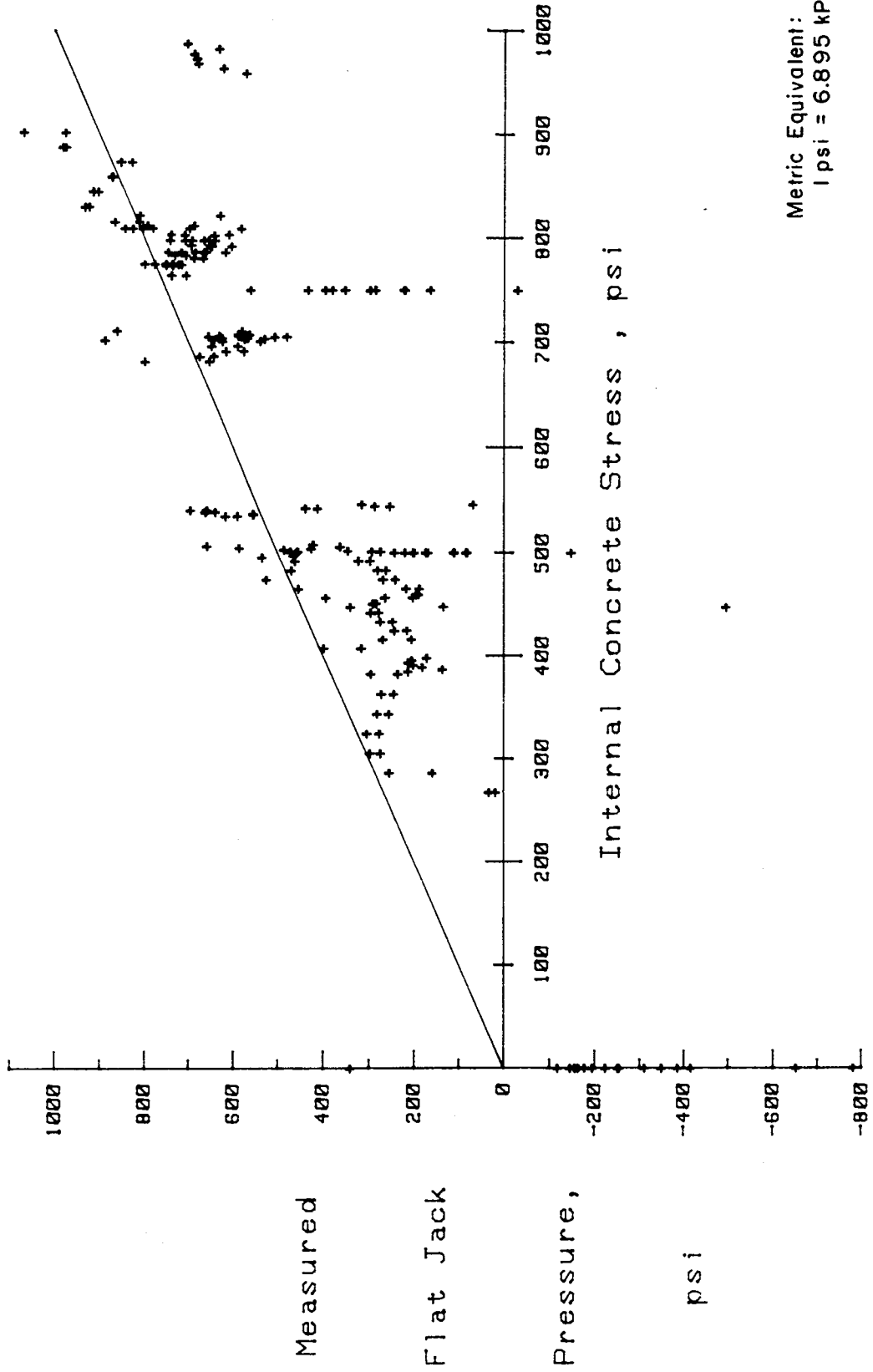
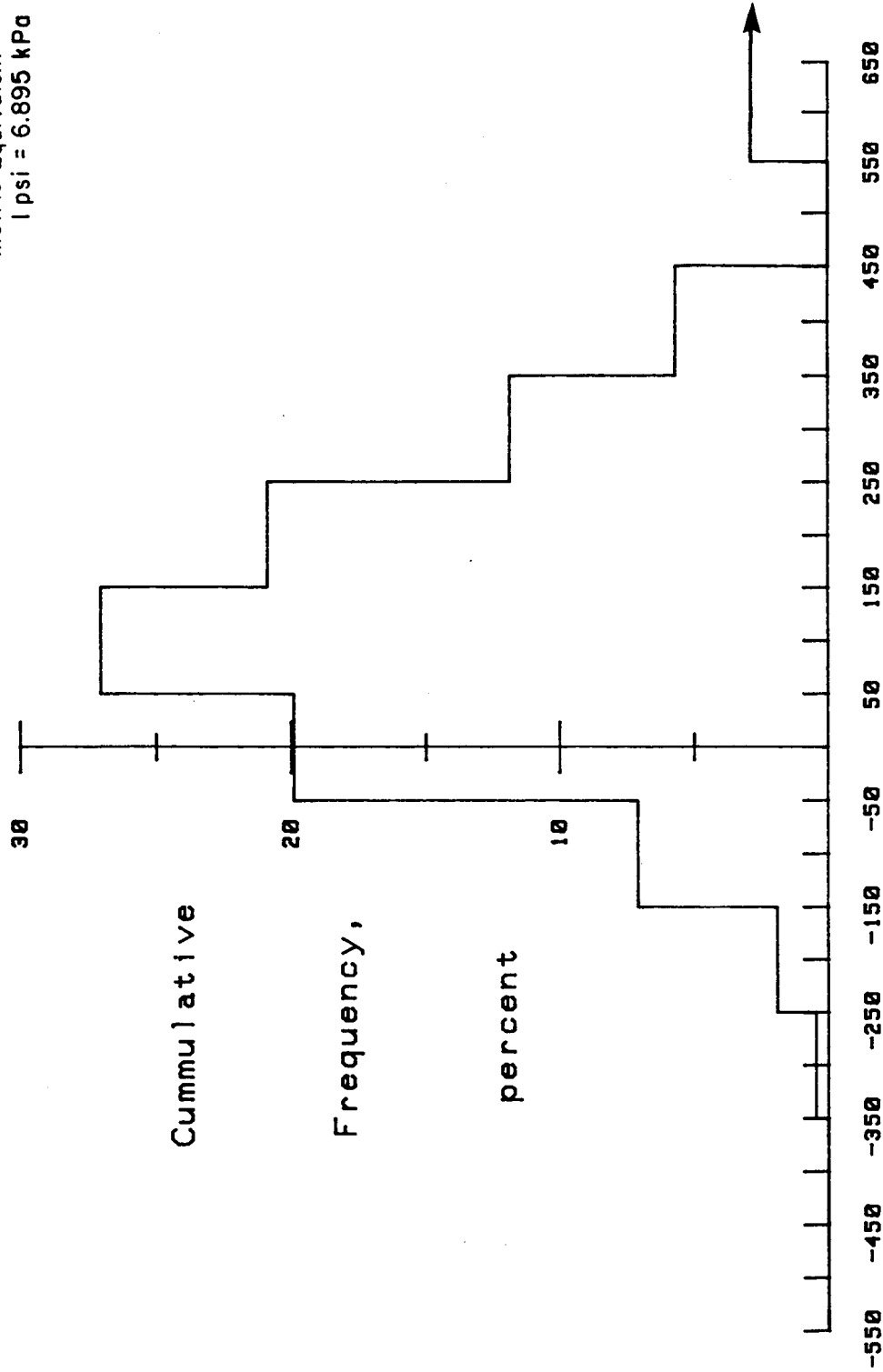


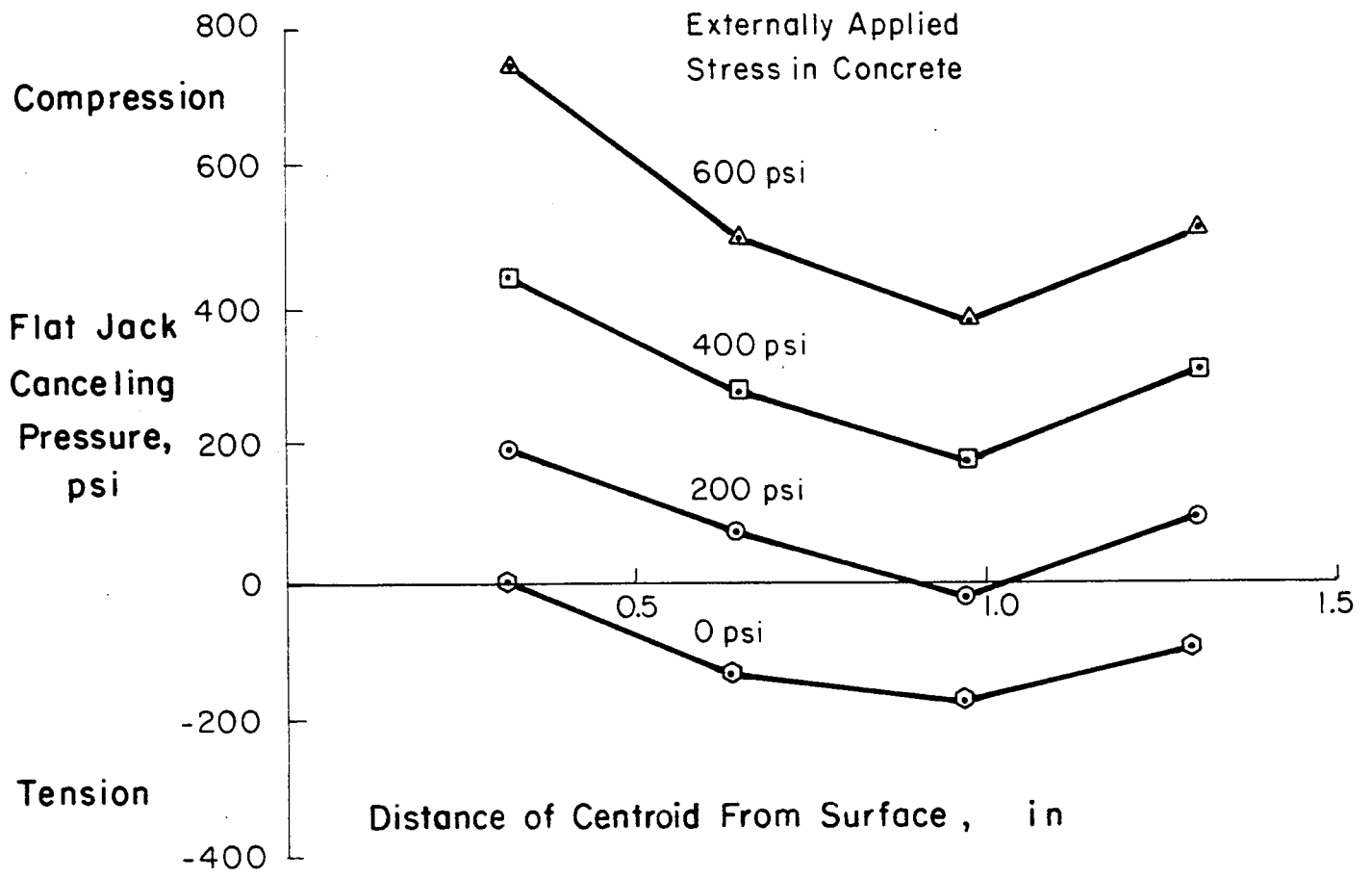
Figure 34. Uncorrected results of specimen cuts.

Metric Equivalent:  
1 psi = 6.895 kPa



Difference Between Applied And Measured Stress, psi

Figure 35. Distribution of uncorrected canceling pressures.



Metric Equivalents  
 1 in = 25.4 mm  
 1 psi = 6.895 kPa

Figure 36. Canceling pressures at various applied stresses.

but is unrealistic for field applications. Prestressed bridge members will be stressed long before measurements are taken.

#### 5.4.5 Multiple Variant Linear Regression Analysis

A multiple variant linear regression analysis was performed on all data from vertical slots with 40-mm (1.57-in) Pfender point spacing. The dependent variables included: longitudinal and transverse canceling pressures. The results of the regression analyses for all slot depths are shown in table 15. Also shown in this table are analyses for combined data and for combined data exclusive of the 20-mm (0.79-in) cut results. The 20-mm cut data were excluded because of microcracking problems discussed in section 5.4.3. The multiple correlation for the combined equation, 30 through 80 mm (1.18 through 3.15 in), when compared to the individual values, indicates that segregation by slot depth is not warranted. Table 16 shows the accuracy of the combined equation for all 30 to 80 mm cuts (1.18 to 3.15 in). The table indicates a 90 percent confidence level at  $\pm 200$  psi (1.38 MPa).

As experimentation progressed, the laboratory technician became more skilled and important variables were controlled as much as possible. Accordingly, stress measurements became more accurate. The multiple correlation values for the last two equations in table 15 indicate better correlation for the later specimens. (Specimen 2 was tested first, then Specimens 1, 3, 4, and 5). The equations indicate that transverse canceling pressures influence the calculated stress value only slightly.

Based on the results of laboratory experimentation, with applied concrete stresses from zero to 1000 psi (0 to 6.90 MPa), the following equation is recommended to determine concrete stress from canceling pressures:

$$\text{Concrete Stress (psi)} = 200 \text{ psi} + 0.80 \times \text{Longitudinal Canceling Pressure (psi)} \quad (10)$$

$$\text{Concrete Stress (kPa)} = 1378 \text{ kPa} + 0.80 \times \text{Longitudinal Canceling Pressure (kPa)}$$



Table 15. Results of multiple linear regression analyses.

Slot Depth mm	Specimens Considered	Number of Points	Concrete Stress* psi	Multiple Correlation
20	1-5	36	$424 + 0.47xA + 0.05xB$	0.635
30	1-5	24	$276 + 0.76xA + 0.11xB$	0.879
40	1-5	36	$415 + 0.66xA + 0.26xB$	0.711
50	1-5	24	$103 + 0.84xA - 0.27xB$	0.830
60	1-5	36	$309 + 0.70xA + 0.11xB$	0.754
70	1-5	24	$220 + 0.72xA - 0.04xB$	0.890
80	1-5	31	$311 + 0.61xA$	0.722
20-80	1-5	211	$335 + 0.63xA + 0.07xB$	0.721
30-80	1-5	175	$310 + 0.70xA + 0.12xB$	0.772
30-80	1, 3, 4, 5	158	$208 + 0.77xA - 0.03xB$	0.872
30-80	4, 5	118	$195 + 0.81xA - 0.03xB$	0.897

\*A = Longitudinal Canceling Pressure  
 B = Transverse Canceling Pressure

Metric Equivalents:  
 1 mm = 0.0394 in  
 1 psi = 6.895 kPa

Table 16. Cumulative frequency data for combined equation.

Error Range ± psi	Number of Points	Percentage of Points
25	43	25
50	81	46
100	125	71
150	144	82
200	158	90
250	168	96
300	172	98
350	173	99
400	174	99
500	175	100

$$\text{Concrete Stress (psi)} = 310 + 0.70 \times \text{Longitudinal Canceling Pressure} + 0.12 \times \text{Transverse Canceling Pressure}$$

Note: Table includes all 30- through 80-mm (1.18- through 3.15-in) slot data.

Metric Equivalent:  
1 psi = 6.895 kPa

The constant of 200 psi (1.38 MPa) represents shrinkage and creep stresses which existed at all times. The 0.8 coefficient for longitudinal canceling pressure indicates that the measured flat-jack pressure is greater than the applied concrete stress. Testing of flat jacks in a testing machine, which is discussed in section 5.4.6, confirmed that in most cases flat-jack pressure is not equal to the applied stress.

The 90 percent confidence level for the recommended equation used for the 30- through 80-mm (1.18- through 3.15-in) cuts on Specimens 4 and 5, is at  $\pm 125$  psi (0.86 MPa), which is significantly more accurate than the equation which considered all the data. Table 17 summarizes the results of the recommended equation. Figure 37 shows the corrected stress plotted versus the internal stress for the data considered in table 17. Figure 38 shows the distribution of these data.

The centroids of flat jacks range in depth from 0.33 to 1.30 in (8.3 to 32.9 mm). In this 0.97-in (24.6-mm) change in depth, stresses typically vary by 100 psi (0.69 MPa) or less. As a result of this fact and the 90 percent confidence level of  $\pm 125$  psi (0.86 MPa), stress gradients could not be determined accurately.

In light of this, the data was reanalyzed using an average applied stress and average canceling pressure for each data set. With 22 resulting data points, the 90 percent confidence level was at  $\pm 90$  psi (0.62 MPa). The 95 percent confidence level was at  $\pm 100$  psi (0.69 MPa).

A final analysis was performed combining the results from the top and bottom sets of Pfender readings. Again the 90 percent confidence level was at  $\pm 90$  psi (0.62 MPa). A word of warning is warranted at this time. As the data base was reduced from over 100 points to 22 points and finally 10 points, the impact of individual points became significant. That is, one or two scattered points could change the distribution significantly. This must be kept in mind when these reanalyses are considered.

Table 17. Cumulative frequency data for recommended equation.

Error Range ± psi	Number of Points	Percentage of Points
100	95	81
105	99	84
110	101	86
115	104	88
120	104	88
125	106	90
130	108	92
135	109	92
140	109	92

Concrete Stress (psi) = 200 psi + 0.80 x Longitudinal Canceling Pressure

Note: Table includes all 30- through 80-mm (1.18- through 3.15-in) slot data for Specimens 4 and 5.

Metric Equivalent:

1 psi = 6.895 kPa

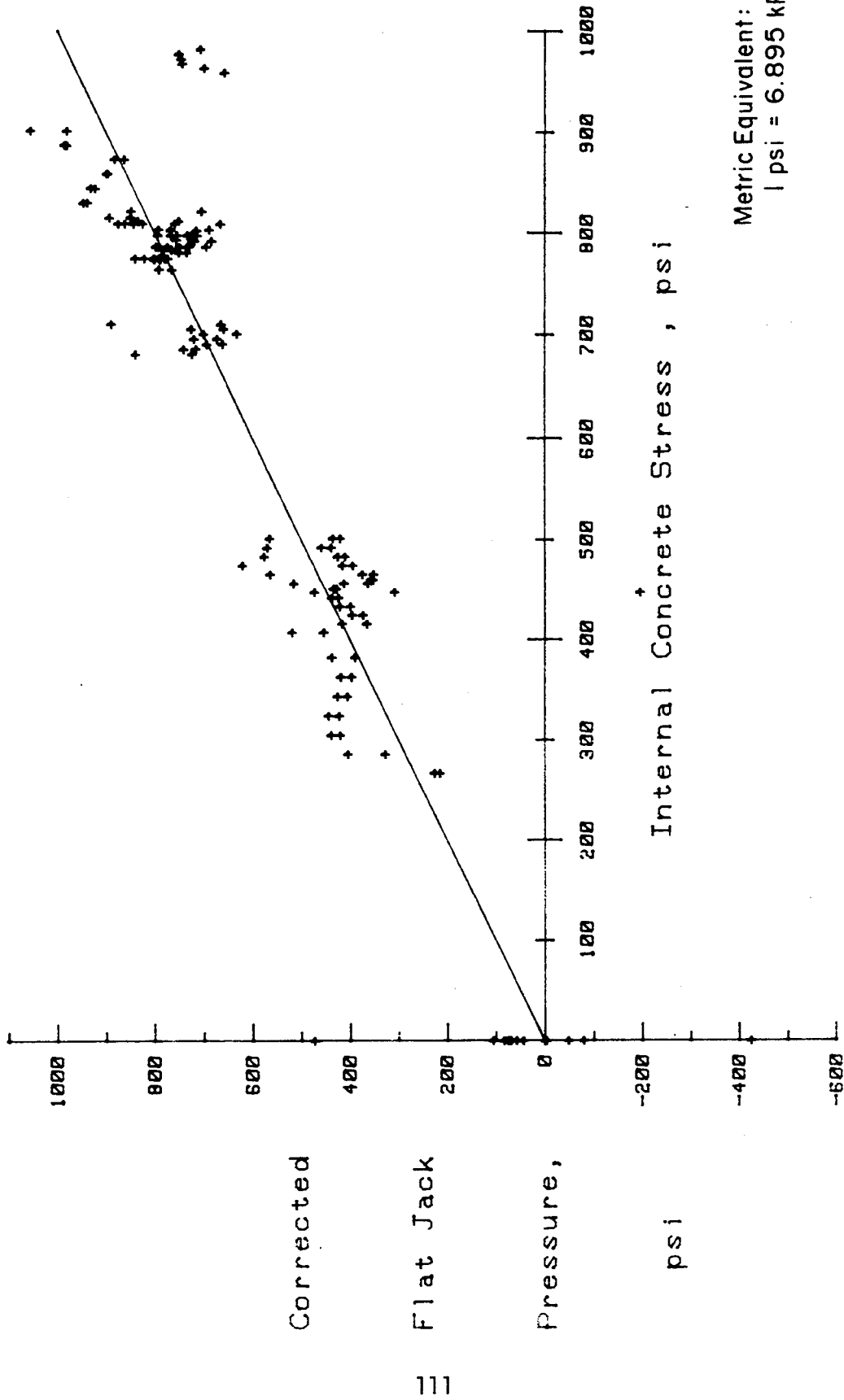
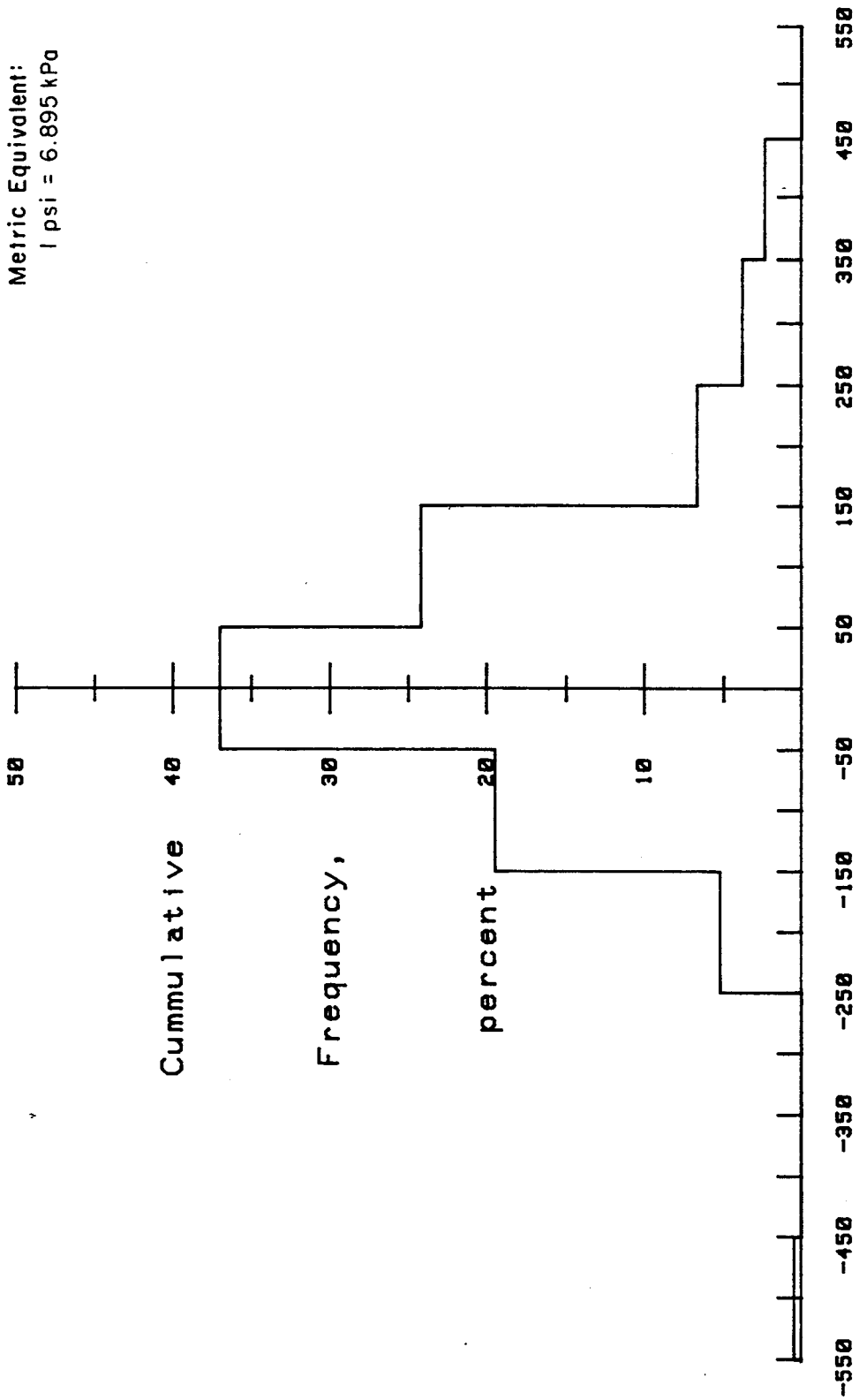


Figure 37. Corrected results of 30-to 80-mm cuts on Specimens S4 and S5.

Metric Equivalent:  
1 psi = 6.895 kPa



Difference Between Applied And Measured Stress, psi

Figure 38. Distribution of corrected concrete stress.

#### 5.4.6 Variables Affecting Canceling Pressures

The main purpose of Task C was to verify the flat-jack measurement technique. During the verification process, it became apparent that several unconsidered variables affect canceling pressures. These variables included:

1. Individual flat-jack characteristics
2. Time between completion of cutting and flat-jack pressurization
3. Length of time specimen is loaded
4. Stress gradient
5. Presence of reinforcing steel
6. Characteristics of individual flat jacks

##### 5.4.6.1 Individual Flat-Jack Characteristics

Three sets of flat jacks were available for testing purposes. A complete set of jacks (20, 30, 40, 50, 60, 70, and 80 mm [0.79, 1.18, 1.57, 1.97, 2.36, 2.76, and 3.15 in]) was typically used to determine concrete stresses. The 20-, 40-, 60-, and 80-mm (0.79-, 1.57-, 2.36-, and 3.15-in) jacks from the three sets of flat jacks were compared on a single member with no applied stress. Figure 39 indicates a scatter of 50 psi (0.34 MPa) for the 40-, 60-, and 80-mm (1.57-, 2.36-, and 3.15-in) cuts. The 130 psi (0.90 MPa) range for the 20-mm (0.79-in) cut confirms the inconsistency of shallow cuts as a result of the overly sensitive nature of the 20-mm jacks due to surface stresses and microcracking.

##### 5.4.6.2 Time Between Completion of Cutting and Flat-Jack Pressurization

The interval of time between completion of cutting and flat-jack pressurization influences canceling pressures. Figure 40 shows measured canceling pressure 0, 10 and 40 minutes after completion of slot cutting. In general, the canceling pressures increased with time, but previous delays did not seem to affect subsequent deeper cuts at the same location. Since the data base and data analysis equation in section 5.4.5 were based on

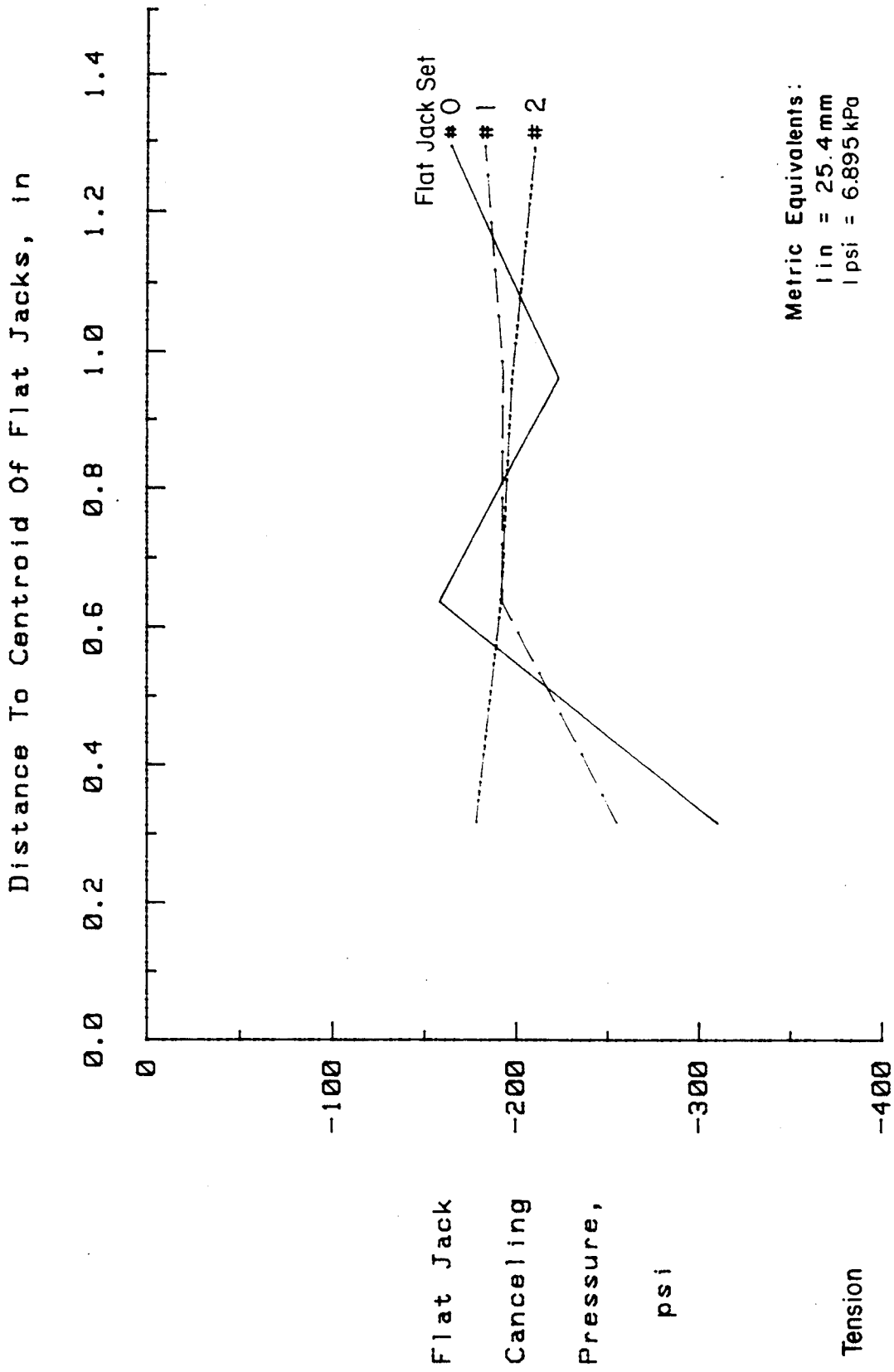


Figure 39. Effect of flat jacks on stress distribution for Specimen S2.



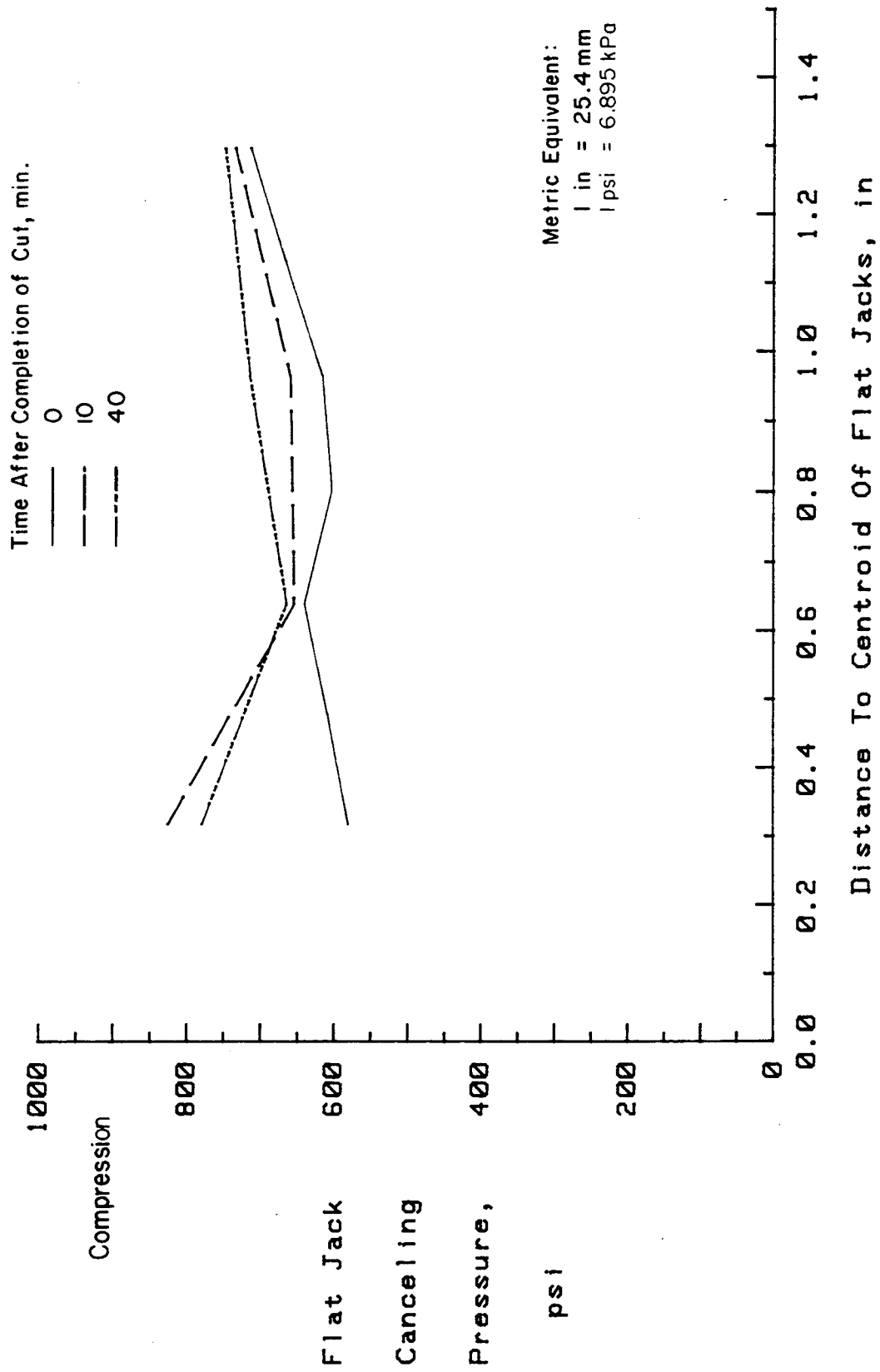


Figure 40. Effect of time on stress distribution for Specimen S5 Slot N1.

virtually no time lag between cutting and flat-jack pressurization, this procedure should be followed to increase the accuracy of results.

#### 5.4.6.3 Length of Time Specimen is Loaded

Figure 41 shows the results of stress measurements taken before application of any external load to the specimen and after load had been applied, maintained, and subsequently removed. Both curves are for vertical cuts, and indicate that time effects are important. With no creep and shrinkage the stress profiles should be at zero. The differences between these stresses is greater than that expected from experimental scatter, so the differences are significant. In general, the measured canceling pressures increased after application of load. This is an important observation for laboratory studies, but since most bridge structures will be stressed when measurements are taken, this should not affect the results.

#### 5.4.6.4 Stress Gradient

Stress gradient influences transverse as well as longitudinal canceling pressures. Figure 42 shows the measured transverse canceling pressures on both sides of Specimen 5. In general, the figure indicates that transverse canceling pressure increases with longitudinal stress. If a relationship is determined between transverse canceling pressure and longitudinal stress, the magnitude of the longitudinal stress may have to be factored into the measured transverse canceling pressure. Ultimately, the determination of internal stress may be an iterative process.

#### 5.4.6.5 Presence of Reinforcing Steel

When cuts were made adjacent to reinforcing steel, no significant deviations of measured canceling pressure were noted. However, the presence of reinforcing steel can affect readings. When cuts were made into reinforcing steel, the measured canceling pressure increased drastically once the bar was cut. Figure 43 indicates this change in measurements. The reinforcing bar

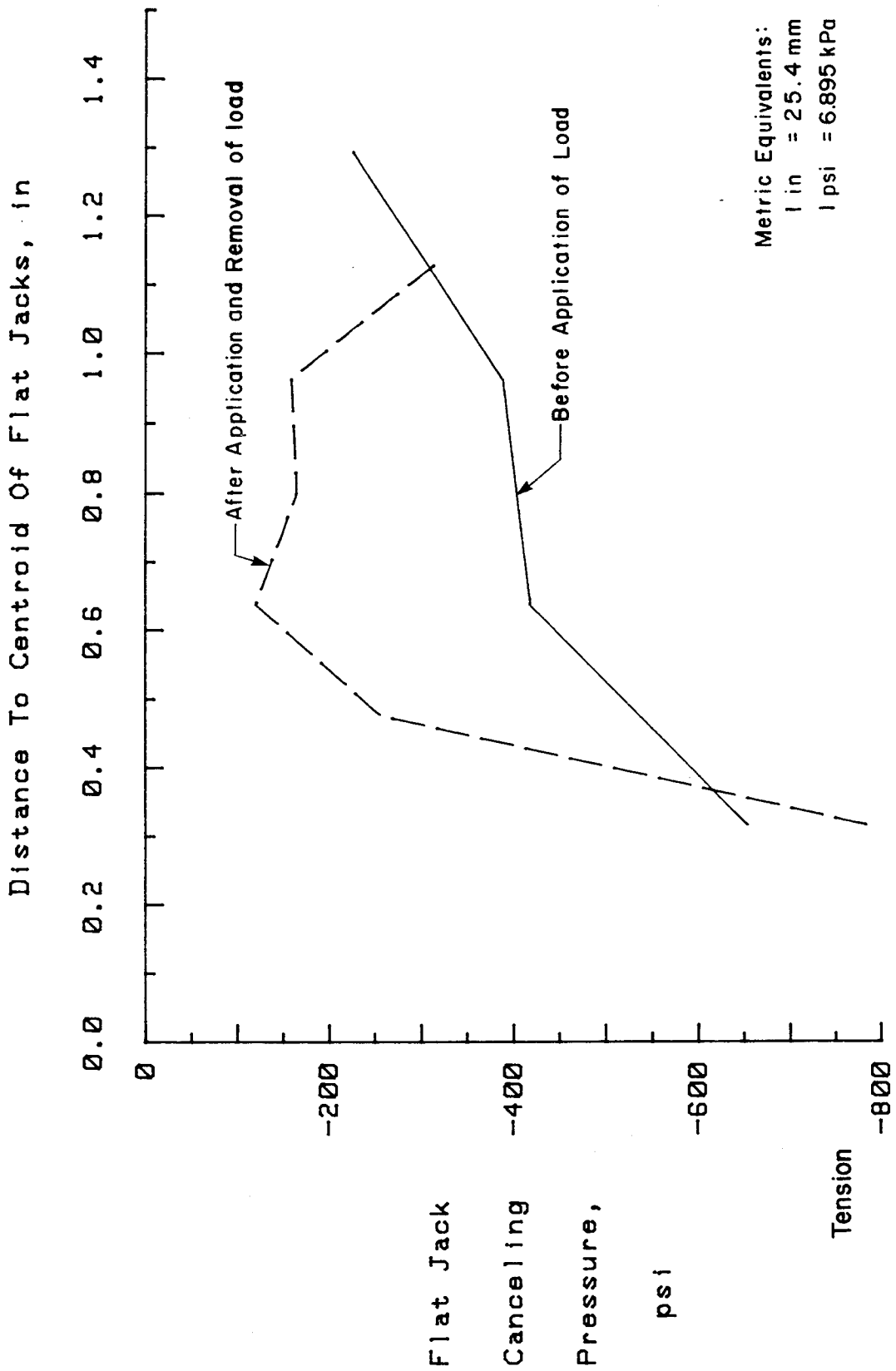


Figure 41. Measured canceling pressures before and after application and removal of load.

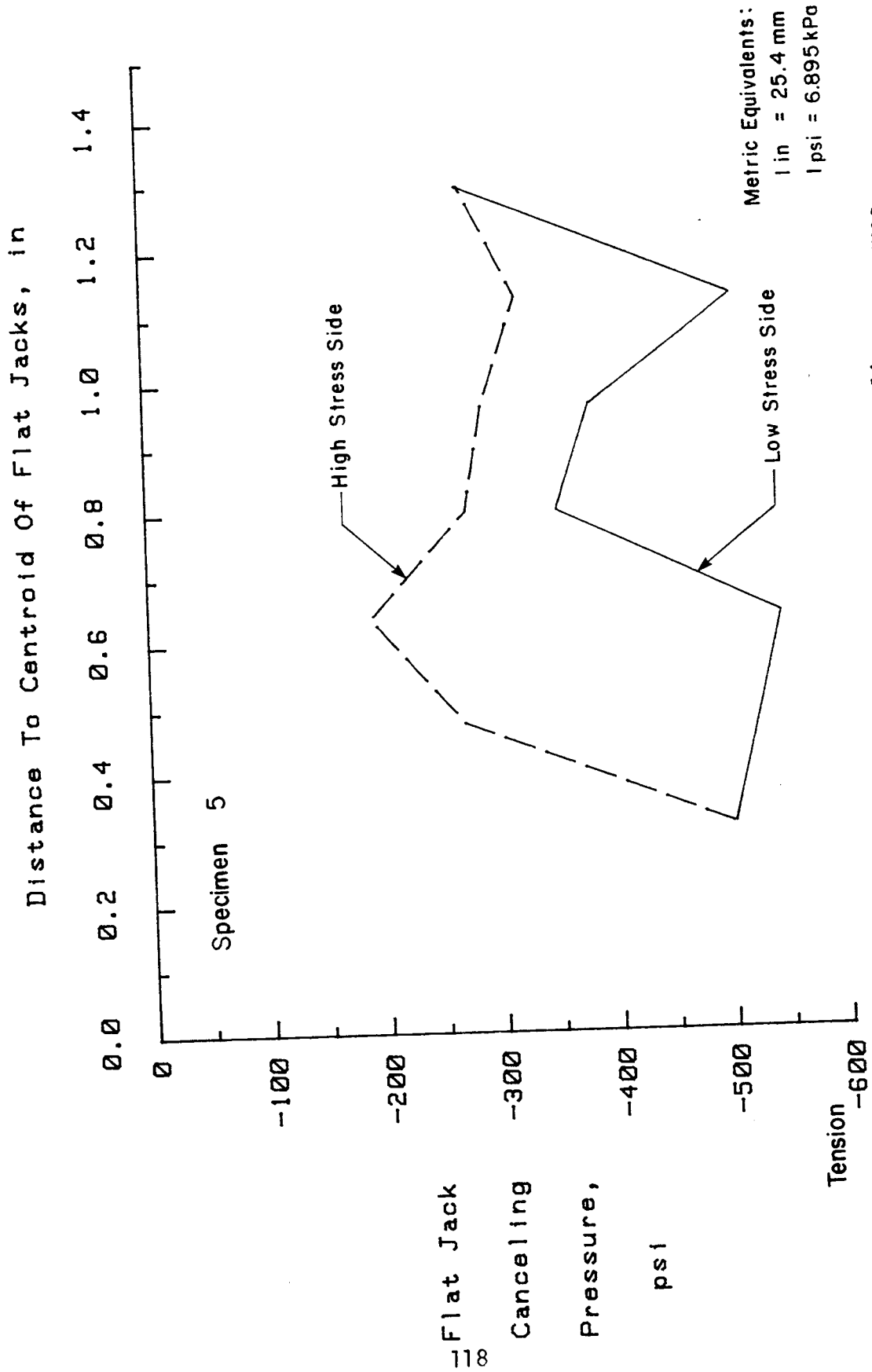
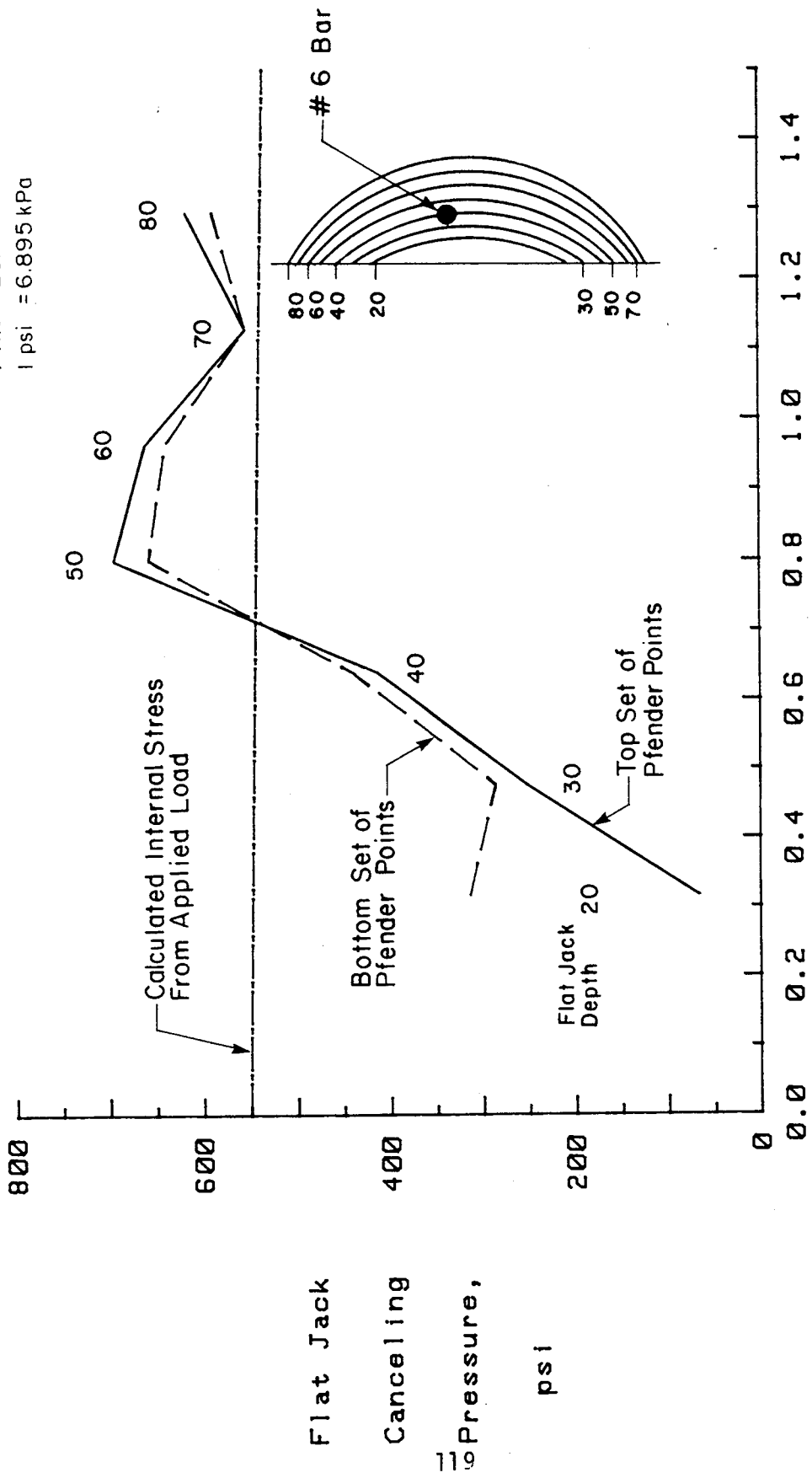


Figure 42. Effect of gradient on measured transverse canceling pressures.

Metric Equivalents:  
 1 in. = 25.4 mm  
 1 psi = 6.895 kPa



Distance To Centroid Of Flat Jacks, in

Figure 43. Effect of cutting into reinforcement.

was first encountered during the 40-mm (1.57-in) cut and was completely severed during the 50-mm (1.97-in) cut. This figure confirms Abdunur's claim that stresses can be determined when reinforcing steel is cut.<sup>[29]</sup> Prior to the time the bar is encountered or cut completely, the bar appears to restrain slot displacement, resulting in canceling pressures that are less than applied stress. After the reinforcing steel is cut completely, reliable results are obtained. The relationship between accuracy of results and proximity of reinforcing steel was not determined in this study. Additional study is needed to determine this relationship. At this time, the reinforcing steel must be cut completely or totally avoided to obtain reliable readings.

#### 5.4.6.6 Characteristics of Individual Flat Jacks

After extensive experimentation, refinement of techniques, and detailed data analysis, it became apparent that Abdunur's claimed accuracy, that canceling pressures were within 43.5 psi (0.30 MPa) of applied concrete stress, was unrealistic. The measurement technique used in this test program was prescribed in conversations with Abdunur. The equipment used was similar, and in the case of the flat jacks, identical, to the equipment used by him. Laboratory tests were performed in a controlled environment. Slot displacement measurement techniques were refined and became extremely consistent. The main component that was assumed to be accurate was the patented flat jacks.

To determine if the flat jacks accurately measure applied stress at various pressures and slot widths, the jacks were pressurized between plates in a testing machine. The tests began by inserting a flat jack between two plates in a testing machine and measuring the distance between the plates at opposite corners. With a slight amount of oil in the jack to prevent crushing, the testing machine load was increased to a predetermined value. As a result of the increased load, the jack was flattened slightly and its internal pressure increased. These values were recorded. With the machine load held at the initial value, the flat-jack pressure was increased causing

the contact area between the plates and the flat jack to decrease and the plate spacing to increase. This procedure was repeated for various applied loads and flat-jack sizes. For comparison, the measured flat-jack pressure (internal jack pressure) was divided by the applied pressure (applied load/nominal flat-jack area). Typical values of this parameter  $\sigma_m/\sigma_a$  (measured pressure/applied pressure) are plotted versus average displacement (average spacing between plates measured through the two dial gages) in figure 44. Measured values were less than the applied when the loading plates bore on the weld along the jacks' edges. Ratios greater than one were measured when the entire jack surface did not make contact with the plates. The figure indicates that accurate readings ( $\sigma_m/\sigma_a = 1$ ) are only possible at a unique displacement and this occurs only when flat jacks are squeezed to a thickness less than the initial thickness of 4.0 mm (0.160 in). The measured pressure is greater than the applied when the plate spacing is greater than the jack thickness which is the typical condition in the sawed cut.

These calibration tests indicate that the flat-jack design has not been perfected. The flat-jack pressures must be greater than the externally applied pressures because of confinement caused by the edge welds. This may explain the linear regression factor of 0.8 which is used to modify the measured canceling pressures. If this is indeed the case, the factor essentially reduces the overpressurization needed to resist the welds.

The results of a least square regression analysis to calculate concrete modulus was inconclusive. Cut depth, pressure/displacement relationship (slope), and applied stress were considered. Because only two different concrete moduli were considered, the results of regression analysis was meaningless.

The equipment and techniques used for the field studies were based on laboratory results. These recommended procedures and equipment include:

1. A Pfender gage to measure slot displacement.
2. Pfender reference points spacing of 40 mm (1.57 in).

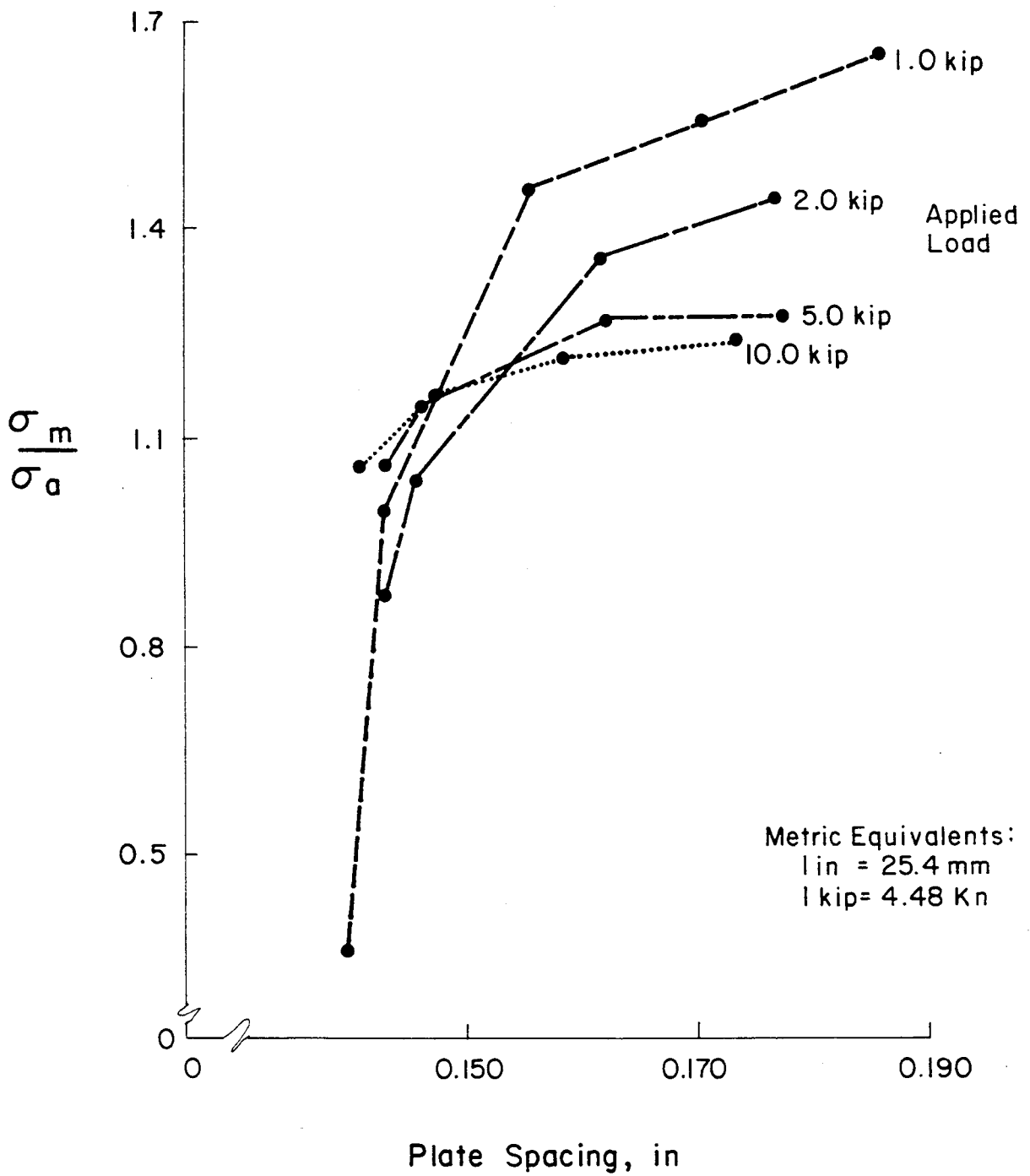


Figure 44. Measured to applied stress at various pressures and plate spacings.



3. Use of two sets (4 points) of Pfender points with each set located 6.4 mm (0.25 in) from the centerline of the cut.
4. Although the technique is not sufficiently accurate to detect stress gradients, all seven flat jacks are used to reduce experimental scatter and because no tests were performed to determine the optimum combination of cuts and the impact of eliminating one or more cuts.
5. No time lag between slot cutting and flat-jack pressurization.

The field studies are detailed in section 6.0. In that section, the prestressed concrete bridge member is discussed along with the results of stress measurements on that member.

## 6.0 TASK D - FIELD STUDIES

Task D included field stress measurements on an existing prestressed concrete bridge member. In this task, the flat-jack technique was evaluated under outdoor conditions.

The specimen consisted of a full-scale prestressed concrete bridge girder with slab. The girder was removed from an Illinois Tollway bridge that was demolished after 25 years of service, due to highway realignment.

The bridge was built in 1958. It carried the southbound traffic on Interstate 94 immediately south of the Wisconsin border. The bridge consisted of three spans, each approximately 42 ft. The superstructure was constructed using precast prestressed Illinois Tollway girders and a cast-in-place, 7-1/2-in-thick, exposed concrete deck. Each span consisted of five I-girders spaced 8 ft on center. In 1969, an asphalt overlay approximately 2-1/2 in. thick was laid down. In 1971, a 1-1/2-in asphalt overlay was added. The bridge was demolished in July 1983 after 25 years of service.

Prior to demolition, three interior girders were chosen for testing. The deck was saw cut half way between girders. Therefore, each test girder included an 8-ft-wide portion of deck. Two girders, including the deck, were tested under a separate study. The third girder was used for this investigation.

The first two girders were subjected to an extensive experimental program. Of interest to this investigation is the test to determine effective prestress. The deck-girder composite section was loaded under a two-point load. The load was applied statically in selected increments until the bottom of the girder cracked in the constant moment region. After unloading the girder, the cracks were instrumented with surface bonded, electrical resistance strain gages, and with crack gages. Then the girder was loaded and unloaded several times to determine the required load to open

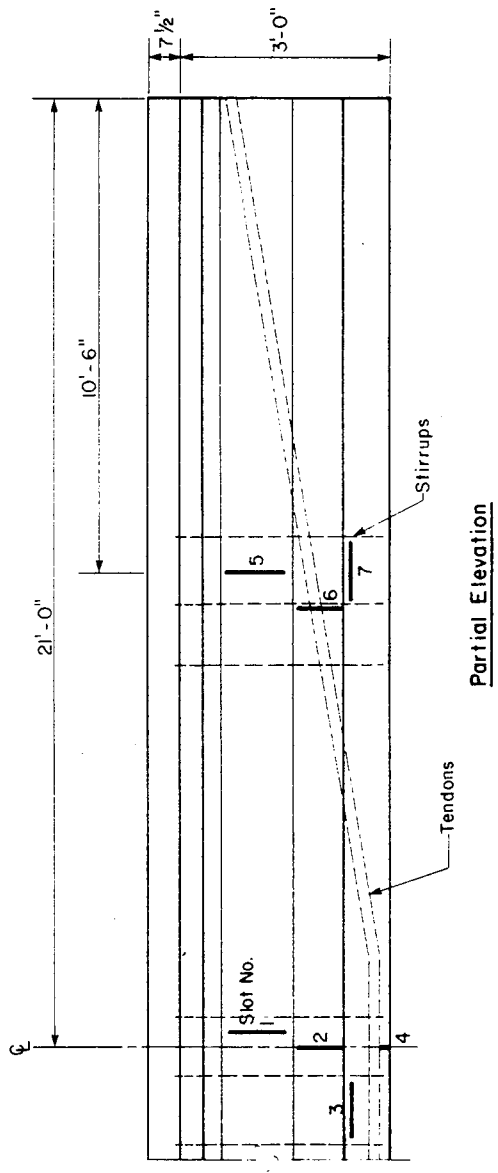
the cracks. This condition corresponded to zero stress in the bottom fiber of the girder. The load necessary to cause zero stress in the bottom fiber of the girder and a knowledge of the girder geometry and location of the prestressing strands were used to compute the effective prestress. As the three girders were manufactured in the same plant, under the same strict quality control, it was justifiably assumed that the three girders have the same effective prestress. The effective prestress, computed from the first two girders, was used to determine the existing stresses in the third girder tested under Task D of this investigation.

Six slots were cut on the side of the girder and one slot on the underside of the lower flange. Figures 45 and 46 show the centerline and quarter point cut locations.

As a result of gross assumptions about the effects of shrinkage, creep, temperature, and plane section behavior, the actual stress in a prestressed member may be quite different from the calculated values. The flat-jack technique was used to measure existing stresses in a member. Existing stress conditions in this girder, determined with the flat jacks, are compared to the stress determined through recent load tests, on two similar girders from the same bridge, performed in the structural laboratory of CTL.

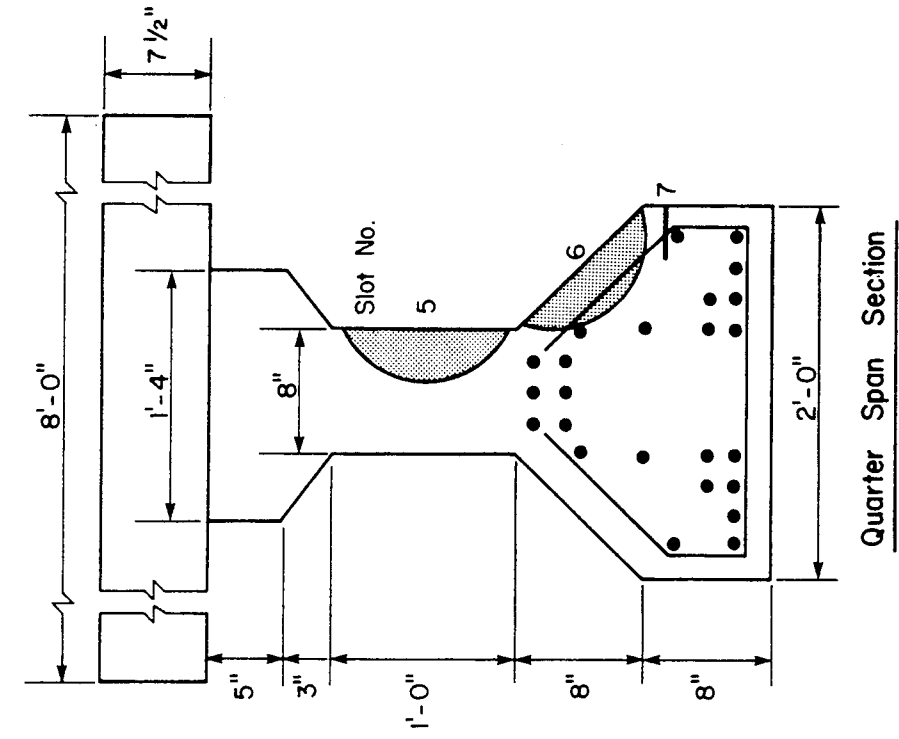
## 6.1 Girder Slots

A total of seven slots were cut in the prestressed concrete girder to determine its state of stress. Stresses at Slots 1, 2, 3, 5, 6, and 7 were measured using all seven flat jacks from 20 through 80 mm (0.79 through 3.15 in). The prestressing strand at Slot 4 limited cut depth to 50 mm (1.97 in). As a result, only the first four jacks were used. Prior to making cuts, a pachometer was used to locate reinforcing and prestressing steel. Consequently, no steel was encountered. As cutting on the girder progressed, the cutting time increased significantly as a result of dulling of the saw blade. The saw blade was damaged during initial cutting of Slot 8 and as a result, data were incomplete and are not reported. Section 11.0,



Metric Equivalents:  
 1 in = 25.4 mm  
 1 ft = 0.304 m

Figure 45. Girder cut locations.



Metric Equivalents:  
 1 in = 25.4 mm  
 1 ft = 0.305 m

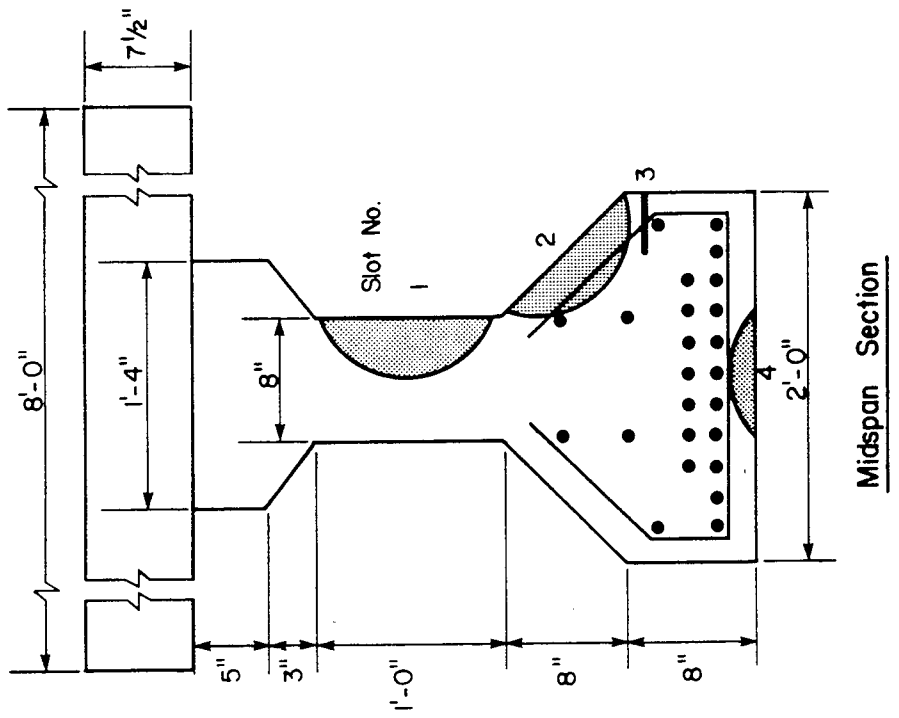


Figure 46. Cross section cut locations.

Appendix C - Field Test Results, reports all cut data for Task D. The appendix includes an explanation of the slot labels, slot displacements, and corresponding pressures, and the resulting stress profile.

## 6.2 Data Analysis

The canceling pressure for all cuts was corrected using the equation recommended in Section 5.0, Laboratory Studies:

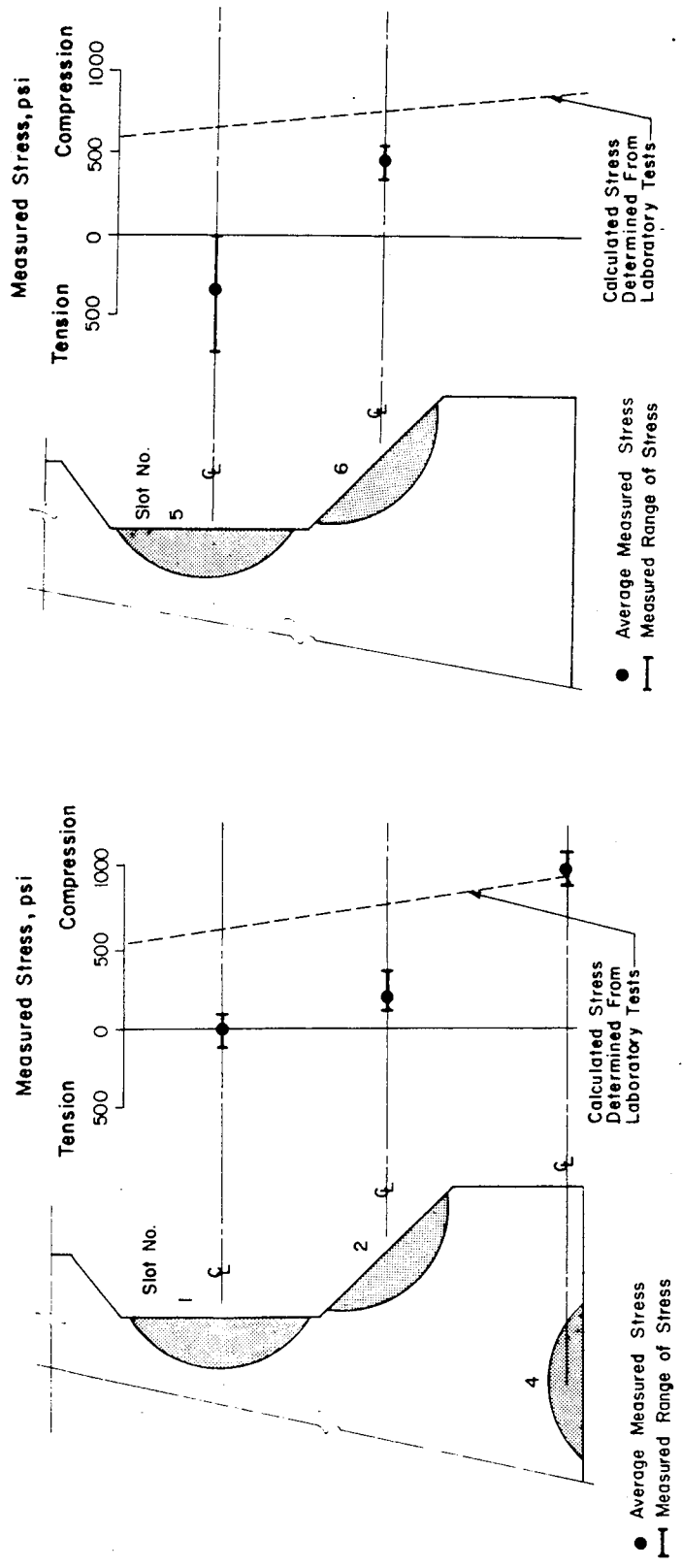
$$\text{Concrete Stress (psi)} = 200 \text{ psi} + 0.80 \times \text{Longitudinal Canceling Pressure (psi)} \quad (10)$$

$$\text{Concrete Stress (kPa)} = 1378 \text{ kPa} + 0.80 \times \text{Longitudinal Canceling Pressure (kPa)}$$

To decrease experimental scatter, two sets of Pfender points were used at each slot. The two separate readings (two sets of Pfender points at each cut, as shown in figure 31) for each cut depth were modified by the above equation then averaged. These individual predicted stresses, for each slot depth, were also averaged. Averaging of all data was performed because laboratory results indicated that stress gradients cannot be determined at this time. In addition, the accuracy of the technique increases when the results are combined.

Average measured stresses were then compared to stresses obtained from laboratory tests. Figure 47 shows the average measured stresses, and their bounds, at mid-span and quarter-span, respectively. The calculated stress shown in figure 47 was the expected value based on laboratory load tests. This stress is shown at the bottom of the section because this was the location at which it was determined. At this location, the stress measurement technique predicted the stress quite accurately.

Stress measurements at Slots 1 and 5 indicate little or no precompression in the web. In contrast, calculations based on simplifying assumptions about the effects of shrinkage, creep, temperature, and plane section behavior indicate that these portions of the web should be in compression.



Metric Equivalent:  
1 psi = 6.895 kPa

Midspan

Quarter-span

Figure 47. Measured stresses.

The nonlinear stress profile given by the stress measurement technique could be attributed to thermal gradient, differential shrinkage or creep, or a combination of these factors.

The results of horizontal cuts at Slots 3 and 7 confirm the laboratory finding that the stress measurement technique is not currently accurate enough to detect transverse shrinkage stresses. The results of these horizontal cuts were inconclusive. The apparent tensile stresses, which were as high as 800 psi (5.5 MPa), did not seem realistic.



## 7.0 CONCLUSIONS AND RECOMMENDATIONS

The objective of this investigation was to develop techniques for measuring existing long-term stresses in prestressed concrete bridges. To determine and develop the most promising stress measurement technique, this project was divided into five tasks.

1. Task A consisted of conducting a state-of-the-art review of techniques used to measure stresses in materials.
2. Task B involved analytical studies to assess the stress measurement techniques and their applicability to prestressed concrete bridges.
3. Task C included experimenting with the selected technique of stress measurement on laboratory specimens under controlled stress conditions.
4. Task D included stress measurements on an existing bridge.
5. Task E consisted of preparing a manual of instruction for engineers and technicians who will use the developed techniques.

This report summarizes the findings of Tasks A through D. The Manual of Instruction, Task E, was prepared as a separate volume and is reference 1.

### 7.1 Conclusions

Based on the state-of-the-art survey, analysis of promising stress measurement techniques and laboratory and field studies the following conclusions are made:

1. Analytical studies indicated that deformations resulting from slitting are larger than deformations due to coring. Therefore, the

slitting technique is more sensitive than the coring technique. As a result, stresses measured through stress relief by slitting are more accurate than stresses measured through stress relief by coring.

2. The flat-jack method of stress measurement, which involves slitting the concrete, was selected as the most promising measurement technique. With this technique, a slot is cut to a predetermined depth, the saw blade is removed, and a flat jack corresponding to the slot depth is inserted into the cut and pressurized. The pressure at which the slot displacement equals the initial distance between two reference points on each side of the slot is the canceling pressure. This canceling pressure is related to the concrete stress.
3. Laboratory experience indicates that the Pfender mechanical gage is the best device for measuring displacement between reference points.
4. A Pfender gage length of 40 mm (1.57 in) was determined to be optimum.
5. Clip gage continuous plots versus flat-jack pressure indicate that the pressure-displacement relationship is linear. Least squares regression analyses for the Pfender data confirm this.
6. The canceling pressure scatter between flat jacks of the same size is generally less than 50 psi (345 kPa).
7. Surface microcracking appears to make results unreliable when the smallest [20 mm (0.79 in)] flat jack is used.
8. In general, the canceling pressure increases with time after the completion of slot cutting.
9. The stress history of a member and longitudinal stress gradient affect the transverse canceling pressure.

10. Application of water to a slot affects displacement readings significantly.
11. For the specimen tested, internal stress could be determined when reinforcing steel was cut.
12. Internal stresses, from zero to 1000 psi (0 to 6.90 MPa), of laboratory specimens could be measured to within  $\pm 125$  psi (0.86 MPa) at a 90 percent confidence level using the following equation:
 
$$\begin{aligned} \text{Internal Concrete Stress (psi)} &= 200 \text{ psi} + 0.8 \times \text{canceling pressure (psi)} & (11) \\ \text{Internal Concrete Stress (kPa)} &= 1378 \text{ kPa} + 0.8 \times \text{canceling pressure (kPa)} \end{aligned}$$
13. The accuracy of the stress measurement technique is not sufficient to detect stress gradients.
14. The flat jacks' pressure-displacement relationships, which were determined from tests in a testing machine, are not linear in the range in which the jacks were intended to be used.
15. Shrinkage stresses are difficult to separate from applied stresses.

## 7.2 Recommendations

Based on the laboratory and field studies and the above conclusions, the following recommendations are made:

1. Development of a new type of flat jack is recommended as a result of the current jacks' nonlinear characteristics and potential availability problems.
2. Additional experimentation is needed to reduce the error in measured stress that corresponds to the 90 percent confidence level. It is

anticipated that as a result of temperature and humidity changes and less than ideal working conditions, the flat-jack technique will not be as accurate in the field as in the laboratory.

3. Field studies on bridges which have active instrumentation are recommended to confirm the accuracy of the flat-jack technique.
4. To minimize technician training time and for more accurate displacement readings, a detachable electronic displacement measurement device, which can be remounted consistently and has a digital readout, should be developed.

## 8.0 REFERENCES

- [1] Overman, T.R. and Hanson, N. W., "Techniques for Measuring Existing Long-Term Stresses in Prestressed Concrete Bridges - Vol. 2, Manual of Instruction," report to Federal Highway Administration, Washington, D. C., submitted by Construction Technology Laboratories, a Division of the Portland Cement Association, Skokie, Illinois, December 1985.
- [2] U.S. Department of Commerce, Bureau of Public Roads, Annual Reports for Fiscal Years 1954 through 1957.
- [3] Rabbat, B.G., Takayanagi, T., and Russell, H.G., "Optimized Sections for Major Prestressed Concrete Bridge Girders", U.S. Department of Transportation, Federal Highway Administration, Report FHWA/RD-82/005, February 1982.
- [4] Ballinger, C.A., Podolny, W., Jr., and Abrahams, M.J., "A Report on the Design and Construction of Segmental Prestressed Concrete Bridges in Western Europe-1977", Federal Highway Administration Report No. FHWA-RD-78-44.
- [5] Barker, James M., "Construction Techniques for Segmental Concrete Bridges", Journal of the Prestressed Concrete Institute, V. 25, No. 4, July-August 1980, pp. 66-86.
- [6] Standard Specifications for Highway Bridges, twelfth edition, American Association of State Highway and Transportation Officials, Washington, D.C., 1977.
- [7] ACI Committee 443, Analysis and Design of Reinforced Concrete Bridge Structures, American Concrete Institute, Detroit, 1977.
- [8] Zia, Paul, and others, "Estimating Prestressed Losses", Concrete International, American Concrete Institute, Vol. 1, No. 6, June 1979, pp. 32-38.
- [9] "Prestressed Girder Shines," Engineering News Record, October 27, 1983, page 16.
- [10] Koretzky, H.P., "What Has Been Learned from the First Prestressed Concrete Bridges - Repair of Such Bridges", Transportation Research Record No. 664, 1978, pp. 37-46.
- [11] Shanafelt, George O. and Horn, Willis B., "Damage Evaluation and Repair Methods for Prestressed Concrete Bridge Members", National Cooperative Highway Research Program Report No. 226, November 1980.
- [12] Carlson, R.W., "Manual for the Use of Strain Meters and Other Instruments for Embedment in Concrete Structures", Carlson Instruments, 24 pp., 1975.

- [13] Tyler, R.G., "Long-Term Strains in Medway Bridge", Great Britain, Department of Environment, TRRL Report LR 539, 1973.
- [14] Dirvy, M., "Etude Experimental des Phenomenes Differs dans les Ouvrages en Beton Precontraint", Laboratoires des Ponts et Chaussees, Rapport No. 50, Ministere de L'Equipment, Paris, December 1975.
- [15] Birkenmaier, M., "Long-Term Measurements on Prestressed Concrete Bridges, FIP Notes No. 89, November-December 1980, pp. 9-12.
- [16] Richardson, J. E., "Field-Measured Post-Tension Prestress Loss in Stress-Relieved Strands," Report No. FHWA/CA/SD-84/02, California Department of Transportation, Sacramento, California, June 1984.
- [17] "Evaluation of Vibra-Tension for Inspection of Tension of Prestressing Strands", Alabama Highway Research, H.R.P. Report No. 74, August 1974.
- [18] "Whittemore Strain Gage", SATEC Systems Inc., Bulletin WG.
- [19] Shiu, K. N., Daniel, J. I., and Russell, H. G., "Time-Dependent Behavior of Segmental Cantilever Concrete Bridges," report to State of Illinois, Department of Transportation, submitted by Construction Technology Laboratories, a division of the Portland Cement Association, Skokie, Illinois, March 1983; 101 pp. and Appendices. Also available through National Technical Information Services, U.S. Department of Commerce, 5285 Port Royal Road, Springfield, Virginia 22161, NTIA Accession No. PB 84-325845.
- [20] Russell, H.G., and others, "Evaluation and Verification of Time-Dependent Deformations in Post-Tensioned Box-Girder Bridges," Transportation Research Record No. 871, 1982, pp 66-70.
- [21] Tyler, R. G., "Developments in the Measurement of Strain and Stress in Concrete Bridge Structures," Ministry of Transport, Road Research Laboratory, Report No. LR 189, United Kingdom, 1968.
- [22] Rotrel, "The Nondestructive Measurement of Residual Stresses," AGARDOGRAPH - AG - 201, Vol. II, February 1976.
- [23] Stengel, B. and Gaymann, T., "Determination of Residual Stresses by Indentation Hardness Testing," AGARD Conference Procedures 53, Conference on Engineering Practice to Avoid Stress Corrosion Cracking, Istanbul, Turkey, 1969.
- [24] Gordon, B.E. and Speidel, T.O.P., "Stress Measurement by Ultrasonic Techniques," Paper presented at 1973 Fall Meeting of the Society for Experimental Stress Analysis, Indianapolis, Indiana.
- [25] Iwayanagi, J. and Abuku, S., "A Contribution to the Magnetic Measurement of Stress in Plastically Deformed Carbon Steel," Proceedings of the Eleventh Japan Congress on Materials Research, 1968.

- [26] Leeman, E.R., "The Measurement of Stress in Rock: A Review of Recent Developments," Proceedings International Symposium on the Determination of Stresses in Rock Masses, Lisbon, Portugal, 1969.
- [27] Redner, S., "Measurement of Residual Stresses by Blind Hole Drilling Method, Principle and Application," Bulletin TDG-5, Photoelastic, Inc., Malvern, Pennsylvania, May 1971.
- [28] Rocha M., Lopes, J.J.B., and Da Silva, J.N., "A New Technique for Applying the Method of the Flat Jack in the Determination of Stresses Inside Rock Masses," Proceedings International Symposium on the Determination of Stresses in Rock Masses, Lisbon, Portugal, 1969.
- [29] Abdunur, C., "Direct Measurement of Stresses in Concrete Structures," Maintenance, Repair, and Rehabilitation of Bridges, International Association for Bridge and Structural Engineering, Washington, D.C., 1982.
- [30] Leeman, E.R., "Absolute Rock Stress Measurements Using a Borehole Trepanning Stress-Relieving Technique," Proceedings of the Sixth Symposium on Rock Mechanics, University of Missouri at Rolla, 1964.
- [31] Leeman, E.R., "The CSIR Doorstopper and Triaxial Rock Stress Measuring Instruments," Proceedings International Symposium on the Determination of Stresses in Rock Masses, Lisbon, Portugal, 1969.
- [32] Mohr, H.F., "Measurement of Rock Pressure," Mine and Quarry Engineering, Vol. 22, No. 5, May 1956.
- [33] Olsen, O.J., "Measurement of Residual Stress by the Strain Relief Method," Quarterly of the Colorado School of Mines, Vol. 52, July 1957.
- [34] Slobodov, M.A., "Test Application of the Load-Relief Method for Investigating Stresses in Deep Rock," Ugol, Vol. 33, No. 7, 1958, Department of Scientific and Industrial Research (D.S.I.R.), British Lending Library, Russian Translation RTS 1068.
- [35] Perrin, J.R. and Scott, J.J., "The White Pine LVDT Biaxial Borehole Deformation Gage," Proceedings Sixth Symposium on Rock Mechanics, University of Missouri at Rolla, 1964.
- [36] Hooker, V.E. and Bickel, D.L., "Overcoring Equipment and Techniques Used in Rock Stress Determination," Information Circular 8618, United States Bureau of Mines, 1974.
- [37] Hooker, V.E., Aggson, J.R., and Bickel, D.L., "Improvements in the Three-Component Borehole Deformation Gage and Overcoring Techniques," Report of Investigations 7894, United States Bureau of Mines, 1974.
- [38] Austin, W.G., "Development of a Stress Relief Method with a Three-Directional Borehole Deformation Gage," Report No. REC-OCE-70-10, United States Bureau of Reclamation, 1970.

- [39] Austin, W.G., "Field and Laboratory Tests for 'Safety in Dams' Investigation at Salt River Project, Arizona," Report No. REC-OCE-70-7, United States Bureau of Reclamation, 1970.
- [40] Bonnechère, F.J. and Cornet, F.N., "In Situ Stress Measurements with a Borehole Deformation Cell," Proceedings International Symposium on Field Measurements in Rock Mechanics, Zurich, Switzerland, 1977.
- [41] Blackwood, R.L., "An Instrument to Measure the Complete Stress Field in Soft Rock or Coal in a Single Operation," Proceedings International Symposium on Field Measurements in Rock Mechanics, Zurich, Switzerland, 1977.
- [42] Filcek, H. and Cyrul, T., "Rigid Inclusion with High Sensitivity," Proceedings International Symposium on Field Measurements in Rock Mechanics, Zurich, Switzerland, 1977.
- [43] Roberts, A., "Progress in the Application of Photoelastic Techniques to Rock Mechanics," Proceedings Sixth Symposium on Rock Mechanics, University of Missouri at Rolla, 1964.
- [44] Yamada, S.E., "Development of In-situ Stress Gauge," Proceedings Joint Conference on Experimental Mechanics, Society for Experimental Stress Analysis, Oahu-Maui, Hawaii, 1982.
- [45] Rocha, M., "New Techniques in Deformability Testing of In Situ Rock Masses," American Society for Testing and Materials (ASTM), ASTM Special Technical Publication STP 477, 1970.
- [46] Panek, L.A., Hornsey, E.E. and Lappi, R.L., "Determination of the Modulus of Rigidity of Rock by Expanding a Cylindrical Pressure Cell in a Drillhole," Proceedings Sixth Symposium on Rock Mechanics, University of Missouri at Rolla, 1964.
- [47] Abdunur, C., Research Engineer, Laboratories Central des Ponts et Chaussees, Paris, France, Personal Communication, February 1984.
- [48] Cooke, R. W. and Seddon, A. E., "The Laboratory Use of Bonded-Wire, Electrical-Resistance Strain Gages on Concrete at the Building Research Station," Magazine of Concrete Research, March 1956, pp. 31-38.
- [49] Neville, A. M., Properties of Concrete, First Edition, Pitman Paperbacks, Surrey, 1970.
- [50] Peterson, R. E., Stress Concentration Factors, John Wiley & Sons, Inc., New York, 1974.
- [51] Timoshenko, S. P., and Goodier, J. N., Theory of Elasticity, McGraw-Hill Book Company, New York, 1970.



- [52] Bathe, K. G., Wilson, E. L., and Peterson, F. E., "SAP IV - A Structural Analysis Program for Static and Dynamic Response of Linear Systems," Report EERC 73-11, College of Engineering, University of California at Berkley, 1974.
- [53] Pickett, Gerald, "Shrinkage Stresses in Concrete," PCA Research Department Bulletin 11, Portland Cement Association, Skokie, Illinois, March 1946.
- [54] Acker, P., "Drying of Concrete - Consequences for the Evaluation of Creep Tests," Fundamental Research on Creep and Shrinkage of Concrete, Edited by F. H. Wittmann, Martinus Nijhoff Publishers, 1982, pp. 149-169.
- [55] Design and Control of Concrete Mixtures, Twelfth Edition, Portland Cement Association, Skokie, Illinois, 1982.
- [56] Leonhardt, F., and Lippoth, W., "Folgerungen aus Schaden an Spannbetonbrücken," Beton-und-Stahlbetonbau, Vol. 65, No. 10, October 1970, pp. 231-244.
- [57] Shiu, K. N., "Seasonal and Diurnal Behavior of Concrete Box-Girder Bridges," Transportation Research Record 982, Washington, D. C., 1984, pp. 50-56.
- [58] Nair, R. S. and Iverson, J. K., "Design and Construction of the Kishwaukee River Bridge," Journal of the Prestressed Concrete Institute, Vol. 27, No. 6, November/December 1982, pp. 22-47.

## 9.0 APPENDIX A - DISPLACEMENT DUE TO CUTTING INTO STRESSED PLATES

### 9.1 Circular Hole in a Stressed Plate

An infinite plate under uniform axial stress is shown in figure 48. The solution for radial displacement near a circular hole can be found from equations given in reference 51. In general, the relation between strain and radial displacement is:

$$\epsilon_r = \frac{\partial u_r}{\partial r} \quad (12)$$

where  $\epsilon_r$  = radial strain in polar coordinates  $(r, \theta)$   
 $u_r$  = the radial displacement in polar coordinates from center of hole  $(r, \theta)$

Hooke's law for plane stress is

$$\epsilon_r = (\sigma_r - \nu\sigma_\theta)/E \quad (13)$$

where  $E$  = the modulus of elasticity  
 $\nu$  = Poisson's ratio  
 $\sigma_r$  = radial stress (figure 48)  
 $\sigma_\theta$  = tangential stress (figure 48)

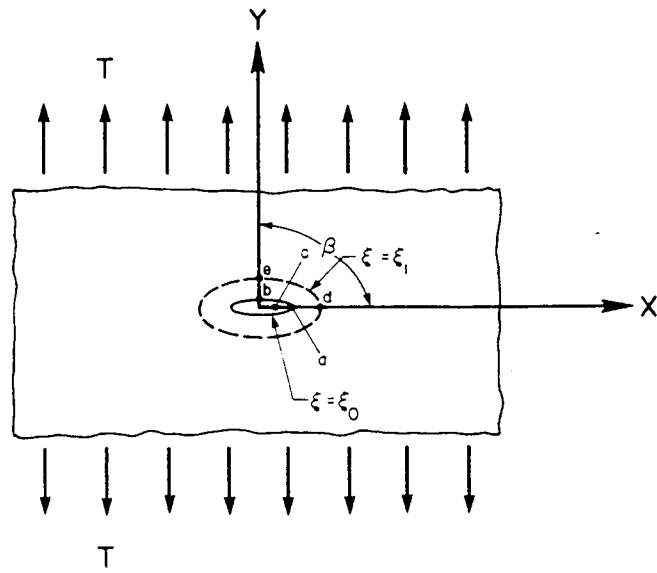
For a plate under uniform axial stress,  $T$ ,  $\sigma_r$  and  $\sigma_\theta$  are as follows:

$$\sigma_r = \frac{T}{2}\left(1 - \frac{a^2}{r^2}\right) + \frac{T}{2}\left(1 + \frac{3a^4}{r^4} - \frac{4a^2}{r^2}\right)\cos 2\theta \quad (14a)$$

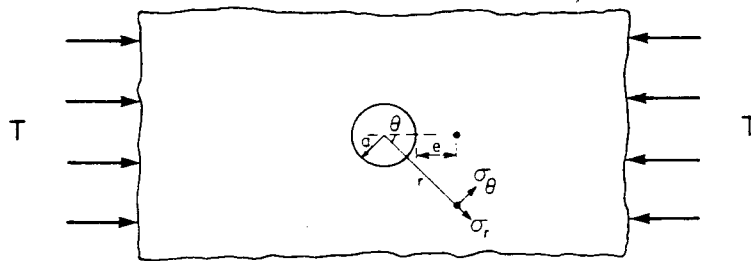
$$\sigma_\theta = \frac{T}{2}\left(1 + \frac{a^2}{r^2}\right) - \frac{T}{2}\left(1 + \frac{3a^4}{r^4}\right)\cos 2\theta \quad (14b)$$

where  $a$  = radius of the circular hole  
 $T$  = uniform axial stress

Substituting expressions for radial and tangential stress into equations 12 and 13, integrating, and disregarding rigid body motion, the following equation for radial displacement is obtained:



(a) With circular hole



(b) With elliptical hole

Figure 48. Infinite plate models.

$$u_r = \frac{T}{2E} \left\{ \left( r + \frac{a^2}{r} \right) + \left( r - \frac{a^4}{r^3} + \frac{4a^2}{r} \right) \cos 2\theta \right. \\ \left. - \nu \left[ \left( r - \frac{a^2}{r} \right) - \left( r - \frac{a^4}{r^3} \right) \cos 2\theta \right] \right\} \quad (15)$$

For radial displacement in the direction of the load (at  $\theta = 0$ ) the above equation reduces to:

$$u_r = \frac{T}{2E} \left[ 2r + (5 + \nu) \frac{a^2}{r} - (1 + \nu) \frac{a^4}{r^3} \right] \quad (16)$$

Equation 16 represents the displacement that occurs when a uniform stress is applied to a plate with a circular hole. This is not the solution for displacement due to cutting a circular hole in a plate under a uniform stress  $T$ . In order to obtain the latter solution, the displacement due to a uniform load on a plate with no hole has to be subtracted from equation 16.

The displacement due to applying a uniform stress  $T$  to a plate with no hole is:

$$u_{r0} = \frac{Tr}{E} \quad (17)$$

The radial displacement at  $\theta = 0$  due to cutting a circular hole of radius  $a$  in a plate under uniform stress  $T$  can be obtained by subtracting equation 17 from equation 16.

$$u_{rc} = \frac{T}{2E} \left[ (5 + \nu) \frac{a^2}{r} - (1 + \nu) \frac{a^4}{r^3} \right] \quad (18)$$

Setting  $r = a + e$ , equation 18 can be rewritten as:

$$u_{rc} = \frac{Ta^2}{2E(a + e)^3} [4a^2 + (5 + \nu)(2ae + e^2)] \quad (19)$$

where  $e$  = the distance from the edge of the hole to the point where the displacement is measured (figure 48).

If the displacement is measured over the diameter  $d_c = 2r$  rather than the radius  $r$ , the equation for displacement is twice the value given by equation 19, that is:

$$d_c = \frac{Ta^2}{E(a+e)^3} [4a^2 + (5+\nu)(2ae + e^2)] \quad (20)$$

## 9.2 Slot in a Stressed Plate

Another infinite plate under uniform axial tension is shown in figure 48. The solution for displacement near an elliptical hole can also be found from equations given in reference 51. The displacements near an elliptical hole are:

$$2G(u - iv) = \frac{3-\nu}{1+\nu} \bar{\Psi}(\bar{z}) + \bar{z}\Psi'(z) - \chi'(z) \quad (21)$$

where  $u$  = displacement in the x-direction  
 $v$  = displacement in the y-direction  
 $G$  = modulus of rigidity  
 $i = \sqrt{-1}$   
 $z = x + iy$

$\Psi(z)$ ,  $\chi(z)$  = complex potentials

The overbar denotes a complex conjugate, while the prime denotes a derivative with respect to  $z$ . The complex potentials for the plate shown in figure 48, are

$$4\Psi(z) = Tc[e^{2\xi_0} \cos 2\beta \cosh \zeta + (1 - e^{2\xi_0 + 2i\beta}) \sinh \zeta] \quad (22a)$$

$$4\chi(z) = -Tc^2[(\cosh 2\xi_0 - \cos 2\beta)\zeta + \frac{1}{2} e^{2\xi_0} \cosh 2(\zeta - \xi_0 - i\beta)] \quad (22b)$$

where  $\beta$  = the angle the load  $T$  makes with the x-axis. (For the case shown in figure 48,  $\beta = \frac{\pi}{2}$ )

$$\zeta = \xi + i\eta,$$

where  $\xi$  and  $\eta$  are elliptical coordinates such that:

$$x = c (\cosh \xi) \cos \eta \quad (23a)$$

$$y = c (\sinh \xi) \sin \eta \quad (23b)$$

The foci of the ellipses are at  $x = \pm c$ .  $\xi$  is constant on a given ellipse while  $\eta$ , the eccentric angle, varies from 0 to  $2\pi$ . On the boundary of

the elliptical hole  $\xi = \xi_0$ . The semiaxes of the elliptical hole, as shown in figure 48, are a and b. Using equations 23a and 23b, these can be written as:

$$a = c \cosh \xi_0 \quad (24a)$$

$$b = c \sinh \xi_0 \quad (24b)$$

The ellipse upon which displacements will be measured is  $\xi = \xi_1$ . As shown in figure 48 its semiaxes are:

$$d = c \cosh \xi_1 \quad (25a)$$

$$e = c \sinh \xi_1 \quad (25b)$$

Setting  $\eta = \frac{\pi}{2}$  to obtain displacement at e, and using equations 22 through 25 with appropriate derivatives and conjugates, the following equations are obtained:

$$\bar{\Psi}(\bar{z}) = i \frac{T}{4} \left[ \frac{a+b}{a-b} (e-d) - d \right] \quad (26a)$$

$$\bar{z}\Psi'(z) = -\frac{iTe}{4d} \left[ \frac{a+b}{a-b} (e-d) + e \right] \quad (26b)$$

$$\chi'(z) = -\frac{iT}{2d} \left\{ a^2 + \frac{1}{(a-b)^2} [de(a^2 + b^2) - ab(d^2 + e^2)] \right\} \quad (26c)$$

Equations 25 are all purely imaginary. By taking the imaginary part of equation 20, the solution for the displacement v becomes:

$$v = \frac{1}{2G} \left\{ \text{Im} \left[ \frac{3-v}{1+v} \bar{\Psi}(\bar{z}) + \bar{z} \Psi'(z) - \chi'(z) \right] \right\} \quad (27)$$

where  $\bar{\Psi}(\bar{z})$ ,  $z\Psi'(z)$  and  $\chi'(z)$  are defined by equations 26.

Equation 27 is the displacement due to a uniform stress on a plate with an elliptical hole. To find the displacement for a slot, let  $b \rightarrow 0$  in equation 26. Equation 27 then reduces to:

$$v = \frac{-T}{8G} \left[ \frac{3-v}{1+v} (e-2d) + \frac{e}{d}(2e-d) - \frac{2}{d}(a^2 + de) \right] \quad (28)$$

Since  $\cosh^2 \xi - \sinh^2 \xi = 1$ , equations 23 and 24 can be written as:

$$a^2 - b^2 = c^2 \quad (29a)$$

$$d^2 - e^2 = c^2 \quad (29b)$$

If  $b = 0$ , then equation 29a indicates that  $a \cong c$ .  $d$  can then be eliminated in equation 28 by setting  $d^2 = e^2 + a^2$ . After some simplification equation 28 becomes:

$$v = \frac{T}{E} \left[ ev + \frac{2a^2 + e^2(1 - \nu)}{\sqrt{a^2 + e^2}} \right] \quad (30)$$

Equation 30 represents the displacement that occurs when a uniform stress  $T$  is applied to a plate with a slot of length  $2a$ . This is not the solution for displacement due to cutting a slot in a plate under a uniform stress  $T$ . In order to obtain the latter solution, the displacement due to a uniform load on a plate with no slot has to be subtracted from equation 30. The displacement due to a uniform stress  $T$  on a plate with no slot is:

$$v_0 = \frac{Te}{E} \quad (31)$$

Subtracting equation 30 from equation 29, the following solution for the displacement at  $e$  due to cutting a slot of length  $2a$  in a plate under uniform stress  $T$  is obtained:

$$v_s = \frac{T}{E} \left[ \frac{2a^2 + e^2(1 - \nu)}{\sqrt{a^2 + e^2}} - e(1 - \nu) \right] \quad (32)$$

If the displacement is measured across the slot then the total displacement,  $d_s$ , is twice that given by equation 33:

$$d_s = \frac{2T}{E} \left[ \frac{2a^2 + e^2(1 - \nu)}{\sqrt{a^2 + e^2}} - e(1 - \nu) \right] \quad (33)$$

## 10.0 APPENDIX B - LABORATORY TEST RESULTS

This appendix contains data from all laboratory specimens. A descriptive alphanumeric label was used for each slot:

a b c d XX/YY e f

- a is the specimen number as shown in figures 26 through 29.
- b indicates side of specimen cut was made on: N is the north side; S is the south side.
- c indicates the slot location as shown in figures 26 through 29.
- d indicates the cut orientation: H denotes horizontal slots where the transverse stress was measured; V denotes a vertical cut used to determine applied stresses.
- XX is applied stress divided by 10, in psi, on the side of the cut.
- YY is the applied stress divided by 10, in psi, on the side opposite the cut.
- e indicates the Pfender points location. For vertical slots, T is the top set of Pfender points and B is the bottom set. For horizontal slots, E the east set and W is the west set. The orientation of Pfender points is shown in figure 31.
- f indicates additional Notations as follows:
  - 20 mm, 60 mm was the spacing of Pfender reference points used to measure displacement. Spacings of "20 mm" and "60 mm" are indicated in the label. If no value is given, 40 mm spacing was used.
  - 10, 40 indicates the time in minutes between the end of slot cutting and the beginning of flat-jack pressurization. Time lags of "10" and "40" minutes were used. If no value is given, immediate pressurization occurred.
  - 0FJ, 1FJ, 2FJ indicates that flat-jack set number used to determine canceling pressures. Flat-jack sets used are "0," "1," and "2." In most cases, set number 0 or 1 was used.

The stress gradients indicated (XX/YY) in the alphanumeric labels were determined using a Whittemore mechanical strain gage with gage points located adjacent to the slots and are labeled on graphs by a dashed line.



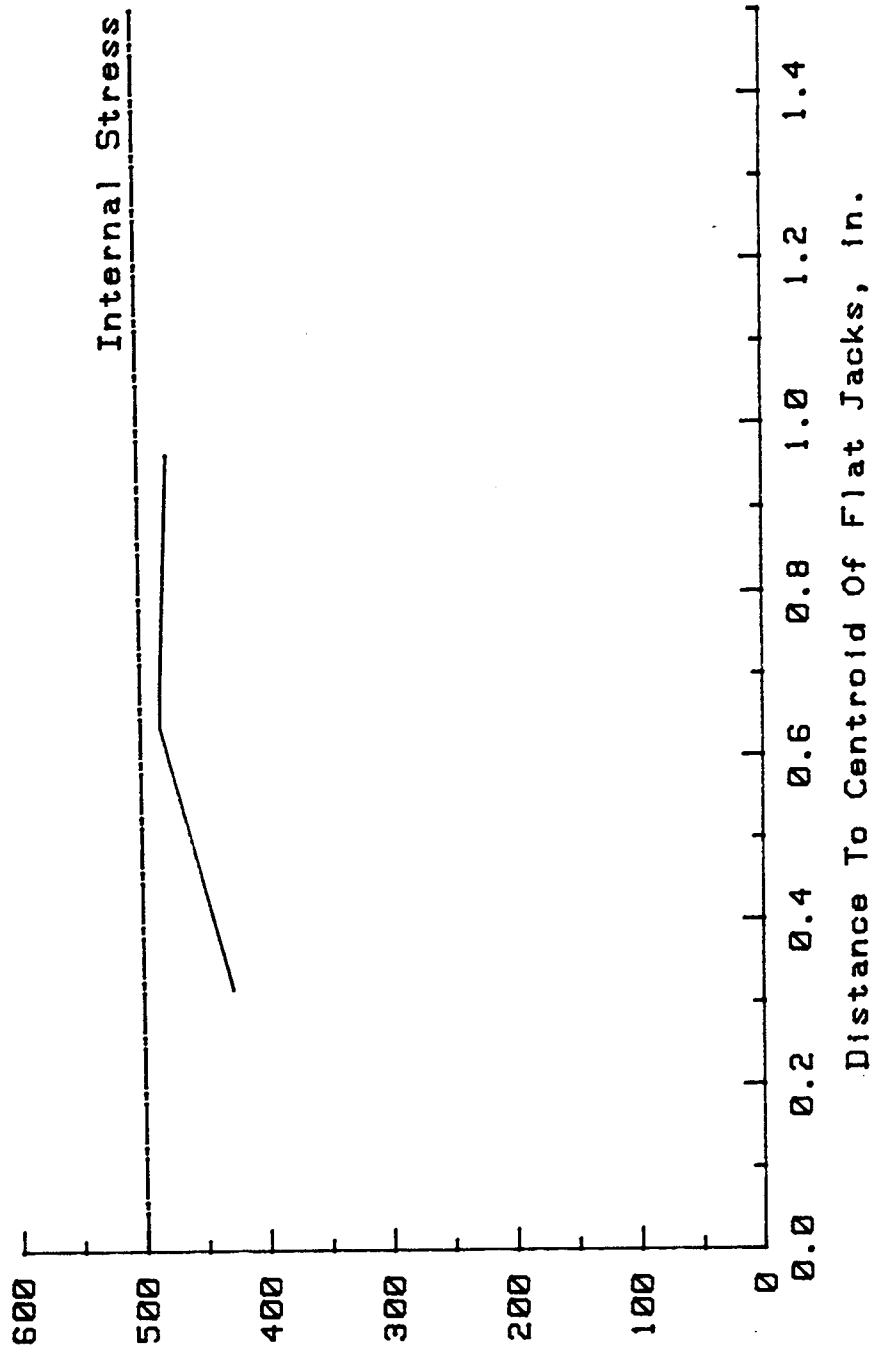
The following results are organized by specimen number followed by slot number. Positive canceling pressures indicate compressive stresses while negative (-) pressures indicate tensile stresses.

This appendix includes tables for modified Pfender gage readings at various pressures and linear regression, least squares, results at various pressures. The Pfender readings were modified based on changes in standard bar readings. This appendix also includes graphs of measured canceling pressures and internal applied stresses at various distances from the surface of the specimen. The canceling pressures were plotted at the centroid of individual flat jacks. The centroids are given in figure 21.

**Table 18. Stress measurement data for specimen 1S1V50/55T20MM.**

FFENDER READINGS							
Out Depth (mm)	Flat Jack Internal Pressure (psi)						
	0	100	200	300	400	500	600
20	-5.0	-4.0	-3.0	0.0	-1.0	0.0	2.0
40		-16.0	-8.0	-3.0	-9.0	-2.0	5.0
60	-23.0	-11.0	-15.0	-7.0	-5.0	-1.0	5.0

LEAST SQUARES CURVE PARAMETERS				
Out Depth (mm)	Slope (ksi/in)	Y-Intercept (Canceling Press,psi)	Correction Coefficient (1=Exact Fit)	Standard Error Of Estimate
20	3.24	429	0.9540	153.7
40	0.93	482	0.8981	184.0
60	0.88	482	0.9532	160.0



Flat Jack  
 Canceling  
 Pressure,  
 psi

Figure 49. Uncorrected stress profile for ISIV50/55T20MM.

Table 19. Stress measurement data for specimen 1S1V50/55B.

PFENDER READINGS							
Cut	Flat Jack Internal Pressure (psi)						
Depth	0	100	200	300	400	500	600
(mm)							
20	0.0	-2.0	-2.0	-1.0	0.0	0.0	2.0
40	-10.0	-7.0	-6.0	-3.0	-0.5	2.0	4.0
60	-9.0	-10.0	-5.0	-3.0	0.0	4.0	9.0
80	-16.0	-18.0	-13.0	-7.0	-2.0	4.0	10.0

LEAST SQUARES CURVE PARAMETERS				
Cut	Slope	Y-Intercept	Correlation	Standard
Depth		(Canceling	Coefficient	Error Of
(mm)	(ksi/in)	Press,psi)	(1=Exact Fit)	Estimate
20	4.03	344	0.6626	396.3
40	1.67	424	0.9968	42.4
60	1.21	361	0.9756	116.1
80	0.79	420	0.9739	120.0

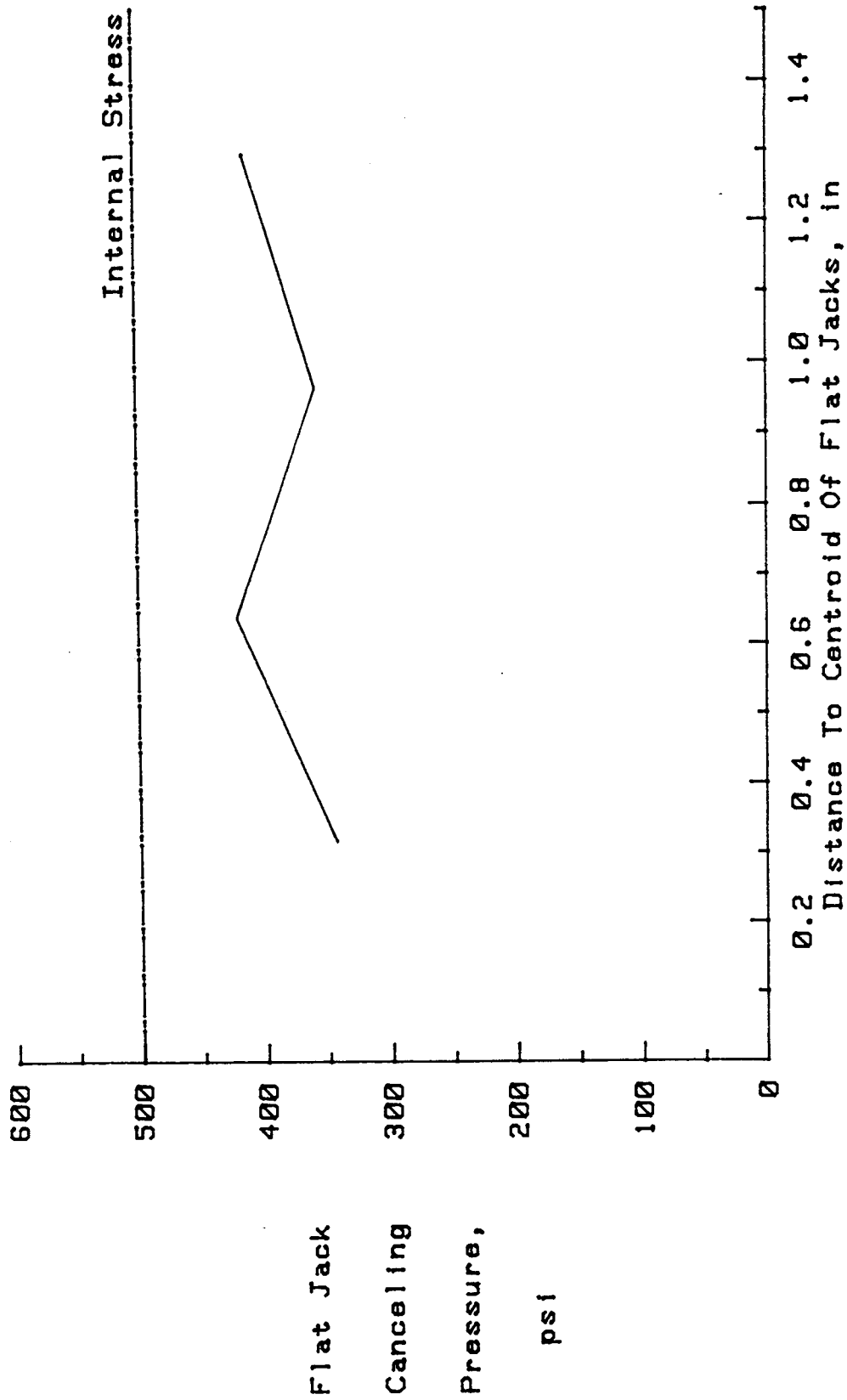


Figure 50. Uncorrected stress profile for 1S1V50/55B.

Table 20. Stress measurement data for specimen 1S2V00/00T.

PFENDER READINGS						
Cut	Flat Jack Internal Pressure (psi)					
Depth (mm)	0	100	200	300	400	500
20	6.0	6.0	8.0	9.0	8.0	9.0
40	10.0	14.0	16.0	18.0	21.0	23.0
60	16.0	19.0	22.0	26.0	31.0	35.0
80	15.0	19.0	24.0	30.0	37.0	44.0

LEAST SQUARES CURVE PARAMETERS				
Cut	Slope	Y-Intercept	Correlation	Standard
Depth		(Canceling	Coefficient	Error Of
(mm)	(ksi/in)	Press,psi)	(1=Exact Fit)	Estimate
20	4.64	-654	0.8607	213.0
40	1.55	-418	0.9939	46.3
60	1.01	-388	0.9953	40.6
80	0.66	-226	0.9946	43.2

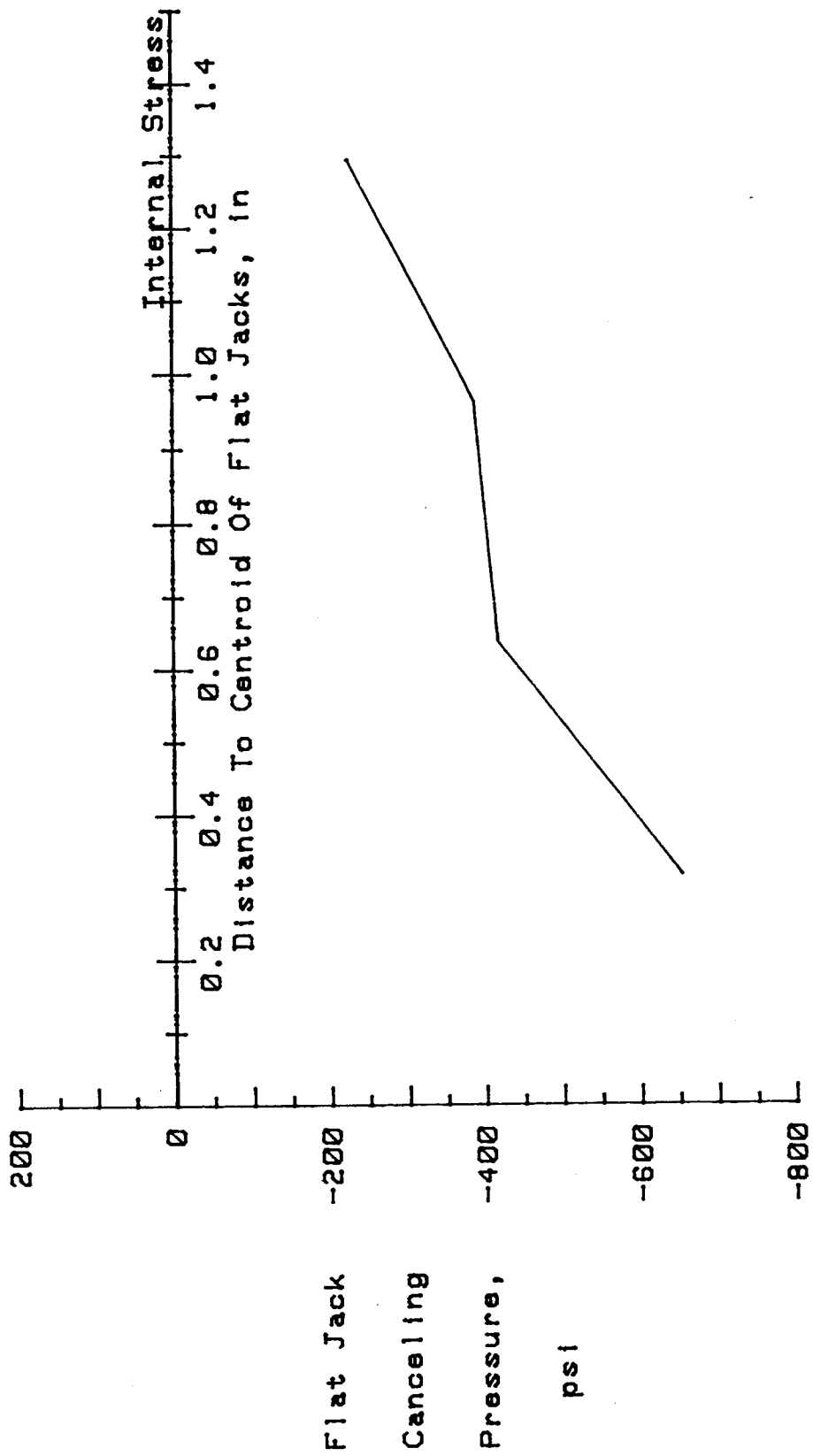


Figure 51. Uncorrected stress profile for 1S2V00/00T.

Table 21. Stress measurement data for specimen 1S2V00/00B60MM.

FFENDER READINGS						
Cut	Flat Jack Internal Pressure (psi)					
Depth (mm)	0	100	200	300	400	500
20	3.0	3.0	3.0	3.0	4.0	4.0
40	7.0	9.0	12.0	14.0	15.0	18.0
60	16.0	16.0	20.0	23.0	26.0	29.0
80	9.0	15.0	21.0	26.0	32.0	38.0

LEAST SQUARES CURVE PARAMETERS				
Cut	Slope	Y-Intercept	Correlation	Standard
Depth (mm)	(ksi/in)	(Canceling Press,psi)	Coefficient (1=Exact Fit)	Error Of Estimate
20	11.81	-750	0.8281	234.5
40	1.81	-325	0.9930	49.5
60	1.36	-501	0.9853	71.5
80	0.69	-159	0.9997	10.2



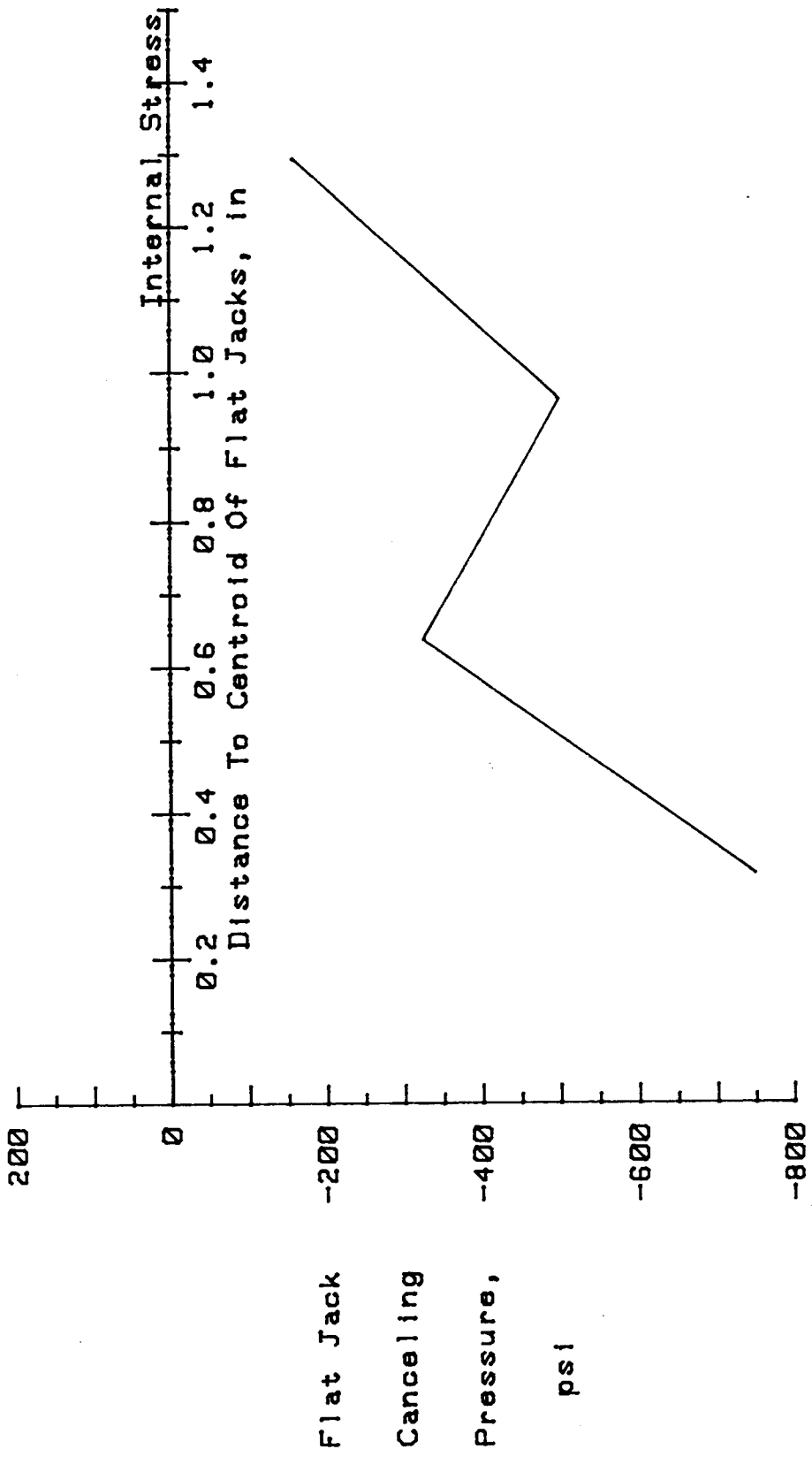


Figure 52. Uncorrected stress profile for 1S2V00/00B60MM.

Table 22. Stress measurement data for specimen 1S4V38/49TK.

PFENDER READINGS				
Cut Depth (mm)	Flat Jack Internal Pressure (psi)			
	0	200	400	600
20	1.0	0.0	2.0	5.0
30	-2.0	0.0	4.0	9.0
40	-6.0	0.0	7.0	13.0
50	-7.0	-1.0	7.0	14.0
60	-9.0	0.0	10.0	20.0
70	-8.0	-2.0	9.0	20.0
80	-7.0	0.0	11.0	22.5

LEAST SQUARES CURVE PARAMETERS				
Cut Depth (mm)	Slope (ksi/in)	Y-Intercept (Canceling Press,psi)	Correlation Coefficient (1=Exact Fit)	Standard Error Of Estimate
20	3.94	100	0.8367	244.9
30	2.06	156	0.9836	80.6
40	1.23	191	0.9995	14.0
50	1.11	209	0.9986	23.5
60	0.81	192	0.9997	11.3
70	0.82	202	0.9918	57.2
80	0.78	168	0.9943	47.6

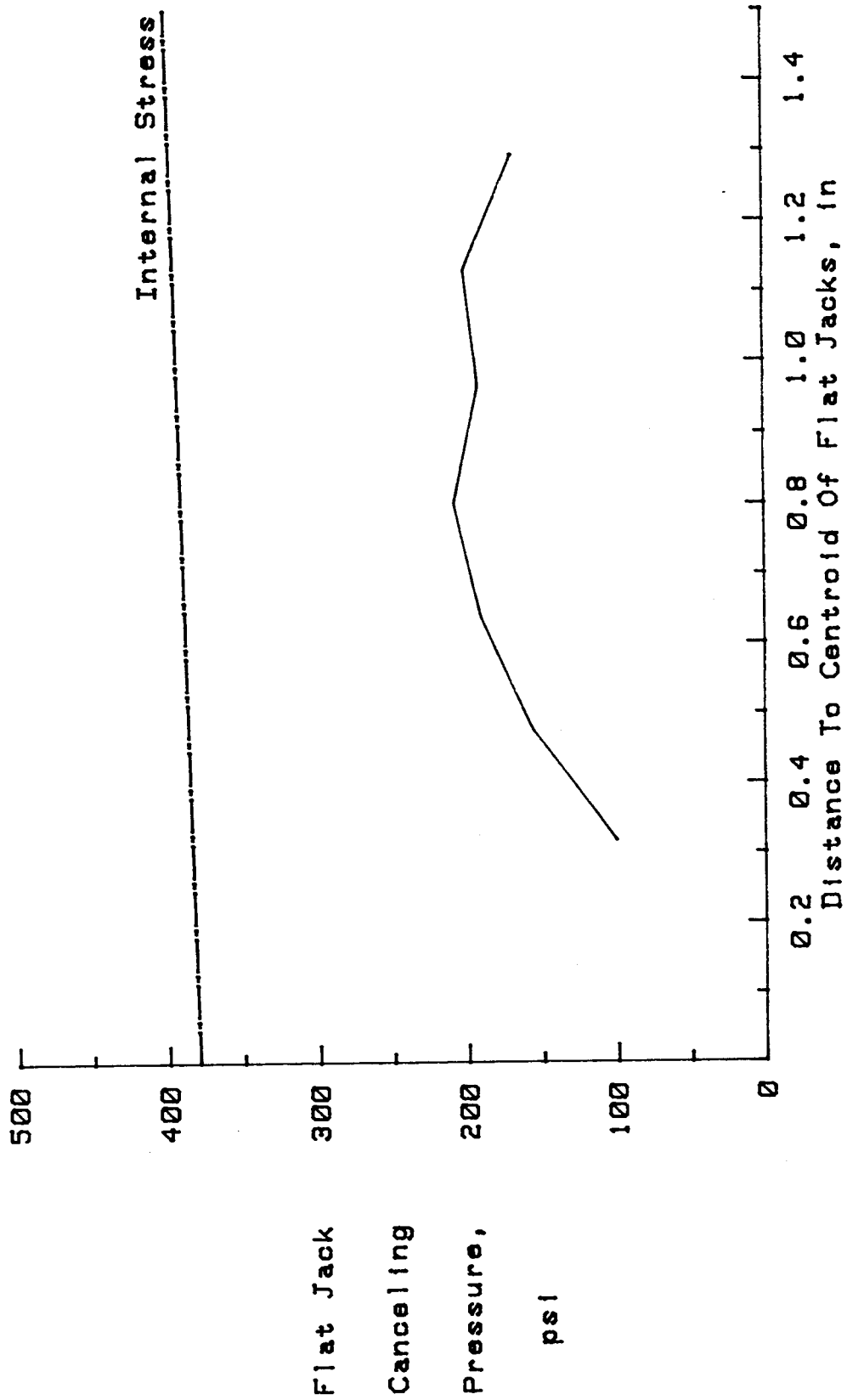


Figure 53. Uncorrected stress profile for 1S4V38/49TK.

Table 23. Stress measurement data for specimen 1S4V38/49B.

PFENDER READINGS				
Cut Depth (mm)	Flat Jack Internal Pressure (psi)			
	0	200	400	600
20	1.5	-1.5	1.5	3.5
30	-1.5	0.5	3.5	6.5
40	-4.5	0.5	5.5	10.5
50	-5.5	-0.5	5.5	12.5
60	-9.5	-0.5	8.5	17.5
70	-7.5	-1.5	8.5	16.5
80	-6.5	-0.5	10.5	22.5

LEAST SQUARES CURVE PARAMETERS				
Cut Depth (mm)	Slope (ksi/in)	Y-Intercept (Canceling Press,psi)	Correlation Coefficient (1=Exact Fit)	Standard Error Of Estimate
20	2.78	212	0.5636	369.4
30	2.89	135	0.9959	40.4
40	1.57	180	1.0000	0.0
50	1.31	201	0.9972	33.2
60	0.87	211	1.0000	0.0
70	0.95	203	0.9959	40.6
80	0.79	170	0.9899	63.2

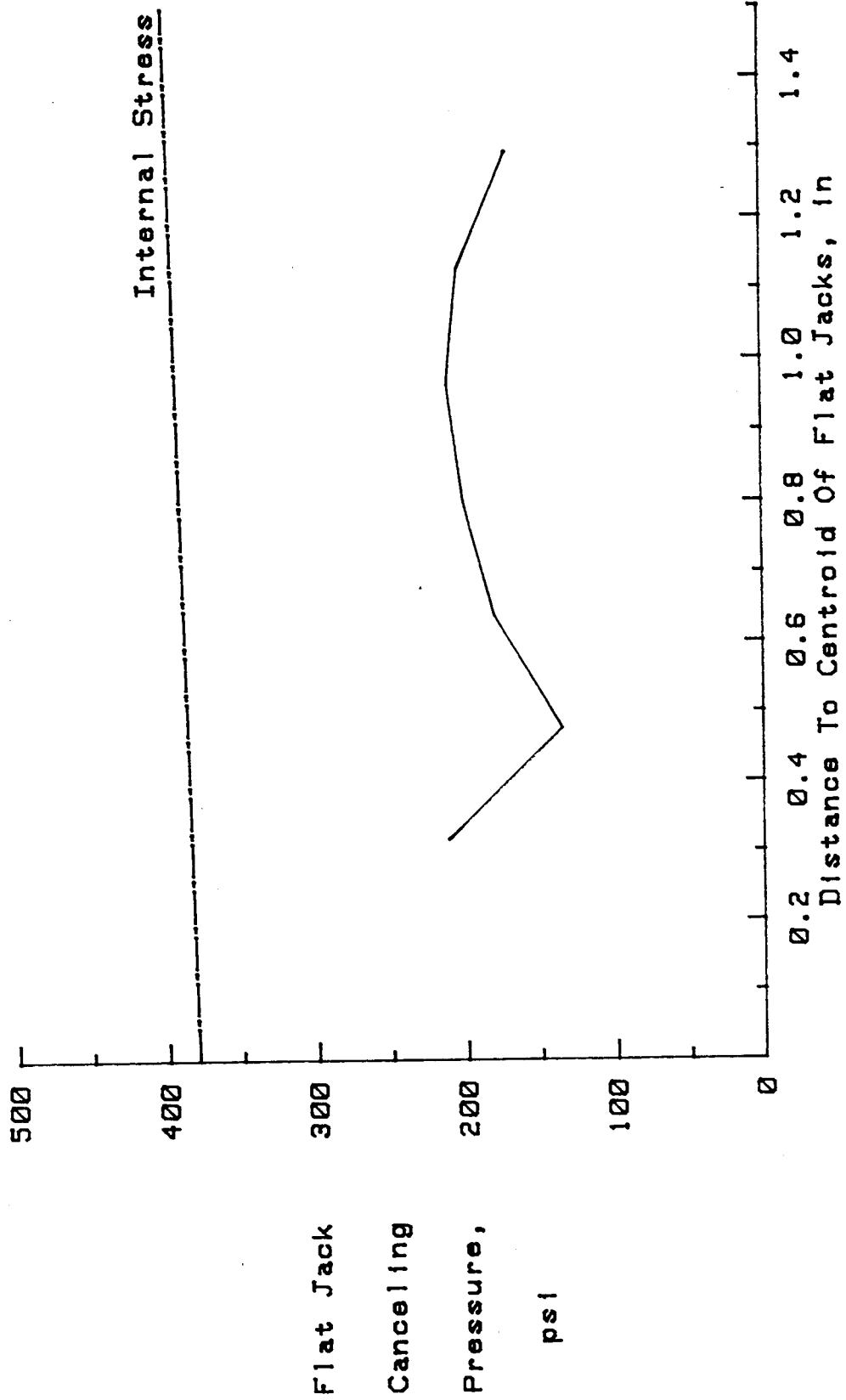


Figure 54. Uncorrected stress profile for 1S4V38/49B.

Table 24. Stress measurement data for specimen 1S5H50/50W.

PFENDER READINGS				
Cut Depth (mm)	Flat Jack Internal Pressure (psi)			
	0	200	400	600
20	4.0	5.0	8.0	10.0
30	-3.0	1.0	4.0	7.0
40	3.0	10.0	17.0	24.0
60	3.0	22.0	28.0	41.0
80	8.0	20.0	30.5	42.0

LEAST SQUARES CURVE PARAMETERS				
Cut Depth (mm)	Slope (ksi/in)	Y-Intercept (Canceling Press,psi)	Correlation Coefficient (1=Exact Fit)	Standard Error Of Estimate
20	3.63	-323	0.9845	78.4
30	2.37	164	0.9973	33.1
40	1.12	-86	1.0000	0.0
60	0.63	-77	0.9804	88.0
80	0.70	-146	0.9997	10.9

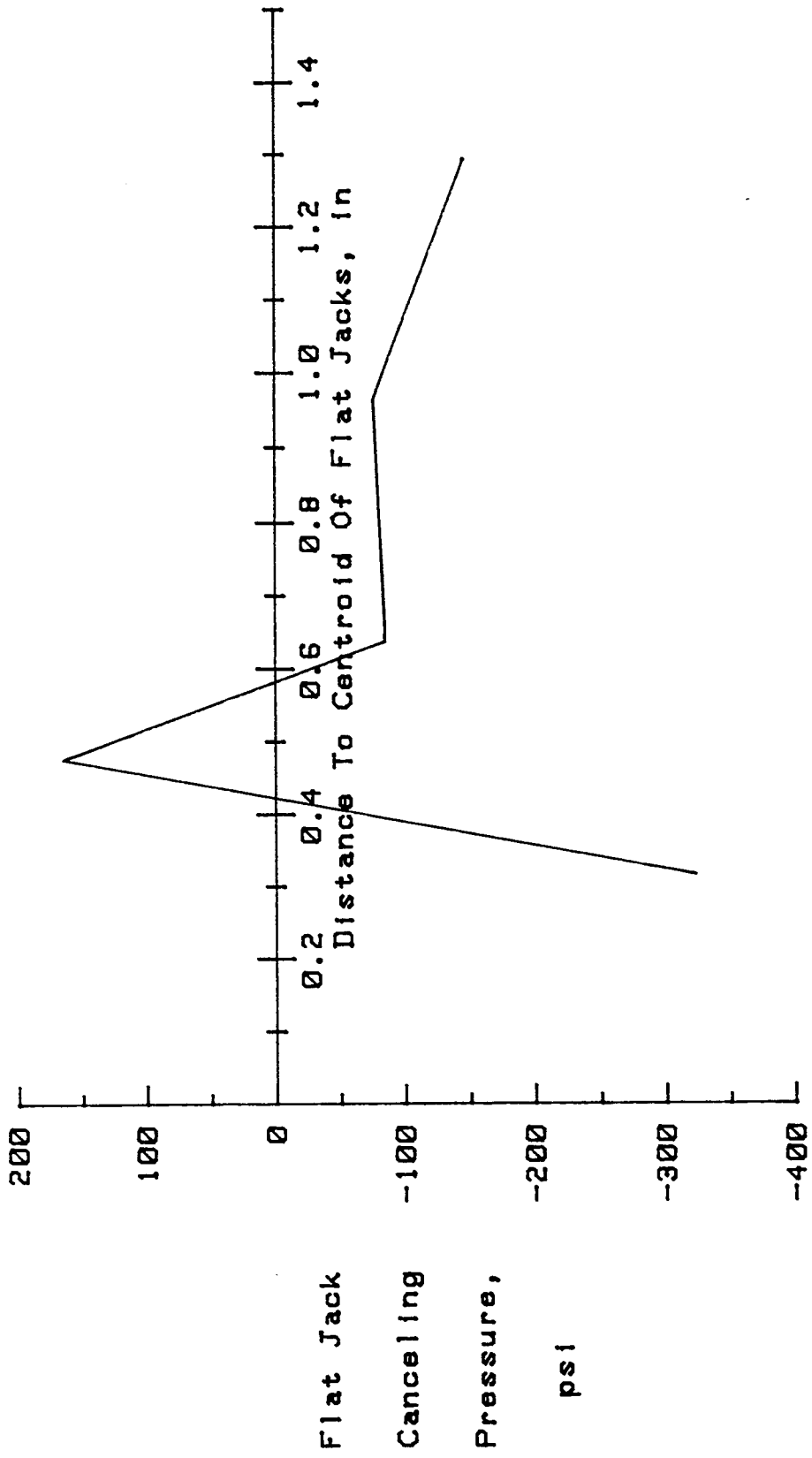


Figure 55. Uncorrected stress profile for 1S5H50/50W.

Table 25. Stress measurement data for specimen 2S3V50/50T.

PFENDER READINGS						
Cut	Flat Jack Internal Pressure (psi)					
Depth (mm)	0	100	200	300	400	500
20	-2.0	-1.0	0.0	1.0	2.0	3.0
40	-1.0	0.0	1.0	3.0	6.0	9.0
60	-5.0	-3.0	0.0	5.0	8.0	11.0
80	-10.0	-6.0	-1.0	4.0	8.0	14.0

LEAST SQUARES CURVE PARAMETERS				
Cut	Slope	Y-Intercept	Correlation	Standard
Depth		(Canceling	Coefficient	Error Of
(mm)	(ksi/in)	Press,psi)	(1=Exact Fit)	Estimate
20	3.94	200	1.0000	0.0
40	1.86	108	0.9726	97.3
60	1.15	172	0.9940	45.9
80	0.82	219	0.9986	21.8



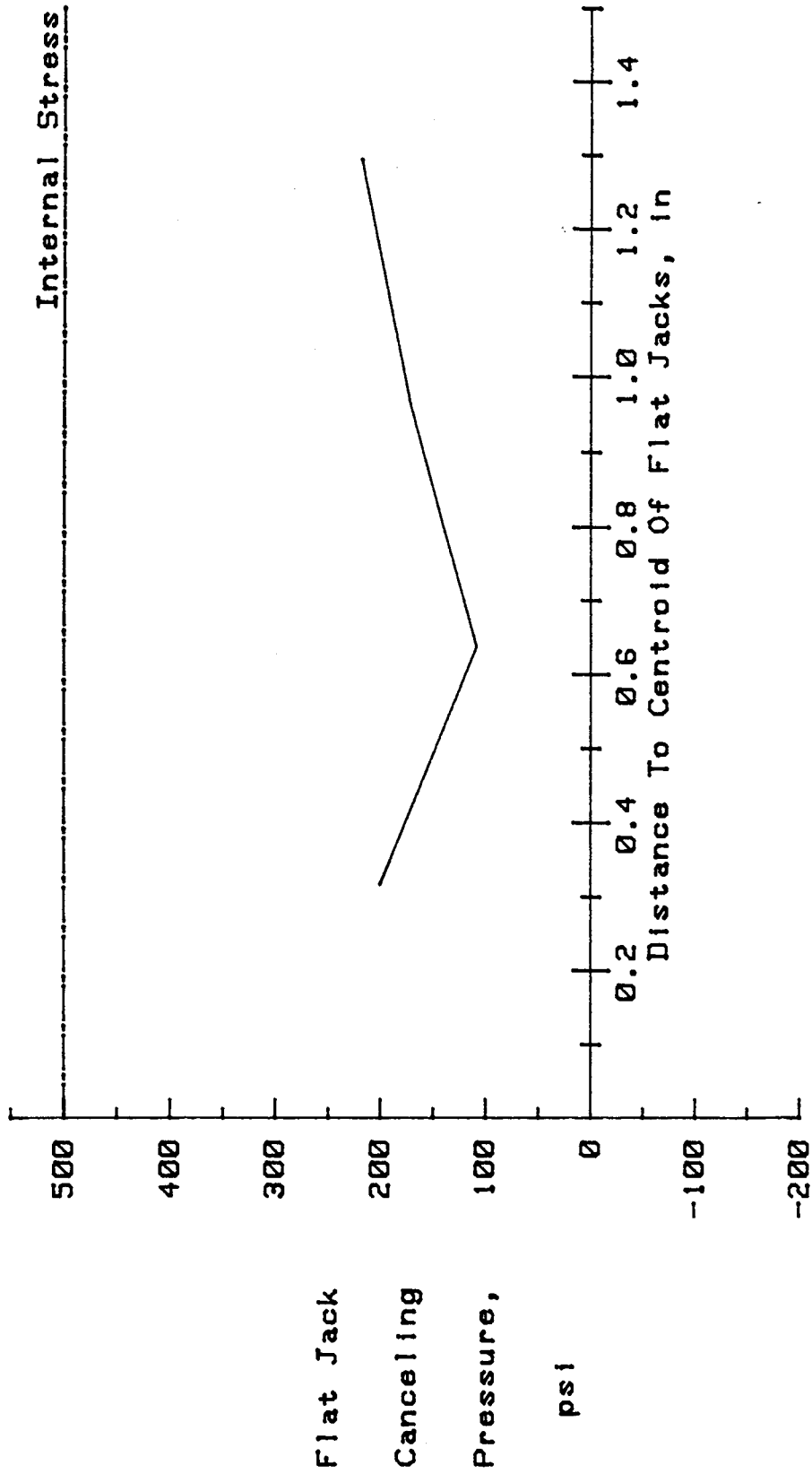
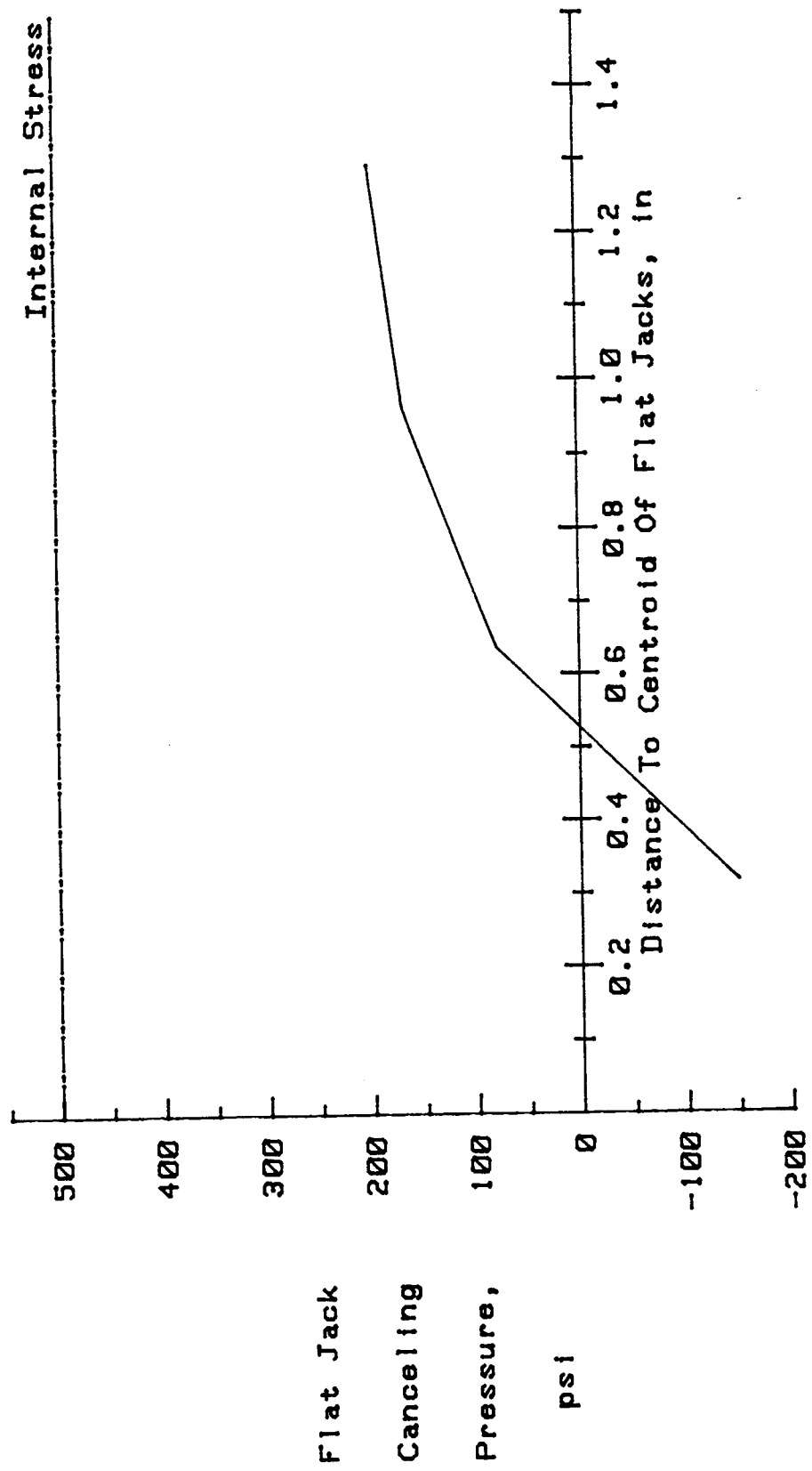


Figure 56. Uncorrected stress profile for 2S3V50/50T.

Table 26. Stress measurement data for specimen 2S3V50/50M.

PFENDER READINGS							
Cut	Flat Jack Internal Pressure (psi)						
Depth (mm)	0	100	200	300	400	500	
20	1.0	2.0	2.0	3.0	4.0	4.0	
40	-1.0	1.0	2.0	4.0	6.0	10.0	
60	-6.0	-2.0	0.0	5.0	9.0	13.0	
80	-10.0	-5.0	0.0	5.0	10.0	16.0	

LEAST SQUARES CURVE PARAMETERS				
Cut	Slope	Y-Intercept	Correlation	Standard
Depth		(Canceling	Coefficient	Error Of
(mm)	(ksi/in)	Press,psi)	(1=Exact Fit)	Estimate
20	5.91	-150	0.9710	100.0
40	1.83	79	0.9786	86.1
60	1.03	167	0.9958	38.3
80	0.76	198	0.9995	13.4



Flat Jack  
 Canceling  
 Pressure,

Figure 57. Uncorrected stress profile for 2S3V50/50M.

Table 27. Stress measurement data for specimen 2S3V50/50B.

PFENDER READINGS						
Cut Depth (mm)	Flat Jack Internal Pressure (psi)					
	0	100	200	300	400	500
20	0.0	0.0	1.0	1.0	4.0	6.0
40	-2.0	1.0	2.0	5.0	6.0	8.0
60	-10.0	-6.0	-1.0	1.0	6.0	12.0
80	-9.0	-4.0	1.0	7.0	12.0	20.0

LEAST SQUARES CURVE PARAMETERS				
Cut Depth (mm)	Slope (ksi/in)	Y-Intercept (Canceling Press,psi)	Correlation Coefficient (1=Exact Fit)	Standard Error Of Estimate
20	2.76	110	0.9165	167.3
40	1.99	82	0.9905	57.6
60	0.92	242	0.9930	49.4
80	0.69	171	0.9967	34.0

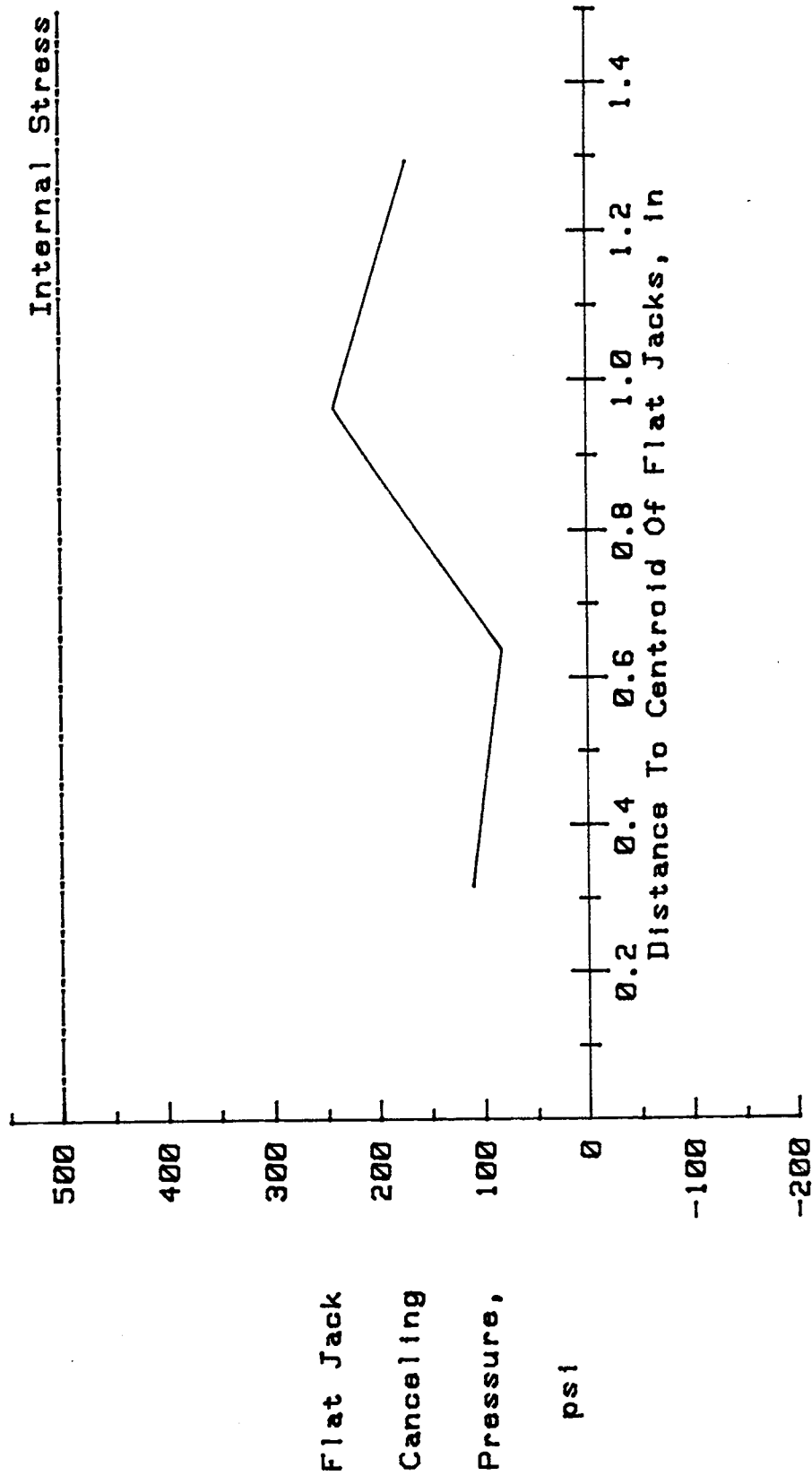


Figure 58. Uncorrected stress profile for 2S3V50/50B.

Table 28. Stress measurement data for specimen 2S4V75/75T.

PFENDER READINGS							
Cut	Flat Jack Internal Pressure (psi)						
Depth (mm)	0	200	400	500	600	700	800
20	-1.0	-4.0	-4.0	1.0	3.0	3.0	5.0
40	1.0	7.0	13.0	14.0	21.0	21.0	23.0
60	-8.0	-2.0	2.0	6.0	9.0	17.0	18.0
80	-15.0	-6.0	4.0	12.0	18.0	24.0	24.0

LEAST SQUARES CURVE PARAMETERS				
Cut	Slope	Y-Intercept	Correlation	Standard
Depth		(Canceling	Coefficient	Error Of
(mm)	(ksi/in)	Press,psi)	(1=Exact Fit)	Estimate
20	2.41	431	0.7701	440.7
40	1.35	-31	0.9866	112.8
60	1.14	284	0.9815	132.2
80	0.73	296	0.9918	88.5

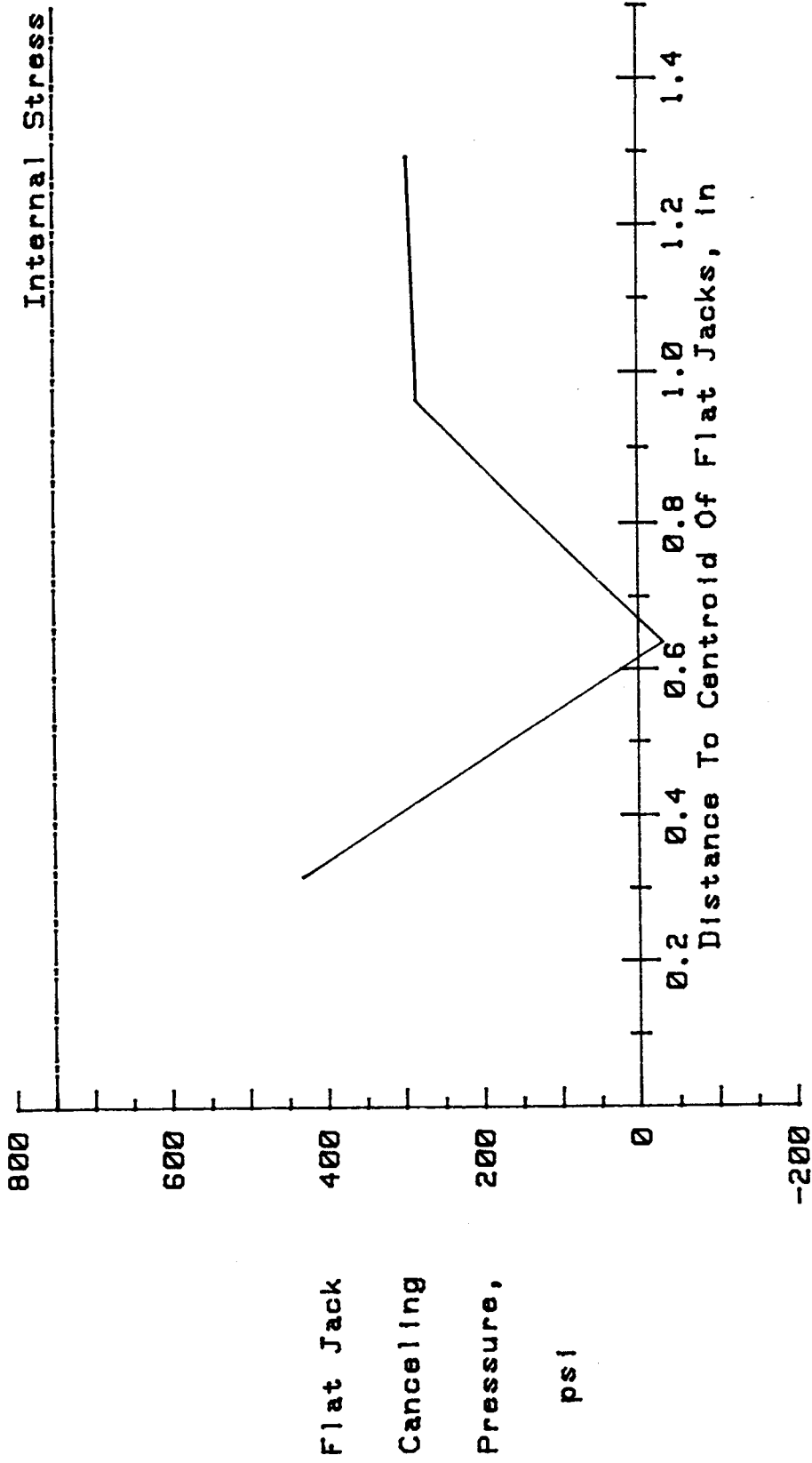


Figure 59. Uncorrected stress profile for 2S4V75/75T.

Table 29. Stress measurement data for specimen 2S4V75/75M.

PFENDER READINGS							
Cut	Flat Jack Internal Pressure						
Depth	(psi)						
(mm)	0	200	400	500	600	700	800
20	-2.0	-6.0	-1.0	-1.0	-2.0	1.0	2.0
40	-8.0	-4.0	2.0	3.0	5.0	9.0	11.0
60	-11.0	-4.0	-1.0	2.0	6.0	10.0	16.0
80	-18.0	-11.0	0.0	6.0	9.0	16.0	20.0

LEAST SQUARES CURVE PARAMETERS				
Cut	Slope	Y-Intercept	Correlation	Standard
Depth		(Canceling	Coefficient	Error Of
(mm)	(ksi/in)	Press,psi)	(1=Exact Fit)	Estimate
20	3.11	559	0.7180	480.8
40	1.64	350	0.9950	68.7
60	1.21	378	0.9814	132.5
80	0.80	393	0.9970	53.4



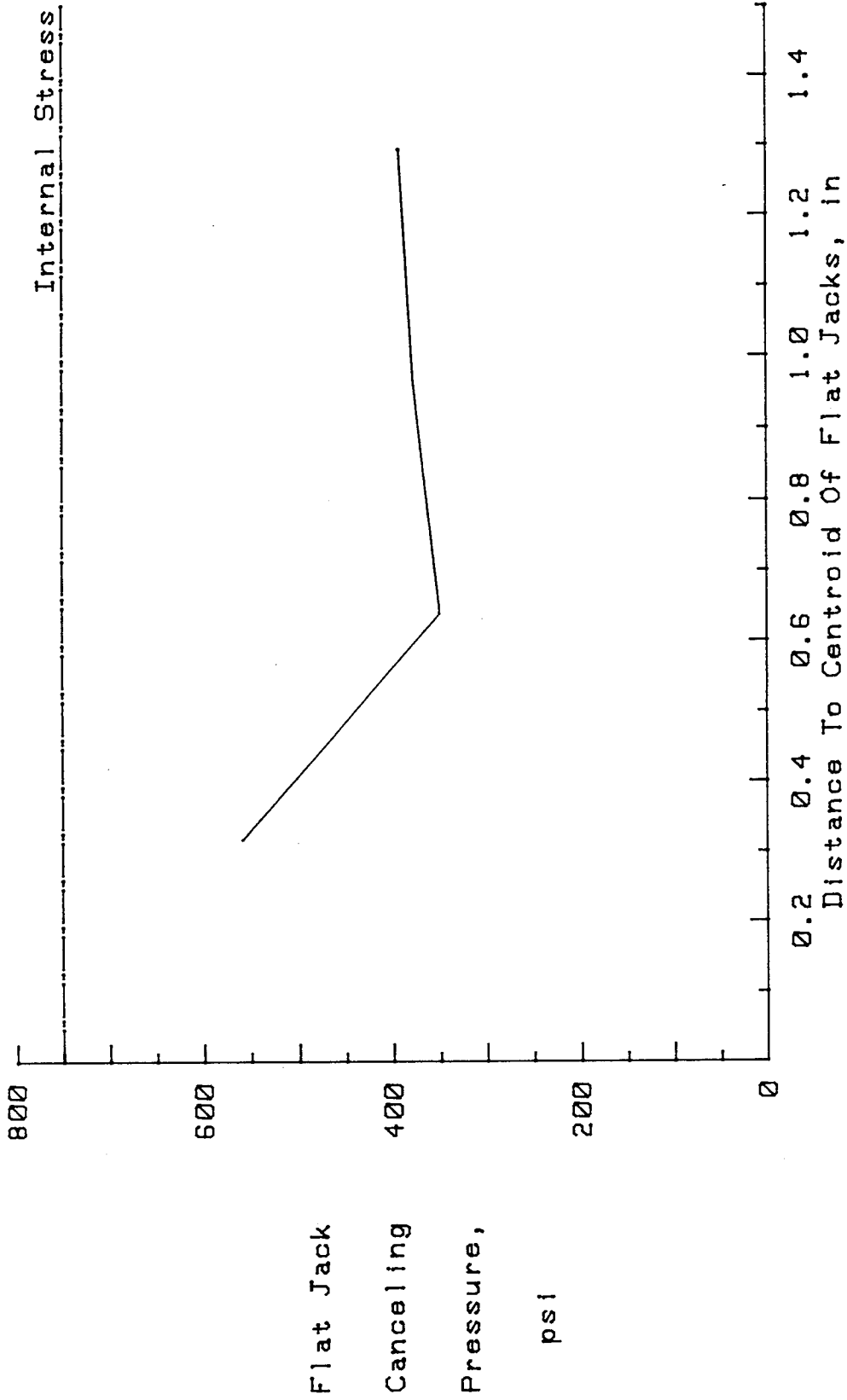
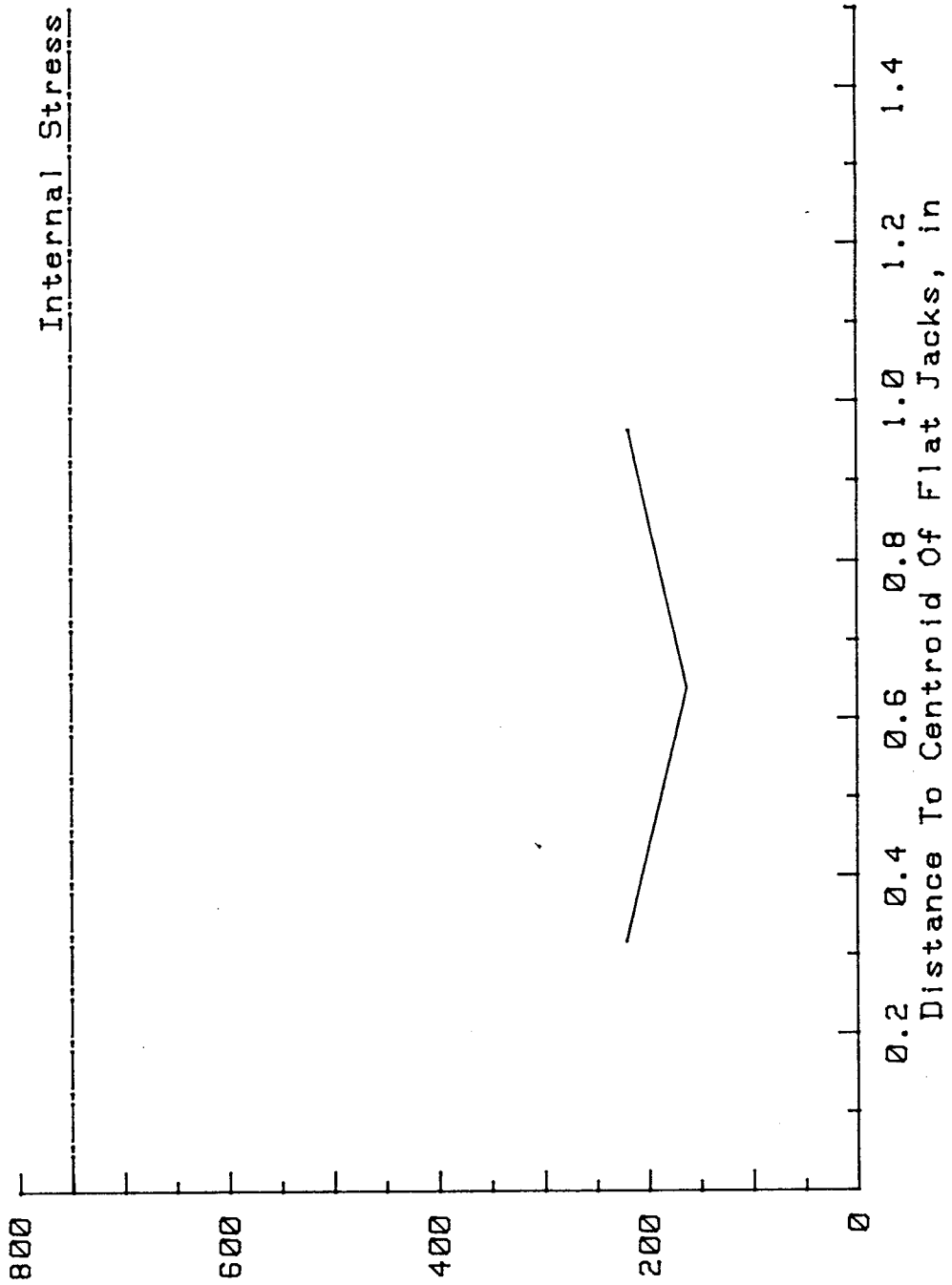


Figure 60. Uncorrected stress profile for 2S4V75/75M.

Table 30. Stress measurement data for specimen 2S4V75/75B.

PFENDER READINGS							
Cut Depth (mm)	Flat Jack Internal Pressure (psi)						
	0	200	400	500	600	700	800
20	2.0	-2.0	3.0	2.0	5.0	7.0	6.0
40	-3.0	0.0	5.0	12.0	10.0	13.0	15.0
60	-4.0	-2.0	4.0	7.0	11.0	10.0	16.0

LEAST SQUARES CURVE PARAMETERS				
Cut Depth (mm)	Slope (ksi/in)	Y-Intercept (Canceling Press,psi)	Correlation Coefficient (1=Exact Fit)	Standard Error Of Estimate
20	2.83	221	0.7750	436.5
40	1.56	163	0.9703	167.2
60	1.49	219	0.9778	100.8



Flat Jack  
 Canceling  
 Pressure,  
 psi

Figure 61. Uncorrected stress profile for 2S4V75/75B.

Table 31. Stress measurement data for specimen 2S5H50/50M.

PFENDER READINGS						
Cut	Flat Jack Internal Pressure (psi)					
Depth	0	100	200	300	400	500
(mm)						
20	4.0	5.0	5.0	7.0	8.0	9.0
40	9.0	11.0	12.0	14.0	17.0	19.0
60	14.0	14.0	18.0	22.0	26.0	31.0
80	16.0	20.0	25.0	30.0	35.0	41.0

LEAST SQUARES CURVE PARAMETERS				
Cut	Slope	Y-Intercept	Correlation	Standard
Depth		(Canceling	Coefficient	Error Of
(mm)	(ksi/in)	Press,psi)	(1=Exact Fit)	Estimate
20	3.67	-340	0.9786	86.1
40	1.93	-421	0.9906	57.2
60	1.06	-309	0.9791	85.0
80	0.79	-305	0.9985	23.1

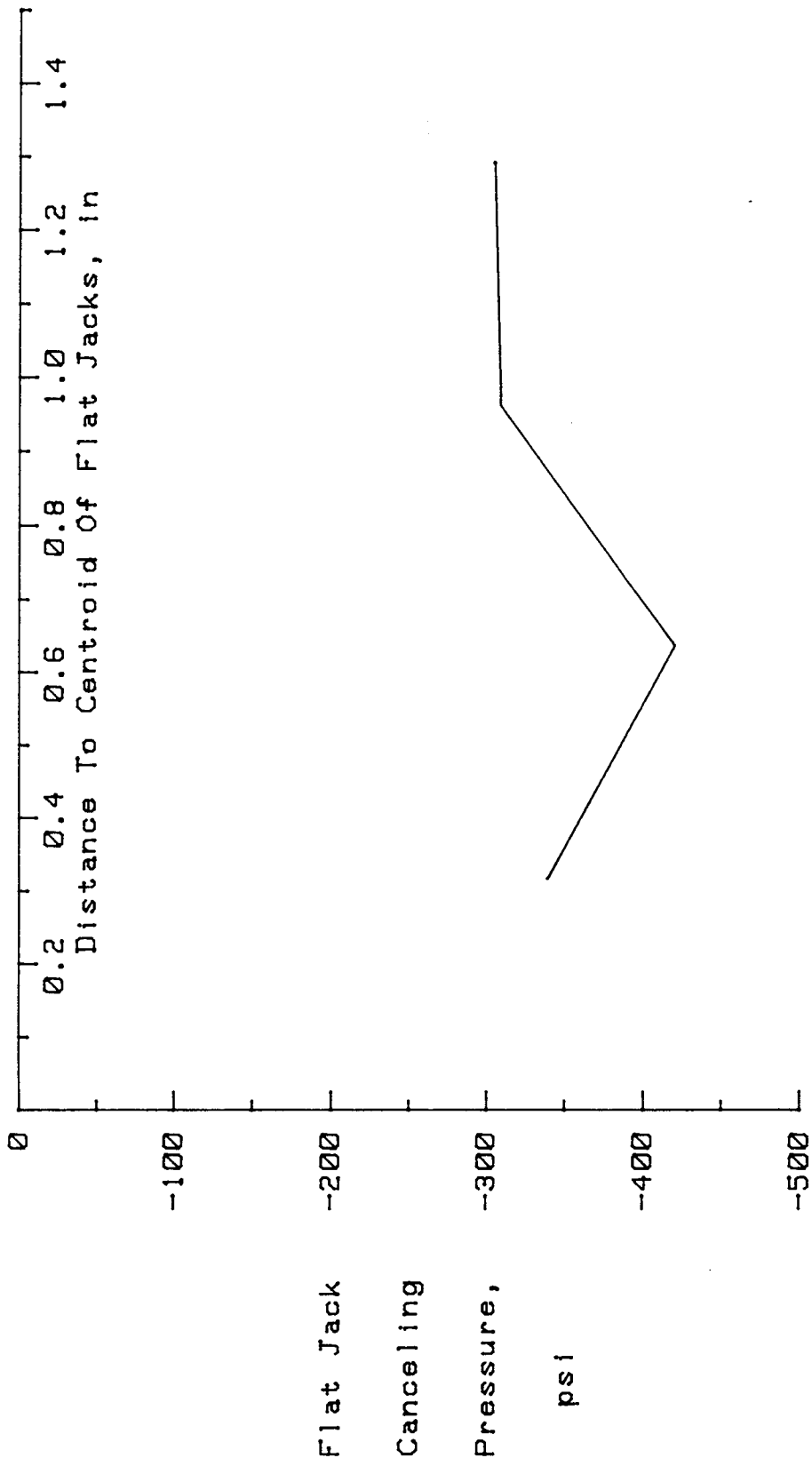


Figure 62. Uncorrected stress profile for 2S5H50/50M.

Table 32. Stress measurement data for specimen 2S6H00/00MOFJ.

PFENDER READINGS							
Cut Depth (mm)	Flat Jack Internal Pressure (psi)						
	0	100	200	300	400	500	
20	4.0	4.0	4.0	6.0	6.0	8.0	
40	5.0	7.0	10.0	12.0	15.0	19.0	
60	9.0	13.0	17.0	20.0	25.0	29.0	
80	10.0	14.0	19.0	25.0	30.0	37.0	

LEAST SQUARES CURVE PARAMETERS				
Cut Depth (mm)	Slope (ksi/in)	Y-Intercept (Canceling Press,psi)	Correlation Coefficient (1=Exact Fit)	Standard Error Of Estimate
20	4.13	-310	0.9165	167.3
40	1.42	-158	0.9937	46.9
60	0.99	-223	0.9985	22.8
80	0.72	-164	0.9969	33.0

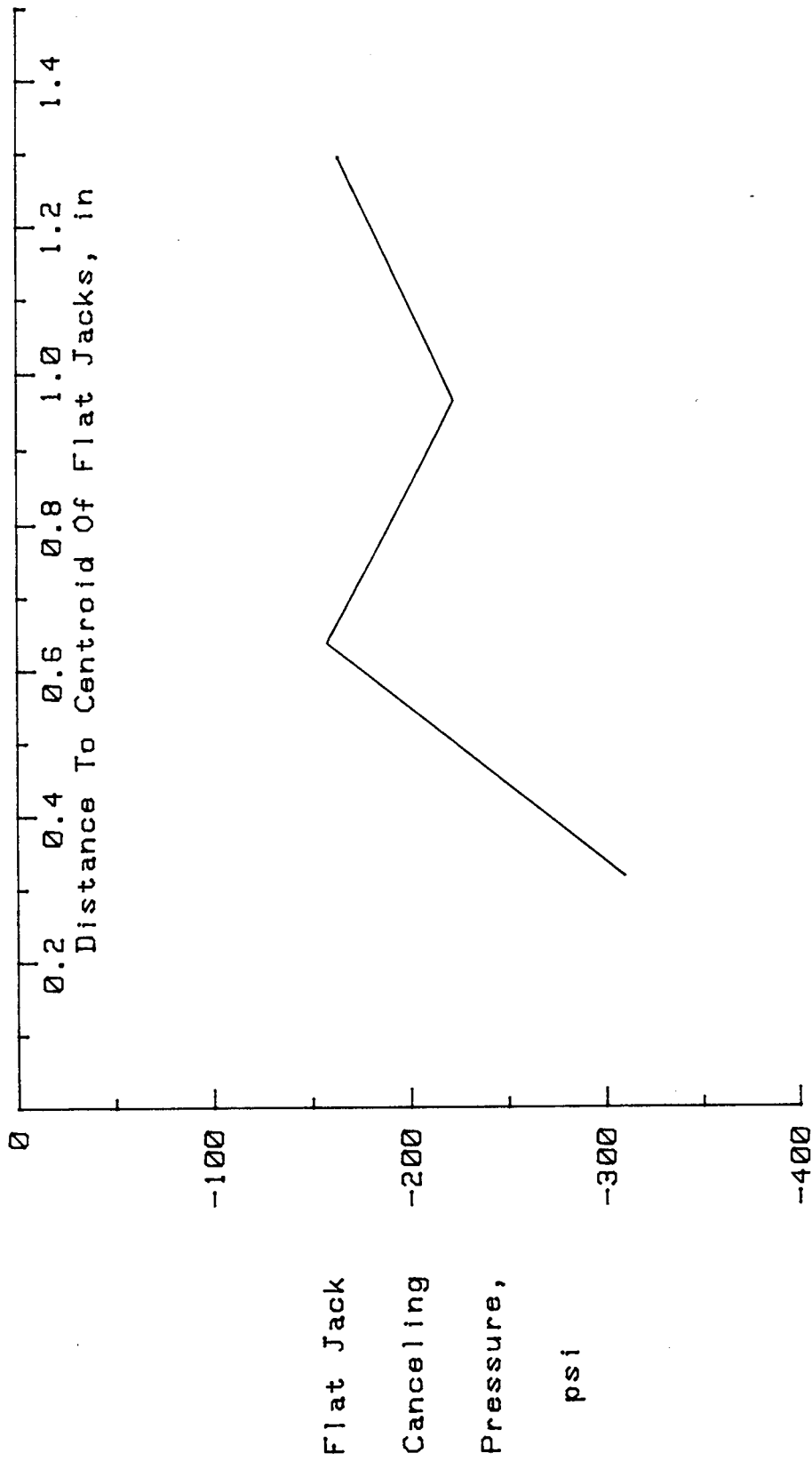


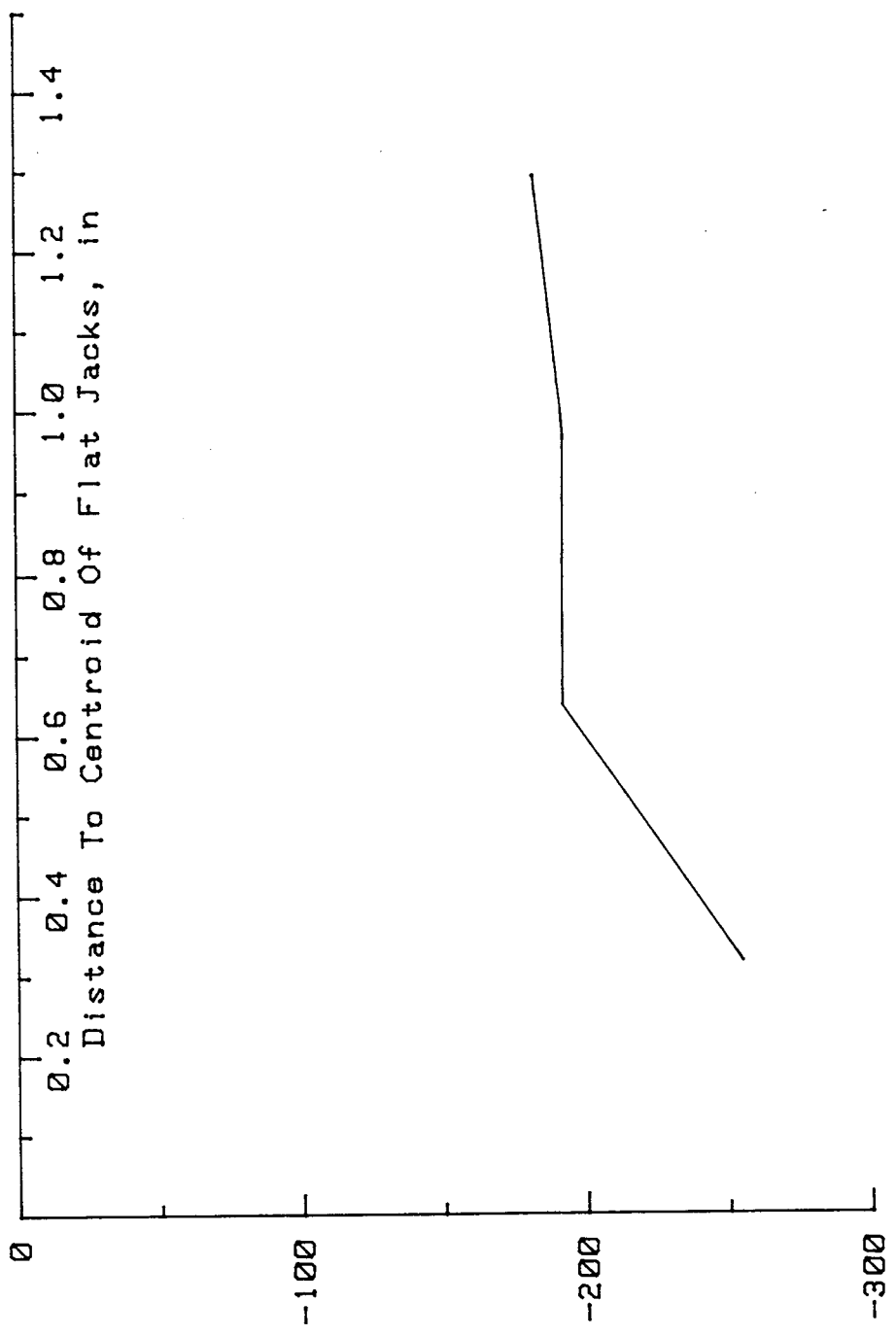
Figure 63. Uncorrected stress profile for 2S6H00/00M0FJ.

Table 33. Stress measurement data for specimen 2S6H00/00M1FJ.

PFENDER READINGS						
Cut Depth (mm)	Flat Jack Internal Pressure (psi)					
	0	100	200	300	400	500
20	3.0	5.0	4.0	5.0	6.0	8.0
40	6.0	9.0	11.0	14.0	17.0	21.0
60	8.0	13.0	17.0	22.0	25.0	30.0
80	11.0	16.0	22.0	28.0	33.0	40.0

LEAST SQUARES CURVE PARAMETERS				
Cut Depth (mm)	Slope (ksi/in)	Y-Intercept (Canceling Press,psi)	Correlation Coefficient (1=Exact Fit)	Standard Error Of Estimate
20	3.85	-255	0.9000	182.4
40	1.34	-192	0.9954	40.0
60	0.91	-193	0.9983	24.3
80	0.68	-182	0.9991	18.0





Flat Jack  
Canceling  
Pressure,  
psi

Figure 64. Uncorrected stress profile for 2S6H00/00M1FJ.

Table 34. Stress measurement data for specimen 2S6H00/00M2FJ.

PFENDER READINGS						
Cut Depth (mm)	Flat Jack Internal Pressure (psi)					
	0	100	200	300	400	500
20	2.0	2.0	4.0	5.0	5.0	6.0
40	6.0	8.0	11.0	14.0	17.0	20.0
60	9.0	12.0	15.0	19.0	23.0	29.0
80	12.0	16.0	21.0	26.0	32.0	38.0

LEAST SQUARES CURVE PARAMETERS				
Cut Depth (mm)	Slope (ksi/in)	Y-Intercept (Canceling Press,psi)	Correlation Coefficient (1=Exact Fit)	Standard Error Of Estimate
20	4.22	-179	0.9583	119.5
40	1.37	-192	0.9983	24.1
60	0.99	-198	0.9913	54.9
80	0.75	-210	0.9975	29.7

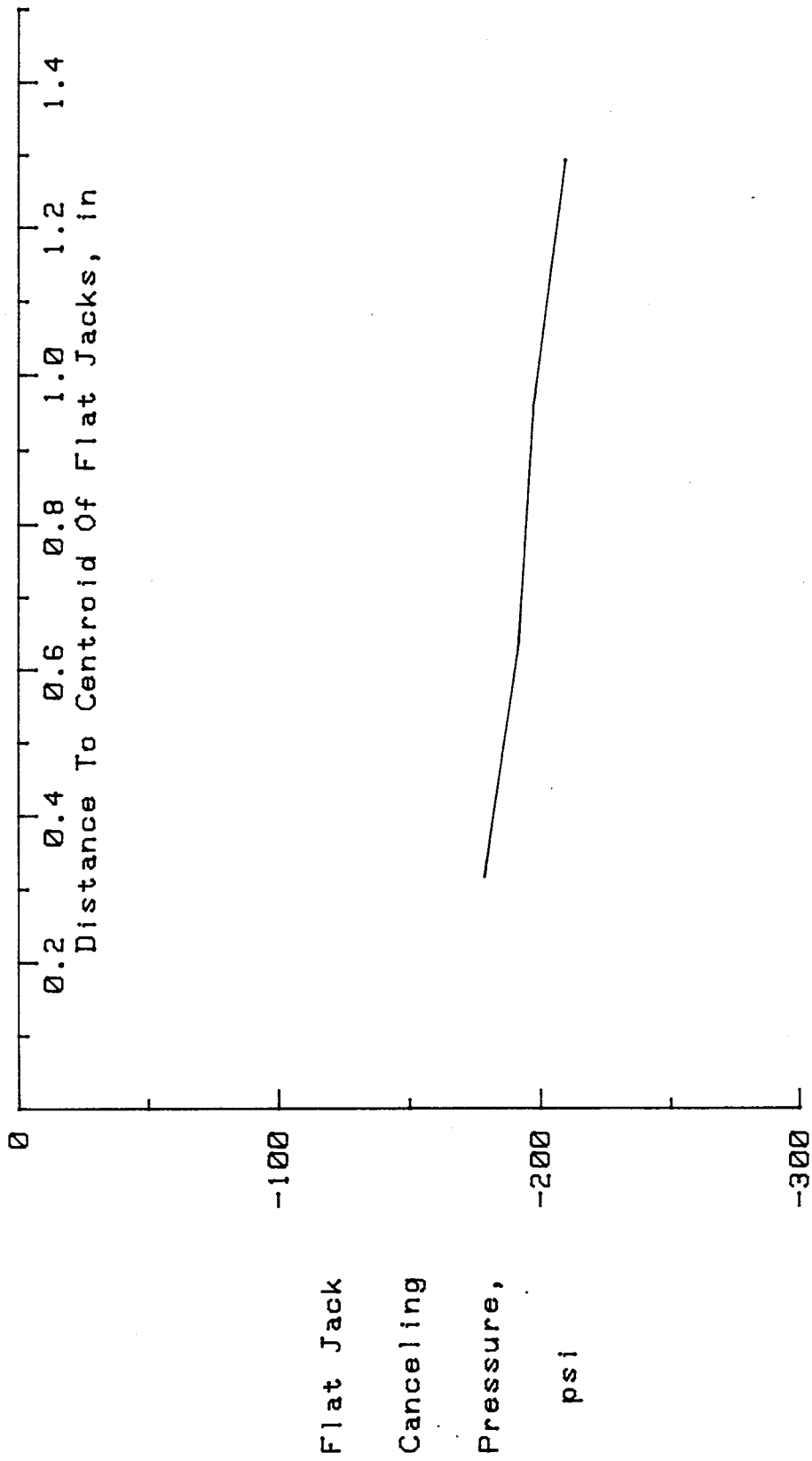


Figure 65. Uncorrected stress profile for 2S6H00/00M2FJ.

Table 35. Stress measurement data for specimen 3N2V70/75T.

PFENDER READINGS				
Cut Depth (mm)	Flat Jack Internal Pressure (psi)			
	0	300	600	900
20	-6.4	-4.6	-2.6	0.4
30	-6.3	-5.7	-0.6	5.4
40	-15.6	-8.6	-1.0	7.4
50	-16.6	-7.6	2.4	14.3
60	-24.2	-12.6	-3.7	12.0
70	-30.6	-14.6	0.4	16.4

LEAST SQUARES CURVE PARAMETERS				
Cut Depth (mm)	Slope (ksi/in)	Y-Intercept (Canceling Press,psi)	Correlation Coefficient (1=Exact Fit)	Standard Error Of Estimate
20	5.19	885	0.9923	83.2
30	2.68	572	0.9542	200.6
40	1.54	624	0.9992	27.4
50	1.15	505	0.9980	42.7
60	0.99	630	0.9937	74.9
70	0.76	587	0.9999	8.6

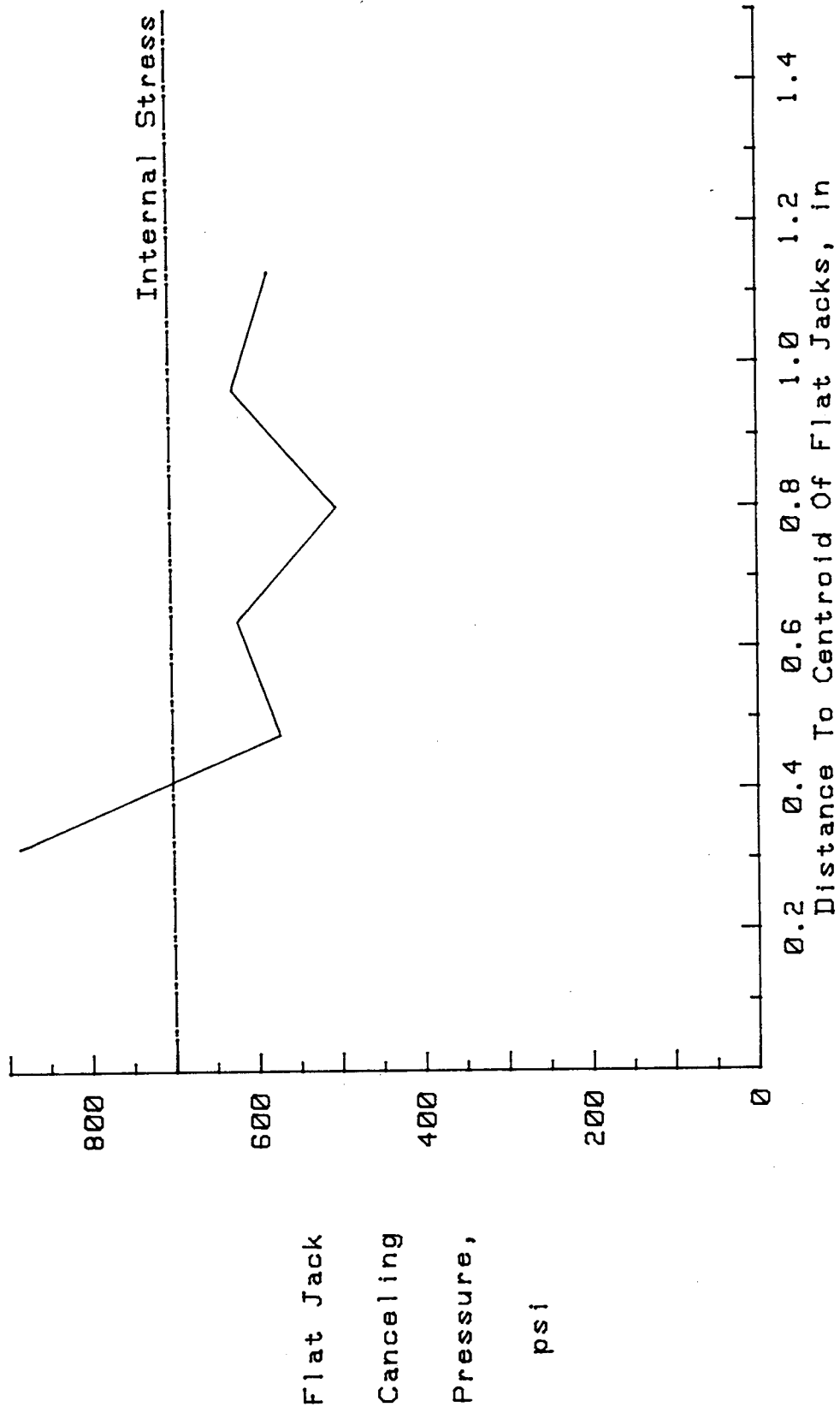
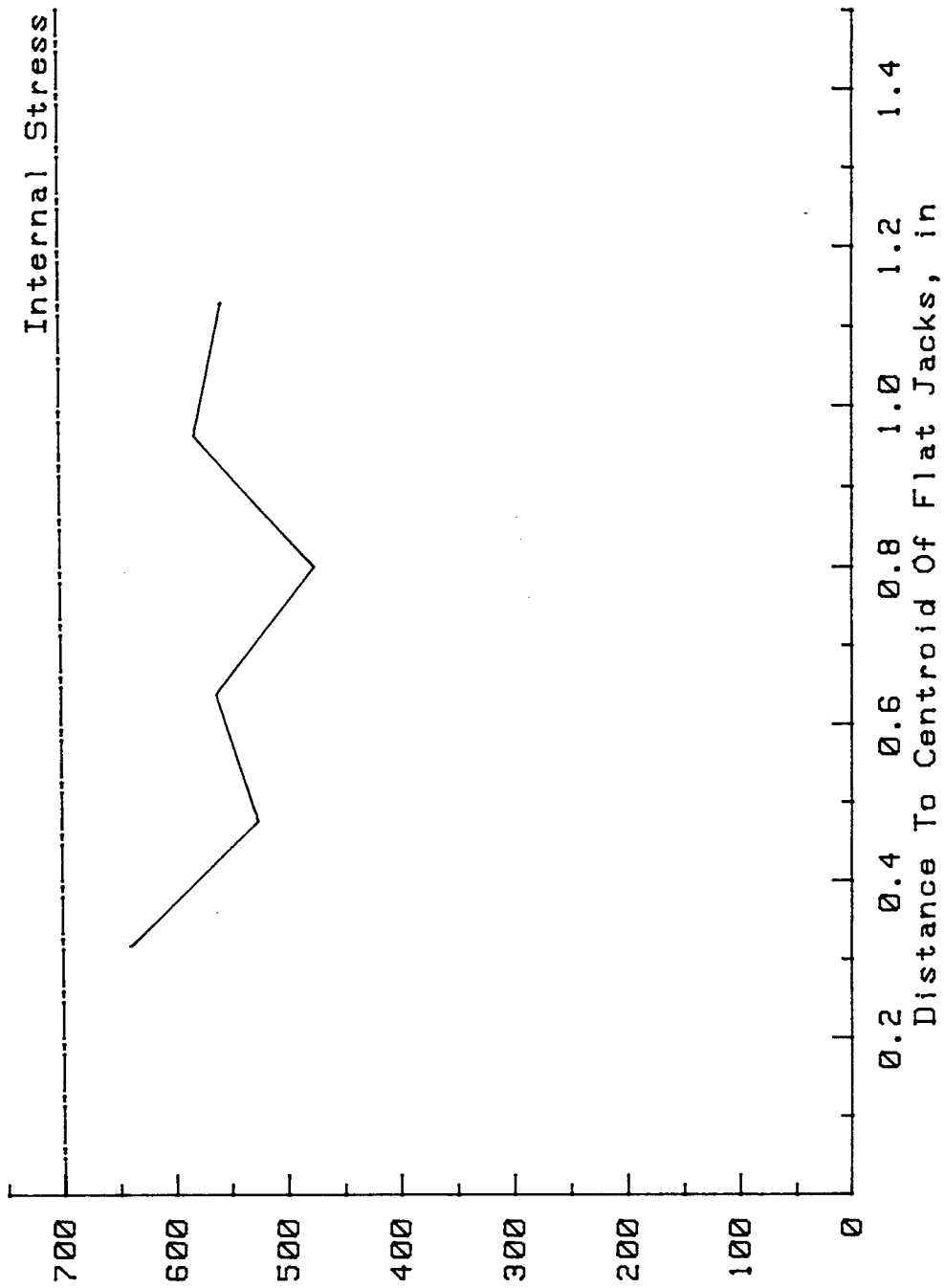


Figure 66. Uncorrected stress profile for 3N2V70/75T.

Table 36. Stress measurement data for specimen 3N2Y70/75B.

PFENDER READINGS				
Cut Depth (mm)	Flat Jack Internal Pressure (psi)			
	0	300	600	900
20	-6.1	-4.1	-0.3	2.7
30	-10.4	-5.3	1.7	7.7
40	-16.3	-7.3	0.7	9.7
50	-17.3	-6.3	4.2	15.4
60	-24.3	-12.3	-0.2	13.9
70	-30.3	-14.3	1.7	18.7

LEAST SQUARES CURVE PARAMETERS				
Cut Depth (mm)	Slope (ksi/in)	Y-Intercept (Canceling Press,psi)	Correlation Coefficient (1=Exact Fit)	Standard Error Of Estimate
20	3.86	641	0.9936	75.7
30	1.92	527	0.9983	38.6
40	1.37	565	0.9997	15.6
50	1.09	478	0.9999	7.9
60	0.93	585	0.9992	26.8
70	0.72	561	0.9999	10.1



Flat Jack  
 Canceling  
 Pressure,  
 psi

Figure 67. Uncorrected stress profile for 3N2V70/75B.

Table 37. Stress measurement data for specimen 3N3V51/42T.

PFENDER READINGS				
Cut Depth (mm)	Flat Jack Internal Pressure (psi)			
	0	200	400	600
20	-5.9	-4.4	-2.4	-0.4
30	-9.4	-6.8	-3.4	0.5
40	-12.4	-7.6	-2.4	3.2
50	-15.4	-9.4	-2.4	4.5
60	-18.8	-11.4	-2.7	6.3
70	-22.8	-13.4	-3.6	7.2
80	-26.1	-18.6	-7.1	4.0

LEAST SQUARES CURVE PARAMETERS				
Cut Depth (mm)	Slope (ksi/in)	Y-Intercept (Canceling Press,psi)	Correlation Coefficient (1=Exact Fit)	Standard Error Of Estimate
20	4.24	657	0.9978	29.5
30	2.34	584	0.9956	41.8
40	1.50	484	0.9993	17.2
50	1.17	470	0.9993	16.3
60	0.93	458	0.9989	20.7
70	0.79	463	0.9994	15.3
80	0.76	532	0.9959	40.7



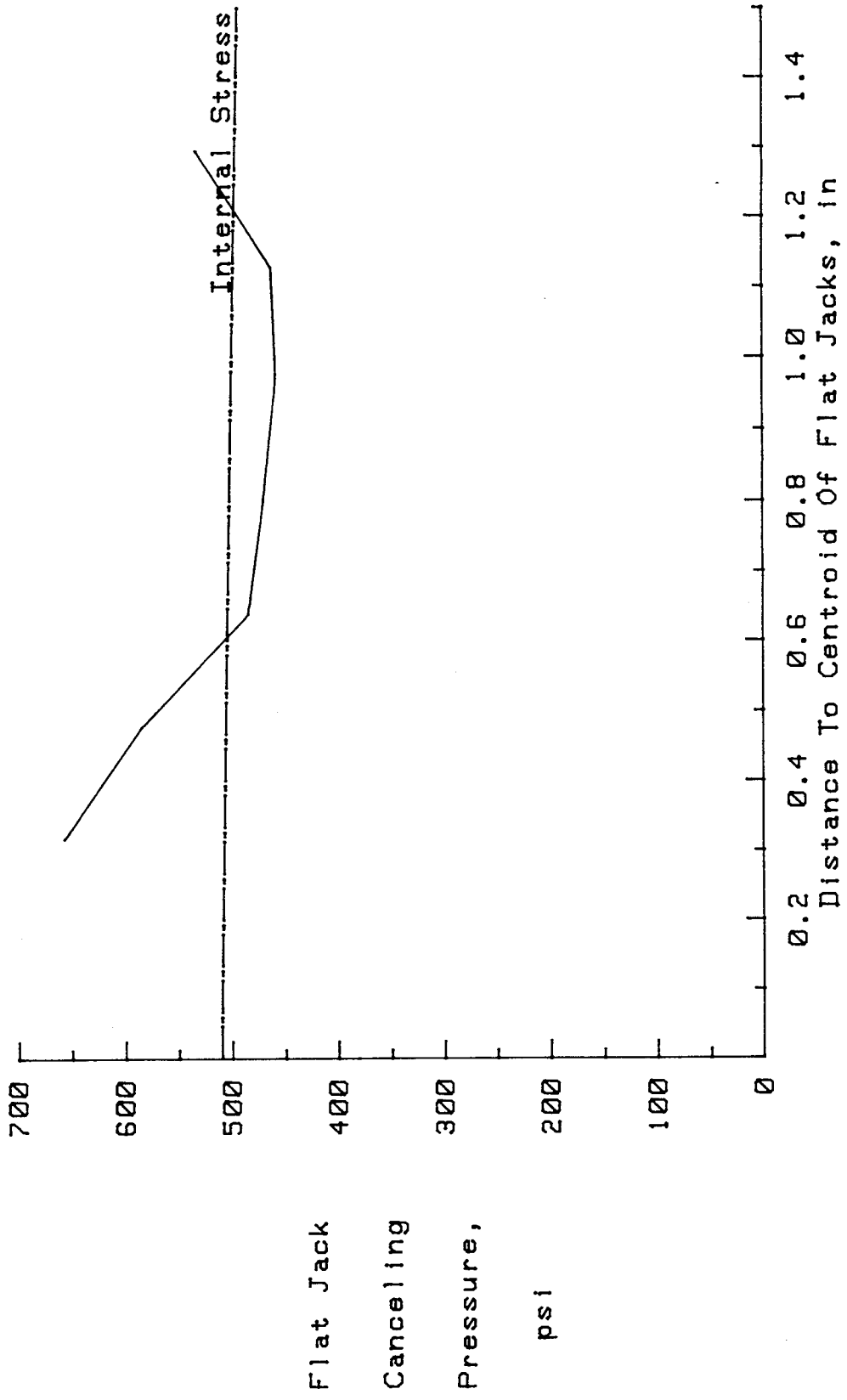


Figure 68. Uncorrected stress profile for 3N3V51/42T.

Table 38. Stress measurement data for specimen 3N4V55/46T.

PFENDER READINGS				
Cut Depth (mm)	Flat Jack Internal Pressure (psi)			
	0	200	400	600
20	0.2	0.2	1.8	3.0
30	-3.0	-1.8	2.4	5.3
40	-8.0	-5.0	-1.0	4.6
50	-20.4	-16.2	-9.9	-2.2
60	-25.0	-18.0	-10.3	-2.0
70	-25.0	-17.5	-8.0	3.0
80	-29.0	-21.7	-11.8	0.2

LEAST SQUARES CURVE PARAMETERS				
Cut Depth (mm)	Slope (ksi/in)	Y-Intercept (Canceling Press,psi)	Correlation Coefficient (1=Exact Fit)	Standard Error Of Estimate
20	7.08	66	0.9483	141.9
30	2.60	252	0.9811	86.5
40	1.85	410	0.9904	61.9
50	1.27	693	0.9918	57.2
60	1.03	660	0.9993	16.9
70	0.84	552	0.9965	37.4
80	0.80	616	0.9942	48.0

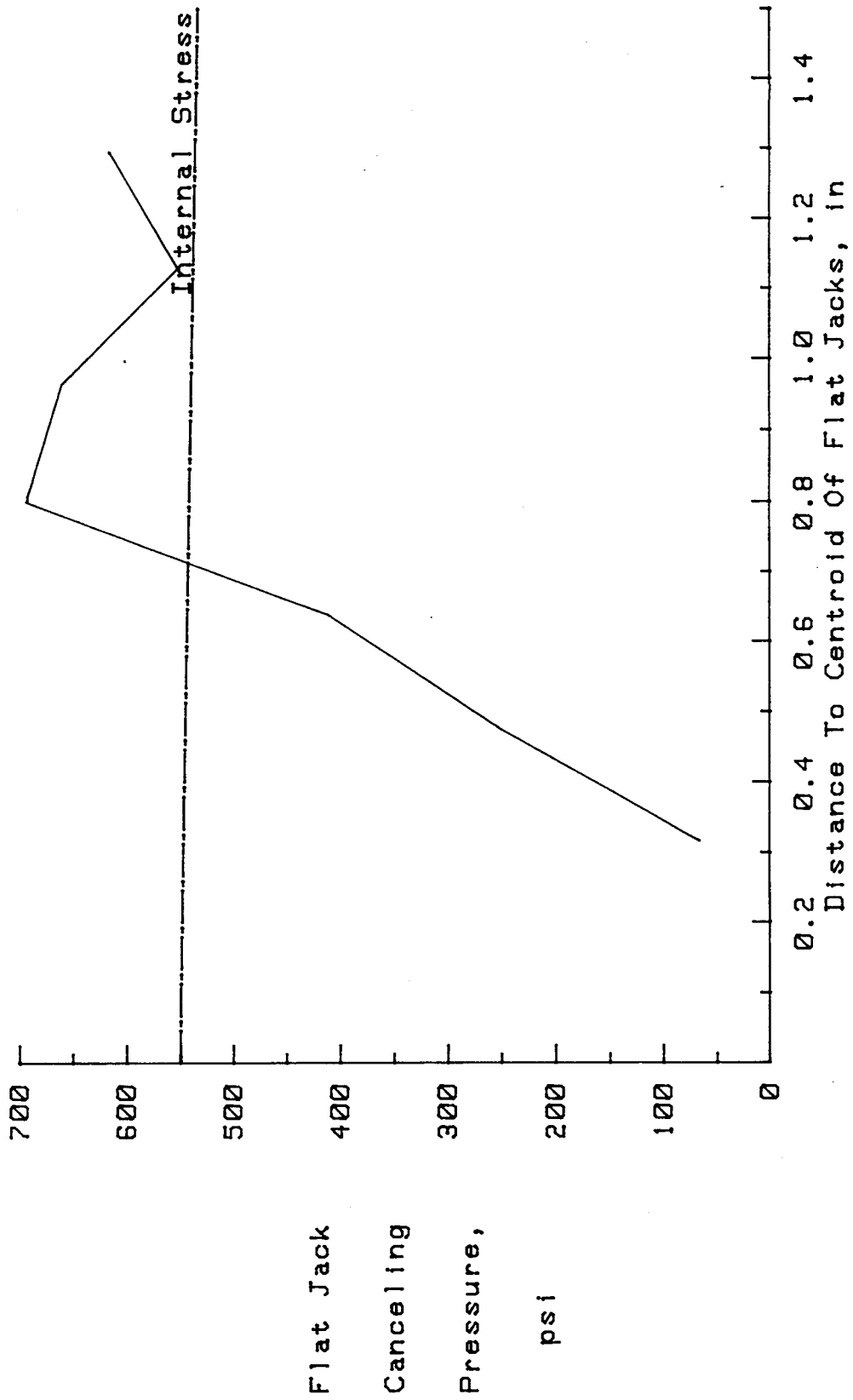


Figure 69. Uncorrected stress profile for 3M4V55/46T.

Table 39. Stress measurement data for specimen 3N4V55/46B.

PFENDER READINGS				
Cut Depth (mm)	Flat Jack Internal Pressure (psi)			
	0	200	400	600
20	-2.1	-0.8	0.8	1.8
30	-4.1	0.6	0.3	4.0
40	-8.6	-5.0	-1.4	3.8
50	-20.3	-16.3	-8.3	-1.5
60	-24.1	-17.1	-9.4	-1.1
70	-25.1	-17.1	-7.8	2.8
80	-28.1	-20.6	-10.4	1.5

LEAST SQUARES CURVE PARAMETERS				
Cut Depth (mm)	Slope (ksi/in)	Y-Intercept (Canceling Press,psi)	Correlation Coefficient (1=Exact Fit)	Standard Error Of Estimate
20	5.70	313	0.9956	41.9
30	2.82	285	0.9323	161.7
40	1.90	437	0.9949	45.1
50	1.20	657	0.9921	56.1
60	1.03	638	0.9993	16.9
70	0.84	553	0.9979	28.9
80	0.78	588	0.9949	45.3

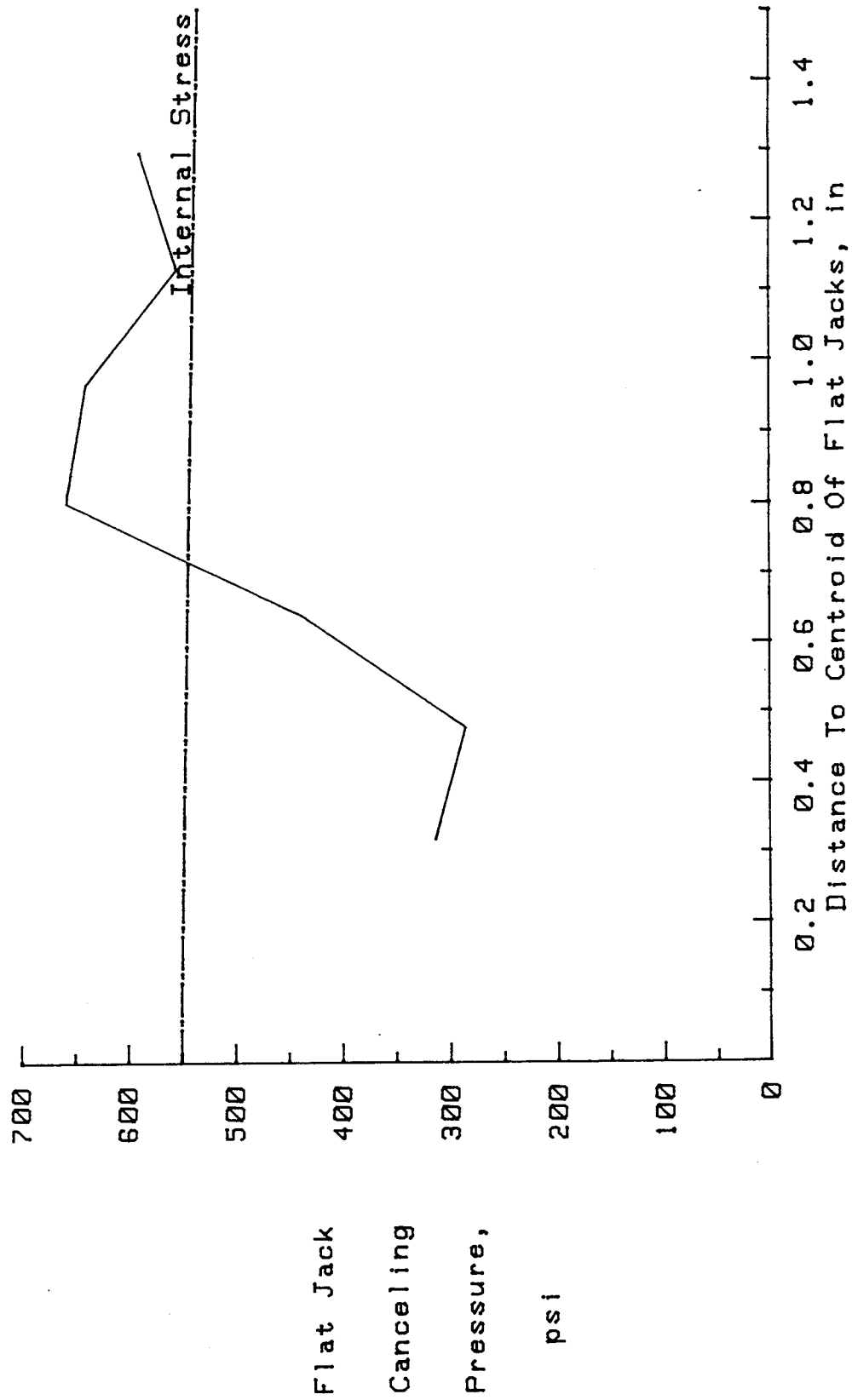


Figure 70. Uncorrected stress profile for 3N4V55/46B.

Table 40. Stress measurement data for specimen 3S5H50/50E.

PFENDER READINGS				
Cut Depth (mm)	Flat Jack Internal Pressure (psi)			
	0	100	200	300
20	1.7	1.7	0.7	1.7
30	2.7	3.7	4.7	6.7
40	4.7	5.7	7.7	10.7
50	5.7	6.7	9.2	12.2
60	7.7	11.2	14.7	17.7
70	8.7	11.7	15.7	20.7
80	8.7	12.7	18.7	23.7

LEAST SQUARES CURVE PARAMETERS				
Cut Depth (mm)	Slope (ksi/in)	Y-Intercept (Canceling Press,psi)	Correlation Coefficient (1=Exact Fit)	Standard Error Of Estimate
20	-2.62	247	-.2582	216.0
30	2.92	-181	0.9827	41.4
40	1.87	-193	0.9759	48.8
50	1.72	-218	0.9790	45.6
60	1.17	-232	0.9993	8.2
70	0.97	-201	0.9938	24.8
80	0.77	-161	0.9973	16.4

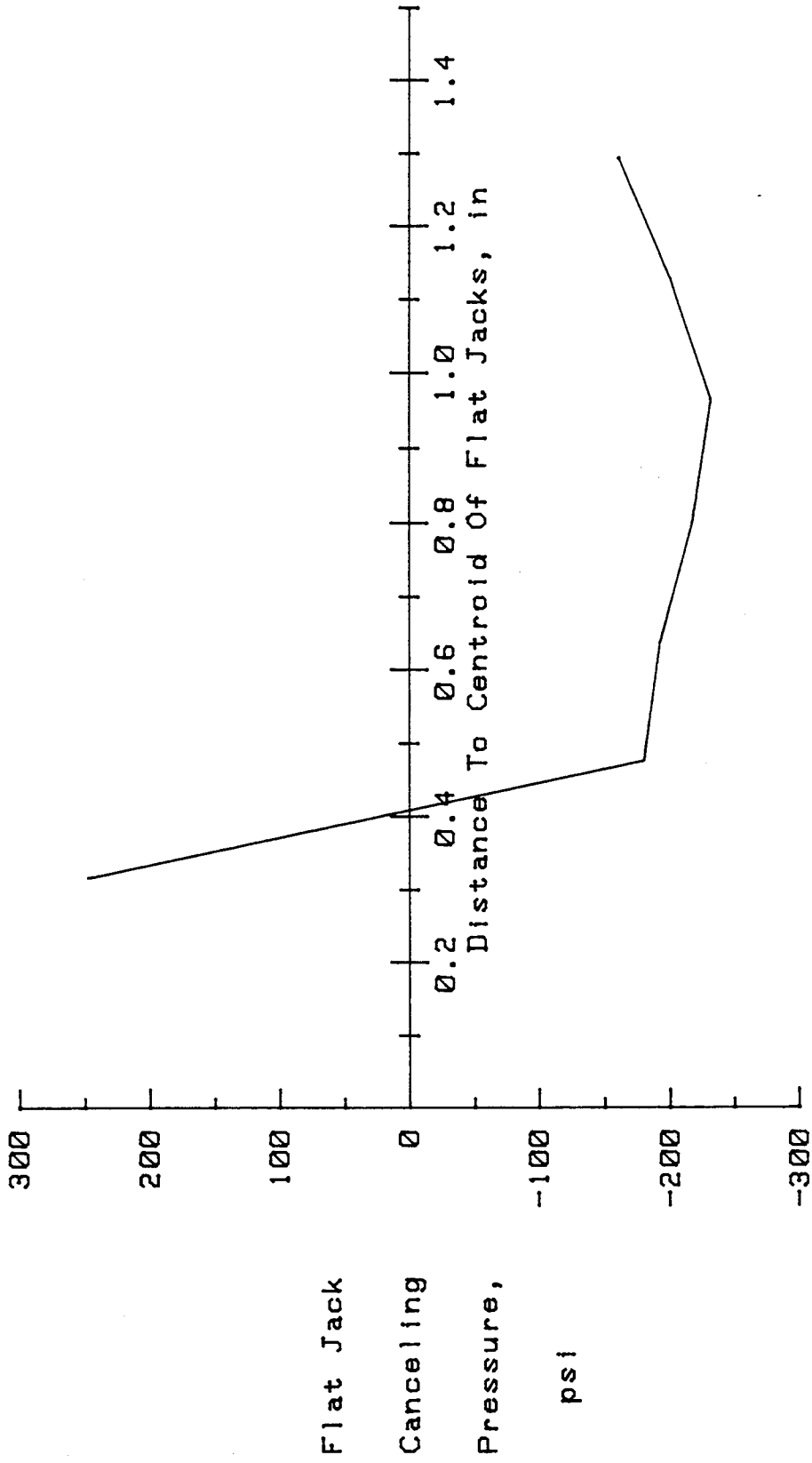


Figure 71. Uncorrected stress profile for 3S5H50/50E.

Table 41. Stress measurement data for specimen 3S5H50/50WK.

PFENDER READINGS				
Cut Depth (mm)	Flat Jack Internal Pressure (psi)			
	0	100	200	300
20	2.9	2.9	2.9	4.9
30	3.9	5.9	6.9	8.9
40	6.9	9.9	11.9	13.9
50	7.9	9.9	12.9	16.4
60	9.9	14.9	17.9	21.9
70	11.9	13.9	17.9	22.9
80	13.6	15.7	20.5	23.6

LEAST SQUARES CURVE PARAMETERS				
Cut Depth (mm)	Slope (ksi/in)	Y-Intercept (Canceling Press,psi)	Correlation Coefficient (1=Exact Fit)	Standard Error Of Estimate
20	3.94	-190	0.7746	141.4
30	2.42	-244	0.9923	27.7
40	1.69	-308	0.9944	23.7
50	1.36	-257	0.9930	26.4
60	1.00	-260	0.9954	21.4
70	1.03	-285	0.9836	40.3
80	1.11	-367	0.9901	31.4



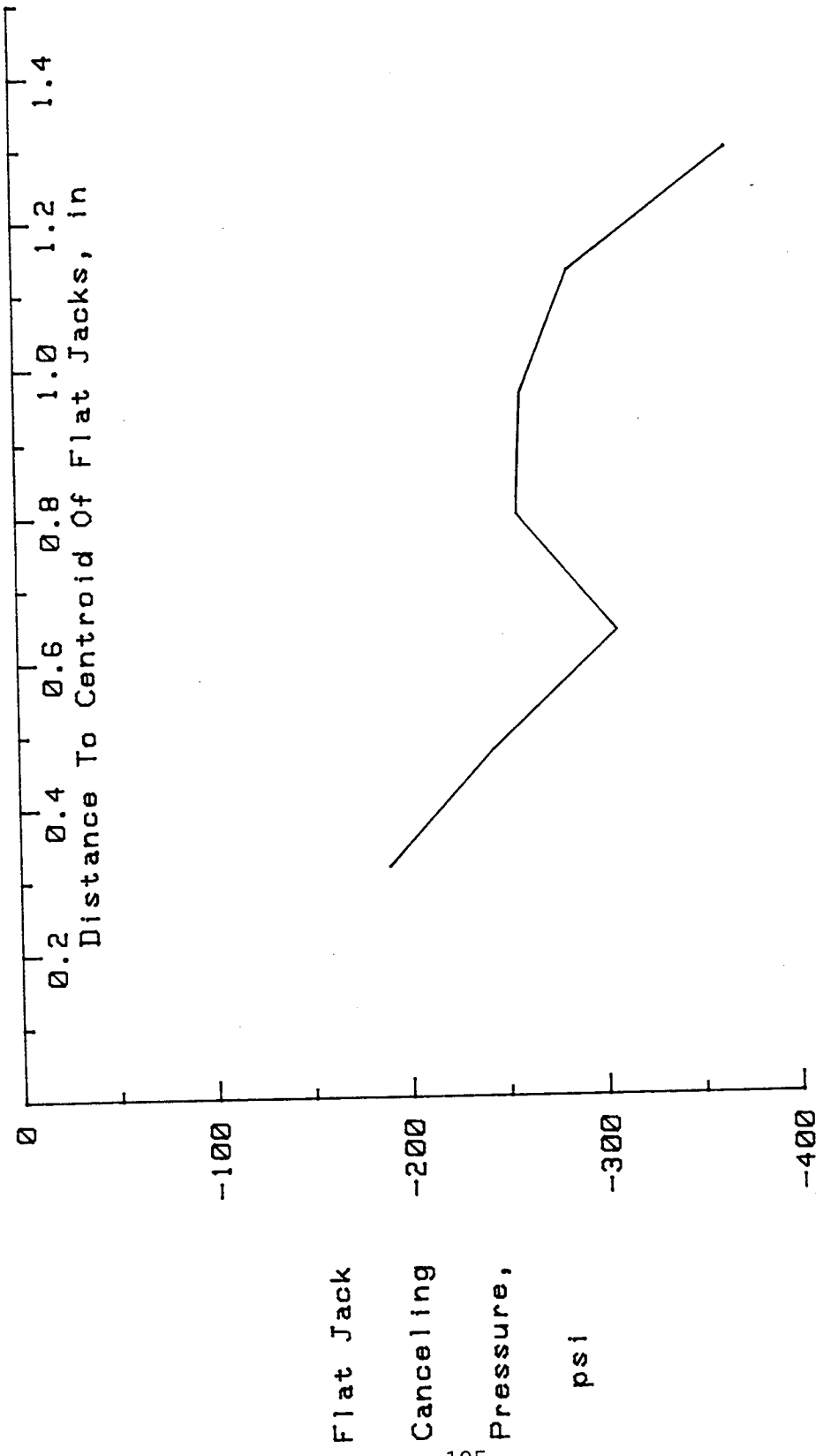


Figure 72. Uncorrected stress profile for 3S5H50/50MK.

Table 42. Stress measurement data for specimen 3S6H00/00E.

PFENDER READINGS					
Cut Depth (mm)	Flat Jack Internal Pressure (psi)				
	0	100	200	300	400
20	1.1	-0.2	2.3	2.3	2.9
40	2.6	3.6	7.7	10.0	12.0
60	5.3	10.7	12.6	16.6	22.9
80	7.3	11.0	24.6	20.4	25.0

LEAST SQUARES CURVE PARAMETERS				
Cut Depth (mm)	Slope (ksi/in)	Y-Intercept (Canceling Press,psi)	Correlation Coefficient (1=Exact Fit)	Standard Error Of Estimate
20	3.92	33	0.7792	198.2
40	1.52	-77	0.9865	51.7
60	0.93	-122	0.9859	52.9
80	0.68	-103	0.8765	152.2

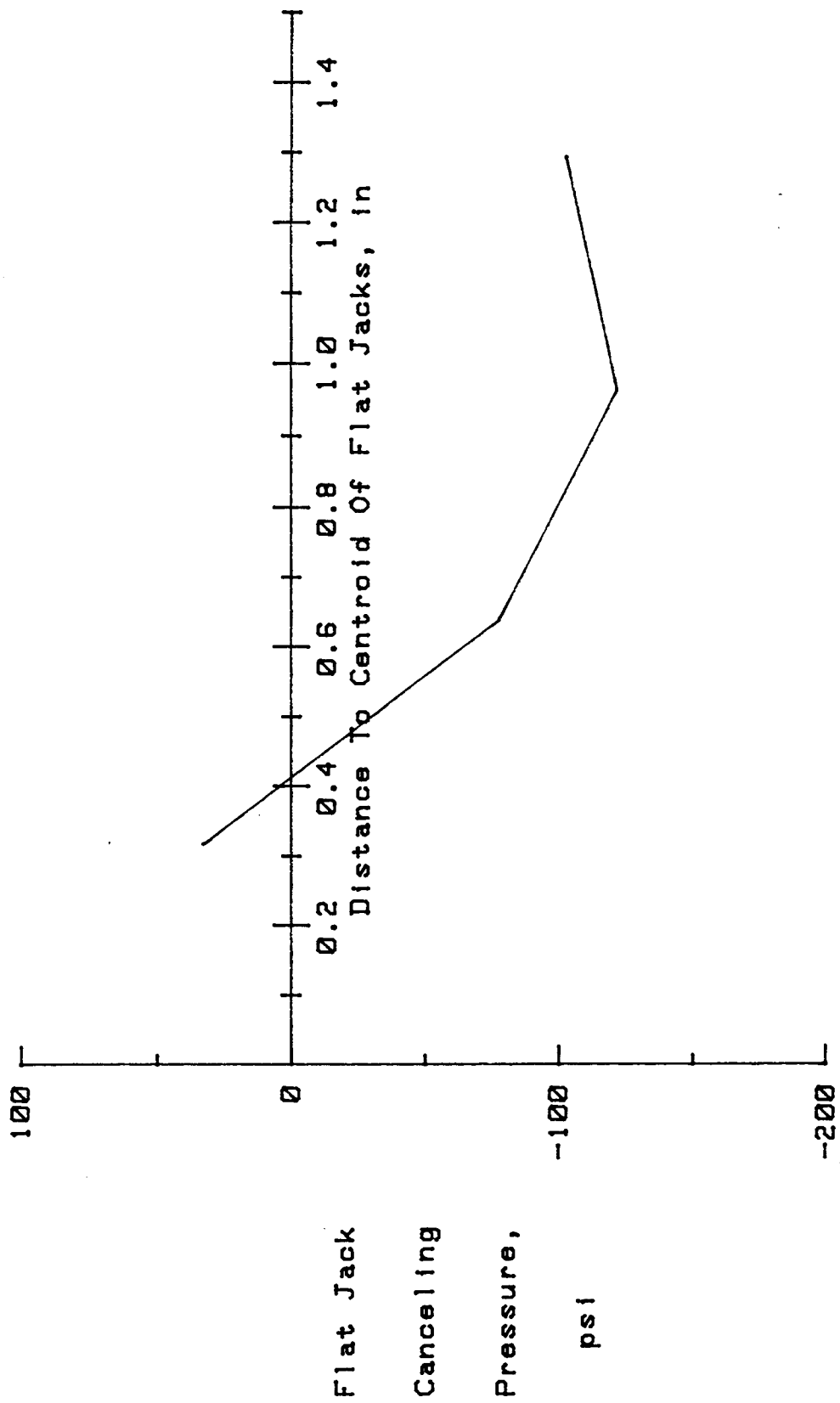


Figure 73. Uncorrected stress profile for 3S6H00/00E.

Table 43. Stress measurement data for specimen 3S6H00/00WK.

PFENDER READINGS					
Cut Depth (mm)	Flat Jack Internal Pressure (psi)				
	0	100	200	300	400
20	-1.4	-0.9	0.6	-1.4	3.8
40	-0.5	3.0	4.6	7.0	9.0
60	4.5	9.0	13.0	17.0	22.8
80	4.7	9.7	14.3	19.7	25.0

LEAST SQUARES CURVE PARAMETERS				
Cut Depth (mm)	Slope (ksi/in)	Y-Intercept (Canceling Press,psi)	Correlation Coefficient (1=Exact Fit)	Standard Error Of Estimate
20	2.01	193	0.7102	222.6
40	1.69	2	0.9926	38.3
60	0.88	-96	0.9974	22.8
80	0.78	-90	0.9996	9.1

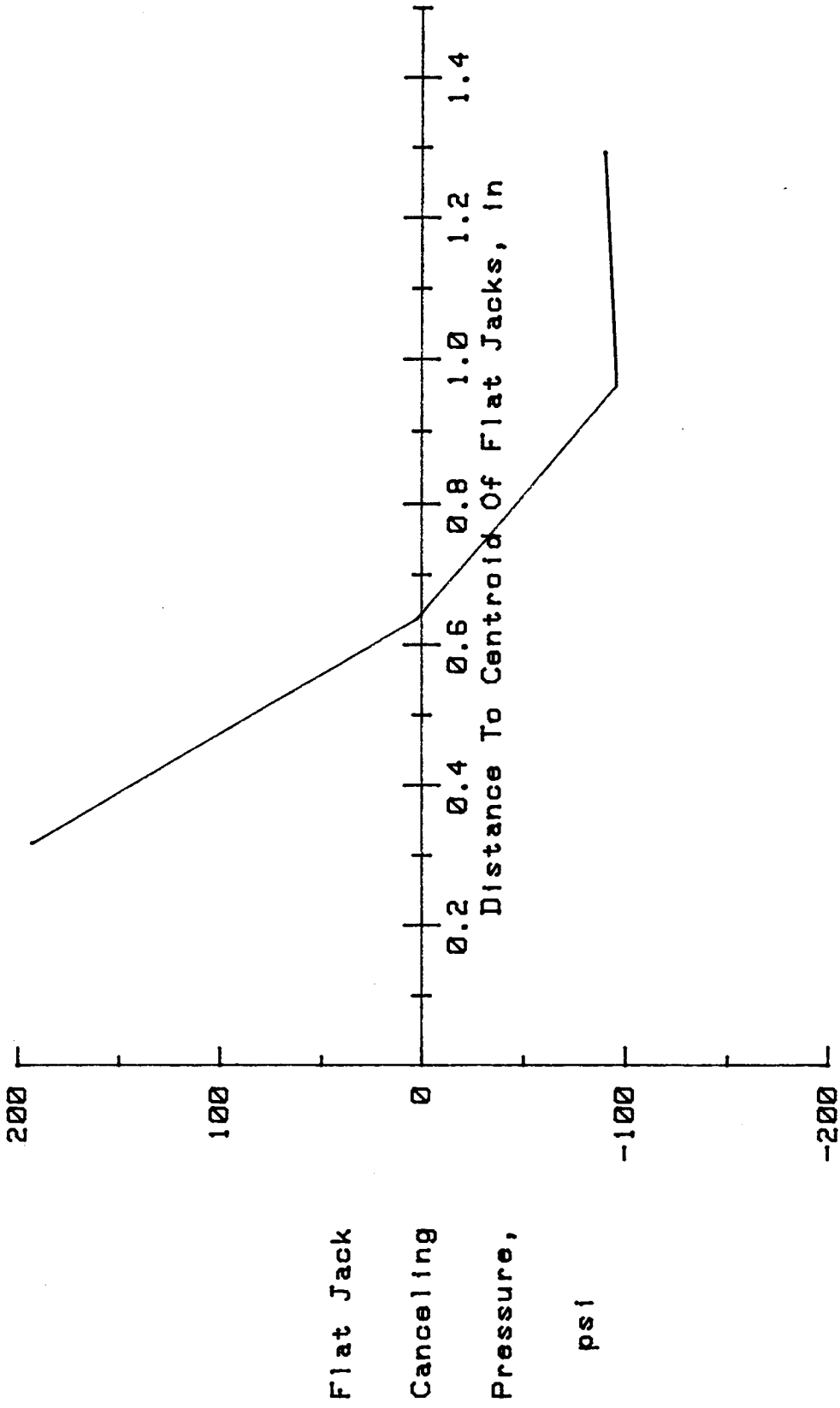


Figure 74. Uncorrected stress profile for 3S6H00/00WK.

Table 44. Stress measurement data for specimen 4N1V00/00T.

PFENDER READINGS				
Cut Depth (mm)	Flat Jack Internal Pressure (psi)			
	0	100	200	300
20	6.2	5.9	6.6	5.9
30	5.0	5.7	7.7	10.0
40	5.5	6.2	9.8	12.5
50	7.5	10.6	14.6	18.5
60	7.5	11.5	17.5	21.8
70	16.8	21.0	26.0	30.9

LEAST SQUARES CURVE PARAMETERS				
Cut Depth (mm)	Slope (ksi/in)	Y-Intercept (Canceling Press,psi)	Correlation Coefficient (1=Exact Fit)	Standard Error Of Estimate
20	-1.19	339	-.0778	222.9
30	2.21	-253	0.9769	47.7
40	1.51	-180	0.9727	51.9
50	1.06	-197	0.9985	12.4
60	0.80	-148	0.9971	17.1
70	0.83	-351	0.9993	8.5

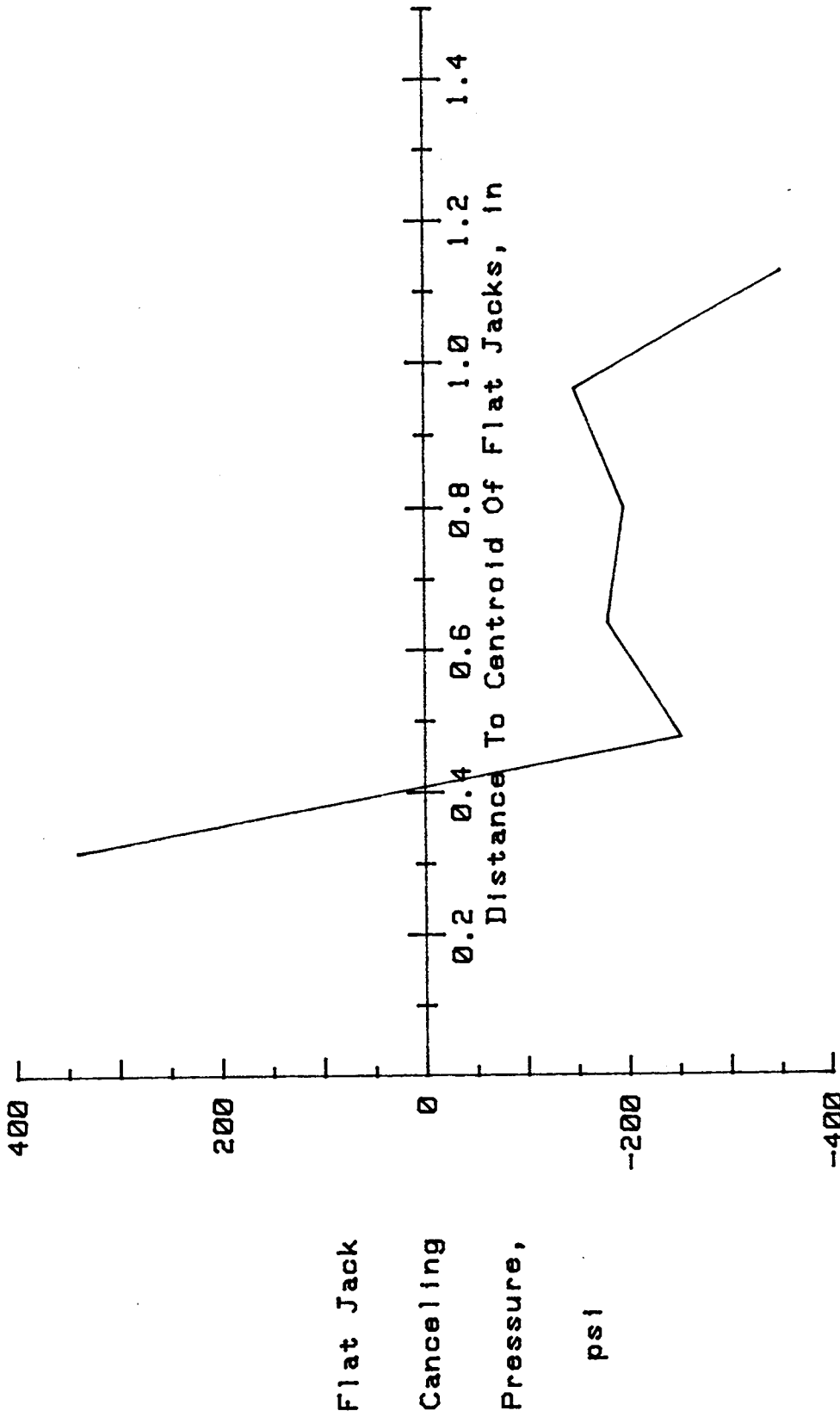


Figure 75. Uncorrected stress profile for 4N1V00/00T.

Table 45. Stress measurement data for specimen 4N1V00/00B.

PFENDER READINGS				
Cut Depth (mm)	Flat Jack Internal Pressure (psi)			
	0	100	200	300
20	4.3	5.0	5.3	6.0
30	4.8	5.8	7.8	9.8
40	3.7	7.6	10.6	13.6
50	6.6	10.6	14.6	18.6
60	7.6	11.9	16.6	21.6
70	15.1	19.4	25.1	29.1

LEAST SQUARES CURVE PARAMETERS				
Cut Depth (mm)	Slope (ksi/in)	Y-Intercept (Canceling Press,psi)	Correlation Coefficient (1=Exact Fit)	Standard Error Of Estimate
20	7.13	-783	0.9892	32.8
30	2.27	-256	0.9898	31.9
40	1.20	-120	0.9977	15.0
50	0.98	-165	1.0000	0.0
60	0.84	-159	0.9994	7.5
70	0.82	-313	0.9978	14.8



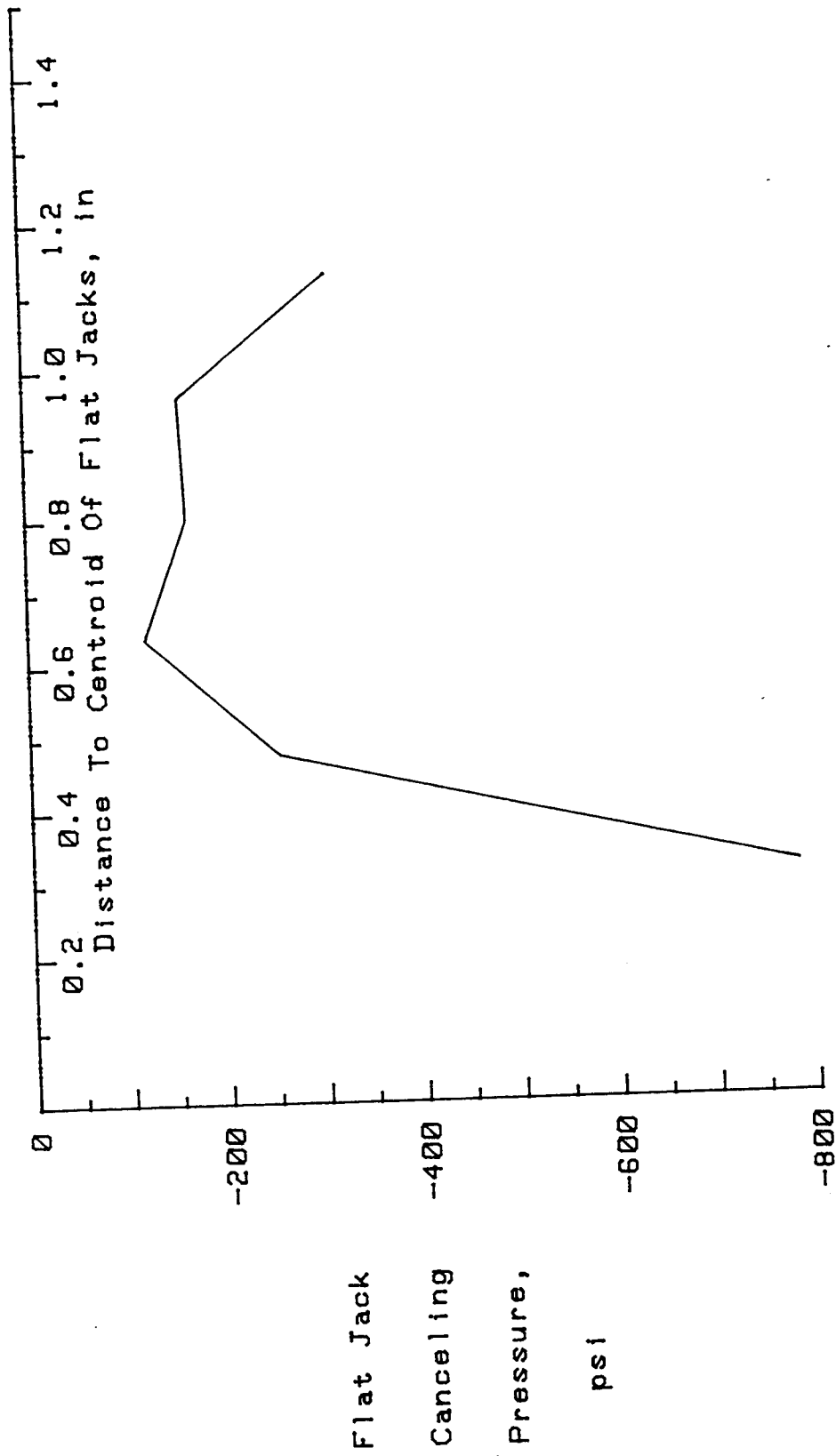


Figure 76. Uncorrected stress profile for 4N1V00/00B.

Table 46. Stress measurement data for specimen 4N2V95/118T.

PFENDER READINGS				
Cut Depth (mm)	Flat Jack Internal Pressure (psi)			
	0	300	600	900
20	-3.1	-2.5	-0.7	2.8
30	-11.3	-7.5	-0.4	5.7
40	-20.0	-11.8	-2.3	6.8
50	-26.4	-14.3	-3.5	8.6
60	-32.3	-18.3	-4.5	10.4
70	-32.9	-17.9	-1.8	14.4
80	-42.8	-24.4	-6.2	12.1

LEAST SQUARES CURVE PARAMETERS				
Cut Depth (mm)	Slope (ksi/in)	Y-Intercept (Canceling Press,psi)	Correlation Coefficient (1=Exact Fit)	Standard Error Of Estimate
20	5.35	570	0.9467	216.0
30	2.00	621	0.9933	77.8
40	1.31	677	0.9995	20.4
50	1.02	680	0.9997	15.6
60	0.83	686	0.9998	12.4
70	0.75	631	0.9998	12.9
80	0.64	701	1.0000	1.5

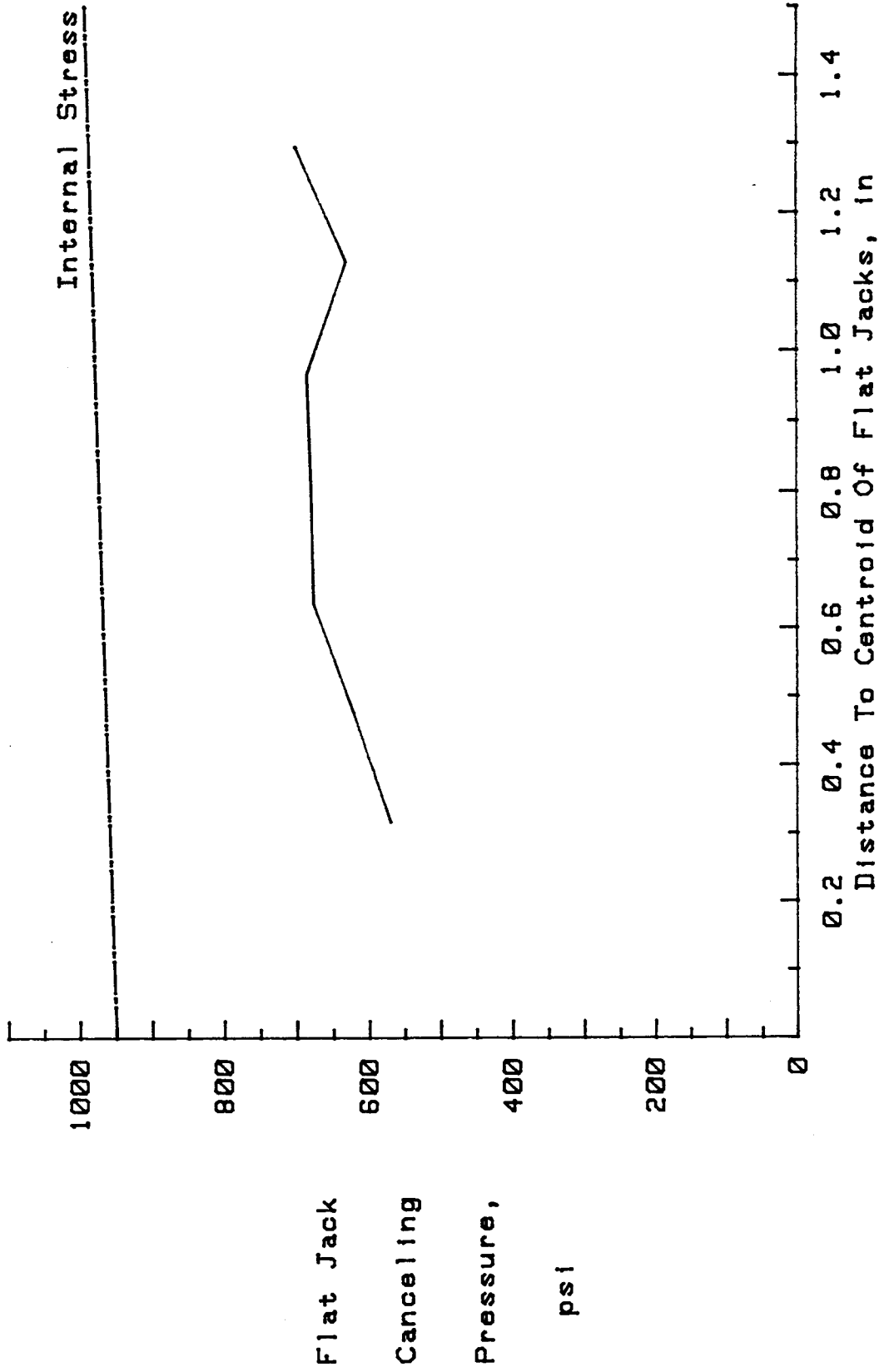


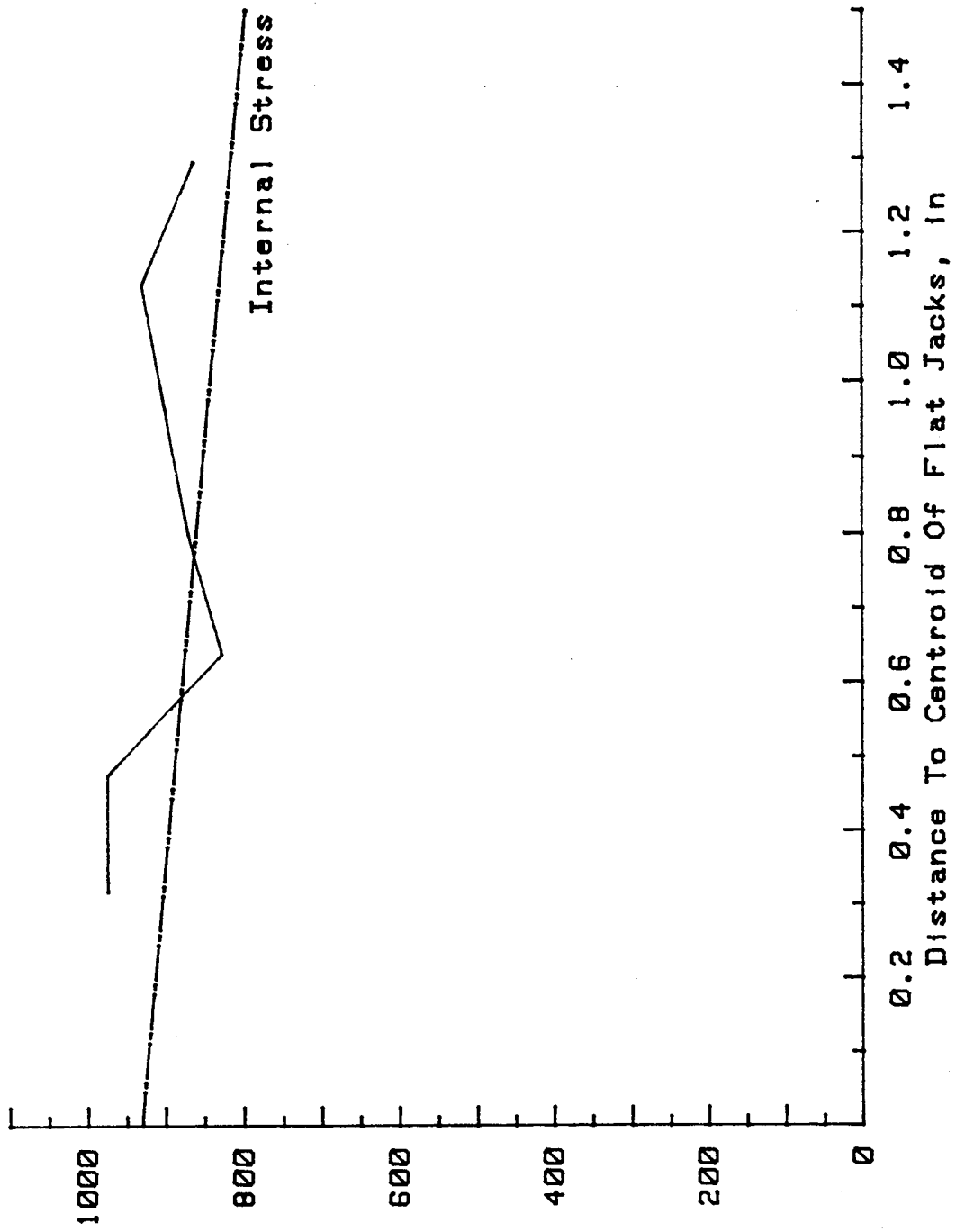
Figure 77. Uncorrected stress profile for 4N2V95/118T.

Flat Jack  
 Canceling  
 Pressure,  
 psi

Table 47. Stress measurement data for specimen 4N3V93/22T.

PFENDER READINGS				
Cut Depth (mm)	Flat Jack Internal Pressure (psi)			
	0	300	600	900
20	-6.7	-6.4	-3.7	-0.2
30	-17.8	-12.8	-7.3	-1.0
40	-21.5	-14.8	-6.5	2.4
50	-29.5	-20.3	-9.7	1.4
60	-37.9	-25.9	-12.6	0.0
70	-50.5	-34.5	-18.0	-1.5
80	-51.1	-33.8	-15.3	2.0

LEAST SQUARES CURVE PARAMETERS				
Cut Depth (mm)	Slope (ksi/in)	Y-Intercept (Canceling Press,psi)	Correlation Coefficient (1=Exact Fit)	Standard Error Of Estimate
20	4.80	973	0.9496	210.4
30	2.11	973	0.9986	35.0
40	1.46	826	0.9979	43.5
50	1.14	870	0.9990	29.4
60	0.93	900	0.9998	13.0
70	0.72	930	1.0000	5.0
80	0.66	864	0.9999	8.7



Flat Jack  
Canceling  
Pressure,  
psi

Figure 78. Uncorrected stress profile for 4N3V93/22T.

Table 48. Stress measurement data for specimen 4N3V93/22B.

PFENDER READINGS				
Cut Depth (mm)	Flat Jack Internal Pressure (psi)			
	0	300	600	900
20	-9.3	-7.3	-4.3	-1.3
30	-19.1	-14.1	-8.1	-1.1
40	-23.1	-16.1	-7.1	1.6
50	-30.4	-20.9	-8.5	0.6
60	-40.0	-27.2	-13.5	-0.5
70	-51.8	-35.8	-18.0	-1.0
80	-47.2	-30.9	-11.7	5.2

LEAST SQUARES CURVE PARAMETERS				
Cut Depth (mm)	Slope (ksi/in)	Y-Intercept (Canceling Press,psi)	Correlation Coefficient (1=Exact Fit)	Standard Error Of Estimate
20	4.34	1066	0.9959	60.6
30	1.96	979	0.9972	49.9
40	1.41	851	0.9985	36.8
50	1.11	869	0.9983	38.9
60	0.89	912	0.9999	8.4
70	0.69	920	0.9998	13.5
80	0.67	809	0.9995	20.2

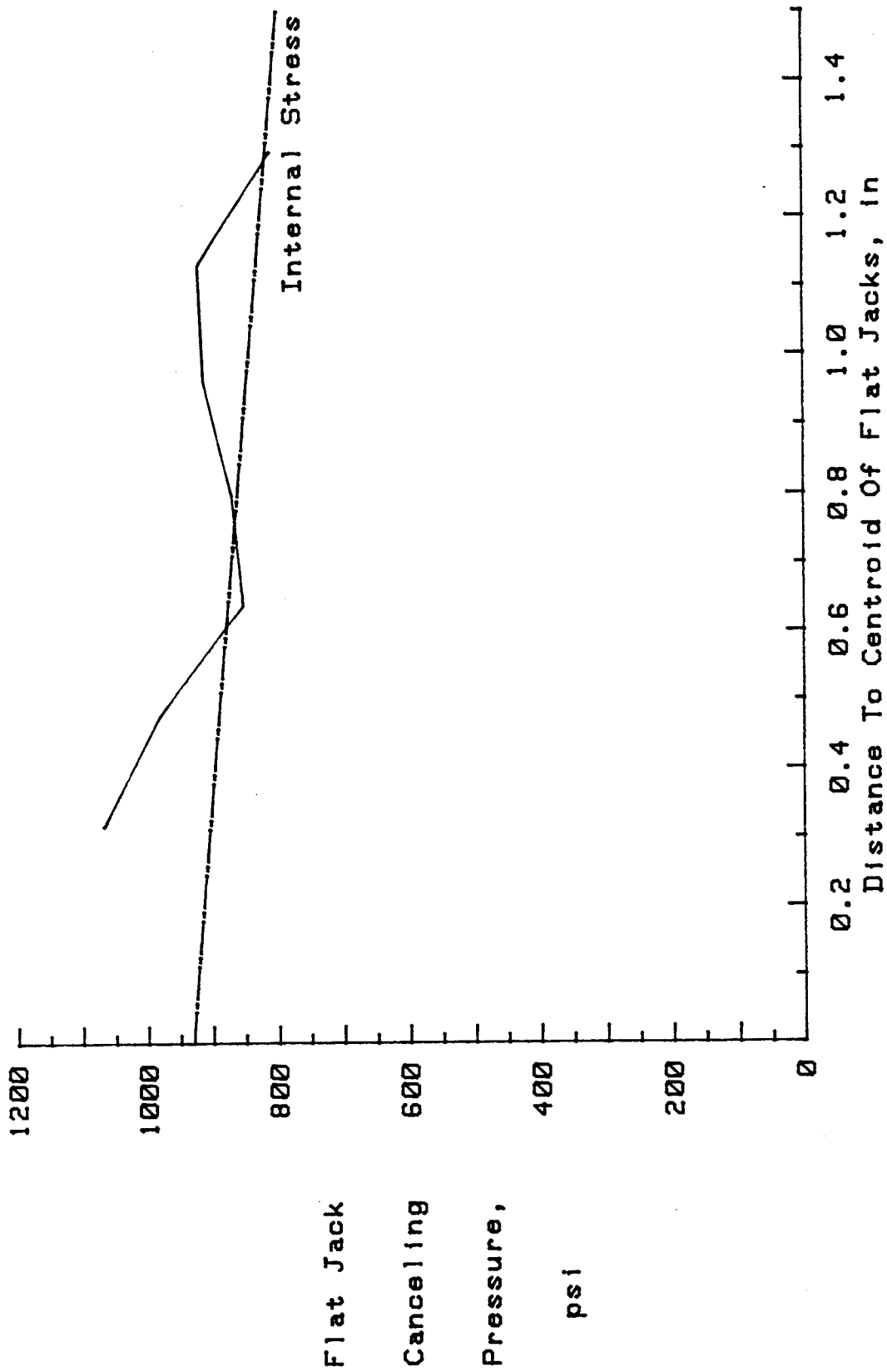


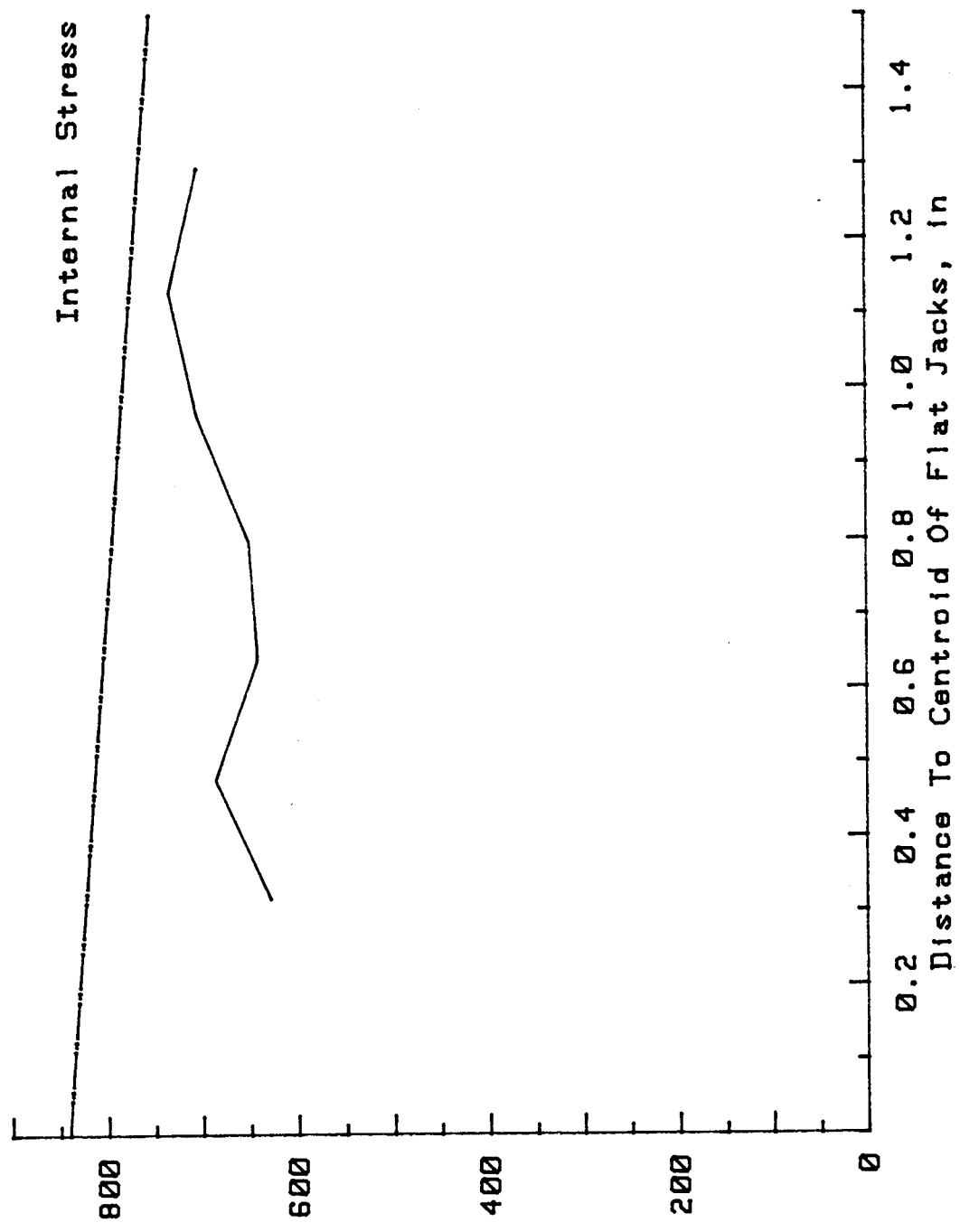
Figure 79. Uncorrected stress profile for 4N3V93/22B.

Table 49. Stress measurement data for specimen 4N4V84/37T.

PFENDER READINGS				
Cut Depth (mm)	Flat Jack Internal Pressure (psi)			
	0	300	600	900
20	-4.3	-3.0	0.0	2.0
30	-10.2	-7.0	-2.0	4.0
40	-14.2	-8.3	-1.3	6.3
50	-19.0	-11.2	-2.0	8.0
60	-24.2	-16.5	-4.5	8.0
70	-31.8	-20.5	-7.5	8.7
80	-35.0	-21.8	-6.2	11.0

LEAST SQUARES CURVE PARAMETERS				
Cut Depth (mm)	Slope (ksi/in)	Y-Intercept (Canceling Press,psi)	Correlation Coefficient (1=Exact Fit)	Standard Error Of Estimate
20	5.29	628	0.9900	94.6
30	2.44	685	0.9913	88.2
40	1.72	641	0.9984	37.5
50	1.31	651	0.9985	36.8
60	1.08	704	0.9945	69.9
70	0.87	733	0.9966	55.0
80	0.77	703	0.9983	39.2





Flat Jack  
 Canceling  
 Pressure,  
 psi

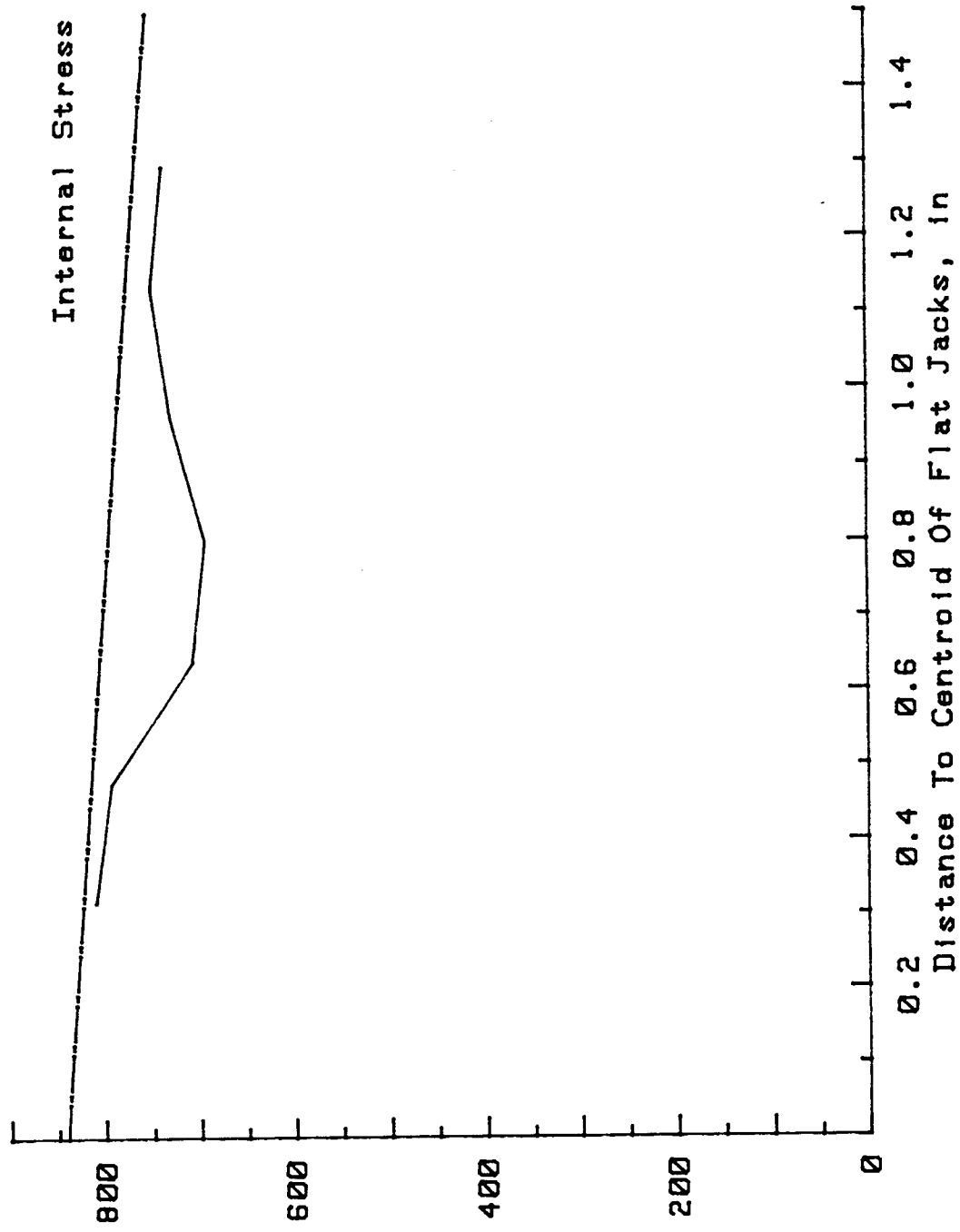
Figure 80. Uncorrected stress profile for 4N4V84/37T.

Table 50. Stress measurement data for specimen 4N4V84/37B.

PFENDER READINGS				
Cut Depth (mm)	Flat Jack Internal Pressure (psi)			
	0	300	600	900
20	-6.0	-4.3	-2.0	1.0
30	-12.2	-8.0	-3.0	1.8
40	-16.0	-10.0	-3.0	5.0
50	-21.0	-13.0	-3.0	6.8
60	-27.6	-18.0	-5.3	7.2
70	-33.8	-22.2	-7.0	7.5
80	-37.7	-24.0	-7.2	9.0

LEAST SQUARES CURVE PARAMETERS				
Cut Depth (mm)	Slope (ksi/in)	Y-Intercept (Canceling Press,psi)	Correlation Coefficient (1=Exact Fit)	Standard Error Of Estimate
20	4.99	808	0.9923	83.1
30	2.51	791	0.9994	23.9
40	1.68	706	0.9980	42.8
50	1.26	692	0.9988	32.9
60	1.00	729	0.9981	41.6
70	0.85	748	0.9984	37.5
80	0.75	736	0.9991	28.6



Flat Jack  
 Canceling  
 Pressure,  
 psi

Figure 81. Uncorrected stress profile for 4N4V84/37B.

Table 51. Stress measurement data for specimen 4N5H88/22E.

PFENDER READINGS				
Cut Depth (mm)	Flat Jack Internal Pressure (psi)			
	0	100	200	300
20	4.7	4.6	5.2	5.9
30	6.7	6.8	7.8	9.7
40	10.0	10.4	13.0	14.9
50	9.2	9.8	13.8	16.8
60	11.0	14.0	18.0	22.0
70	15.7	18.2	22.2	26.2
80	14.8	17.8	23.8	27.8

LEAST SQUARES CURVE PARAMETERS				
Cut Depth (mm)	Slope (ksi/in)	Y-Intercept (Canceling Press,psi)	Correlation Coefficient (1=Exact Fit)	Standard Error Of Estimate
20	7.80	-860	0.9122	91.6
30	3.39	-517	0.9277	83.5
40	2.14	-505	0.9687	55.5
50	1.38	-284	0.9681	56.1
60	1.06	-287	0.9978	14.8
70	1.10	-423	0.9947	23.0
80	0.86	-311	0.9927	27.0

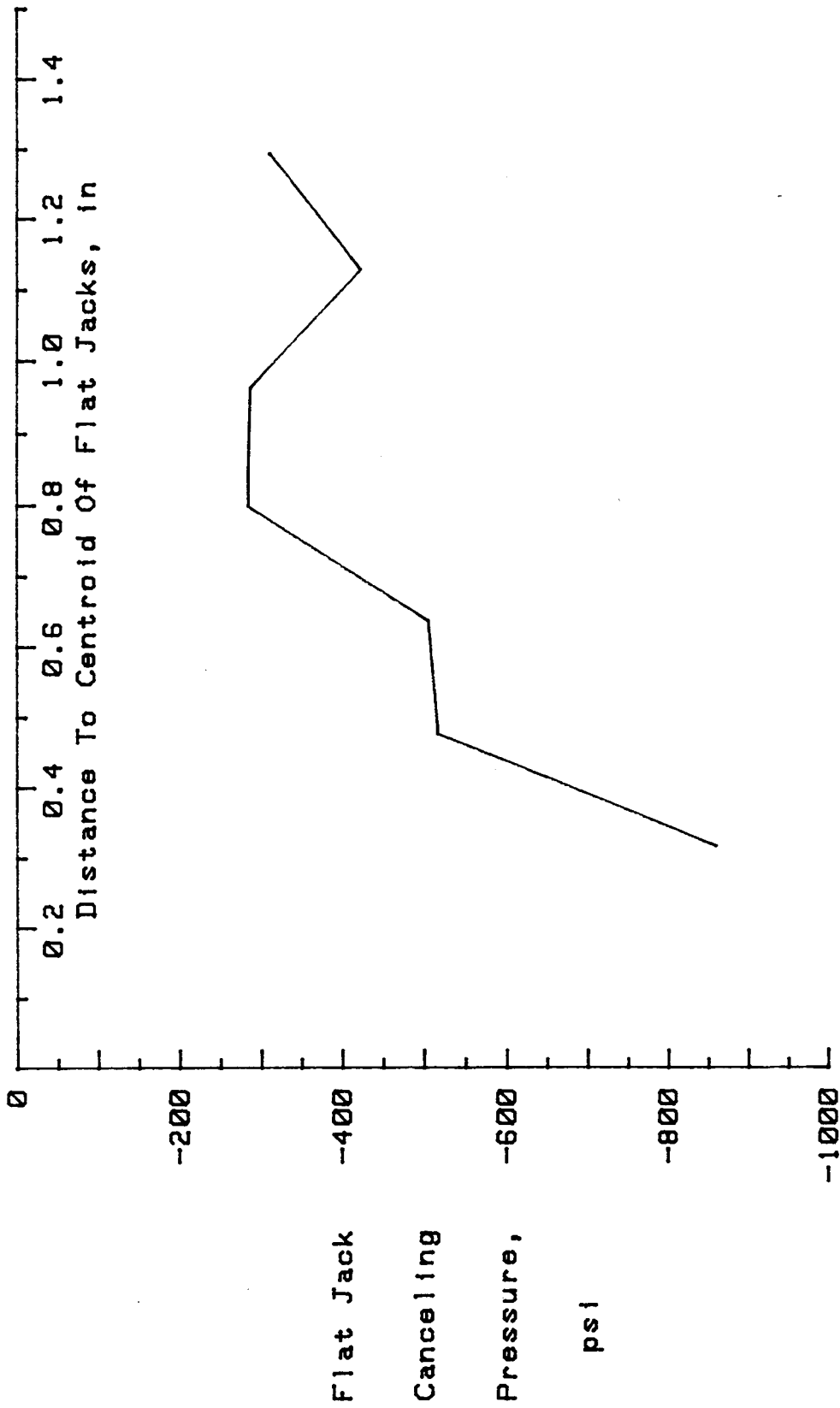


Figure 82. Uncorrected stress profile for 4N5H88/22E.

Table 52. Stress measurement data for specimen 4N5H88/22W.

PFENDER READINGS				
Cut Depth (mm)	Flat Jack Internal Pressure (psi)			
	0	100	200	300
20	5.1	4.1	4.1	4.1
30	5.6	6.3	7.3	9.2
40	9.5	9.5	11.5	13.5
50	9.0	9.3	12.3	15.3
60	10.2	12.5	16.5	20.5
70	15.7	16.7	21.2	25.7
80	13.3	17.3	22.8	27.3

LEAST SQUARES CURVE PARAMETERS				
Cut Depth (mm)	Slope (ksi/in)	Y-Intercept (Canceling Press,psi)	Correlation Coefficient (1=Exact Fit)	Standard Error Of Estimate
20	-7.87	1020	-.7746	141.4
30	3.16	-421	0.9739	50.7
40	2.51	-550	0.9439	73.9
50	1.65	-330	0.9573	64.6
60	1.11	-272	0.9930	26.5
70	1.07	-391	0.9705	53.9
80	0.83	-273	0.9983	12.9

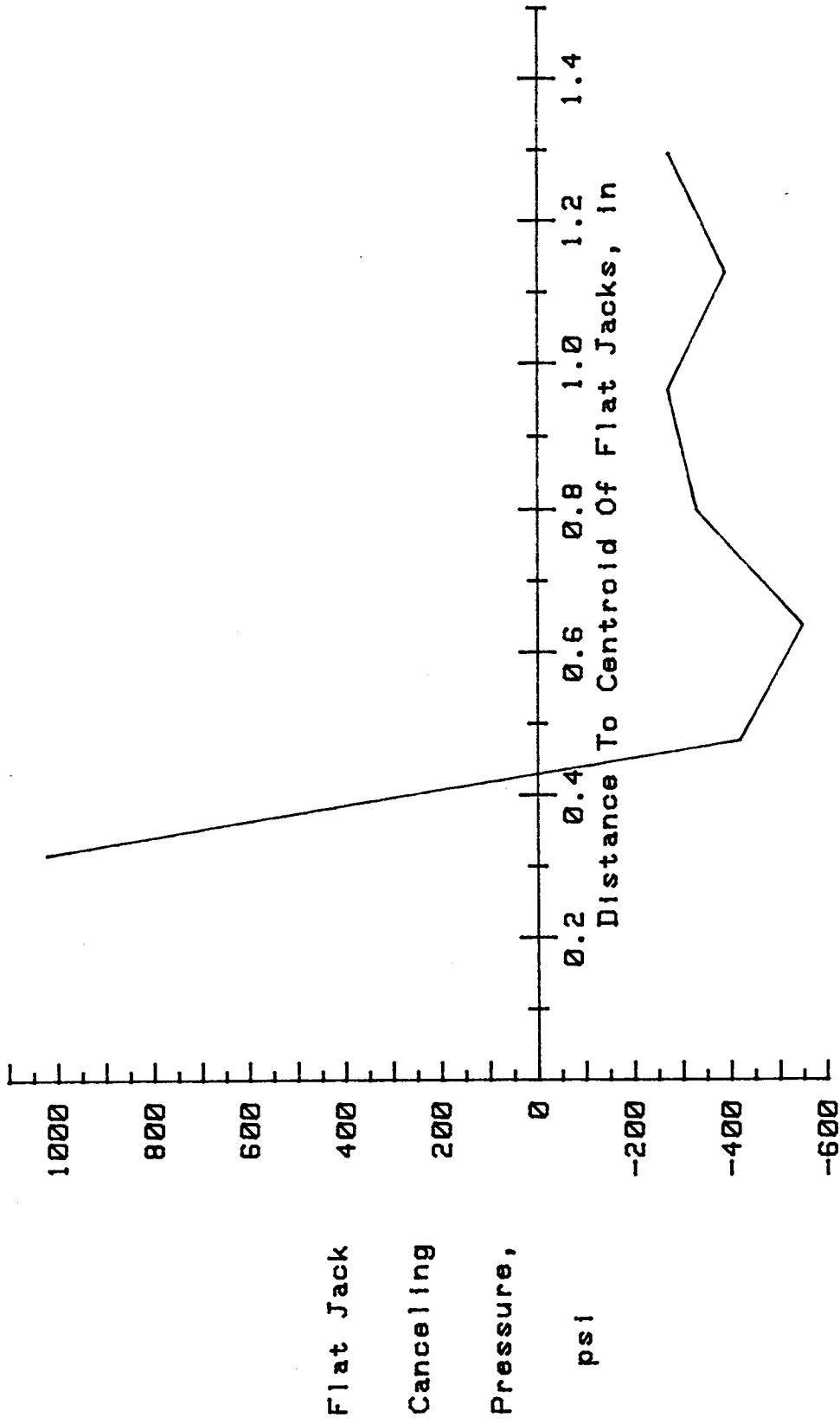


Figure 83. Uncorrected stress profile for 4N5H88/22W.

Table 53. Stress measurement data for specimen 4S6V23/117T.

PFENDER READINGS				
Cut Depth (mm)	Flat Jack Internal Pressure (psi)			
	0	200	400	600
20	-0.0	1.4	2.4	4.4
30	-2.4	1.3	2.8	6.2
40	-5.3	-3.0	2.6	8.3
50	-8.9	-2.9	3.6	11.6
60	-9.1	-3.0	5.8	13.3
70	-10.3	-2.4	7.0	15.6
80	-8.3	-3.7	6.9	16.6

LEAST SQUARES CURVE PARAMETERS				
Cut Depth (mm)	Slope (ksi/in)	Y-Intercept (Canceling Press,psi)	Correlation Coefficient (1=Exact Fit)	Standard Error Of Estimate
20	5.34	16	0.9918	57.2
30	2.79	157	0.9881	68.8
40	1.63	272	0.9845	78.4
50	1.15	275	0.9978	29.6
60	1.03	254	0.9977	30.6
70	0.90	243	0.9994	15.1
80	0.90	234	0.9879	69.3



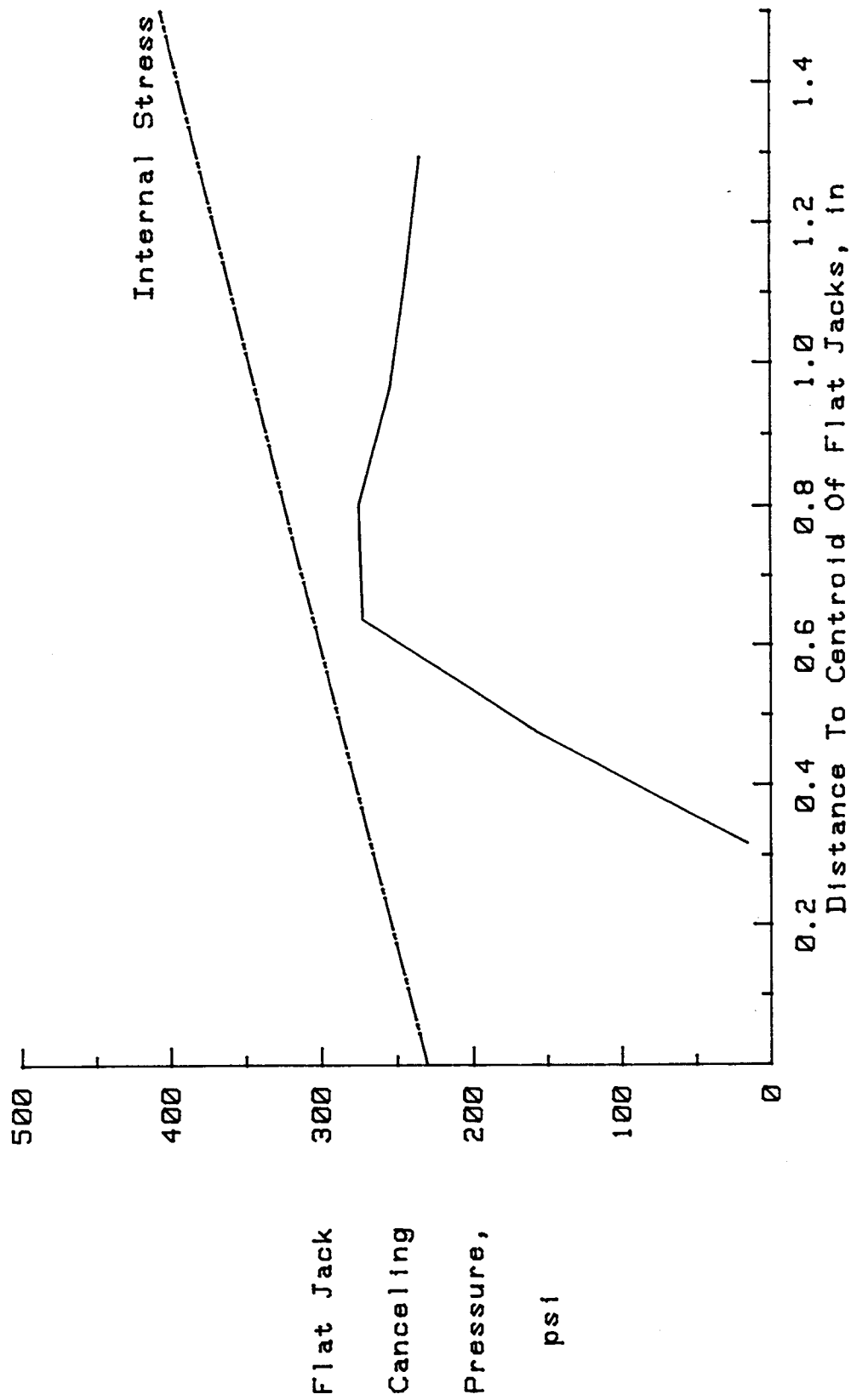


Figure 84. Uncorrected stress profile for 4S6V23/117T.

Table 54. Stress measurement data for specimen 4S6V23/117B.

PFENDER READINGS				
Cut Depth (mm)	Flat Jack Internal Pressure (psi)			
	0	200	400	600
20	0.8	0.4	1.8	3.5
30	-3.4	-1.4	2.1	5.6
40	-7.0	-2.3	2.7	7.0
50	-9.7	-3.6	3.0	10.0
60	-9.8	-4.0	4.2	12.7
70	-11.0	-3.9	5.0	15.0
80	-13.0	-5.5	4.7	15.0

LEAST SQUARES CURVE PARAMETERS				
Cut Depth (mm)	Slope (ksi/in)	Y-Intercept (Canceling Press,psi)	Correlation Coefficient (1=Exact Fit)	Standard Error Of Estimate
20	6.53	30	0.8876	206.0
30	2.54	253	0.9928	53.5
40	1.67	296	0.9996	12.8
50	1.20	302	0.9995	13.7
60	1.03	280	0.9965	37.6
70	0.90	271	0.9972	33.5
80	0.83	294	0.9974	32.1

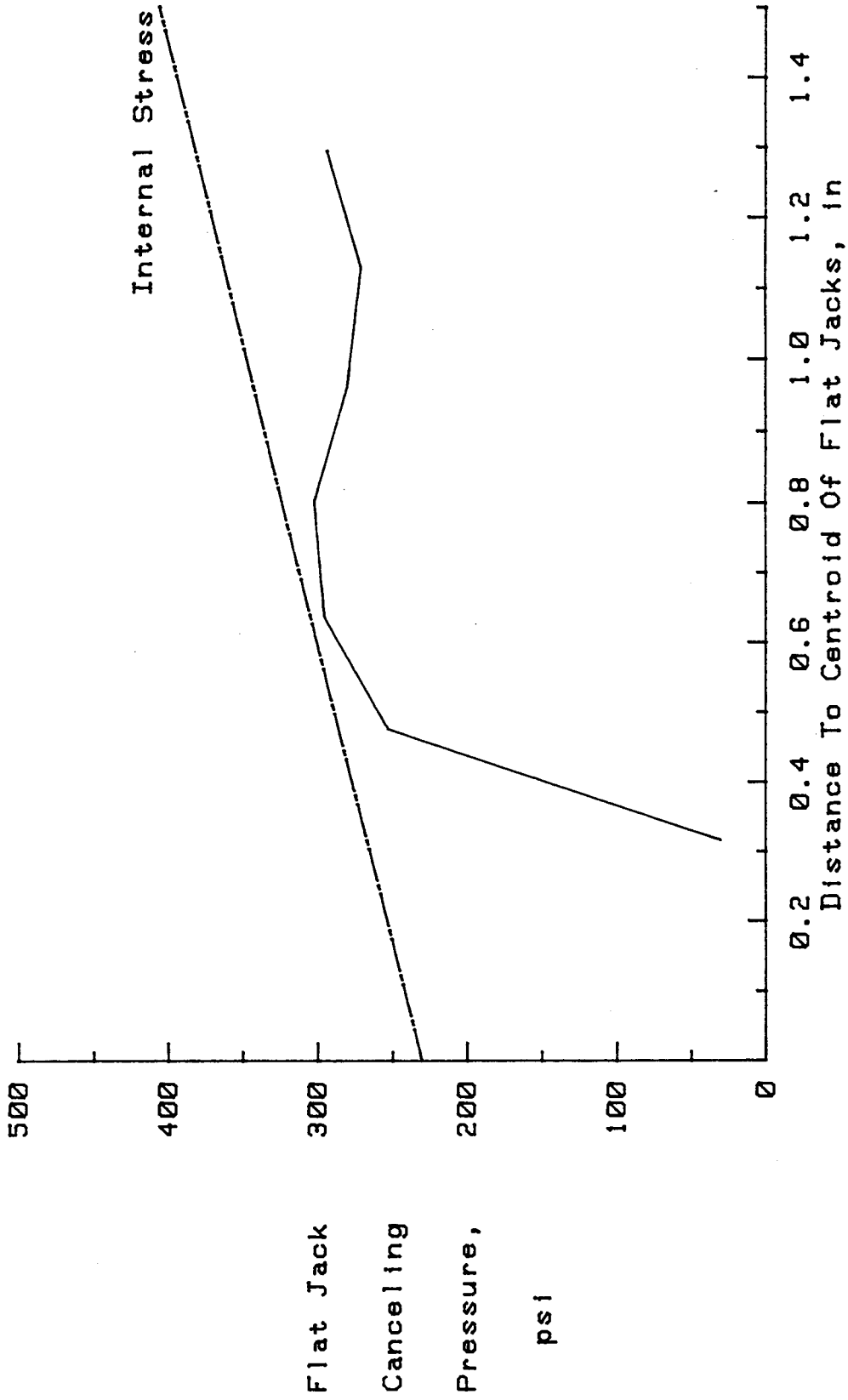


Figure 85. Uncorrected stress profile for 4S6V23/117B.

Table 55. Stress measurement data for specimen 5S0V43/87T.

PFENDER READINGS				
Cut Depth (mm)	Flat Jack Internal Pressure (psi)			
	0	200	400	600
20	2.2	3.1	2.9	4.4
30	-2.4	-0.4	2.6	5.5
40	-4.0	0.0	5.0	9.0
50	-6.1	-2.7	4.6	11.6
60	-9.5	-2.7	5.3	12.8
70	-10.9	-4.4	3.5	12.5
80	-13.3	-4.3	6.7	46.6

LEAST SQUARES CURVE PARAMETERS				
Cut Depth (mm)	Slope (ksi/in)	Y-Intercept (Canceling Press,psi)	Correlation Coefficient (1=Exact Fit)	Standard Error Of Estimate
20	9.96	-497	0.8997	195.2
30	2.93	201	0.9963	38.3
40	1.79	187	0.9990	20.3
50	1.27	240	0.9889	66.5
60	1.05	261	0.9995	13.8
70	1.00	296	0.9974	32.0
80	0.78	272	0.9983	16.3

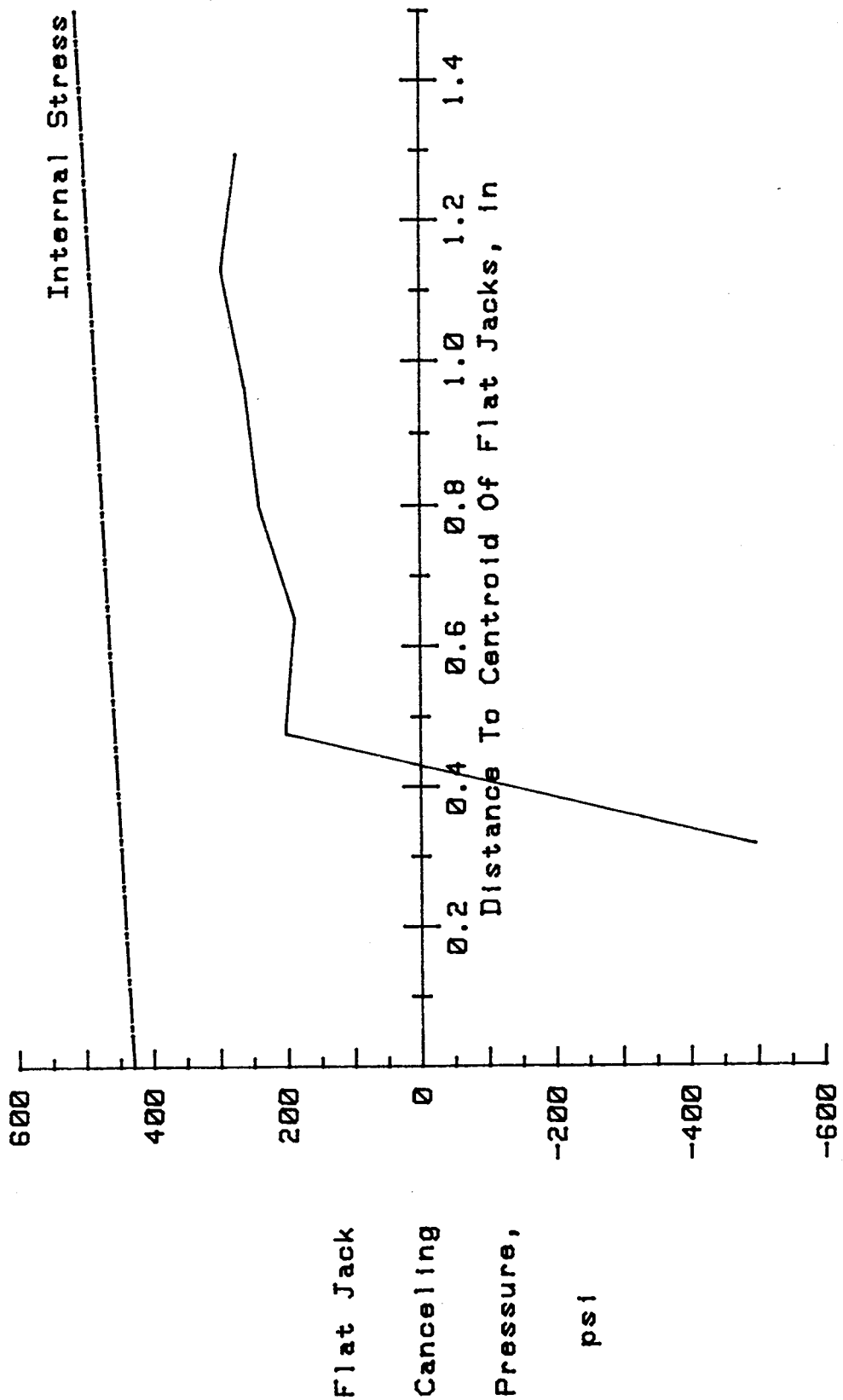


Figure 86. Uncorrected stress profile for 5S0V43/87T.

Table 56. Stress measurement data for specimen 5S0V43/87B.

PFENDER READINGS				
Cut Depth (mm)	Flat Jack Internal Pressure (psi)			
	0	200	400	600
20	-0.8	0.2	2.2	4.2
30	-3.5	-1.4	1.6	5.6
40	-5.1	-0.1	4.0	9.0
50	-8.5	-2.4	4.5	10.6
60	-10.2	-3.2	4.7	11.8
70	-12.1	-6.0	2.7	12.0
80	-14.0	-5.3	5.7	46.6

LEAST SQUARES CURVE PARAMETERS				
Cut Depth (mm)	Slope (ksi/in)	Y-Intercept (Canceling Press,psi)	Correlation Coefficient (1=Exact Fit)	Standard Error Of Estimate
20	4.54	133	0.9898	63.8
30	2.55	263	0.9903	62.1
40	1.69	216	0.9992	17.3
50	1.23	267	0.9997	11.1
60	1.06	279	0.9997	10.4
70	0.96	321	0.9958	40.8
80	0.80	292	0.9977	19.0

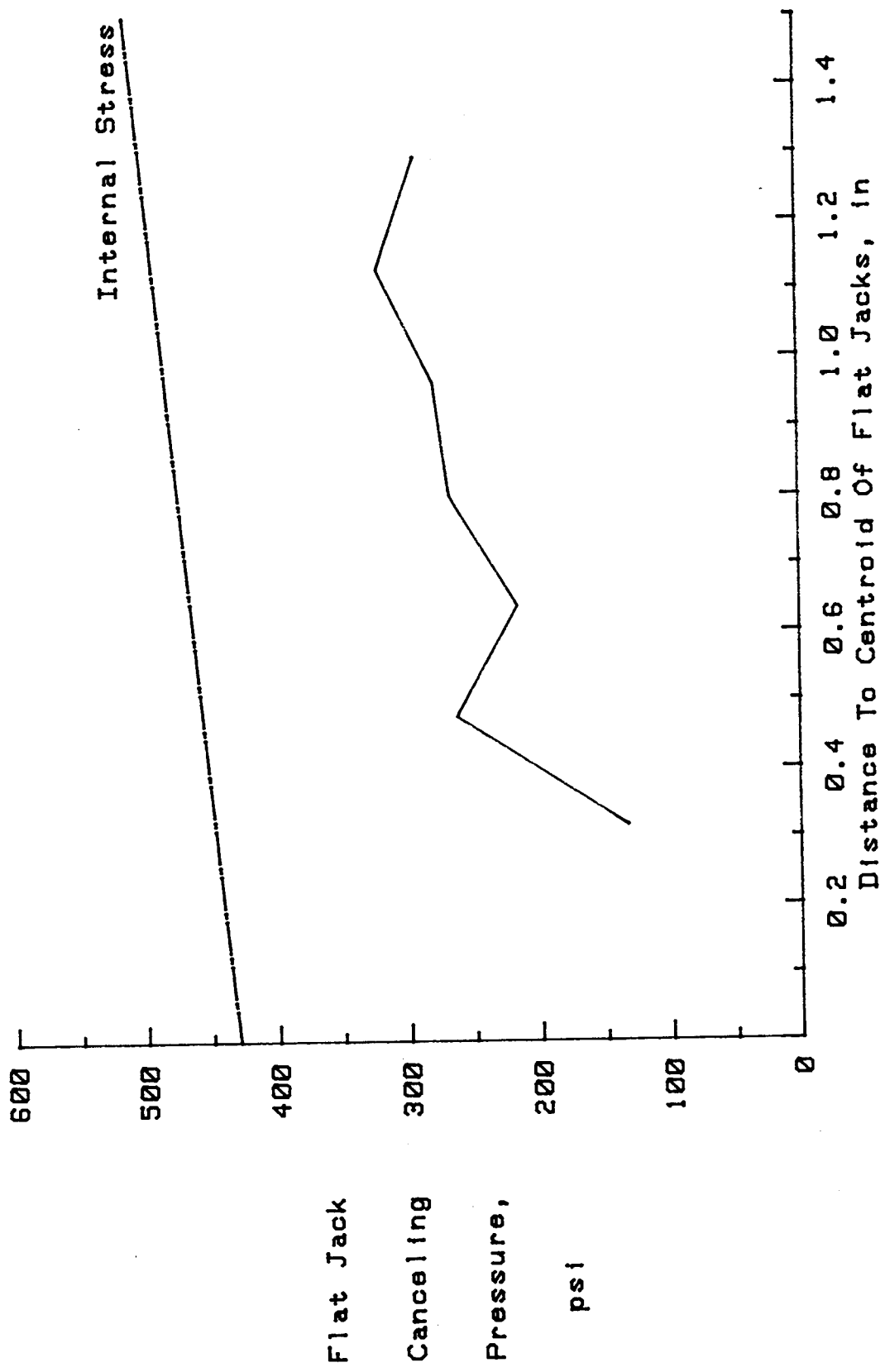


Figure 87. Uncorrected stress profile for 5S0V43/87B.

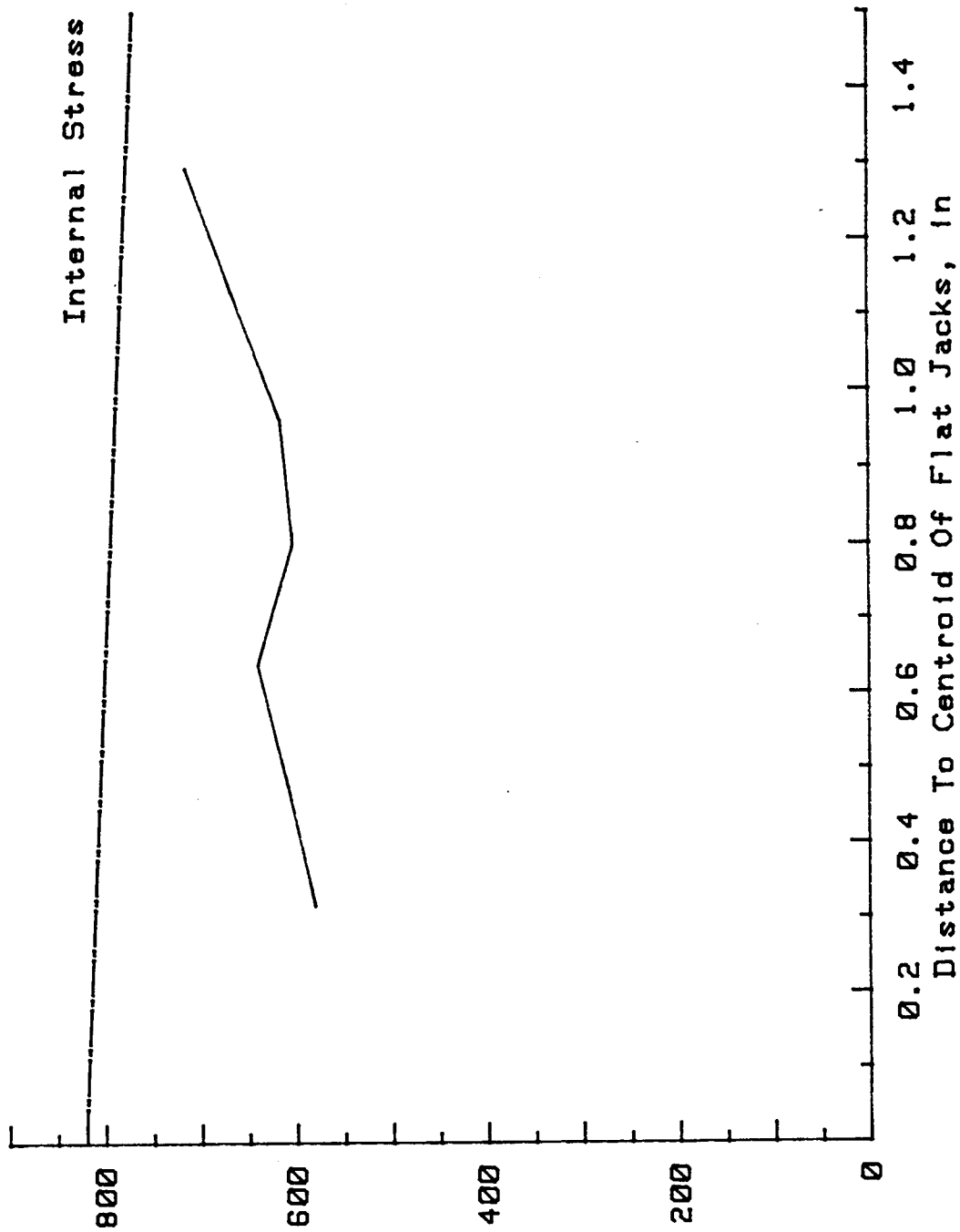
Table 57. Stress measurement data for specimen 5N1V82/54T00.

PFENDER READINGS				
Cut Depth (mm)	Flat Jack Internal Pressure (psi)			
	0	200	400	600
20	-4.3	-3.2	-1.8	0.4
30	-8.9	-6.6	-3.6	0.2
40	-13.6	-10.6	-5.5	-0.6
50	-17.6	-13.6	-6.6	0.4
60	-24.6	-16.9	-8.6	-0.6
70	-30.0	-21.6	-12.6	-2.6
80	-37.5	-26.5	-17.3	-5.6

LEAST SQUARES CURVE PARAMETERS				
Cut Depth (mm)	Slope (ksi/in)	Y-Intercept (Canceling Press,psi)	Correlation Coefficient (1=Exact Fit)	Standard Error Of Estimate
20	4.95	580	0.9871	71.5
30	2.57	608	0.9939	49.2
40	1.76	639	0.9941	48.7
50	1.27	602	0.9928	53.5
60	0.98	616	0.9999	6.3
70	0.86	666	0.9992	17.6
80	0.75	713	0.9990	19.5





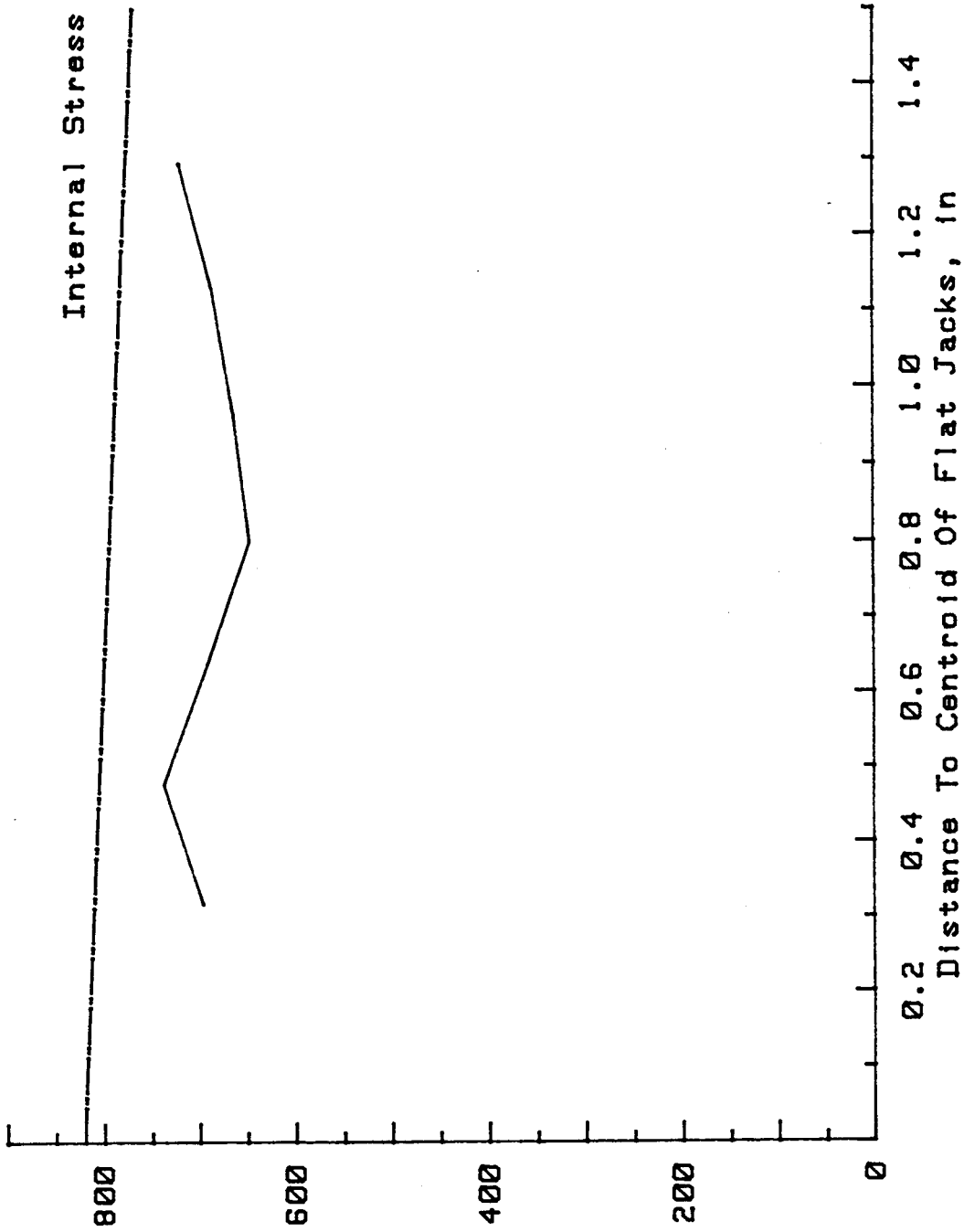
Flat Jack  
 Canceling  
 Pressure,  
 psi

Figure 88. Uncorrected stress profile for 5N1V82/54T00.

Table 58. Stress measurement data for specimen 5N1V82/54B00.

PFENDER READINGS				
Cut Depth (mm)	Flat Jack Internal Pressure (psi)			
	0	200	400	600
20	-4.9	-4.6	-2.6	-0.6
30	-9.6	-7.6	-4.6	-1.7
40	-15.6	-9.9	-6.6	-2.2
50	-21.1	-14.1	-8.0	-1.6
60	-26.6	-18.6	-10.4	-2.6
70	-31.3	-22.5	-13.6	-3.6
80	-37.5	-23.3	-17.4	-6.6

LEAST SQUARES CURVE PARAMETERS				
Cut Depth (mm)	Slope (ksi/in)	Y-Intercept (Canceling Press,psi)	Correlation Coefficient (1=Exact Fit)	Standard Error Of Estimate
20	4.90	695	0.9631	120.4
30	2.93	737	0.9963	38.3
40	1.79	690	0.9946	46.5
50	1.22	646	0.9996	12.5
60	0.98	663	1.0000	4.2
70	0.86	685	0.9995	13.9
80	0.78	720	0.9883	68.3



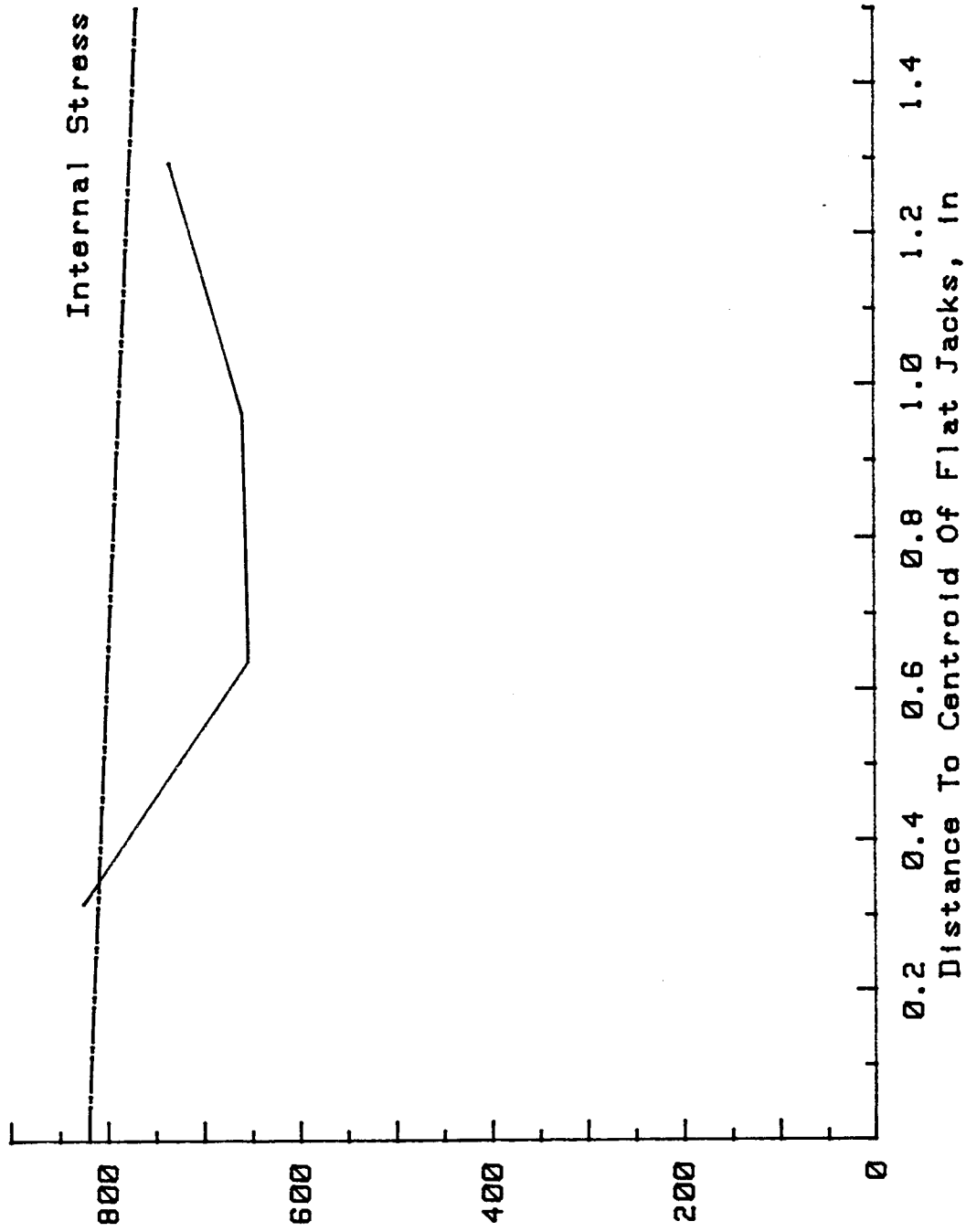
Flat Jack  
 Canceling  
 Pressure,  
 psi

Figure 89. Uncorrected stress profile for 5N1V82/54B00.

**Table 59. Stress measurement data for specimen 5N1V82/54T10.**

PFENDER READINGS				
Cut Depth (mm)	Flat Jack Internal Pressure (psi)			
	0	200	400	600
20	-5.3	-4.2	-2.5	-1.6
40	-17.6	-11.8	-6.6	-1.6
60	-27.6	-19.6	-10.6	-2.6
80	-38.7	-29.1	-18.6	-6.6

LEAST SQUARES CURVE PARAMETERS				
Cut Depth (mm)	Slope (ksi/in)	Y-Intercept (Canceling Press,psi)	Correlation Coefficient (1=Exact Fit)	Standard Error Of Estimate
20	6.07	824	0.9935	51.0
40	1.48	653	0.9994	15.4
60	0.94	659	0.9997	10.6
80	0.74	734	0.9987	22.6



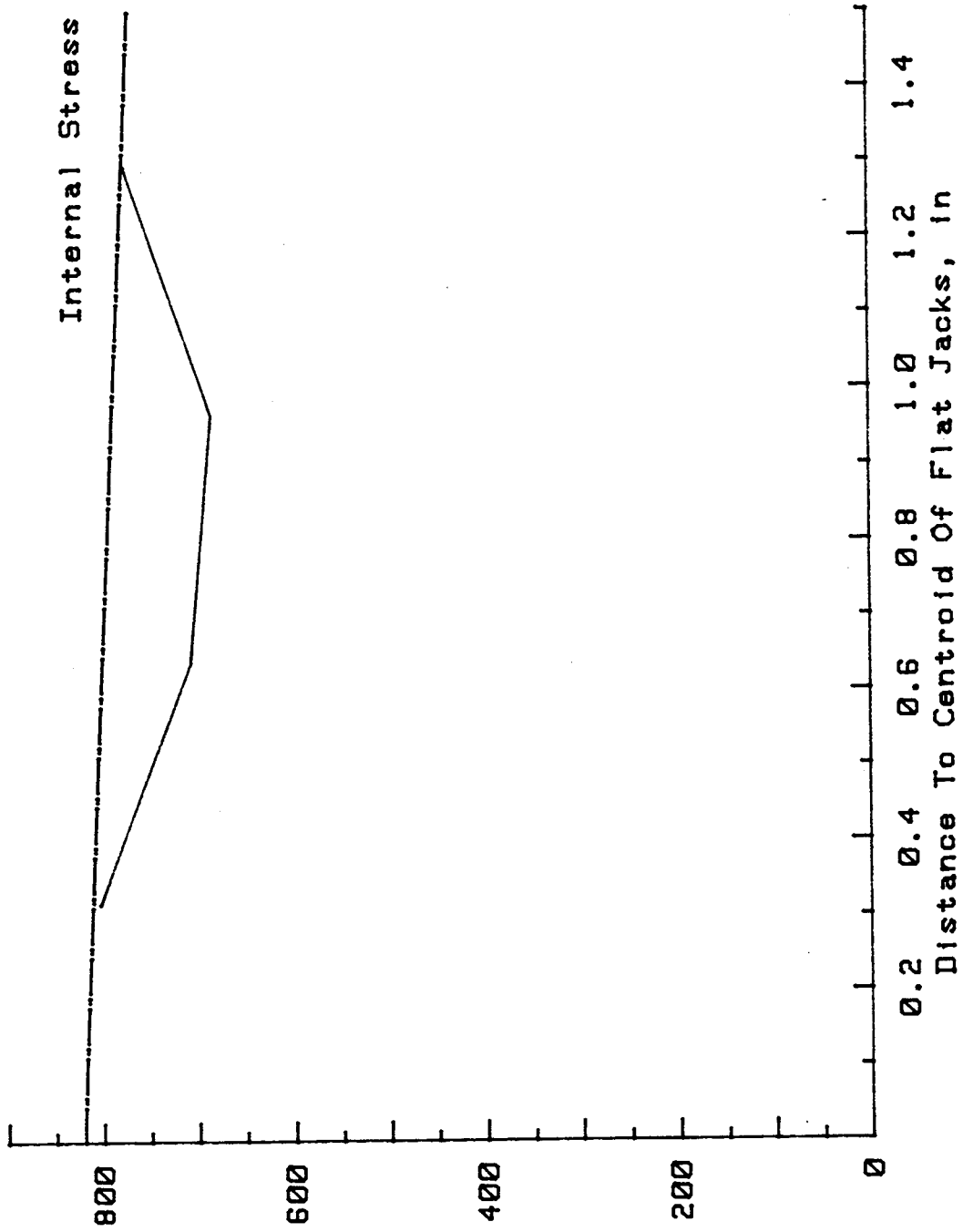
Flat Jack  
 Canceling  
 Pressure,  
 psi

Figure 90. Uncorrected stress profile for 5N1V82/54T10.

Table 60. Stress measurement data for specimen 5N1V82/54B10.

FFENDER READINGS				
Cut Depth (mm)	Flat Jack Internal Pressure (psi)			
	0	200	400	600
20	-6.6	-5.6	-3.6	-1.6
40	-18.1	-12.6	-8.1	-2.6
60	-28.6	-20.4	-11.6	-3.6
80	-39.6	-30.6	-19.6	-8.7

LEAST SQUARES CURVE PARAMETERS				
Cut Depth (mm)	Slope (ksi/in)	Y-Intercept (Canceling Press,psi)	Correlation Coefficient (1=Exact Fit)	Standard Error Of Estimate
20	4.54	801	0.9898	63.8
40	1.54	705	0.9992	17.5
60	0.94	683	0.9998	7.8
80	0.76	774	0.9990	20.4



Flat Jack  
 Cancelling  
 Pressure,  
 psi

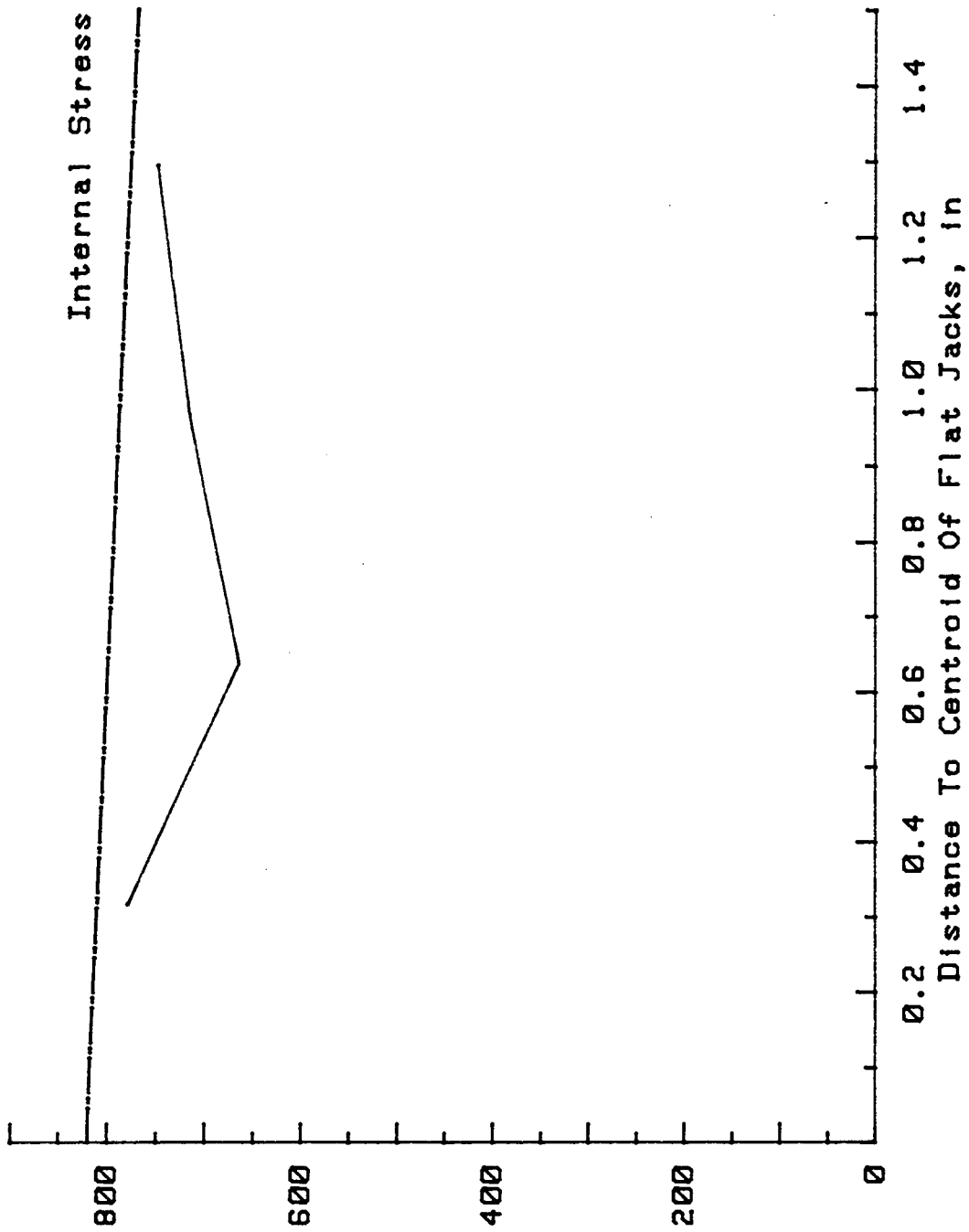
Figure 91. Uncorrected stress profile for 5N1V82/54B10.

Table 61. Stress measurement data for specimen 5N1V82/54T40.

PFENDER READINGS				
Cut Depth (mm)	Flat Jack Internal Pressure (psi)			
	0	200	400	600
20	-6.4	-5.2	-3.6	-1.3
40	-17.4	-12.4	-7.4	-1.4
60	-28.6	-21.5	-12.7	-4.5
80	-40.4	-30.6	-19.6	-7.6

LEAST SQUARES CURVE PARAMETERS				
Cut Depth (mm)	Slope (ksi/in)	Y-Intercept (Canceling Press,psi)	Correlation Coefficient (1=Exact Fit)	Standard Error Of Estimate
20	4.56	778	0.9894	64.9
40	1.48	663	0.9989	20.6
60	0.97	714	0.9991	18.6
80	0.72	748	0.9990	20.1





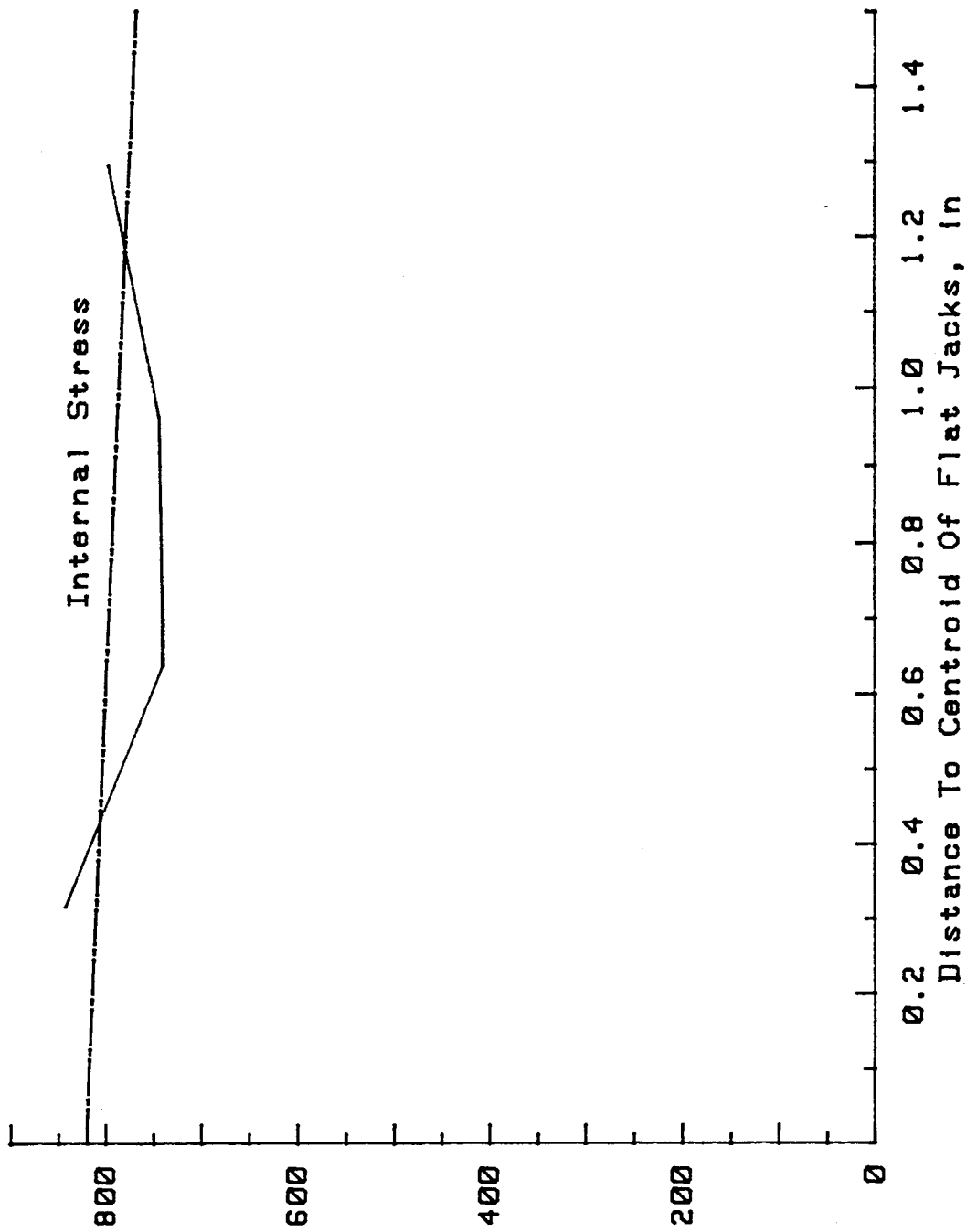
Flat Jack  
 Cancelling  
 Pressure,  
 psi

Figure 92. Uncorrected stress profile for 5N1V82/54T40.

Table 62. Stress measurement data for specimen 5N1V82/54B40.

PFENDER READINGS				
Cut Depth (mm)	Flat Jack Internal Pressure (psi)			
	0	200	400	600
20	-7.6	-5.6	-4.6	-2.0
40	-18.2	-13.7	-8.4	-3.4
60	-29.6	-22.6	-14.6	-5.3
80	-40.0	-30.7	-20.6	-9.6

LEAST SQUARES CURVE PARAMETERS				
Cut Depth (mm)	Slope (ksi/in)	Y-Intercept (Canceling Press,psi)	Correlation Coefficient (1=Exact Fit)	Standard Error Of Estimate
20	4.31	842	0.9868	72.5
40	1.58	739	0.9995	14.1
60	0.97	744	0.9980	28.4
80	0.78	797	0.9993	16.8



Flat Jack  
 Canceling  
 Pressure,  
 psi

Figure 93. Uncorrected stress profile for 5NIV82/54B40.

Table 63. Stress measurement data for specimen 5S1V43/87T.

PFENDER READINGS				
Cut Depth (mm)	Flat Jack Internal Pressure (psi)			
	0	200	400	600
20	-2.2	-1.2	0.7	1.7
30	-5.9	-3.2	-0.2	3.6
40	-11.2	-6.4	-1.2	3.7
50	-17.2	-11.2	-4.1	2.7
60	-18.2	-10.8	-2.8	5.4
70	-21.1	-12.3	-2.8	6.6
80	-24.5	-10.6	-5.3	8.0

LEAST SQUARES CURVE PARAMETERS				
Cut Depth (mm)	Slope (ksi/in)	Y-Intercept (Canceling Press,psi)	Correlation Coefficient (1=Exact Fit)	Standard Error Of Estimate
20	5.51	338	0.9899	63.2
30	2.46	392	0.9963	38.5
40	1.57	452	0.9999	6.7
50	1.17	523	0.9994	16.0
60	0.99	468	0.9997	11.5
70	0.85	460	0.9998	8.3
80	0.74	454	0.9871	71.7

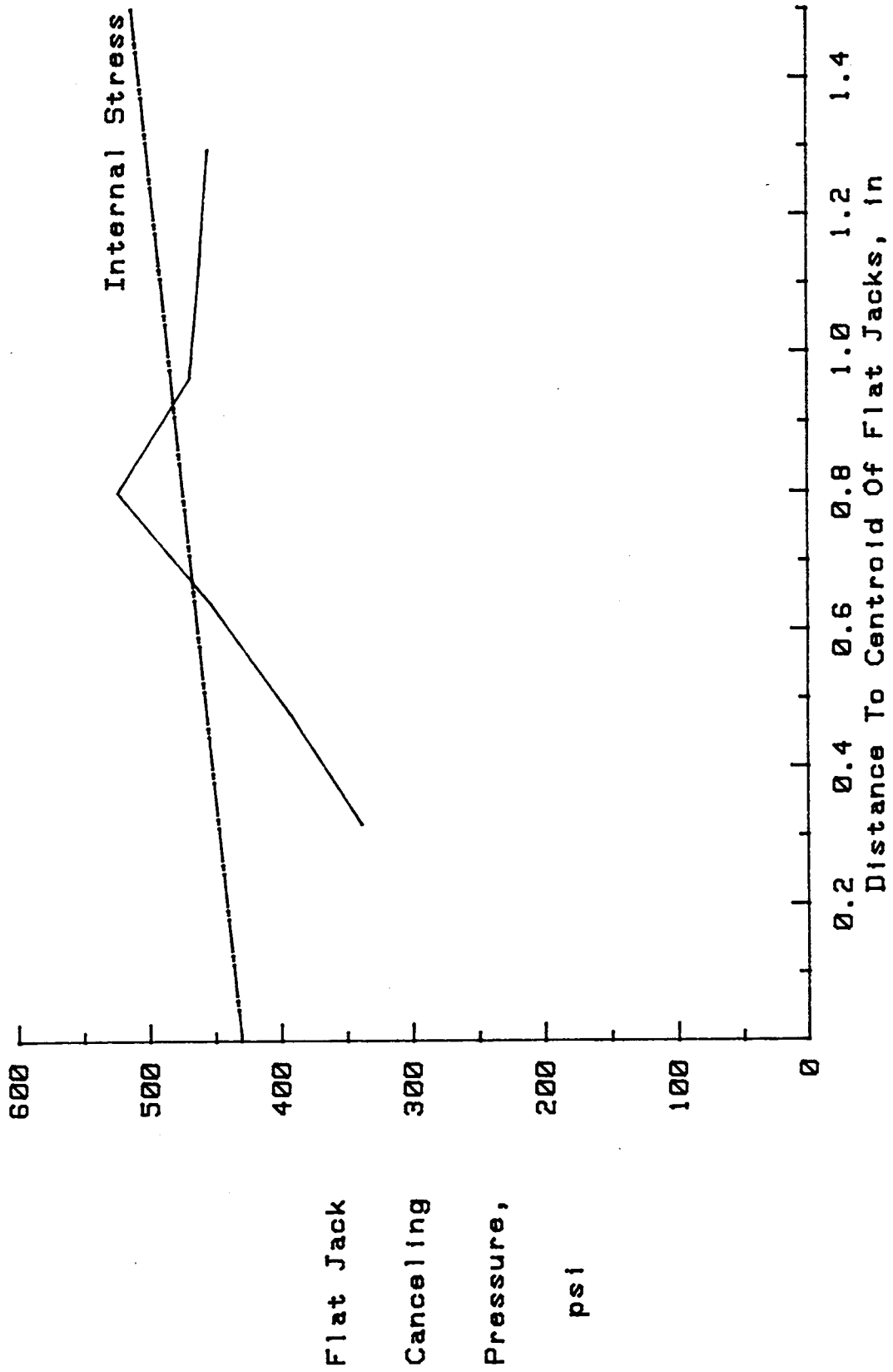
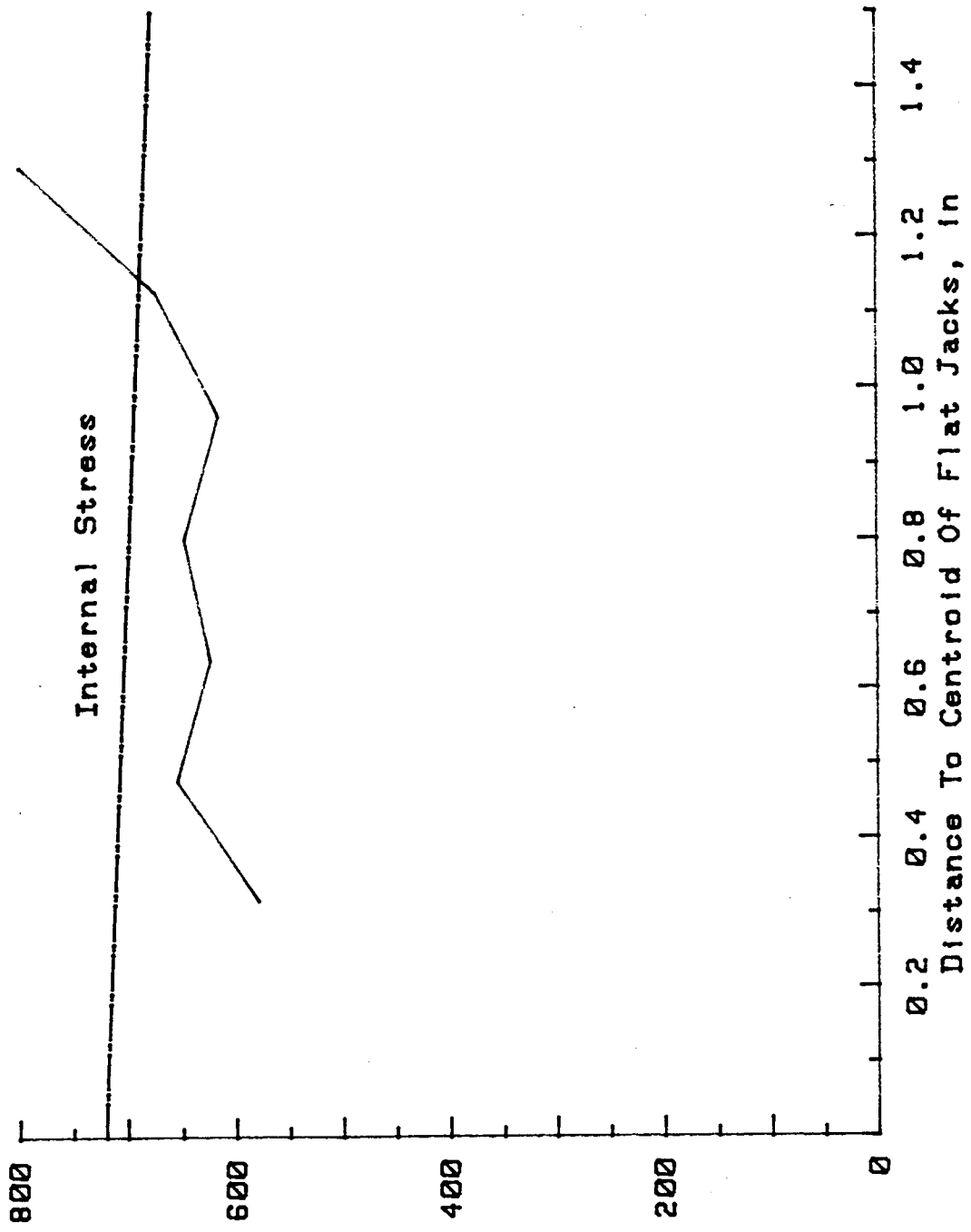


Figure 94. Uncorrected stress profile for 5S1V43/87T.

Table 64. Stress measurement data for specimen 5N4V72/48T.

PFENDER READINGS				
Cut Depth (mm)	Flat Jack Internal Pressure (psi)			
	0	200	400	600
20	-4.1	-5.0	-5.5	-3.4
30	-6.9	-6.3	-2.8	-0.6
40	-12.5	-10.1	-5.0	-0.1
50	-22.1	-16.0	-9.2	-1.1
60	-24.0	-16.4	-9.1	-0.1
70	-31.0	-22.1	-13.1	-3.0
80	-37.0	-27.1	-15.6	-11.1

LEAST SQUARES CURVE PARAMETERS				
Cut Depth (mm)	Slope (ksi/in)	Y-Intercept (Canceling Press,psi)	Correlation Coefficient (1=Exact Fit)	Standard Error Of Estimate
20	2.40	578	0.2210	436.2
30	3.31	654	0.9710	107.0
40	1.82	623	0.9891	65.9
50	1.12	647	0.9979	28.8
60	0.99	615	0.9989	21.0
70	0.85	673	0.9995	13.8
80	0.86	796	0.9865	73.3



Flat Jack  
 Canceling  
 Pressure,  
 psi

Figure 95. Uncorrected stress profile for 5N4V72/48T.

Table 65. Stress measurement data for specimen 5N4V72/48B.

PFENDER READINGS				
Cut Depth (mm)	Flat Jack Internal Pressure (psi)			
	0	200	400	600
20	-4.8	-5.1	-4.0	-1.6
30	-7.7	-5.4	-2.4	0.5
40	-11.5	-8.6	-3.6	1.9
50	-21.9	-15.2	-6.6	0.3
60	-22.6	-15.7	-7.1	1.3
70	-30.3	-21.9	-11.6	-1.7
80	-37.7	-26.8	-15.0	-2.6

LEAST SQUARES CURVE PARAMETERS				
Cut Depth (mm)	Slope (ksi/in)	Y-Intercept (Canceling Press,psi)	Correlation Coefficient (1=Exact Fit)	Standard Error Of Estimate
20	5.58	859	0.8709	219.8
30	2.81	571	0.9981	27.4
40	1.70	537	0.9908	60.6
50	1.04	588	0.9989	21.1
60	0.97	574	0.9988	22.2
70	0.82	642	0.9991	18.9
80	0.67	651	0.9996	12.9



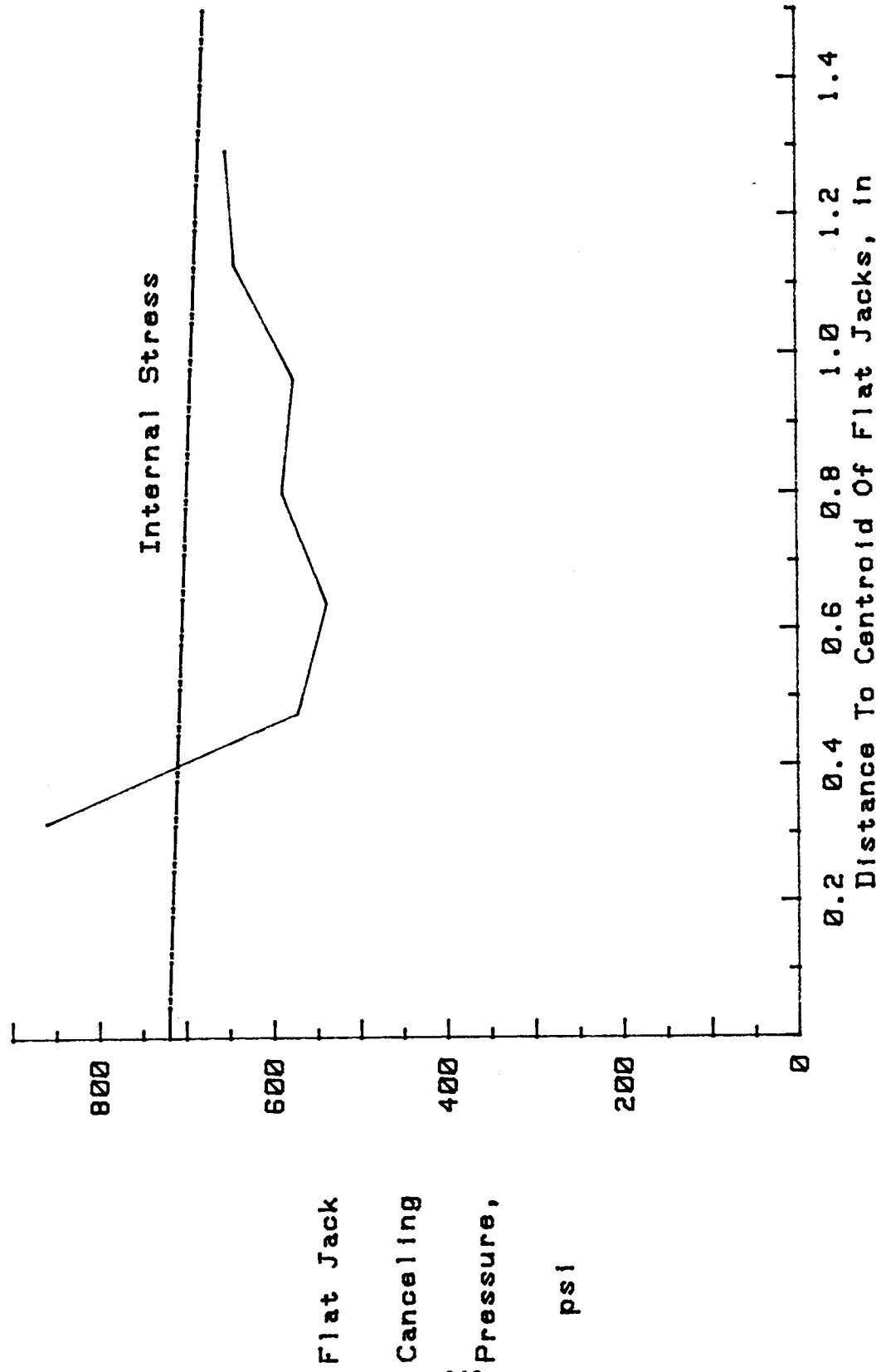


Figure 96. Uncorrected stress profile for 5N4V72/488.

Table 66. Stress measurement data for specimen 5S4V39/82T.

PFENDER READINGS				
Cut Depth (mm)	Flat Jack Internal Pressure (psi)			
	0	200	400	600
20	-2.0	-1.5	-0.4	1.5
30	-4.3	-0.9	1.7	5.6
40	-5.5	-1.5	4.0	8.5
50	-8.2	-2.5	3.5	10.5
60	-11.4	-3.5	3.8	12.0
70	-12.0	-3.9	4.6	13.1
80	-9.0	0.4	10.0	20.5

LEAST SQUARES CURVE PARAMETERS				
Cut Depth (mm)	Slope (ksi/in)	Y-Intercept (Canceling Press,psi)	Correlation Coefficient (1=Exact Fit)	Standard Error Of Estimate
20	6.33	396	0.9653	116.7
30	2.42	268	0.9973	32.9
40	1.65	242	0.9983	25.7
50	1.27	273	0.9988	21.5
60	1.02	294	0.9998	9.5
70	0.94	289	0.9999	5.2
80	0.80	188	0.9997	11.7

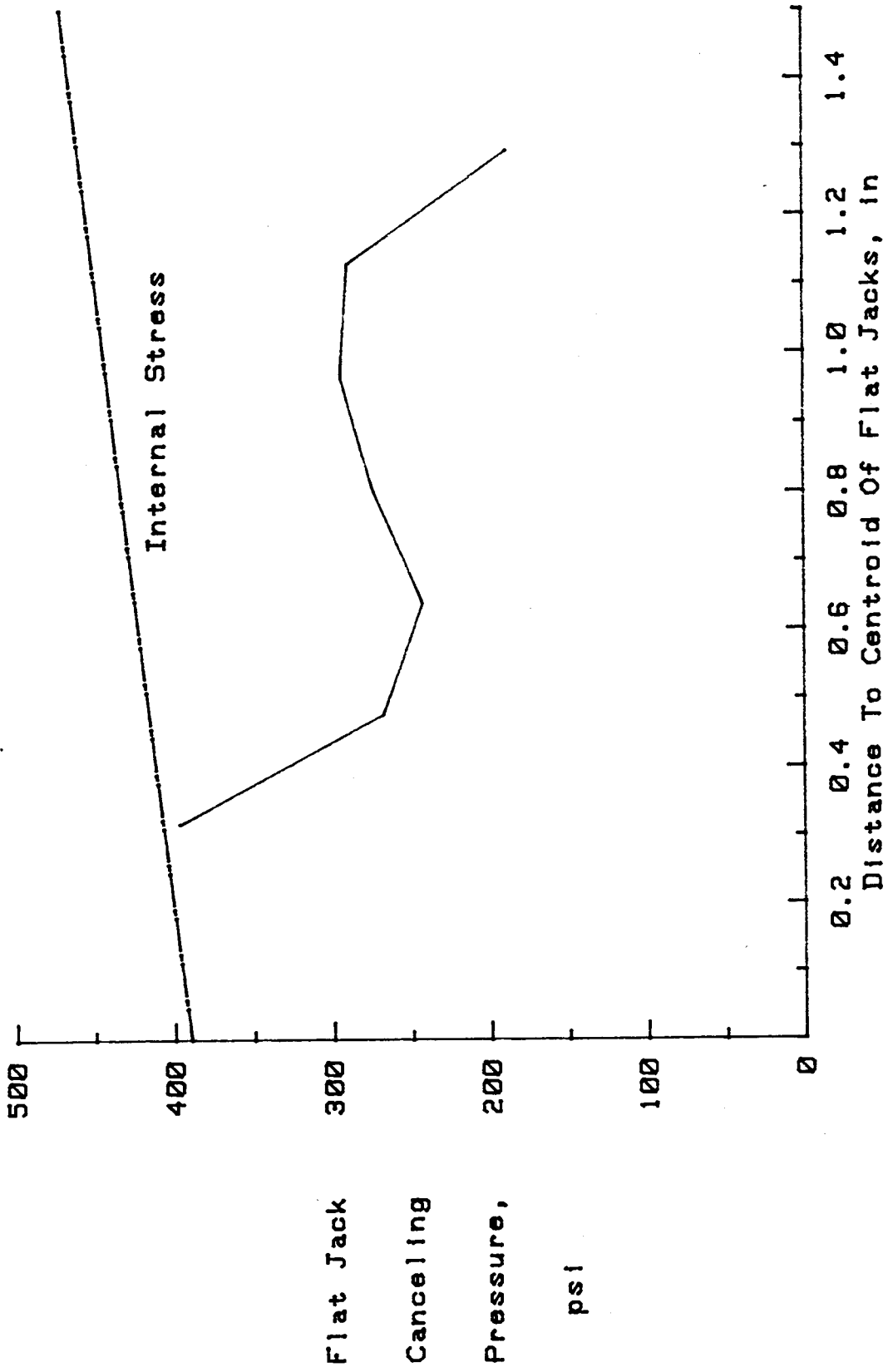


Figure 97. Uncorrected stress profile for 5S4V39/82T.

Table 67. Stress measurement data for specimen 5S4V39/82B.

PFENDER READINGS				
Cut Depth (mm)	Flat Jack Internal Pressure (psi)			
	0	200	400	600
20	-1.7	-1.2	0.2	2.2
30	-2.5	-0.5	2.4	6.4
40	-4.7	-0.7	4.2	9.2
50	-6.7	-1.7	4.2	10.3
60	-10.2	-2.9	4.5	12.0
70	-11.2	-4.2	4.2	14.2
80	-8.8	-0.2	9.7	19.7

LEAST SQUARES CURVE PARAMETERS				
Cut Depth (mm)	Slope (ksi/in)	Y-Intercept (Canceling Press,psi)	Correlation Coefficient (1=Exact Fit)	Standard Error Of Estimate
20	5.49	314	0.9699	109.0
30	2.57	204	0.9891	65.9
40	1.67	214	0.9986	23.3
50	1.37	246	0.9990	20.4
60	1.06	277	1.0000	2.9
70	0.92	282	0.9969	35.2
80	0.82	193	0.9994	16.0

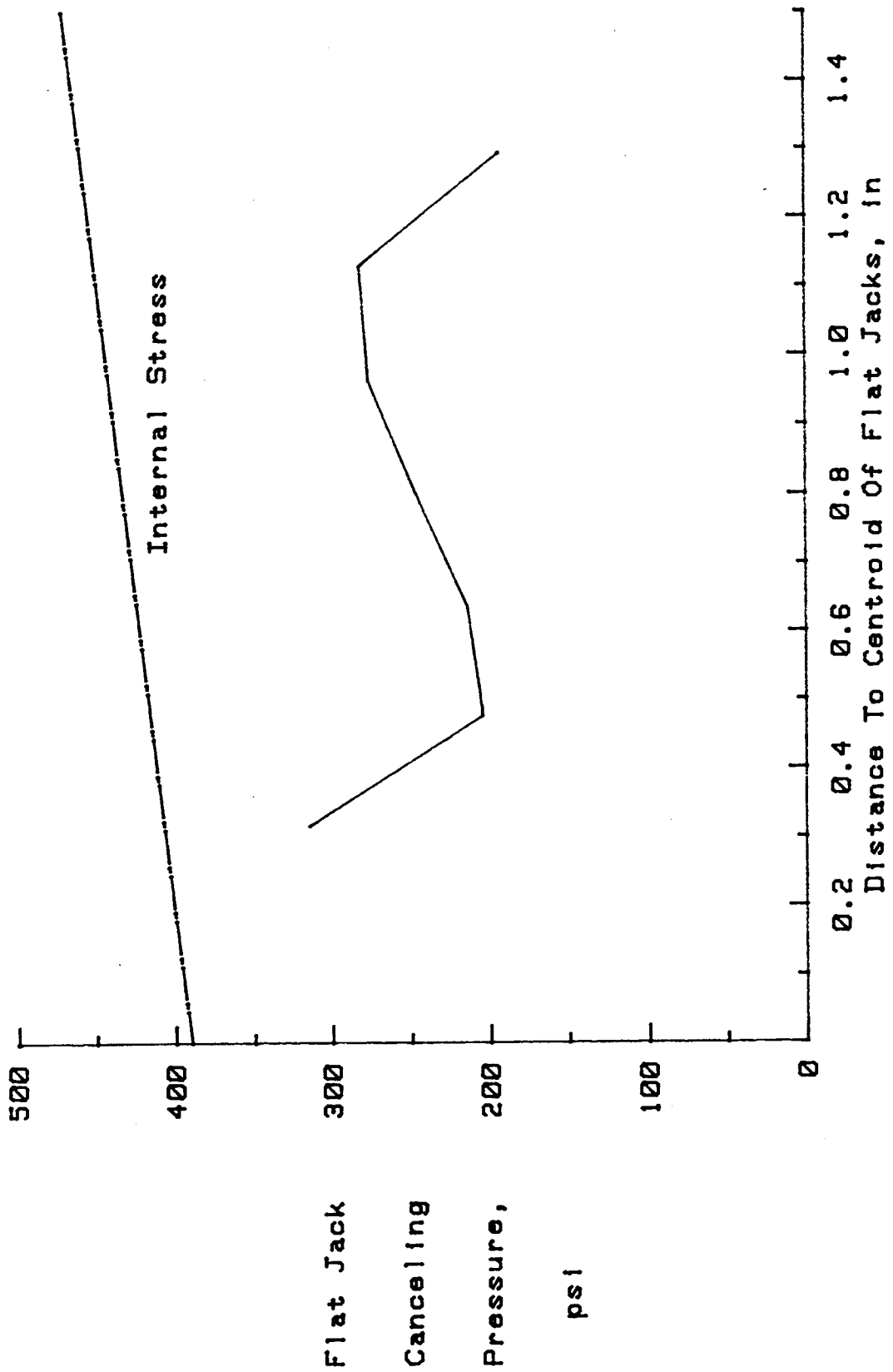


Figure 98. Uncorrected stress profile for 5S4V39/82B.

Table 70. Stress measurement data for specimen 5S5H38/80T.

PFENDER READINGS				
Cut Depth (mm)	Flat Jack Internal Pressure (psi)			
	0	100	200	300
20	5.8	5.7	7.8	7.8
40	10.7	13.6	14.1	38.8
50	12.8	17.0	20.1	50.0
60	13.7	16.7	20.7	34.0
70	16.1	18.2	22.1	32.1
80	14.0	19.3	24.3	40.9

LEAST SQUARES CURVE PARAMETERS				
Cut Depth (mm)	Slope (ksi/in)	Y-Intercept (Canceling Press,psi)	Correlation Coefficient (i=Exact Fit)	Standard Error Of Estimate
20	3.79	-502	0.8830	105.0
40	1.99	-546	0.9260	53.4
50	1.07	-352	0.9962	12.3
60	1.12	-383	0.9966	11.6
70	1.27	-508	0.9853	24.1
80	0.76	-273	0.9999	2.4

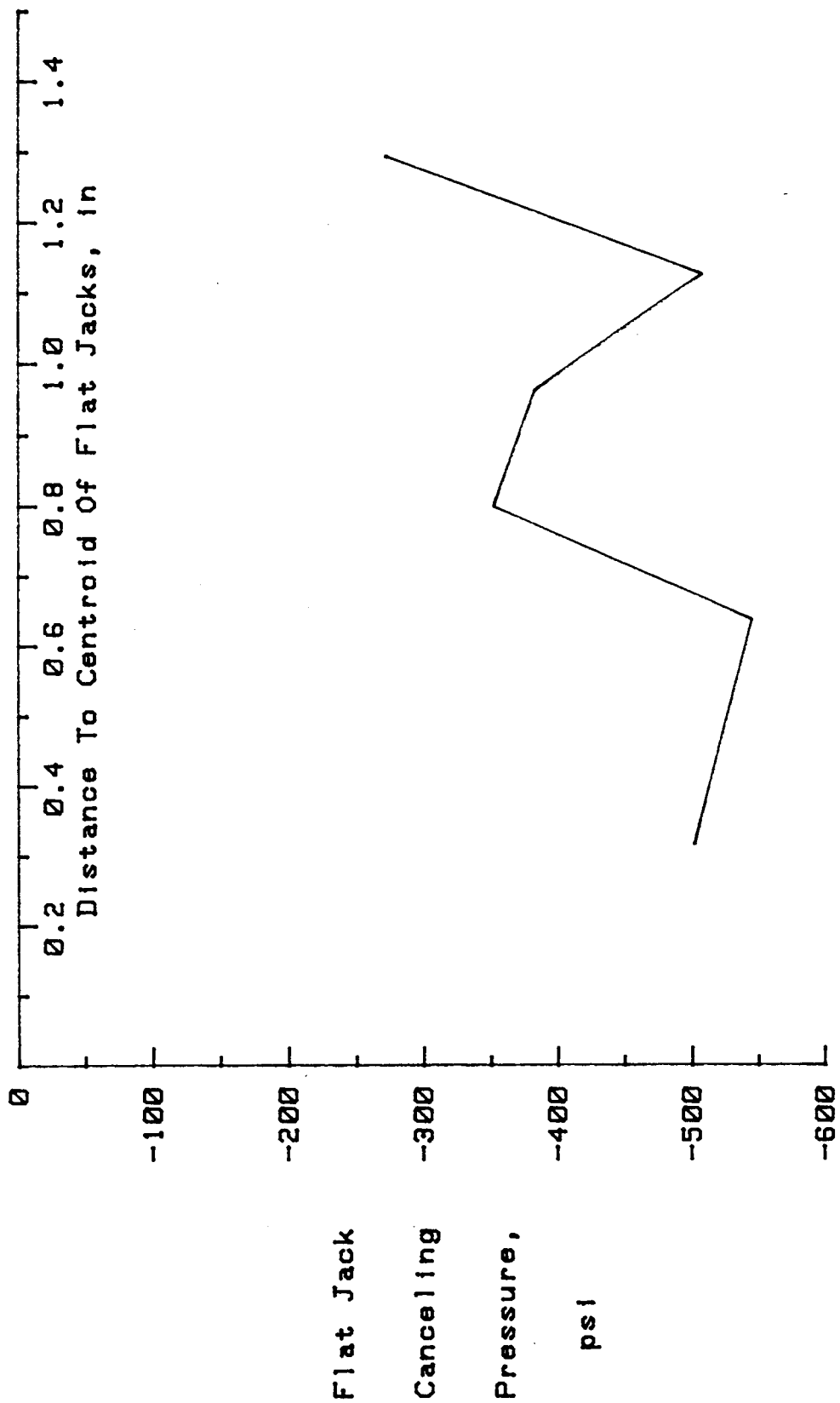


Figure 102. Uncorrected stress profile for 5S5H38/80T.

Table 71. Stress measurement data for specimen 5S5H38/80B.

PFENDER READINGS				
Cut Depth (mm)	Flat Jack Internal Pressure (psi)			
	0	100	200	300
20	5.3	5.5	5.5	6.2
40	10.5	10.9	13.1	38.8
50	11.2	16.6	16.5	50.0
60	11.5	14.2	19.0	34.0
70	12.6	14.8	19.5	32.1
80	11.7	16.7	21.7	40.9

LEAST SQUARES CURVE PARAMETERS				
Cut Depth (mm)	Slope (ksi/in)	Y-Intercept (Canceling Press,psi)	Correlation Coefficient (1=Exact Fit)	Standard Error Of Estimate
20	11.37	-1491	0.8830	105.0
40	2.61	-666	0.9286	52.5
50	1.09	-312	0.8578	72.7
60	1.02	-289	0.9872	22.6
70	1.09	-336	0.9788	29.0
80	0.79	-235	1.0000	0.0



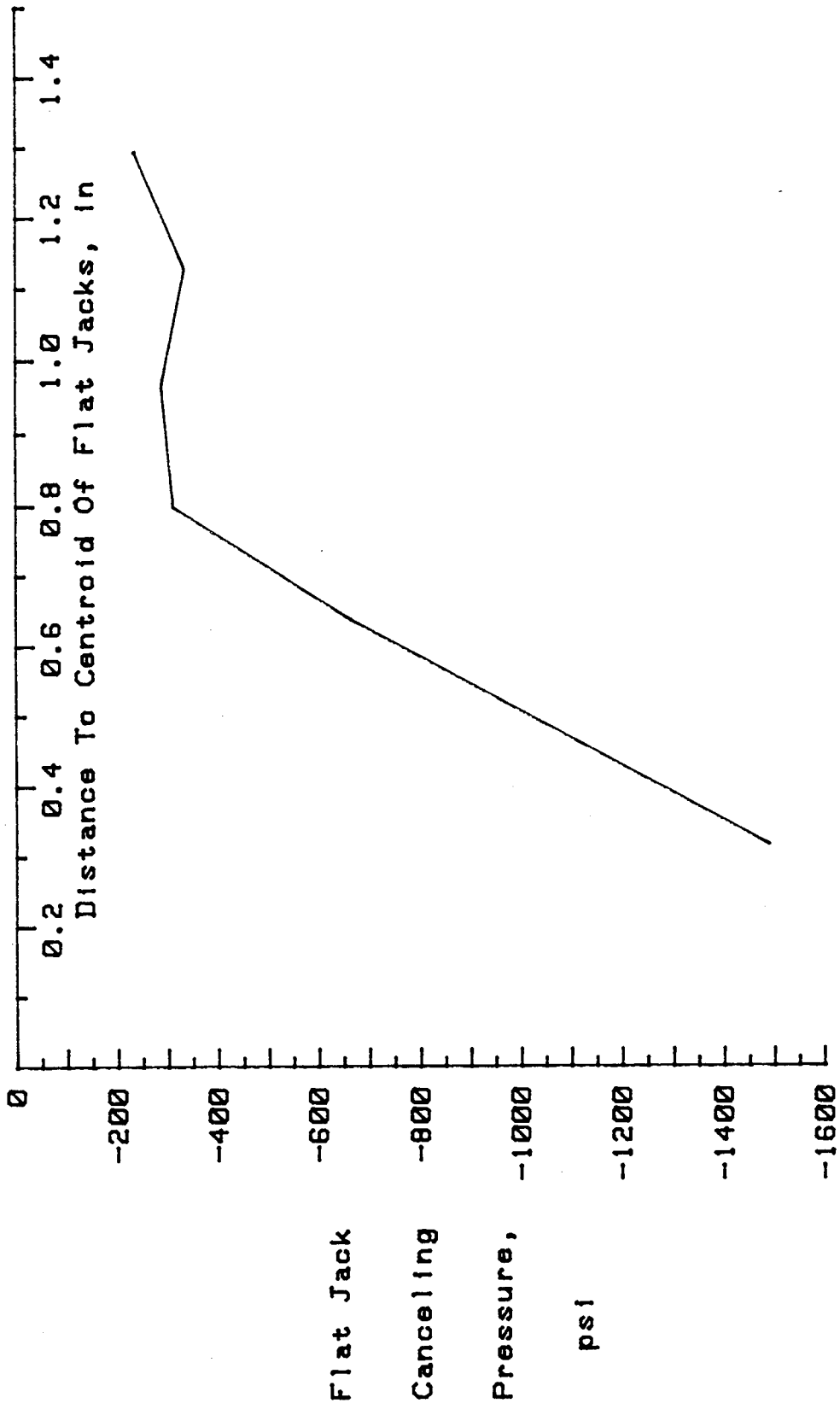


Figure 103. Uncorrected stress profile for 5S5H38/80B.

Table 72. Stress measurement data for specimen 5S6H38/80T.

PFENDER READINGS			
Cut Depth (mm)	Flat Jack Internal Pressure (psi)		
	0	100	200
40	12.1	13.7	16.4
50	11.9	13.2	16.9
60	15.5	16.9	19.2
70	23.0	24.5	28.5
80	25.1	26.1	30.1

LEAST SQUARES CURVE PARAMETERS				
Cut Depth (mm)	Slope (ksi/in)	Y-Intercept (Canceling Press,psi)	Correlation Coefficient (1=Exact Fit)	Standard Error Of Estimate
40	1.79	-544	0.9893	20.7
50	1.46	-423	0.9637	37.8
60	2.09	-816	0.9903	19.7
70	1.34	-765	0.9672	35.9
80	1.41	-871	0.9449	46.3

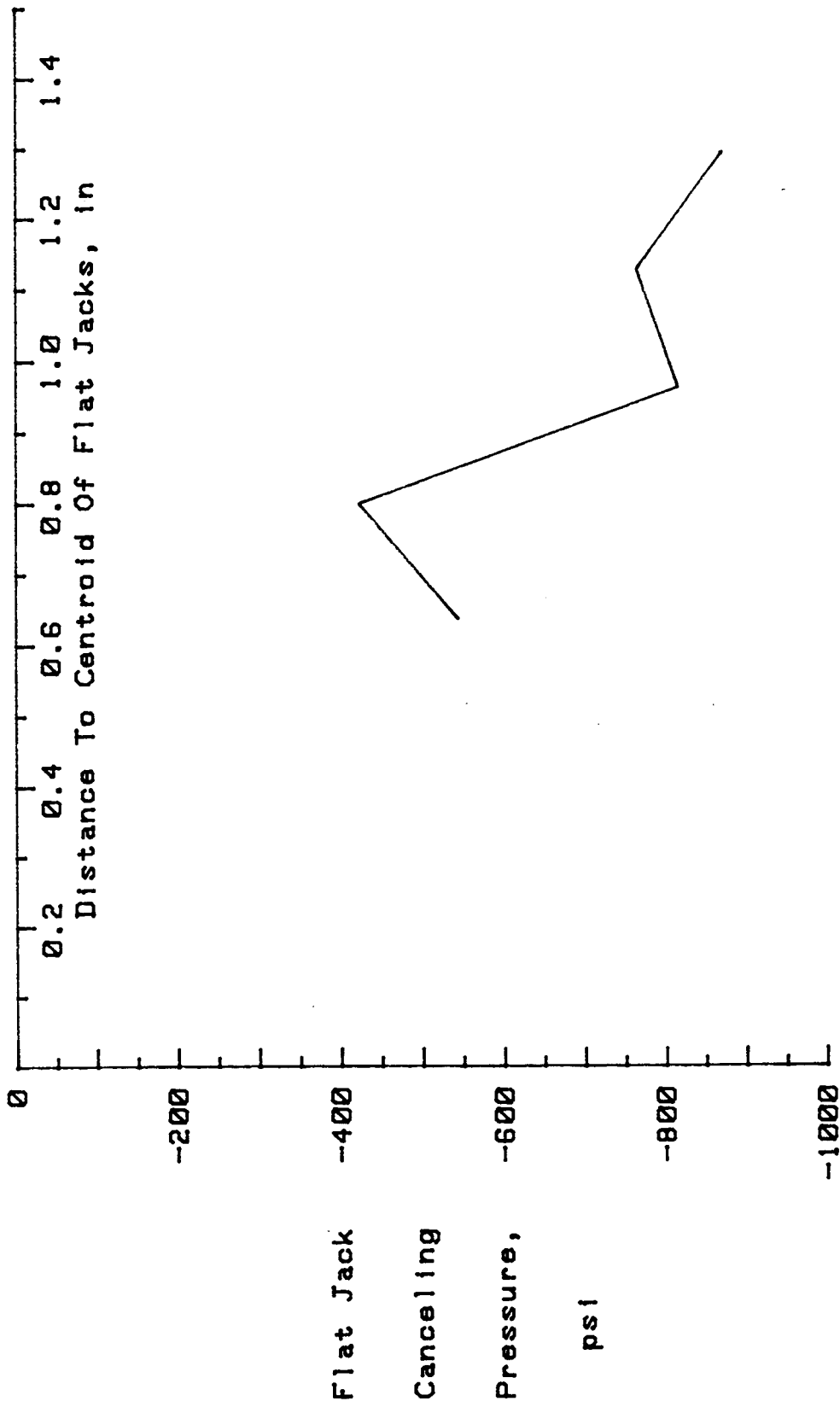


Figure 104. Uncorrected stress profile for 5S6H38/80T.

Table 73. Stress measurement data for specimen 5S6H38/80B.

PFENDER READINGS				
Cut Depth (mm)	Flat Jack Internal Pressure (psi)			
	0	100	100	200
40	9.2	11.2	11.2	13.5
50	10.3	12.4	12.4	15.4
60	12.7	14.7	14.7	16.7
70	20.5	22.0	22.0	26.0
80	21.6	23.6	23.6	27.6

LEAST SQUARES CURVE PARAMETERS				
Cut Depth (mm)	Slope (ksi/in)	Y-Intercept (Canceling Press,psi)	Correlation Coefficient (1=Exact Fit)	Standard Error Of Estimate
40	1.83	-425	0.9992	5.7
50	1.53	-393	0.9948	14.3
60	1.97	-635	1.0000	0.0
70	1.34	-677	0.9672	35.9
80	1.27	-680	0.9820	26.7

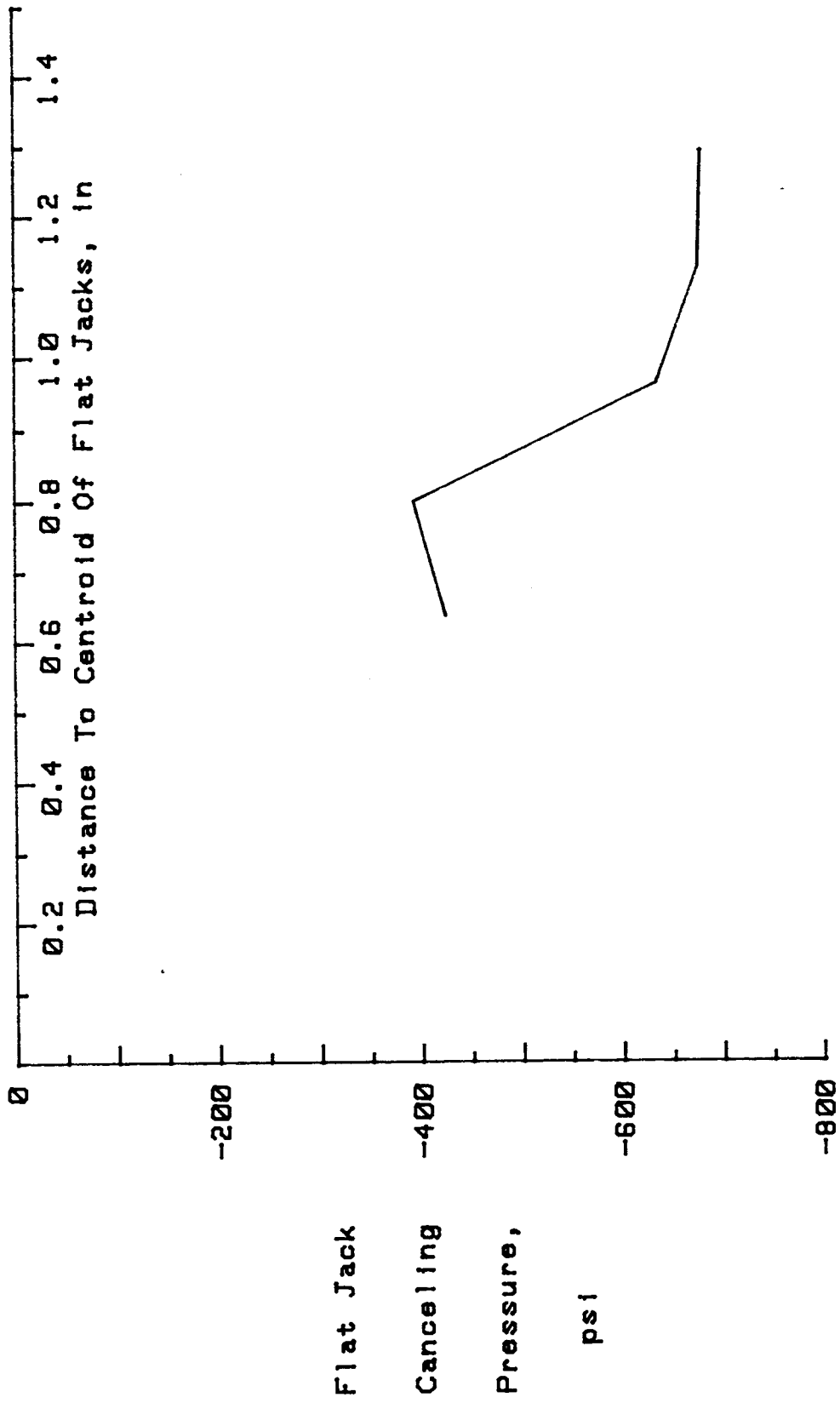


Figure 105. Uncorrected stress profile for 5S6H38/80B.

## 11.0 APPENDIX C - FIELD TEST RESULTS

This appendix contains data from all field cuts. A descriptive alphanumeric label was used for each slot:

TW a b c e

TW indicates that cuts were made on the tollway girder.

a indicates side of specimen cut was made on: S is the south side; B is the bottom side.

b indicates the slot location as shown in figures 45 and 46.

c indicates the cut orientation: H denotes horizontal slots and V denotes vertical slots.

e indicates the Pfender points location. For vertical slots, T is the top set of Pfender points and B is the bottom set. For horizontal slots, E the east set and W is the west set. For bottom side cuts, N the north set and S is the south set. The orientation of Pfender points is shown in figure 31.

The following results are organized by slot number first then Pfender point location (top, east, or north first, bottom, west, or south second). Positive canceling pressures indicate compressive stresses while negative (-) pressures indicate tensile stresses.

This appendix includes tables for modified Pfender gage readings at various pressures, and also contains linear regression, least squares, results at various pressures. The Pfender readings were modified based on changes in standard bar readings. This appendix also includes graphs of measured canceling pressures and internal applied stresses at various distances from the surface of the specimen. The canceling pressures were plotted at the centroid of individual flat jacks. The centroids are given in figure 21.

Table 74. Stress measurement data for specimen TWS1VT.

PFENDER READINGS				
Cut Depth (mm)	Flat Jack Internal Pressure (psi)			
	0	200	400	600
20	4.0	5.0	6.3	8.0
30	4.6	7.1	10.8	13.1
40	6.6	9.6	14.6	18.4
50	8.3	12.1	17.8	23.3
60	11.1	15.7	20.9	27.4
70	10.6	16.4	23.6	30.6
80	9.1	17.0	25.9	35.6

LEAST SQUARES CURVE PARAMETERS				
Cut Depth (mm)	Slope (ksi/in)	Y-Intercept (Canceling Press,psi)	Correlation Coefficient (1=Exact Fit)	Standard Error Of Estimate
20	5.84	-574	0.9931	52.4
30	2.67	-309	0.9959	40.2
40	1.93	-307	0.9959	40.4
50	1.54	-305	0.9964	38.2
60	1.45	-392	0.9968	35.5
70	1.17	-305	0.9989	20.8
80	0.89	-196	0.9990	20.4

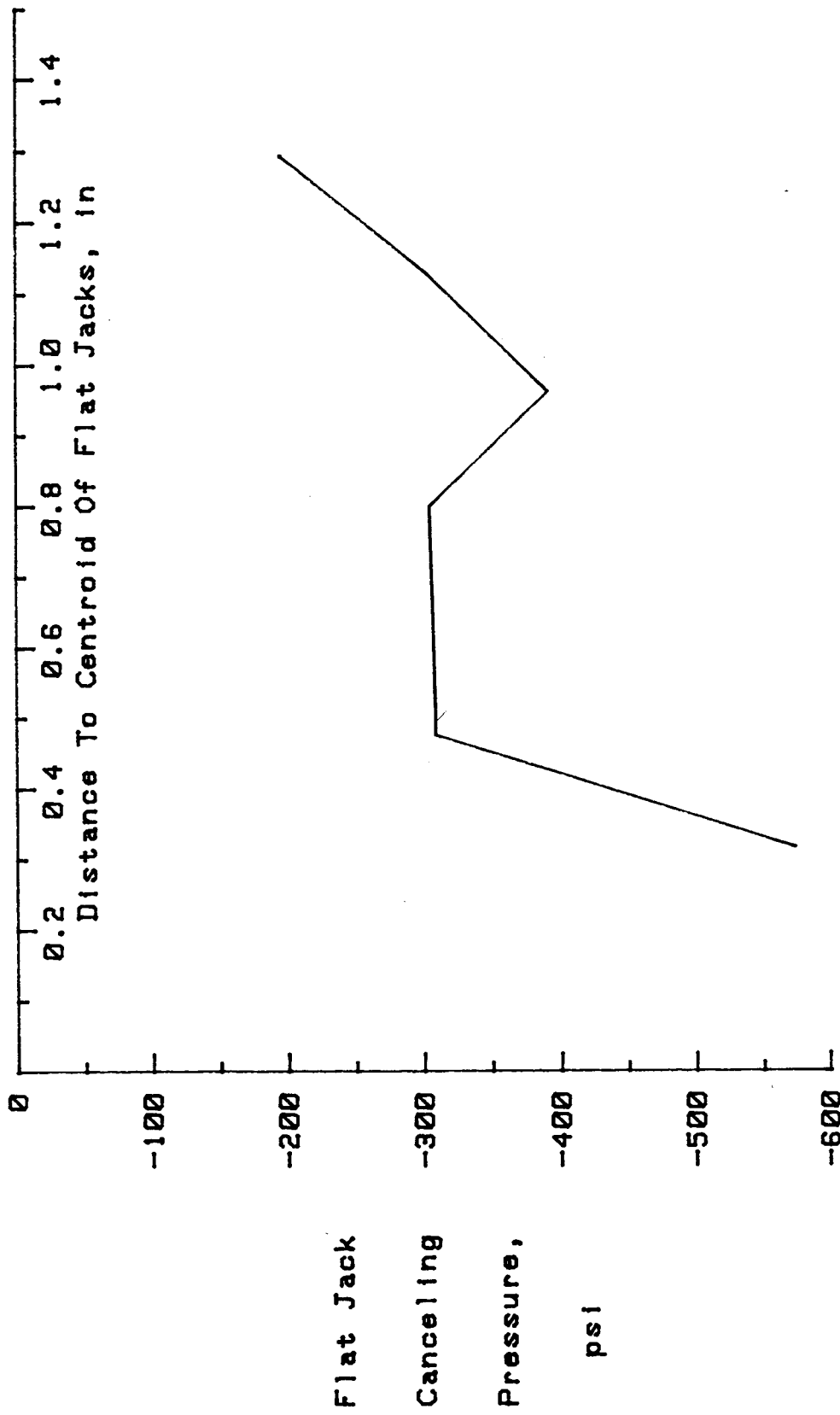


Figure 106. Uncorrected stress profile for TWS1VT.



Table 75. Stress measurement data for specimen TWS1VB.

PFENDER READINGS				
Cut Depth (mm)	Flat Jack Internal Pressure (psi)			
	0	200	400	600
20	2.0	2.4	3.4	5.6
30	3.0	4.0	7.5	10.3
40	4.0	7.3	11.2	15.7
50	5.7	9.9	14.9	20.5
60	8.3	13.1	18.3	24.5
70	8.3	14.0	20.7	27.7
80	6.3	14.0	23.0	32.8

LEAST SQUARES CURVE PARAMETERS				
Cut Depth (mm)	Slope (ksi/in)	Y-Intercept (Canceling Press,psi)	Correlation Coefficient (1=Exact Fit)	Standard Error Of Estimate
20	5.96	-218	0.9454	145.8
30	2.98	-174	0.9801	88.7
40	2.01	-191	0.9976	30.7
50	1.59	-217	0.9980	28.3
60	1.46	-297	0.9982	26.4
70	1.21	-246	0.9989	20.6
80	0.89	-130	0.9986	23.8

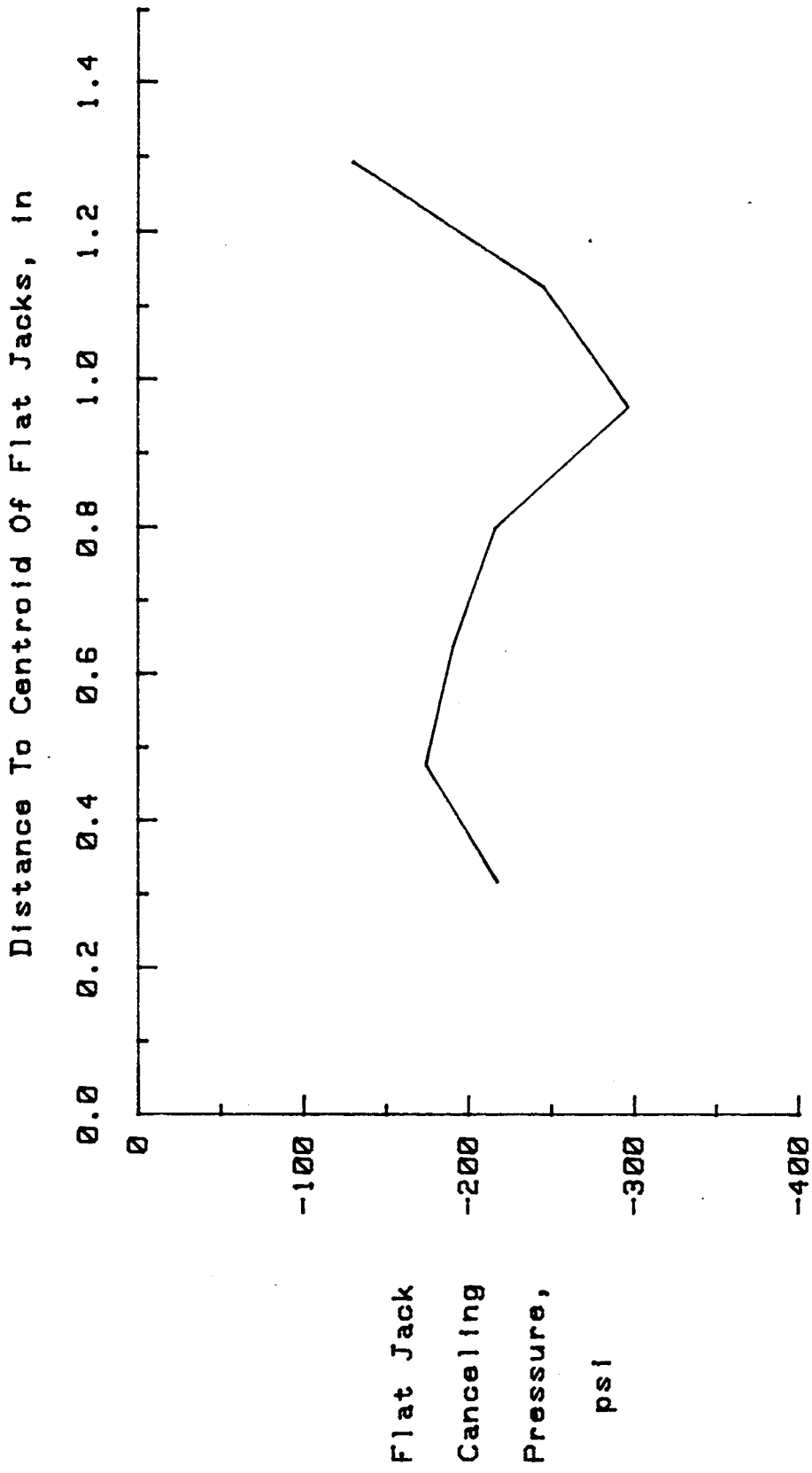


Figure 107. Uncorrected stress profile for TWS1VB.

Table 76. Stress measurement data for specimen TWS2VT.

PFENDER READINGS				
Cut Depth (mm)	Flat Jack Internal Pressure (psi)			
	0	200	400	600
20	3.1	2.4	5.1	7.1
30	2.1	4.4	7.1	10.6
40	0.3	4.0	8.0	12.7
50	3.9	4.9	10.9	14.9
60	7.6	12.1	20.0	19.3
70	-0.4	4.6	11.3	18.6
80	-3.4	4.1	12.1	19.8

LEAST SQUARES CURVE PARAMETERS				
Cut Depth (mm)	Slope (ksi/in)	Y-Intercept (Canceling Press,psi)	Correlation Coefficient (1=Exact Fit)	Standard Error Of Estimate
20	4.30	-187	0.8957	198.9
30	2.77	-128	0.9954	42.8
40	1.91	-4	0.9985	24.6
50	1.90	-119	0.9705	107.9
60	1.59	-297	0.9321	162.0
70	1.22	35	0.9969	35.0
80	1.01	91	1.0000	4.2

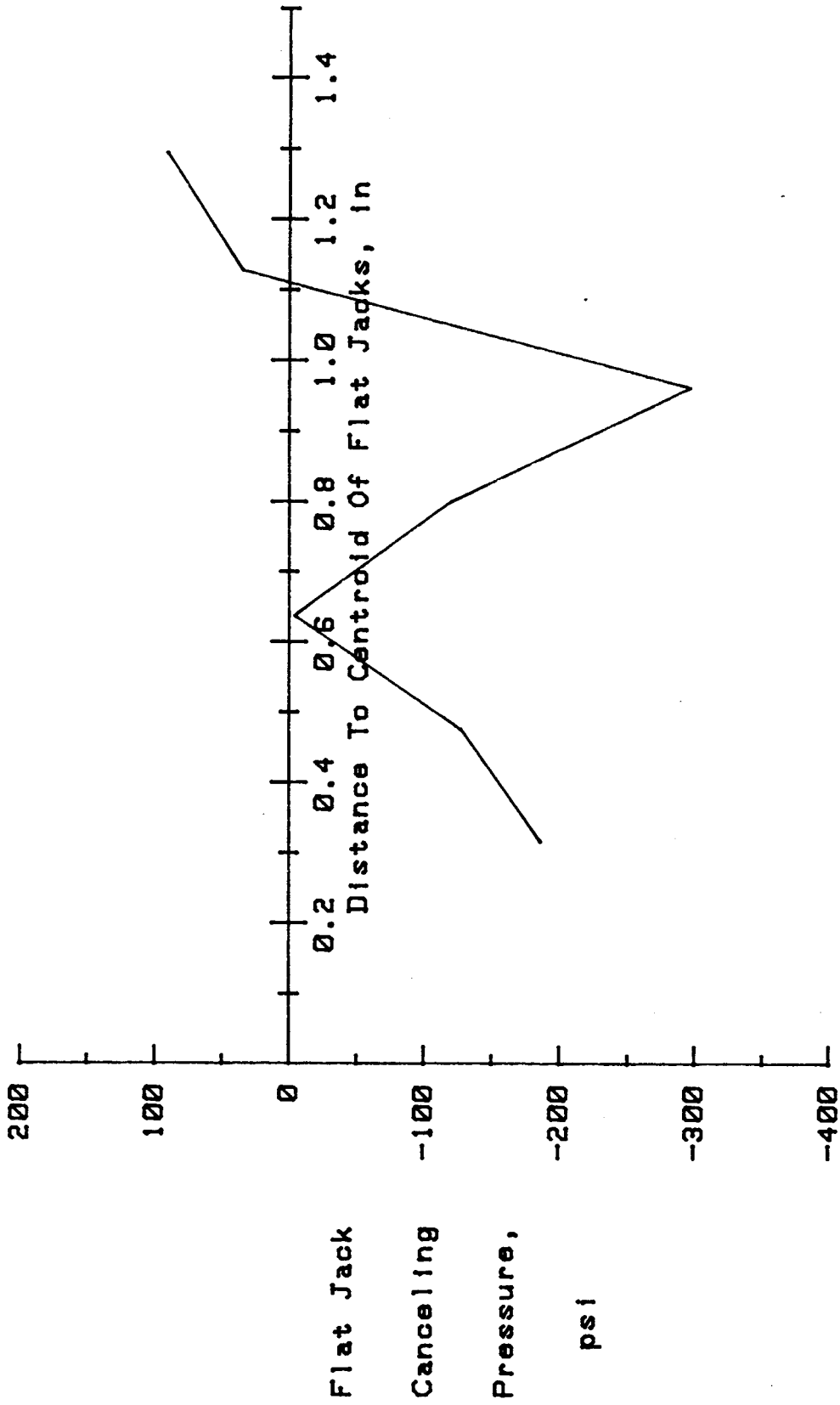


Figure 108. Uncorrected stress profile for TMS2VT.

Table 77. Stress measurement data for specimen TWS2VB.

PFENDER READINGS				
Cut Depth (mm)	Flat Jack Internal Pressure (psi)			
	0	200	400	600
20	1.9	1.3	3.0	5.8
30	0.7	3.0	5.7	7.8
40	-0.9	2.1	5.1	9.7
50	-1.2	1.8	6.3	13.0
60	-1.5	5.7	10.7	12.7
70	-5.9	0.5	6.8	12.5
80	-7.9	-0.1	5.6	13.6

LEAST SQUARES CURVE PARAMETERS				
Cut Depth (mm)	Slope (ksi/in)	Y-Intercept (Canceling Press,psi)	Correlation Coefficient (1=Exact Fit)	Standard Error Of Estimate
20	4.42	-37	0.8671	222.7
30	3.27	-58	0.9990	20.4
40	2.23	73	0.9937	50.0
50	1.62	95	0.9848	77.6
60	1.56	26	0.9713	106.4
70	1.28	187	0.9996	11.9
80	1.12	221	0.9980	28.1

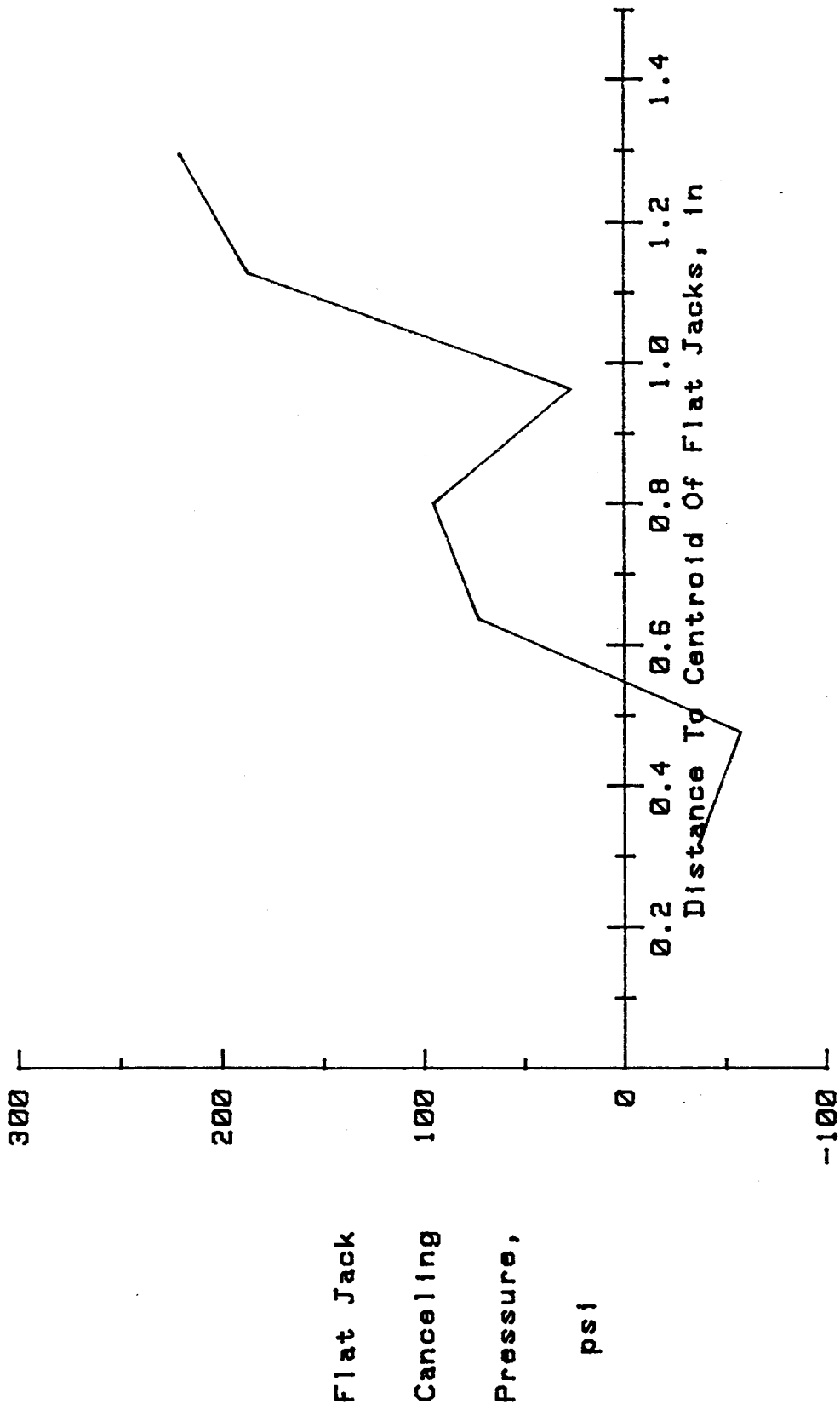


Figure 109. Uncorrected stress profile for TWS2VB.

Table 78. Stress measurement data for specimen TWS3HE.

PFENDER READINGS				
Cut Depth (mm)	Flat Jack Internal Pressure (psi)			
	0	100	200	300
20	4.4	6.5	7.2	9.1
30	5.8	7.7	7.9	8.7
40	10.1	10.7	12.7	14.7
50	16.2	17.7	19.8	23.1
60	19.9	20.7	23.8	27.7
70	26.2	29.7	34.7	40.2
80	27.7	32.7	39.7	45.7

LEAST SQUARES CURVE PARAMETERS				
Cut Depth (mm)	Slope (ksi/in)	Y-Intercept (Canceling Press,psi)	Correlation Coefficient (1=Exact Fit)	Standard Error Of Estimate
20	2.58	-300	0.9845	39.2
30	3.87	-597	0.9353	79.1
40	2.38	-583	0.9772	47.4
50	1.67	-669	0.9844	39.3
60	1.39	-664	0.9660	57.8
70	0.83	-541	0.9953	21.7
80	0.64	-447	0.9981	13.7

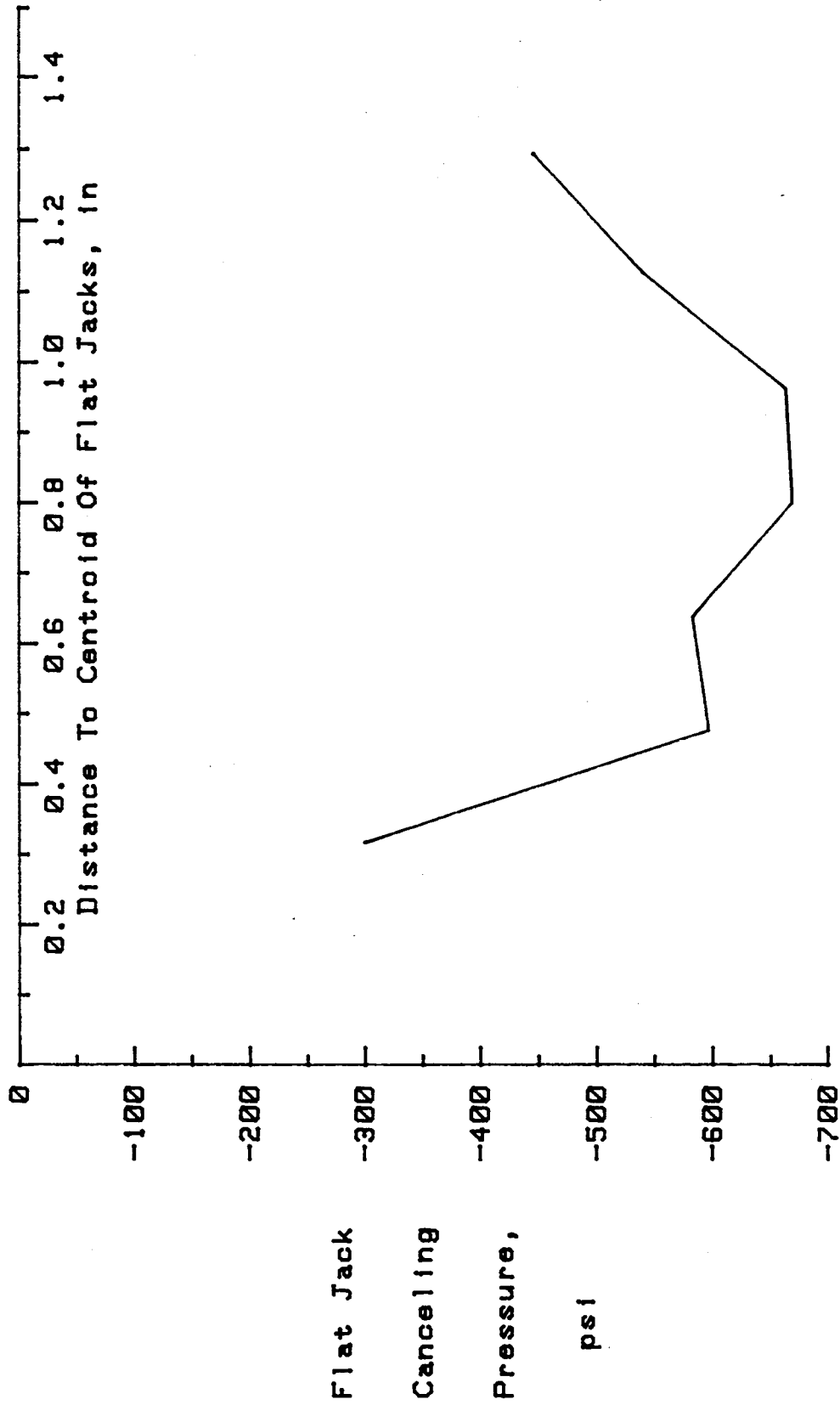


Figure 110. Uncorrected stress profile for TWS3HE.



Table 79. Stress measurement data for specimen TWS3HW.

PFENDER READINGS				
Cut Depth (mm)	Flat Jack Internal Pressure (psi)			
	0	100	200	300
20	3.7	3.4	3.4	4.4
30	4.4	5.4	7.4	9.4
40	10.9	10.9	12.5	15.4
50	17.4	18.5	20.8	23.4
60	21.4	21.6	24.4	28.4
70	27.8	30.6	35.9	40.9
80	31.0	34.2	40.4	46.6

LEAST SQUARES CURVE PARAMETERS				
Cut Depth (mm)	Slope (ksi/in)	Y-Intercept (Canceling Press,psi)	Correlation Coefficient (1=Exact Fit)	Standard Error Of Estimate
20	6.19	-443	0.5747	183.0
30	2.27	-236	0.9898	31.9
40	2.20	-547	0.9187	88.3
50	1.88	-811	0.9857	37.7
60	1.46	-741	0.9403	76.1
70	0.87	-597	0.9920	28.2
80	0.73	-555	0.9905	30.7

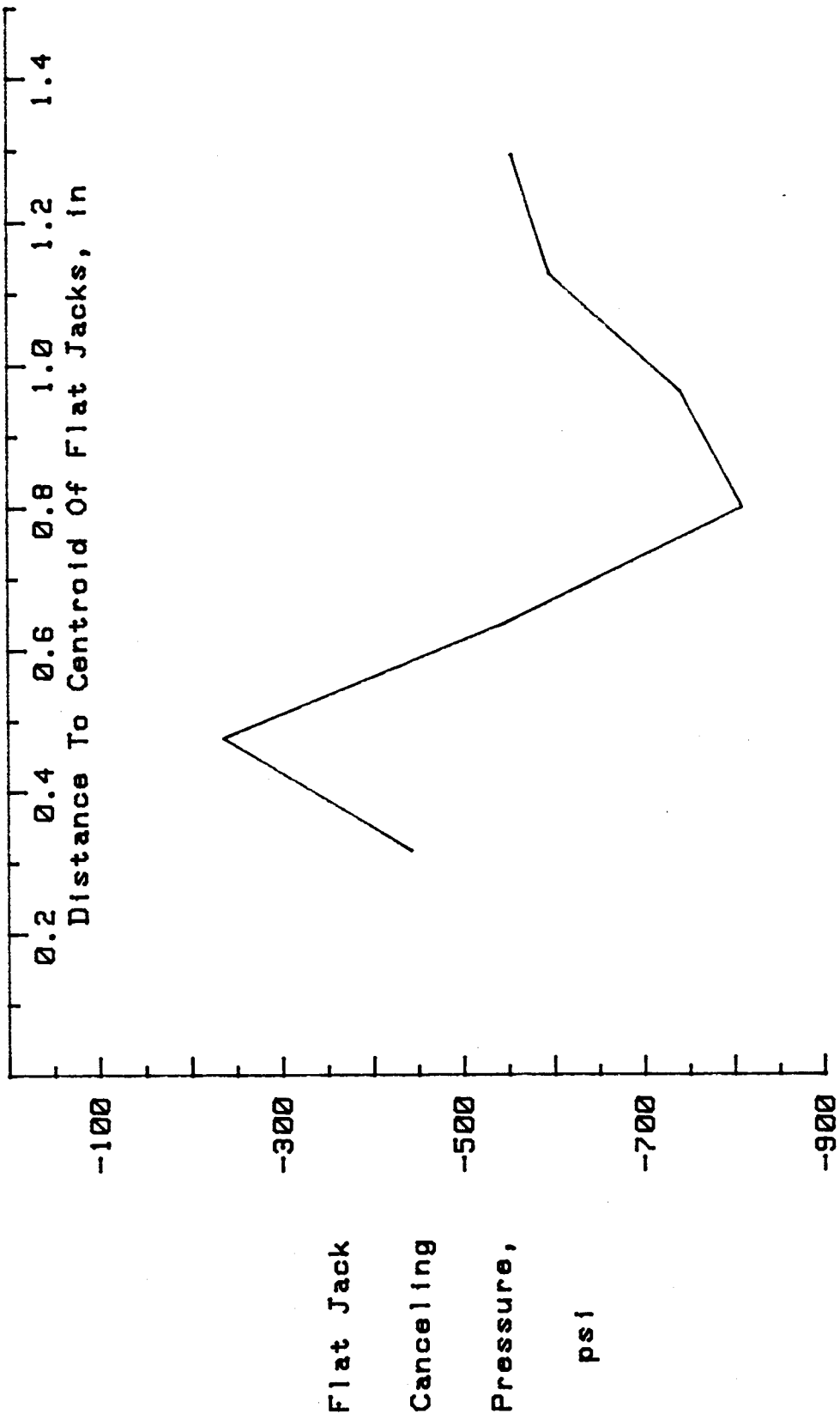
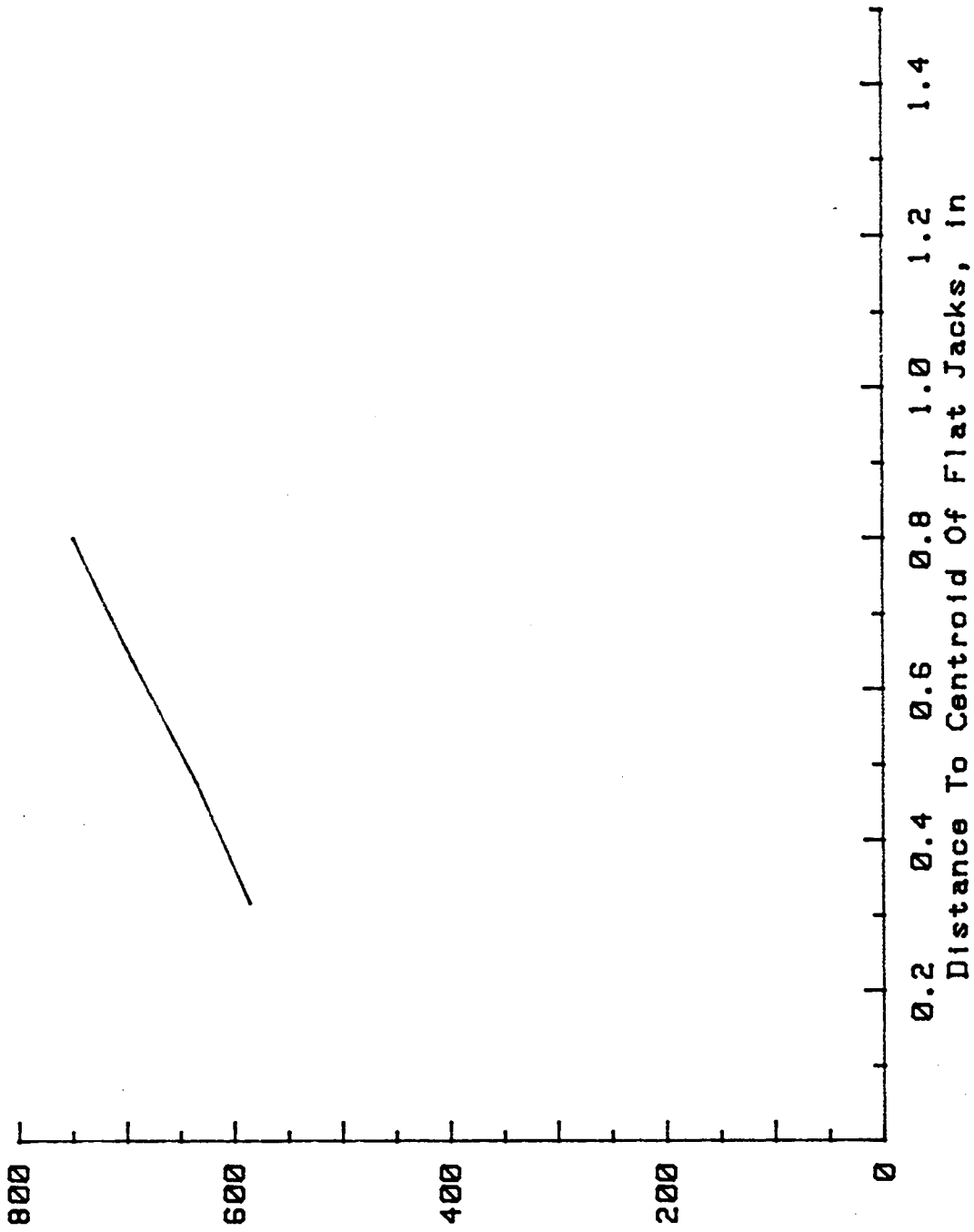


Figure 111. Uncorrected stress profile for TWS3HW.

Table 80. Stress measurement data for specimen TWB4VN.

PFENDER READINGS				
Cut Depth (mm)	Flat Jack Internal Pressure (psi)			
	0	200	400	600
20	-4.9	-2.0	-1.5	-0.5
30	-6.5	-5.3	-2.5	-0.3
40	-11.4	-8.1	-5.1	-1.4
50	-13.4	-11.8	-7.4	-2.4

LEAST SQUARES CURVE PARAMETERS				
Cut Depth (mm)	Slope (ksi/in)	Y-Intercept (Canceling Press,psi)	Correlation Coefficient (1=Exact Fit)	Standard Error Of Estimate
20	5.04	585	0.9362	157.2
30	3.60	634	0.9894	64.9
40	2.38	693	0.9992	18.2
50	2.02	748	0.9783	92.6



Flat Jack  
Canceling  
Pressure,  
psi

Figure 112. Uncorrected stress profile for TWB4VN.

Table 81. Stress measurement data for specimen TWB4VS.

PFENDER READINGS				
Cut Depth (mm)	Flat Jack Internal Pressure (psi)			
	0	200	400	600
20	-11.4	-11.4	-9.4	-7.4
30	-14.1	-13.1	-11.4	-8.4
40	-19.5	-16.5	-13.5	-9.7
50	-22.1	-19.3	-16.3	-12.3

LEAST SQUARES CURVE PARAMETERS				
Cut Depth (mm)	Slope (ksi/in)	Y-Intercept (Canceling Press,psi)	Correlation Coefficient (1=Exact Fit)	Standard Error Of Estimate
20	5.01	1561	0.9439	147.7
30	3.96	1483	0.9724	104.4
40	2.42	1211	0.9982	27.0
50	2.41	1373	0.9963	38.5

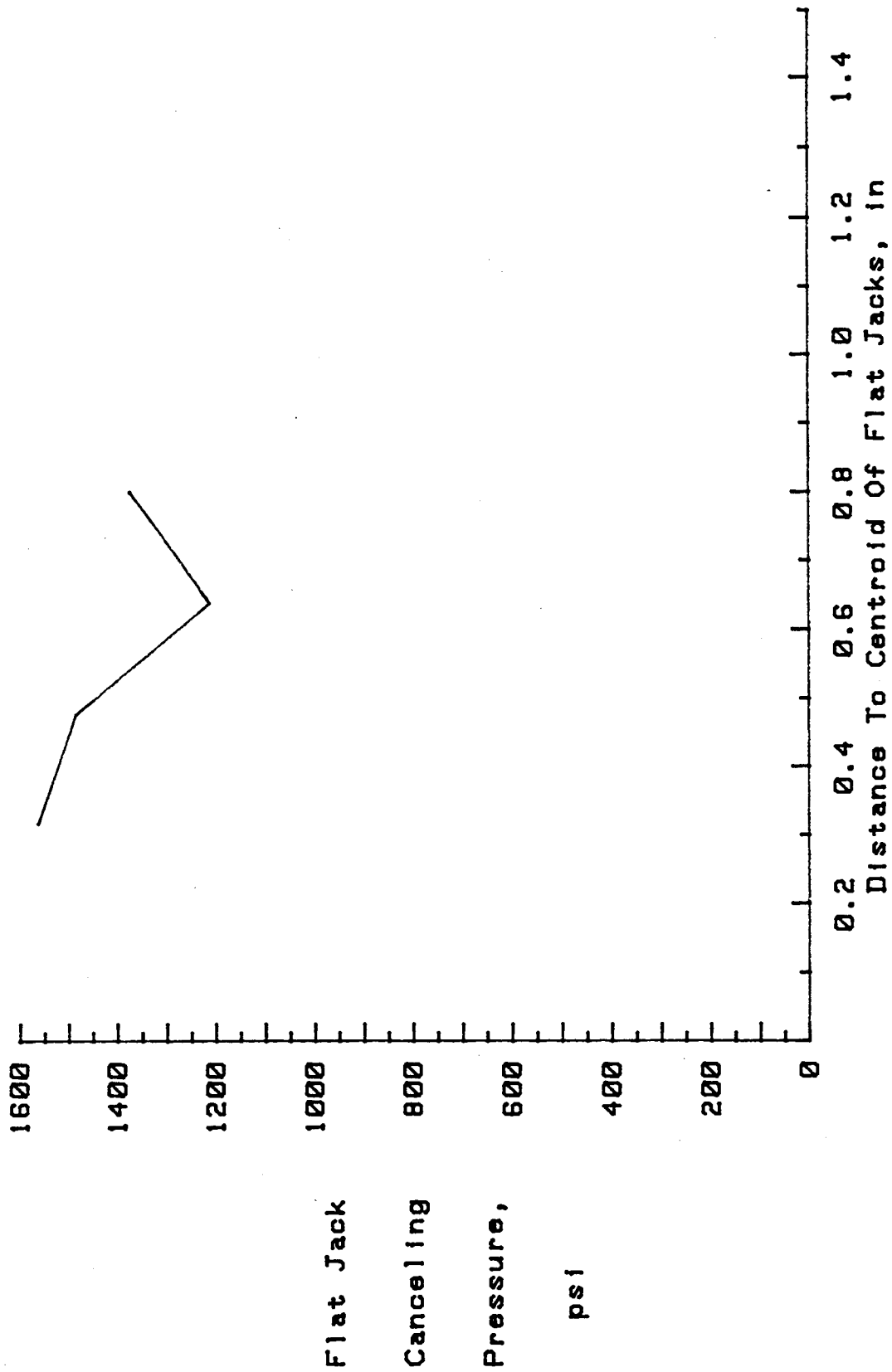


Figure 113. Uncorrected stress profile for TWB4VS.

Table 82. Stress measurement data for specimen TWS5VT.

PFENDER READINGS				
Cut Depth (mm)	Flat Jack Internal Pressure (psi)			
	0	200	400	600
20	5.2	5.9	6.1	7.7
30	6.2	8.2	10.0	12.2
40	11.9	14.8	17.8	21.6
50	16.9	19.7	23.7	27.7
60	17.2	21.3	26.1	32.6
70	18.2	21.9	27.9	33.9
80	11.2	16.7	24.4	32.9

LEAST SQUARES CURVE PARAMETERS				
Cut Depth (mm)	Slope (ksi/in)	Y-Intercept (Canceling Press,psi)	Correlation Coefficient (1=Exact Fit)	Standard Error Of Estimate
20	9.06	-1145	0.9411	151.3
30	3.97	-629	0.9993	16.9
40	2.44	-729	0.9978	29.6
50	2.15	-904	0.9968	36.0
60	1.53	-644	0.9943	47.6
70	1.47	-651	0.9944	47.2
80	1.07	-282	0.9956	41.9

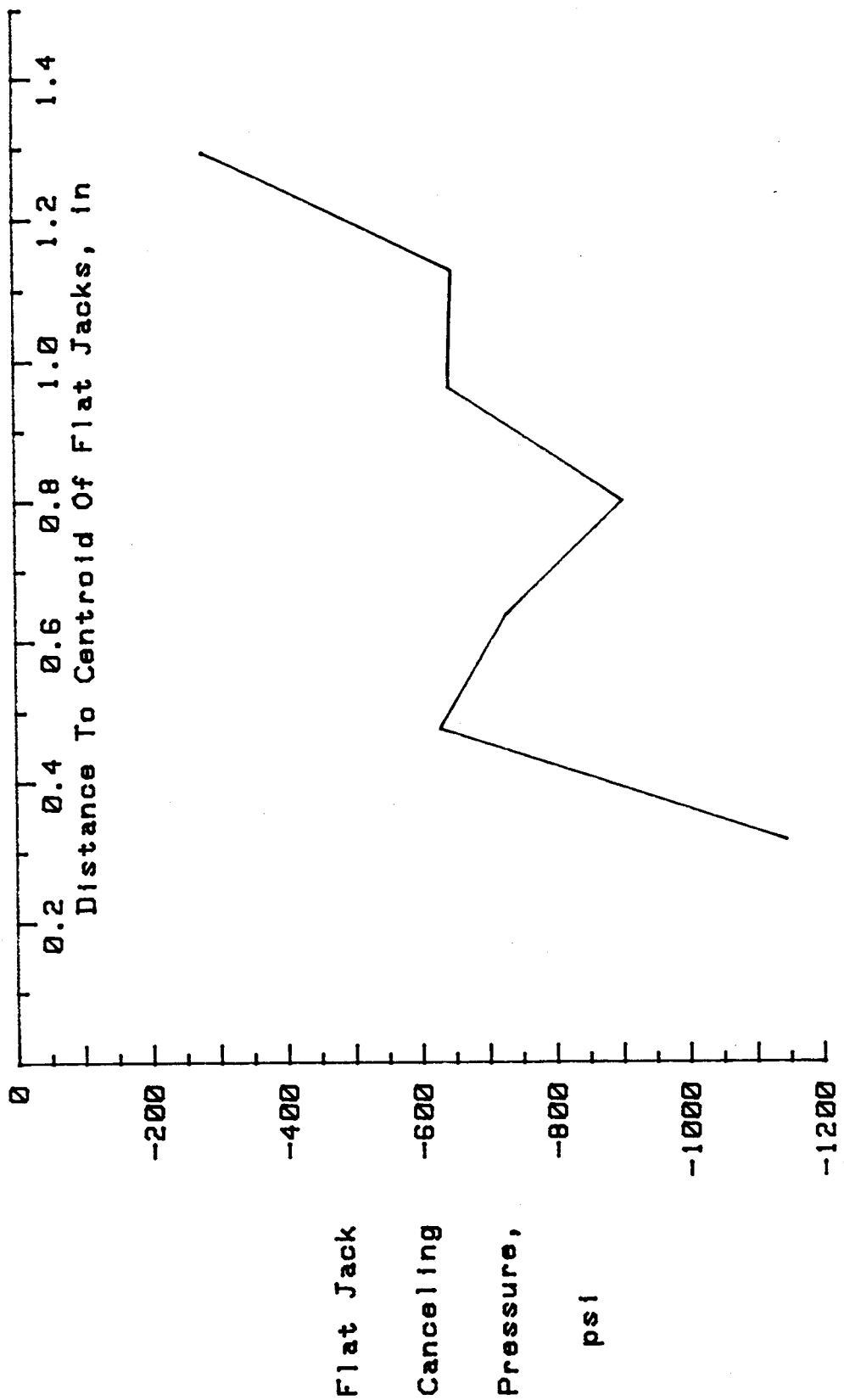


Figure 114. Uncorrected stress profile for TWS5VT.



Table 83. Stress measurement data for specimen TWS5VB.

PFENDER READINGS				
Cut Depth (mm)	Flat Jack Internal Pressure (psi)			
	0	200	400	600
20	5.2	6.4	7.1	7.9
30	6.4	8.4	9.6	13.2
40	11.6	14.6	18.0	21.6
50	17.4	20.0	23.7	27.9
60	17.1	21.6	26.3	33.1
70	19.1	22.4	27.9	34.9
80	10.0	16.5	26.2	32.2

LEAST SQUARES CURVE PARAMETERS				
Cut Depth (mm)	Slope (ksi/in)	Y-Intercept (Canceling Press,psi)	Correlation Coefficient (1=Exact Fit)	Standard Error Of Estimate
20	8.82	-1208	0.9926	54.3
30	3.47	-537	0.9762	97.0
40	2.35	-688	0.9992	18.1
50	2.21	-956	0.9947	45.8
60	1.48	-624	0.9946	46.3
70	1.45	-665	0.9879	69.3
80	1.02	-254	0.9958	40.8

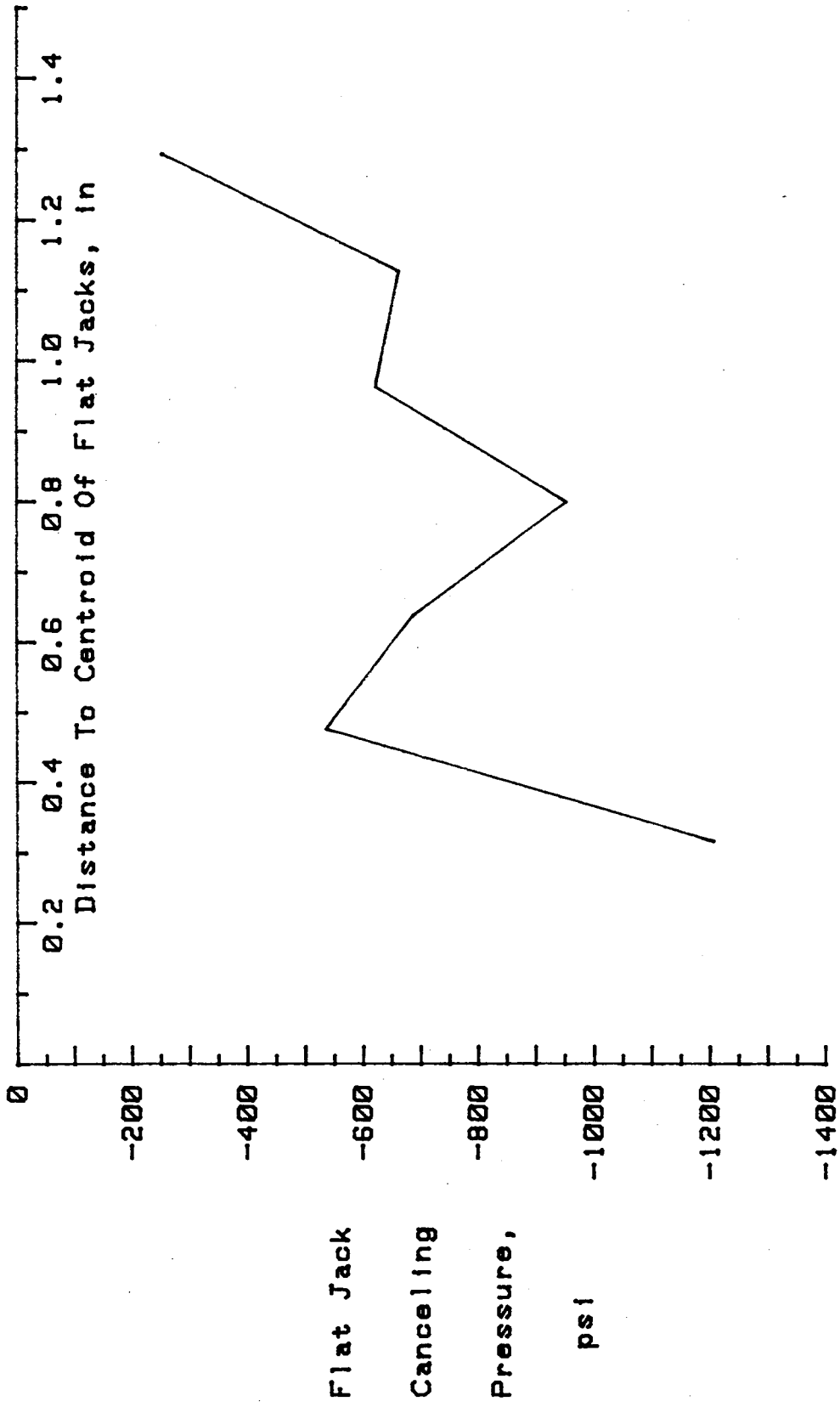


Figure 115. Uncorrected stress profile for TWS5VB.

**Table 84. Stress measurement data for specimen TWS6VT.**

PFENDER READINGS				
Cut Depth (mm)	Flat Jack Internal Pressure (psi)			
	0	200	400	600
20	-1.4	-0.4	1.5	2.5
30	-4.9	-2.4	0.0	2.7
40	-9.5	-4.8	-0.7	3.7
50	-9.5	-3.6	0.7	5.8
60	-9.0	-3.7	1.9	9.6
70	-9.7	-4.7	1.3	10.2
80	-16.6	-8.9	-0.1	11.0

LEAST SQUARES CURVE PARAMETERS				
Cut Depth (mm)	Slope (ksi/in)	Y-Intercept (Canceling Press,psi)	Correlation Coefficient (1=Exact Fit)	Standard Error Of Estimate
20	5.51	218	0.9899	63.2
30	3.07	387	0.9998	8.6
40	1.79	428	0.9997	11.1
50	1.55	364	0.9984	25.0
60	1.26	309	0.9959	40.4
70	1.17	321	0.9911	59.6
80	0.85	379	0.9963	38.5

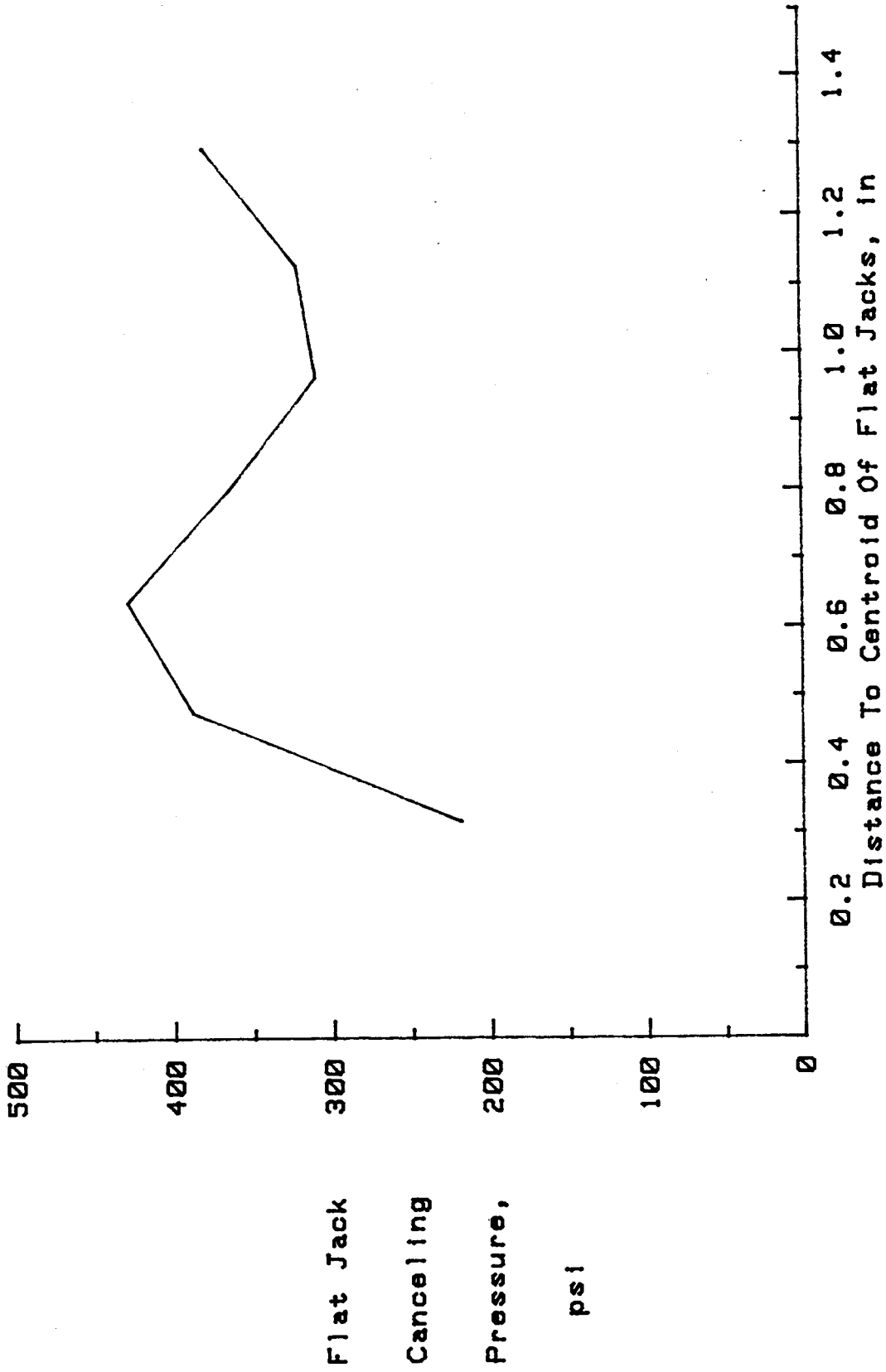


Figure 116. Uncorrected stress profile for TMS6VT.

Table 85. Stress measurement data for specimen TWS6VB.

PFENDER READINGS				
Cut Depth (mm)	Flat Jack Internal Pressure (psi)			
	0	200	400	600
20	0.6	-0.4	2.4	3.9
30	-0.4	-1.6	1.1	4.3
40	-7.2	-3.5	0.2	5.2
50	-3.8	-1.6	4.7	8.8
60	-6.7	-1.5	2.9	11.3
70	-5.9	-3.1	4.2	11.5
80	-11.8	-4.8	4.7	13.7

LEAST SQUARES CURVE PARAMETERS				
Cut Depth (mm)	Slope (ksi/in)	Y-Intercept (Canceling Press,psi)	Correlation Coefficient (1=Exact Fit)	Standard Error Of Estimate
20	4.44	116	0.8499	235.6
30	3.34	229	0.8540	232.6
40	1.90	365	0.9972	33.6
50	1.72	212	0.9851	76.9
60	1.31	251	0.9897	64.0
70	1.27	246	0.9832	81.5
80	0.91	290	0.9980	28.4

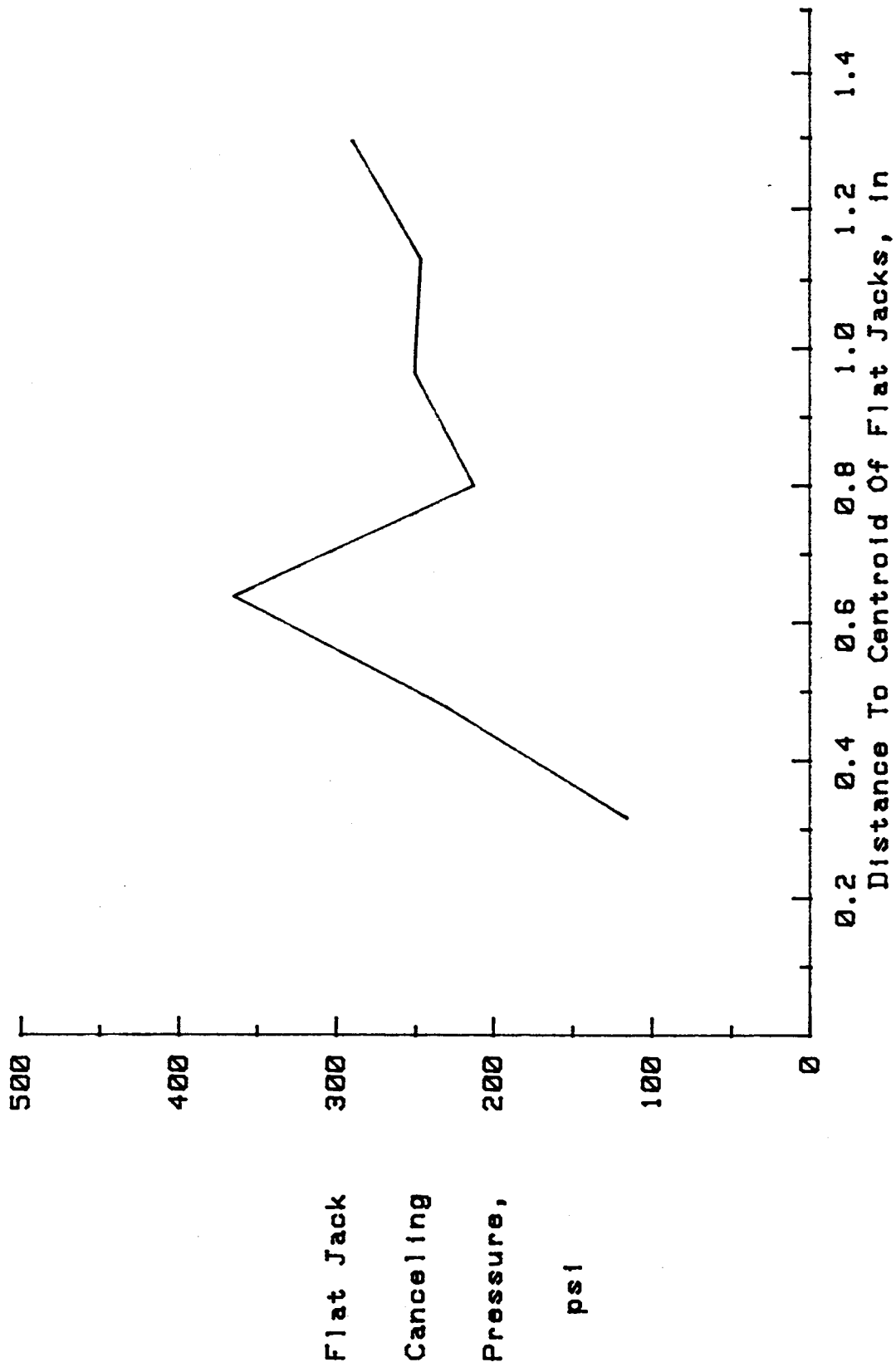


Figure 117. Uncorrected stress profile for TWS6VB.

Table 86. Stress measurement data for specimen TWS7HE.

PFENDER READINGS					
Cut Depth (mm)	Flat Jack Internal Pressure (psi)				
	0	100	200	300	400
20	0.0	-0.0	1.0	3.9	112.8
30	7.9	7.0	9.7	10.9	12.9
40	8.7	9.7	13.2	17.0	48.1
50	16.4	17.4	21.7	24.9	43.6
60	21.7	22.0	29.4	33.9	33.3
70	33.8	35.9	42.7	49.7	32.2
80	39.7	41.9	50.7	56.9	23.0

LEAST SQUARES CURVE PARAMETERS				
Cut Depth (mm)	Slope (ksi/in)	Y-Intercept (Canceling Press,psi)	Correlation Coefficient (1=Exact Fit)	Standard Error Of Estimate
20	5.32	59	0.8220	80.5
30	2.46	-406	0.9327	114.0
40	1.31	-256	0.9738	50.9
50	1.26	-493	0.9763	48.4
60	0.82	-404	0.9547	66.6
70	0.69	-560	0.9772	47.5
80	0.62	-599	0.9782	46.5

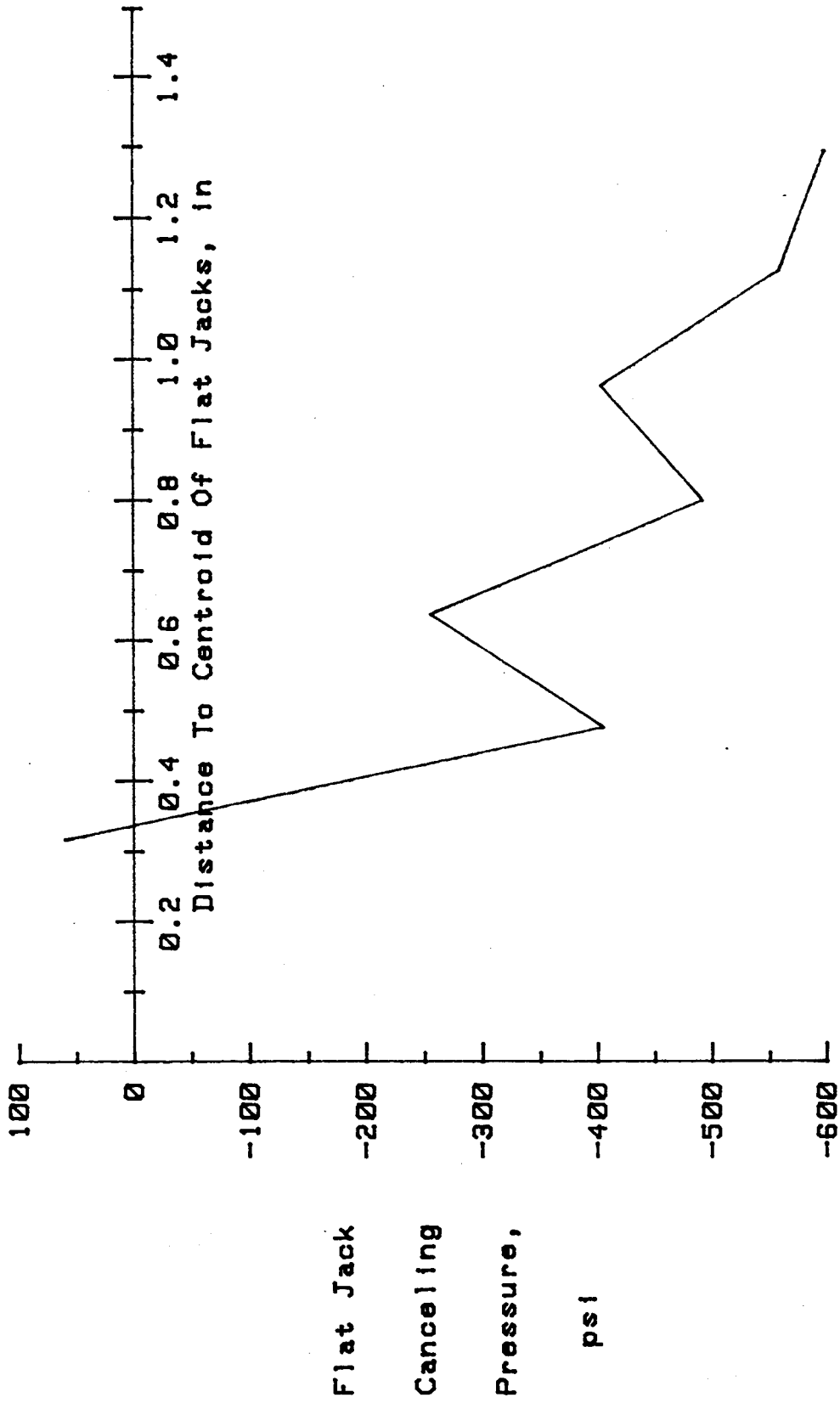


Figure 118. Uncorrected stress profile for TWS7HE.



Table 87. Stress measurement data for specimen TWS7HW.

PFENDER READINGS					
Cut Depth (mm)	Flat Jack Internal Pressure (psi)				
	0	100	200	300	400
20	5.7	4.7	4.7	5.7	6.5
30	7.0	6.7	9.0	10.7	12.9
40	7.2	9.4	13.7	16.7	48.1
50	15.6	18.2	21.6	25.4	43.6
60	20.5	21.9	29.0	33.9	33.3
70	32.7	35.2	42.7	49.2	32.2
80	38.7	41.2	49.9	56.2	23.0

LEAST SQUARES CURVE PARAMETERS				
Cut Depth (mm)	Slope (ksi/in)	Y-Intercept (Canceling Press,psi)	Correlation Coefficient (1=Exact Fit)	Standard Error Of Estimate
20	4.35	-404	0.5361	266.9
30	2.30	-341	0.9606	87.9
40	1.18	-203	0.9932	26.0
50	1.19	-462	0.9966	18.4
60	0.79	-377	0.9735	51.2
70	0.67	-527	0.9826	41.5
80	0.62	-581	0.9810	43.3

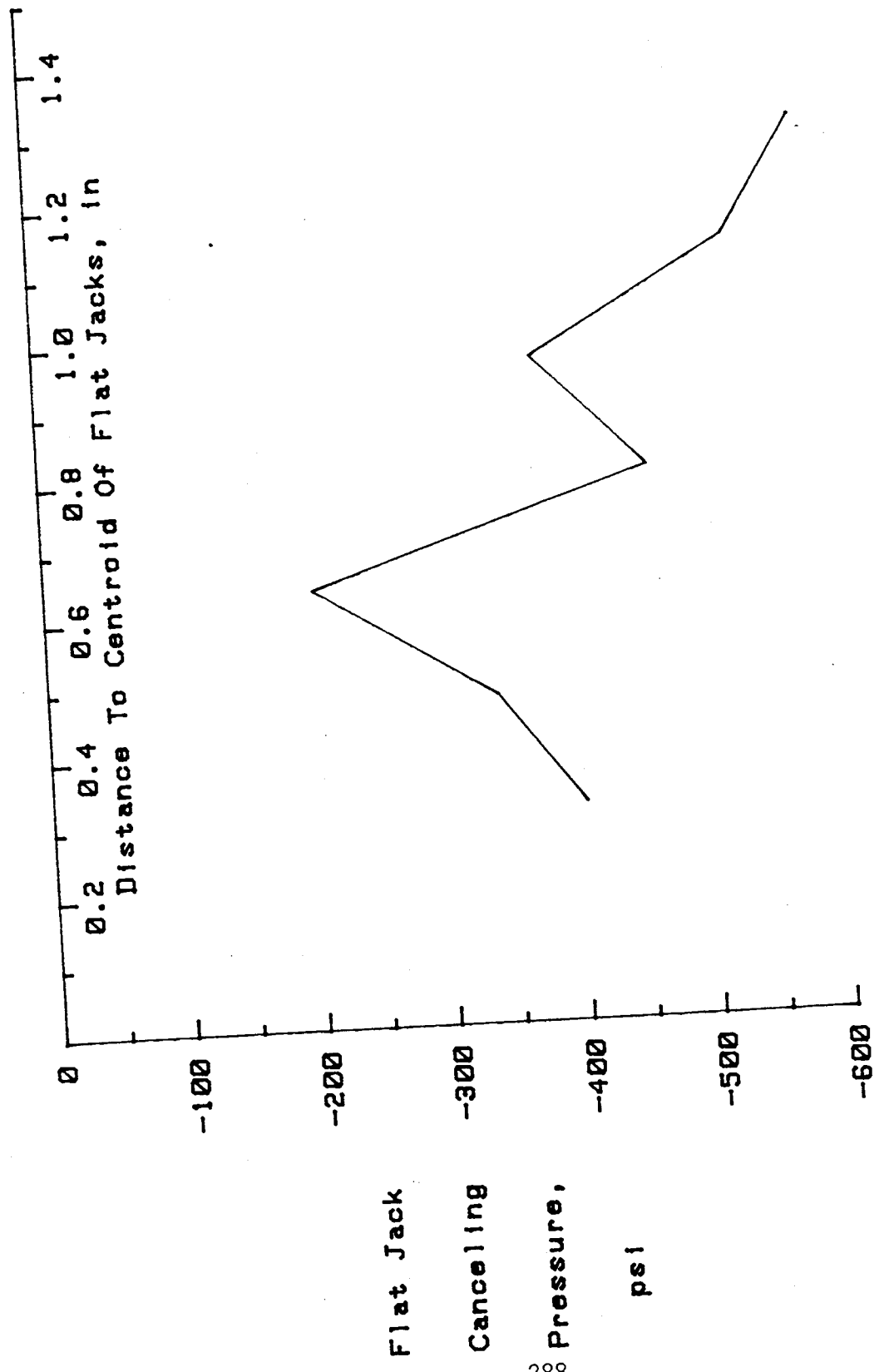


Figure 119. Uncorrected stress profile for TWS7HW.